UNIVERSIDAD DE CHILE
FACULTAD DE CIENCIAS FÍSICAS Y MATEMÁTICAS
DEPARTAMENTO DE INGENIERÍA MATEMÁTICA

UNIVERSITÉ DE PAU ET DES PAYS DE L'ADOUR
LABORATOIRE DE MATHÉMATIQUES ET DE LEURS APPLICATIONS DE PAU

SHAPE OPTIMIZATION FOR THIN LAYERS HEAT EXCHANGERS

TESIS PARA OPTAR AL GRADO DE
DOCTORADO EN CIENCIAS DE LA INGENIERÍA, MENCIÓN MODELACIÓN MATEMÁTICA

EN COTUTELA CON L'UNIVERSITÉ DE PAU ET DES PAYS DE L'ADOUR

RODRIGO ANDRE ZELADA MANCINI

PROFESORES GUÍA:
FABIEN CAUBET (UPPA)
CARLOS CONCA (UCH)
MARC DAMBRINE (UPPA)

MIEMBROS DE LA COMISIÓN:
CHARLES DAPOGNY (REPORTER)
LEÏLA RAHMANI (REPORTER)
BENIAMIN BOGOSEL
YANNICK PRIVAT
JORGE SAN MARTÍN

Este trabajo ha sido parcialmente financiado por ANID Beca Doctorado Nacional 2021-21211704 y CMM ANID BASAL FB210005.

SANTIAGO DE CHILE
2025

Resumen

Esta tesis aborda dos grandes temas en matemáticas aplicadas: el análisis numérico de EDPs y la optimización de forma/topológica. El objectivo es considerar el caso de un intercambiador de calor fluido-fluido en un régimen de convección forcada, donde los fluidos están separados por un solido de espesor pequeño (capa fina). Así, al abordar los retos que plantean las condiciones de transmisión no estándar, este trabajo contribuye a avanzar en las herramientas teóricas y numéricas utilizadas para tratar sistemas físicos acoplados en la optimización de la forma.

Comenzamos por proponer un modelo asintótico que toma en cuenta el intercambio de calor en la capa fina solida a través de condiciones de transmisión efectivas de tipo Ventcel en la interface. En primer lugar, estudiamos la resolución numérica de este modelo, donde desarrollamos y analizamos un método de elementos finitos extendidos de tipo Nitsche, dando resultados de consistencia, estabilidad y estimaciones de error, que validamos tanto teorica como numéricamente. Enseguida, nos interesamos en un problema de optimización de forma motivado por un isolante térmico: obtenemos las derivadas de forma para el problema de diseño óptimo que consiste en minimizar el flujo de calor al exterior de un tubo cubierto pour un isolante térmico a volume fijo, y realizamos simulaciones numéricas utilizando el método de level-set para adaptación de mallas. Finalmente, nos concentramos en el problema de diseño óptimo de intercambiadores de calor fluido-fluido, para maximizar el intercambio de calor bajo restricciones de disipación de energía y de volumen, consideramos un modelo debilmente acoplado entre las ecuaciones de Navier-Stokes estacionarias y la ecuación de convección-difusión con condiciones de transmisión de tipo Ventcel, analizamos la sensibilidad respecto a la forma del sistema y realizamos simulaciones numéricas 3D.

Palabras clave: Optimización de forma; método de level set; modelo asintótico; condiciones de transmición de Ventcel; elementos finitos extendidos tipo Nitsche; ecuaciones de Navier-Stokes; ecuación de convención-diffusión.

Résumé

Cette thèse s'inscrit dans deux domaines majeurs des mathématiques : l'analyse numérique des EDP et l'optimisation de forme/topologique. L'objectif est de considérer le cas d'un échangeur de chaleur à deux fluides en régime de convection forcée, dans le cas où les fluides sont séparés par une fine couche solide. Ainsi, en abordant les défis posés par des conditions de transmission non standard, ce travail contribue à faire progresser les outils théoriques et numériques utilisés pour traiter des systèmes physiques couplés en optimisation de la forme.

Nous commençons par proposer un modèle asymptotique qui prend en compte l'échange de chaleur dans la couche solide mince impliquant des conditions de transmission de type Ventcel à l'interface. Tout d'abord, la résolution numérique de ce modèle est étudiée, où nous développons et analysons une méthode d'éléments finis étendues de type Nitsche en donnant des résultats de consistence, de stabilité et des estimations d'erreur, que nous validons à la fois théoriquement et numériquement. Ensuite, nous nous intéressons à un problème d'optimisation de forme motivé par l'isolation thermique : nous obtenons les dérivées de forme pour le problème de conception optimale consistant à minimiser le flux de chaleur à l'extérieur d'un tuyau entouré d'un isolant thermique de volume fixe, et nous mettons en œuvre des simulations numériques à l'aide de la méthode des lignes de niveaux. Enfin, nous nous concentrons sur la conception d'échangeurs de chaleur fluide-fluide en 3D : pour maximiser l'échange de chaleur sous des contraintes de dissipation d'énergie et de volume, nous considérons un modèle couplé impliquant les équations de Navier-Stokes stationnaires et une équation de convection-diffusion avec des conditions de transmission de type Ventcel, nous analysons la sensibilité par rapport à la forme du système et nous réalisons des simulations numériques 3D.

Mots-clés: Optimisation de forme; méthode des lignes de niveaux; modéle asymptotique; conditions de transmission de Ventcel; élements finis étendus de Nitsche; équations de Navier-Stokes; équation de convection-diffusion.

Abstract

This thesis falls within two major areas of mathematics: numerical analysis of PDEs and shape/ topology optimization. We are interested in the optimal design of a heat exchanger. The aim is to consider the case of a two-fluid heat exchanger in a forced convection regime, in the case where the fluids are separated by a thin solid layer. Then, by addressing challenges arising from non-standard transmission conditions, this work contributes to advancing the theoretical and computational tools used to tackle coupled physical systems in shape optimization.

We begin by proposing an asymptotic model that takes into account heat exchange in the thin solid layer involving Ventcel-type transmission conditions at the interface. Firstly, the numerical resolution of this model is studied and we develop and analyze a Nitsche-type finite element method providing consistency, stability, and error estimates, validated both theoretically and numerically. Secondly, we turn to a shape optimization problem motivated by thermal insulation: we compute shape derivatives for the optimal design problem of minimizing the heat flux outside a pipe surrounded by a thermal insulation of fixed volume, and we implement numerical simulations using the level set method. Finally, we focus on the design of 3D fluid-to-fluid heat exchangers: to maximize heat exchange under energy dissipation and volume constraints, we consider a coupled model involving steady-state Navier-Stokes equations and a convection-diffusion equation with Ventcel-type transmission conditions, analyze the shape sensitivity of the system, and provide 3D numerical simulations.

Keywords: Shape optimization; level-set method; asymptotic model; Ventcel transmission conditions; Nitsche extended finite elements; Navier-Stokes equations; convection-diffusion equation.

Contents

List of Tables

List of Figures

Introducción

Esta tesis se enmarca en dos grandes temas de las matemáticas aplicadas: análisis numérico de PDEs y optimización de forma/topologica. Motivados por un problema real de intercambiadores de calor a partir del trabajo de nuestros colegas *Aldor et al.* del SIAME (Laboratoire des Sciences pour l'Ingénieur Appliquées à la Mécanique et au génie Electrique), que han propuesto un novedoso intercambiador de calor sinusoidal [3], estamos interesados en el diseño óptimo de un intercambiador de calor. Se trata de considerar el caso de un intercambiador de calor de dos fluidos en régimen de convección forzada, en el que los fluidos están separados por una capa fina sólida, como en la Figura 7. A continuación, al abordar los retos derivados de las condiciones de transmisión no estándar, este trabajo contribuye al avance de las herramientas teóricas y numéricas utilizadas para abordar sistemas físicos acoplados y optimización de forma.

Comenzamos proponiendo un modelo asintótico que toma en cuenta el intercambio de calor en la capa fina sólida que implica condiciones de transmisión de tipo Ventcel en la interfaz. En primer lugar, se estudia la resolución numérica de este modelo, donde desarrollamos y analizamos un método de elementos finitos de tipo Nitsche demostrando consistencia, estabilidad y dando estimaciones de error, validadas tanto teórica como numéricamente. En segundo lugar, abordamos un problema de optimización de forma motivado por el aislamiento térmico: obtenemos las derivadas de forma para el problema de diseño óptimo de minimización del flujo de calor en el exterior de una tubería rodeada por de un aislante térmico de volumen fijo, y realizamos simulaciones numéricas utilizando el método de level-set. Finalmente, nos centramos en el diseño de intercambiadores de calor 3D fluido-fluido: para maximizar el intercambio de calor bajo restricciones de disipación de energía y volumen, consideramos un modelo acoplado que involucra las ecuaciones de Navier-Stokes en estado estacionario y una ecuación de convección-difusión con condiciones de transmisión tipo Ventcel, analizamos la sensibilidad a la forma del sistema, y proporcionamos simulaciones numéricas 3D.

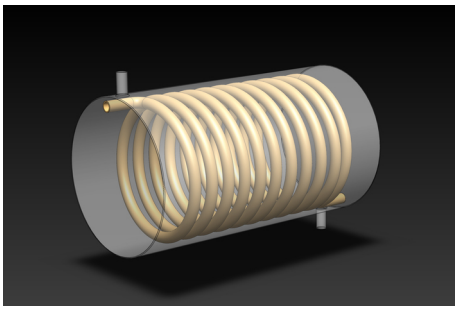

Figure 1: Intercambiador de calor helicoidal. Figura extraída de [88].

Contexto general de optimización de forma y topológica

Aunque la optimización de forma es una técnica matemática antigua que se remonta a 1908 por Jacques Hadamard [69], sólo en las últimas décadas este campo ha recibido una atención considerable, debido a la necesidad de soluciones más eficientes e innovadoras que demandan industrias como la aeroespacial [114, 103], intercambiadores de calor [76, 60, 67], ingeniería civil [19], fotónica [77, 82], etc.

La optimización de forma consiste en cambiar la geometría moviendo la frontera mientras se mantiene la misma topología. Esto hace que el diseño final dependa bastante del dominio inicial, y la respuesta a este problema se llama optimización topológica, que, a diferencia de la optimización de forma, permite cambios en la topología. El objetivo tanto de la optimización de forma como topológica es mejorar el rendimiento de un sistema de ingeniería con respecto a alguna cantidad o criterio físico, como reducir la disipación de energía, reducir el peso, minimizar la complianza, etc., lo que a menudo da lugar a diseños que son contrarios a la intuición de los métodos de ingeniería tradicionales. En algunos casos, la complejidad del diseño final ha hecho difícil o imposible su fabricación, pero la llegada de la fabricación aditiva ha ampliado aún más las capacidades de optimización tanto de forma como topológica.

Por un lado, en la optimización de forma, los dos métodos principales son la variación de frontera y el enfoque de level-set. Por otro lado, la optimización topológica incluye la derivada topológica, la homogeneización y los métodos SIMP (Solid Isotropic Material with Penalization). Comenzaremos por discutir brevemente estos dos enfoques a continuación.

Optimización de forma

Para resolver un problema de optimización general, la estrategia habitual es utilizar un algoritmo de descenso. Hay muchos algoritmos bien estudiados, tanto para casos con restricciones como sin ellas, como el método del gradiente, el método de Newton, el BFGS, el gradiente conjugado o la programación lineal, véase [92]. Para ello, necesitamos proporcionar al menos la primera derivada (en algunos casos, incluso la segunda derivada, como en el método de Newton). La optimización de forma es un problema de optimización de dimensión infinita en el que la variable es un dominio y la derivada es con respecto al dominio. El primer paso, entonces, es definir, en cierto sentido, el concepto de *derivada de forma*. En su trabajo seminal, Hadamard [69] definió este concepto, que a grandes rasgos toma en cuenta pequeñas perturbaciones de la frontera. La derivada de forma de Hadamard proporciona el marco teórico y, desde el punto de vista numérico, tenemos diferentes maneras de actualizar la geometría en cada paso del proceso de optimización.

El primer enfoque, conocido como *optimización de forma geométrica*, consiste en tener una representación explícita de un dominio mediante una malla y utilizar las direcciones de descenso para mover los nodos de esta malla. Remitimos a [13] para una aplicación práctica en el contexto de la optimización estructural o, más recientemente, al trabajo didáctico de Dapogny *et al.* [50] en el contexto de la mecánica de fluidos, ambos utilizando el software de elementos finitos de código abierto FreeFem++. El principal inconveniente de este método es que el proceso de mover vértices puede producir triángulos degenerados (superpuestos o no conformes), lo que afecta a la calidad de la malla. Otro problema es que mantiene la misma conectividad, por lo que tiene sentido utilizarlo

cuando tenemos una idea *a priori* de la solución.

Un segundo enfoque se basa en el método de *level-set*. El método de level-set fue desarrollado por Osher y Sethian en [95], concebido originalmente para seguir la evolución de fronteras o interfaces en movimiento, como curvas o superficies. Resultó ser muy útil en diversas áreas, como la segmentación de imágenes, la visión por ordenador, los problemas fluido-estrucras y, lo que nos interesa, la optimización de forma y topológica. Al introducir un dominio fijo desde el punto de vista computacional que contiene el dominio de interés original, la función de level-set permite representar implícitamente la frontera mediante el level-set cero de la función. Esto resulta especialmente útil en la optimización de forma, donde pueden obtenerse cambios topológicos. Inicialmente, la función de level-set se consideraba en una malla fija [12, 111]. Sin embargo, presenta un inconveniente. Como la malla es fija y la evolución es seguida implícitamente por la función de level-set, las ecuaciones diferenciales parciales consideradas no pueden resolverse directamente. Una solución que suele considerarse en los problemas de optimización de forma consiste en introducir un material ficticio de relleno entre el dominio computacional y el dominio de interés, lo que permite resolver estas ecuaciones aproximadas.

Hoy en día, el enfoque moderno se conoce como *el método de evolución de malla de level-set*, introducido por Allaire *et al.* en [10]. La idea principal es tener dos representaciones diferentes de la geometría, cada una con un propósito diferente. Más concretamente, utilizamos la función de level-set como antes para manejar las deformaciones de la geometría (posibles cambios de topología) y, en cada paso de optimización, remallar de acuerdo con el level-set cero, a continuación, la malla del dominio se puede utilizar para resolver las ecuaciones diferenciales parciales en consideración.

Optimización topológica

La lista de métodos de optimización topológica es bastante extensa. Aquí nos limitaremos a una breve descripción de los más utilizados, especialmente en aplicaciones de intercambiadores de calor.

En primer lugar, además de la derivada de forma, existe la *derivada topológica* [93, 94, 14], basada en expansiones asintóticas, que pretende crear pequeños agujeros en el dominio o añadir pequeñas burbujas al mismo dependiendo del contexto estudiado.

En segundo lugar, existen otro tipo de métodos: los llamados *métodos de densidad*, en los que tenemos el *método de homogeneización* (véase [90, 100, 43, 105] para una introducción general a la teoría matemática de la homogeneización y [6, 41] en el contexto de la optimización de forma y topológica) y el método *SIMP* (Solid Isotropic Material with Penalty) (véase [22, 62]). Ambos se basan en una función de densidad que aproxima la función característica, que es 1 dentro del dominio variable y 0 fuera. Esto significa que el problema de optimización de forma/topológica se relaja, al aceptar como admisibles las estructuras compuestas. Mientras que el método de homogeneización aboga por caracterizar las propiedades de la microestructura (lo cual no es tarea fácil), el método SIMP las aproxima en términos de la densidad mediante alguna heurística (generalmente como un polinomio de la densidad). El principal inconveniente es que obtenemos una densidad continua que tenemos que penalizar para obtener una estructura binaria.

Optimización de forma y topológica de intercambiadores de calor

Como se ha mencionado anteriormente, uno de los objetivos de esta tesis es centrarse en el diseño de intercambiadores de calor. El problema del intercambiador de calor es multifísico (implica temperatura y flujo de fluidos, descritos por las ecuaciones de convección-difusión y Navier-Stokes, respectivamente) e incluye también una restricción de distancia mínima, que garantiza que los fluidos no se mezclen, y que desempeña un papel clave en este problema.

En la comunidad de optimización de forma y topológica, el problema del intercambiador de calor se ha abordado utilizando las diferentes herramientas que hemos descrito anteriormente, principalmente el método SIMP y de evolución de malla de level-set combinado con la derivada de Hadamard. Los primeros trabajos fueron en 2009, considerando un único fluido [51, 52, 112]. El caso de dos fluidos fue tratado en la tesis de máster de Papazoglou en 2015 [97] y luego le siguieron [76, 81]. Como hemos señalado, el principal inconveniente del método SIMP es cómo obtener la estructura binaria introduciendo una penalización adecuada que toma aún más relevancia en este problema multifísico, con geometría compleja y donde la restricción de distancia no es trivial de tener en cuenta. Es por ello que el método de evolución de malla de level-set parece más adecuado para este problema: este es el enfoque seguido recientemente en 2021 en la tesis de Feppon [67]. Cabe señalar que el método SIMP es actualmente preferido por una comunidad más amplia de ingenieros, a pesar de los problemas que hemos explicado, debido a que el método de deformación de malla de level-set con derivada de Hadamard es reciente.

Objetivo y principales dificultades

En esta tesis, el objetivo principal es optimizar un intercambiador de calor teniendo en cuenta la fina capa que separa los dos fluidos, como suele ocurrir en las aplicaciones reales. En el proceso surgen varias dificultades técnicas que explicamos a continuación.

Condiciones de transmisión no estándar de Ventcel

Para comprender mejor estas dificultades, necesitamos explicitar las condiciones de transmisión efectivas. Explicaremos informalmente estas condiciones de transmisión (los detalles rigurosos y los resultados de convergencia se dan en el Capítulo 1). Sea $\eta > 0$ un parámetro pequeño. Comenzamos considerando $\Omega^\eta \subset \mathbb{R}^d$, dividido en tres subdominios $\Omega_1^\eta, \Omega_s^\eta, \Omega_2^\eta$, donde la parte sólida Ω_s^η separa los dominios fluidos Ω_1^η y Ω_2^η. El parámetro η representa el grosor del sólido Ω_s^η (que modela la pared de la tubería que contiene el fluido caloportador). La interfaz entre Ω_i^η y Ω_s^η se denomina $\Gamma_i^\eta := \partial\Omega_i^\eta \cap \partial\Omega_s^\eta$, $i = 1, 2$. Con el propósito de simplificar esta introducción, consideramos sólo las condiciones de borde de Dirichlet en la frontera $\Gamma_{\mathrm{D}}^\eta := \partial\Omega^\eta$, y definimos $\Gamma_{\mathrm{D,i}}^\eta := \partial\Omega_i^\eta \setminus \Gamma_i^\eta$ la parte Dirichlet de Ω_i^η, $i = 1, 2$, y $\Gamma_{\mathrm{D,s}}^\eta := \partial\Omega_i^\eta \setminus (\Gamma_1^\eta \cup \Gamma_2^\eta)$ la parte Dirichlet de Ω_s^η. Suponemos que $\Gamma_{\mathrm{D,i}}^\eta$ toca Γ_i^η, $i = 1, 2$.

Sean $\kappa_1, \kappa_2, \kappa_s$ tres números reales positivos (difusividades térmicas). Consideramos entonces

u^η la solución de la ecuación de convección-difusión en Ω^η, con restricciones $u_i^\eta := u|_{\Omega_i^\eta}^\eta$, $i = 1, 2, s$, condiciones de transmisión continua en las interfaces Γ_i^η, $i = 1, 2$ y condición de borde de Dirichlet homogénea en $\Gamma_{\mathrm{D,i}}^\eta$, $i = 1, 2, s$:

$$\begin{cases} -\operatorname{div}(\kappa_i \nabla u_i^\eta) &= f|_{\Omega_i^\eta} & \text{en } \Omega_i^\eta, i = 1, 2, \\ -\operatorname{div}(\kappa_s \nabla u_s^\eta) &= f|_{\Omega_s^\eta} & \text{en } \Omega_s^\eta, \\ u_i^\eta &= 0 & \text{en } \Gamma_{\mathrm{D,i}}^\eta, i = 1, 2, s, \\ u_s^\eta &= u_i^\eta & \text{en } \Gamma_i^\eta, i = 1, 2, \\ \kappa_s \dfrac{\partial u_s^\eta}{\partial n} &= \kappa_i \dfrac{\partial u_i^\eta}{\partial n} & \text{en } \Gamma_i^\eta, i = 1, 2, \end{cases} \tag{1}$$

donde $\boldsymbol{n}$ es la normal unitaria en Γ_i^η apuntando hacia Ω_2^η y $f \in \mathrm{L}^2(\Omega^\eta)$ tal que $f = 0$ en Ω_s^η .

Debido a que Ω_s^η es demasiado fina, no podemos malla directamente, ya que sería muy costoso para resolver numéricamente (en particular en 3D). Una técnica eficiente para tratar este tipo de problemas son los modelos asintóticos como en el trabajo de Enquist y Nedelec [58] o más recientemente en [110, 16]. Un modelo asintótico similar (tres materiales con una capa fina en el medio) se obtuvo en [40] considerando una física diferente.

La idea es pasar el límite η en la geometría, obteniendo $\Omega_1 \cup \Omega_2$, independiente de η y sin capa delgada, donde Ω_i es el límite de Ω_i^η cuando $\eta \to 0$. Sea $\Gamma := \partial\Omega_1 \cap \partial\Omega_2$ la interfase entre Ω_1 y Ω_2, que coincide con la curva media entre Γ_1^η y Γ_2^η. Análogamente, $\Gamma_{\mathrm{D},i} := \partial\Omega_i \setminus \Gamma$.

Una primera aproximación consiste en despreciar completamente el efecto sólido, es decir, no tener en cuenta la difusión en Ω_s^η, lo que conduce al modelo de orden cero:

$$\begin{cases} -\operatorname{div}(\kappa_i \nabla u_i^0) &= f|_{\Omega_i} & \text{en } \Omega_i, i = 1, 2, \\ u_i^0 &= 0 & \text{en } \Gamma_{\mathrm{D,i}}, i = 1, 2, \\ u_1^0 &= u_2^0 & \text{en } \Gamma, \\ \kappa_1 \dfrac{\partial u_1^0}{\partial n} &= \kappa_2 \dfrac{\partial u_2^0}{\partial n} & \text{en } \Gamma, \end{cases}$$

donde u^0 es la solución asociada al modelo de orden cero, con restricciones u_1^0 y u_2^0 a Ω_1 y Ω_2, respectivamente. En términos generales, esto significa que Ω_s^η es tan fina, que la temperatura u_s^η es constante siguiendo la dirección normal $\boldsymbol{n}$ en Ω_s^η.

Proponemos un modelo más complejo en el que ya no se supone que la temperatura sea constante en la capa delgada. Se trata de un modelo de primer orden, que tiene en cuenta el efecto de la difusión en Ω_s^η utilizando condiciones de transmisión de tipo Ventcel:

$$\begin{cases} -\operatorname{div}(\kappa_i \nabla u_i^1) &= f|_{\Omega_i} & \text{en } \Omega_i, i = 1, 2, \\ u_i^1 &= 0 & \text{en } \Gamma_{\mathrm{D,i}}, i = 1, 2, \\ \left\langle \kappa \dfrac{\partial u^1}{\partial n} \right\rangle &= -\dfrac{\kappa_s}{\eta}[u^1] & \text{en } \Gamma, \\ \left[\kappa \dfrac{\partial u^1}{\partial n} \right] &= \eta \operatorname{div}_\tau(\kappa_s \nabla_\tau \left\langle u^1 \right\rangle) - \kappa_s H[u^1] & \text{en } \Gamma, \end{cases} \tag{2}$$

donde u^1 es la solución asociada del modelo de orden uno, con restricciones u_1^1 y u_2^1 a Ω_1 y Ω_2, respectivamente, div_τ es la divergencia tangencial, ∇_τ es el gradiente tangencial, H es la curvatura

media de Γ y $[\cdot]$, $\langle\cdot\rangle$ denota el salto y la media en Γ, definida para cada función suave definida en Ω con restricciones $\phi_i := \phi|_{\Omega_i}$ en Ω_i como:

$$[\phi] := \phi_1 - \phi_2 \quad \text{y} \quad \langle\phi\rangle := \frac{1}{2}(\phi_1 + \phi_2) \text{ en } \Gamma.$$

Aquí y en lo sucesivo no utilizaremos más el superíndice [1] para denotar el modelo de orden uno, por lo que llamaremos u a la solución del modelo asintótico. El modelo de orden uno con condiciones de transmisión Ventcel no estándar (2) es el modelo que consideraremos a lo largo de esta tesis. A grandes rasgos, esto significa que Ω_s^η es tan fina, que la temperatura u_s^η es lineal siguiendo la dirección normal $\boldsymbol{n}$ en Ω_s^η.

Nótese que el efecto de difusión de volumen $\mathrm{div}(\kappa_s \nabla u_s^\eta)$ en Ω_s^η aparece claramente como $\mathrm{div}_\tau(\kappa_s \nabla_\tau \langle u\rangle)$ en Γ, en el modelo asintótico.

Resolución numérica de un problema de transmisión

Es importante señalar que la resolución numérica del modelo asintótico anterior (2) presenta varias dificultades.

- Las condiciones de transmisión no estándar cambian la naturaleza del problema. La solución del modelo exacto u^η pertenece a $\mathrm{H}^1(\Omega^\eta)$, mientras que la solución del modelo asintótico no es H^1 globalmente, ya que hay un salto sobre Γ en las condiciones de transmisión (2). El problema se plantea entonces en un espacio de *broken Sobolev*:

$$\mathcal{H}^1(\Omega_1, \Omega_2) := \{\phi = (\phi_1, \phi_2) \in \mathrm{H}^1(\Omega_1) \times \mathrm{H}^1(\Omega_2);\ \langle\phi\rangle \in \mathrm{H}^1(\Gamma)\}.$$

- La implementación discreta del espacio de broken Sobolev $\mathcal{H}^1(\Omega_1, \Omega_2)$ no es sencilla y no está disponible en softwares de elementos finitos de código abierto (véase [9] para más detalles sobre este tema).

- Aunque, podemos programar nuestro propio MEF discontinuo Galerkin sólo duplicando los grados de libertad en la interfaz (donde hay discontinuidades), si η es demasiado pequeño, la matriz de rigidez asociada al modelo asintótico está mal condicionada, debido al término $-\frac{\kappa_s}{\eta}[u]$ que explota cuando $\eta \to 0$. Nótese que es razonable tomar valores pequeños de η para nuestros experimentos numéricos, ya que η es el parámetro del desarrollo asintótico.

Necesitamos un método de elementos finitos que sea estable y bien condicionado con respecto a η para calcular el campo de temperatura. Para ello, introducimos una nueva formulación de tipo Nitsche, que estudiamos. Demostramos que esta formulación cumple dichos requisitos (véase el Capítulo 2 para más detalles).

Análisis de sensibilidad de forma

Volviendo al problema de diseño óptimo, debemos calcular las derivadas de forma de las ecuaciones involucradas: en nuestras aplicaciones consideramos un acoplamiento débil entre las ecuaciones de

Navier-Stokes y las ecuaciones de convección-difusión aproximadas/asintóticas, siendo un problema multifísico. Como señalamos anteriormente, se obtuvieron derivadas similares en [63] cuando la parte sólida Ω_s^η no es una capa delgada.

En cuanto a las ecuaciones consideradas en esta tesis, la dificultad adicional en comparación con [63] son las condiciones de transmisión Ventcel no estándar. Más concretamente, las derivadas de material y forma pertenecerán a un espacio de broken Sobolev y además la derivación de las derivadas tangenciales (como ∇_τ) en la superficie es mucho más complicada que la de las derivadas usuales en el volumen debido a la dependencia de la normal unitaria $\boldsymbol{n}$ de Γ, que cambia cuando cambia Γ. La dificultad no radica en calcular la derivada de forma del operador de Laplace-Beltrami: es bien conocida en la literatura, véase por ejemplo [54, 39, 46] en un contexto simplificado. La dificultad real proviene del hecho de que estas derivadas de superficie están implicadas en una condición de salto en una interfaz y están acopladas con discontinuidades de coeficiente. Nótese que tenemos también la curvatura media H, cuya derivada de forma requiere un tratamiento delicado desde el punto de vista numérico. Estas cuestiones se tratan gradualmente en los Capítulos 3 y 4.

Resolución numérica de problemas a gran escala

Por último, nos interesan las aplicaciones reales, *i.e.* simulaciones numéricas en 3D que son costosas desde el punto de vista computacional, en las que pondremos en práctica todas las herramientas anteriores. Se necesitan al menos cien iteraciones para lograr la convergencia del algoritmo de optimización. En cada iteración, tenemos que resolver las ecuaciones de Navier-Stokes, las ecuaciones de convección-difusión aproximadas y algunas ecuaciones adjuntas, deducir una dirección de descenso y, a continuación, remallar. En concreto, las ecuaciones de Navier-Stokes son la parte más costosa, ya que tienen millones de grados de libertad en nuestros casos de prueba a gran escala. Esto no puede hacerse sin paralelismo ni utilizando factorización LU estándar, en primer lugar por la memoria necesaria. Además, tiene que ser razonablemente rápido, lo que requiere precondicionadores adecuados para acelerar la resolución del sistema lineal.

Principales contribuciones

Esta investigación explora y amplía la aplicación de técnicas de optimización de forma y topológica al diseño de intercambiadores de calor de capa fina. El objetivo es desarrollar modelos más realistas que den lugar a soluciones fabricables. Los aportes de este trabajo se refieren a dos áreas principales: el análisis numérico y la optimización de forma.

Basado en el método de Nitsche [91], el método de Nitsche para condiciones de borde generales [79], y el método de elementos finitos extendido de Nitsche [70], esta tesis propone en primer lugar un método de Nitsche modificado para resolver un problema de convección-difusión no estándar. El método está diseñado para mejorar el condicionamiento de la matriz de rigidez asociada a problemas de convección-difusión con condiciones de transmisión no estándar. Las principales características del método propuesto son la robustez con respecto al espesor de la capa permaneciendo consistente, estable e independiente con respecto a los coeficientes de difusividad.

Este desarrollo proporciona un marco marco numérico eficaz para tratar discontinuidades y condiciones de transmisión complejas en problemas de convección-difusión.

A continuación, se propone un nuevo modelo para la optimización de aislantes térmicos. Este modelo es más realista que la literatura existente sobre optimización de forma para aislantes térmicos como [27, 28, 108]. De hecho, nuestro modelo toma en cuenta los efectos de difusión en la interfaz del dominio sólido delgado, utilizando condiciones de transmisión de tipo Ventcel, lo que lo hace más realista para aplicaciones prácticas. Este modelo también incorpora un acoplamiento débil entre las ecuaciones de Navier-Stokes (que describen la dinámica de fluidos) y la ecuación de convección-difusión (que describe la transferencia de calor). En este caso, el dominio del fluido es fijo y sólo se optimiza el material aislante. Consideramos el problema de optimización de forma cuyo objetivo es minimizar el flujo de calor fuera de un aislante con un volumen dado: caracterizamos la derivada de forma del funcional objetivo y realizamos simulaciones numéricas en 3D utilizando el método de evolución de level-set.

Posteriormente, consideramos nuestro problema inicial introduciendo un nuevo modelo para intercambiadores de calor 3D fluido-fluido en convección forzada, donde la capa sólida delgada se representa mediante condiciones de transmisión no estándar. También en este caso, estas condiciones tienen en cuenta los efectos de difusión en la interfaz a través del operador Laplace-Beltrami. El objetivo es optimizar la forma del tubo que contiene el fluido caloportador. En este problema, las condiciones de transmisión de Ventcel se imponen en la interfaz que se pretende optimizar. De ahí que realicemos un análisis de sensibilidad a la forma y calculemos las derivadas de forma asociadas. Hasta donde sabemos, estas derivadas de forma no se han calculado antes. Los resultados obtenidos pueden considerarse un complemento de trabajos anteriores como el de Feppon [63, 67]. De hecho, nuestro modelo incluye la difusión superficial en la interfaz, mientras que los trabajos anteriores suponían la difusión volumétrica en el interior del sólido. Además, destacamos que el análisis de sensibilidad de forma para problemas de transmisión con coeficientes de difusividad discontinuos merece atención y cuidado. Mencionemos los trabajos [74, 96, 1] donde se considera la ecuación de calor en un problema de transmisión con coeficientes de difusividad discontinuos. Es importante destacar que la derivada de forma debe calcularse con precaución en este caso, debido a que el método de derivación rápido de Cea puede llevar a errores en la fórmula de la derivada de forma o en el problema adjunto como se señaló en [96]. En esta tesis, se realiza una derivación rigurosa de las derivadas de forma utilizando primero las derivadas materiales, siguiendo la metodología de [1]. Nuestro trabajo puede verse como una extensión de [9], donde consideraban la ecuación de difusión con una solución discontinua en la interfaz y el flujo normal es continuo y proporcional al salto de la solución, más precisamente (en nuestra notación):

$$\begin{aligned} \left[\kappa \frac{\partial u}{\partial n}\right] &= 0 && \text{en } \Gamma, \\ \left\langle \kappa \frac{\partial u}{\partial n} \right\rangle &= -\kappa_s [u] && \text{en } \Gamma, \end{aligned}$$

que modelan interfaces imperfectas para la fabricación aditiva. En nuestro caso de transmisión por difusión en la interfaz, tenemos unas condiciones de transmisión más complicadas de derivar,

ya que el flujo normal no es continuo y depende del operador de Laplace-Beltrami:

$$\begin{aligned}\left[\kappa\frac{\partial u}{\partial n}\right] &= \eta\,\mathrm{div}_\tau(\kappa_s\nabla_\tau\langle u\rangle) - \kappa_s H[u] \quad \text{en } \Gamma,\\ \left\langle\kappa\frac{\partial u}{\partial n}\right\rangle &= -\frac{\kappa_s}{\eta}[u] \qquad\qquad\qquad\qquad \text{en } \Gamma.\end{aligned}$$

Finalmente, la última contribución es la realización de simulaciones complejas con el objetivo de avanzar un paso más hacia aplicaciones industriales que permitan mejorar el diseño de intercambiadores de calor, con un código que permita integrar las diferentes herramientas para un problema acoplado de ecuaciones multifísicas y no estándar. Al abordar estos problemas y dificultades técnicas, este trabajo pretende ampliar los límites de la optimización de formas que involucran capas delgadas y proporcionar conocimientos que conduzcan a soluciones de gestión térmica más eficientes energéticamente y sostenibles para diferentes aplicaciones.

Organización de la tesis

Capítulo 1: Análisis asintótico de un problema de difusión de tres materiales

En este capítulo preliminar, consideramos un marco simplificado de un modelo de difusión trifásica, con una capa delgada de espesor η entre los otros dos dominios. La convección puede añadirse, pero no desempeña ningún rol, ya que la velocidad es cero en la interfaz (condición de borde antideslizante).

Describimos cómo obtener un modelo asintótico, que contiene condiciones de transmisión efectivas de orden uno. Este es el modelo que consideraremos en lo sucesivo a lo largo de esta tesis. Para ello, utilizamos las herramientas clásicas en el desarrollo asintótico y terminamos proporcionando estimaciones de error.

Una pequeña parte de este capítulo se publicó como artículo en los proceedings Monografías Matemáticas "García de Galeano" [35]:

F. Caubet, C. Conca, M. Dambrine and R. Zelada. Shape optimization for heat exchangers with a thin layer. In *Sixteenth International Conference Zaragoza-Pau on Mathematics and its Applications*, volume 43 of Monogr. Mat. García Galdeano, pages 51–61. Prensas Univ. Zaragoza, Zaragoza, 2024.

Capítulo 2: Método de elementos finitos extendido de Nitsche para un problema de transmisión con discontinuidades en la interfaz

Este capítulo se centra en el análisis numérico del modelo asintótico obtenido del Capítulo 1. Por simplicidad despreciamos la parte convectiva, ya que la velocidad es nula en la interfaz y aquí nos centramos en las condiciones de transmisión no estándar. El objetivo de este capítulo es proponer un método estable y bien condicionado con respecto al parámetro de espesor η.

Comenzamos definiendo el marco variacional y luego consideramos la versión discontinua discreta de Galerkin. Observamos que un término explota cuando η es demasiado pequeño y que la matriz de rigidez está mal condicionada.

A continuación proponemos un método de elementos finitos de Nitsche ampliado. La formulación variacional discreta puede parecer extraña a primera vista, por lo que explicamos cómo obtenerla forzando la coercitividad para deducir las desigualdades que deben verificar algunos coeficientes. A continuación damos las estimaciones de error, que requieren de desigualdades inversas. Por último, discutimos el uso de algunos métodos iterativos, que no hemos explorado con demasiada profundidad y que podrían ser objeto de futuros trabajos para disponer de métodos rápidos, en particular para los casos de prueba de optimización de formas 3D como en el Capítulo 4.

La mayor parte del contenido de este capítulo está publicado en ESAIM: Mathematical Modelling and Numerical Analysis [30]:

D. Capatina, F. Caubet, M. Dambrine, and R. Zelada. Nitsche extended finite element method of a Ventcel transmission problem with discontinuities at the interface. ESAIM: Mathematical Modelling and Numerical Analysis, 59(2):999–1021, 2025.

Capítulo 3: Optimización de forma de un aislante térmico

Como primer paso hacia la optimización de forma de un intercambiador de calor de capa fina, en este capítulo estudiamos la optimización de forma de un aislante térmico en el que consideramos sólo un fluido y el material aislante (sólido), separados por una interfaz que es fija. Estamos interesados en la forma del aislante, más concretamente, en su frontera exterior.

Modelamos un aislante térmico utilizando un acoplamiento débil entre las ecuaciones de Navier-Stokes y el modelo asintótico del Capítulo 1, añadiendo una condición de borde de Robin en la frontera exterior. Estamos interesados en minimizar el aislamiento térmico fijando un cierto volumen para el material aislante. En primer lugar, mostramos la diferenciabilidad ya que se trata de un problema no estándar. En segundo lugar, calculamos las derivadas de forma para un caso de temperatura exterior determinista y variable aleatoria. Por último, realizamos algunos experimentos numéricos en 3D (véase un ejemplo en la Figura 8) para validar estas fórmulas mediante la aplicación de los métodos numéricos desarrollados en el Capítulo 2 para calcular las ecuaciones de convección-difusión y su adjunto.

La mayor parte del contenido de este capítulo es un artículo de revista en Journal of Optimization Theory and Applications [36]:

F. Caubet, C. Conca, M. Dambrine, and R. Zelada. How to Insulate a Pipe? Journal of Optimization Theory and Applications, 207(3):46, 2025.

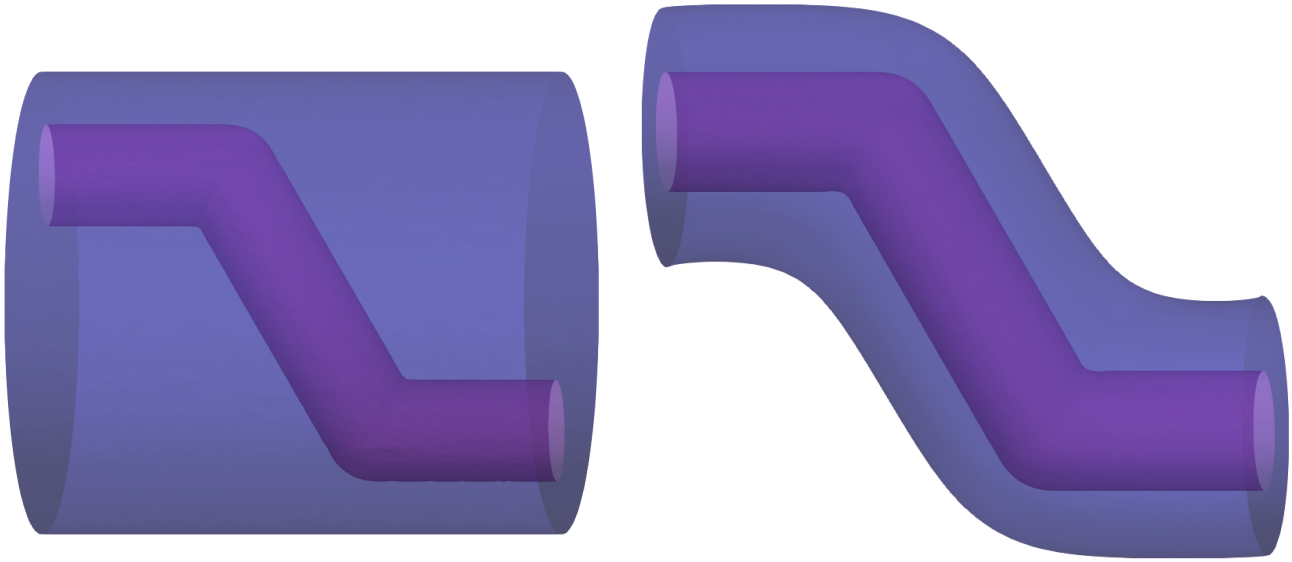

(a) Dominio inicial Ω. (b) Dominio final Ω.

Figure 2: Un ejemplo de los resultados obtenidos al optimizar la forma de un aislante térmico.

Capítulo 4: Optimización de forma de un intercambiador de calor con condiciones de transmisión de Ventcel

Este capítulo es el núcleo de esta tesis, donde utilizamos todas las herramientas desarrolladas en los capítulos anteriores. Consideramos un intercambiador de calor de dos fluidos en convección forzada, separados por una interfaz que es nuestra variable sujeta a optimización.

Lo modelamos a través de las ecuaciones de Navier-Stokes en estado estacionario y la ecuación asintótica de convección-difusión. Demostramos la diferenciabilidad y luego calculamos las derivadas de forma, obteniendo una expresión complicada debido a las condiciones de transmisión no estándar que implican saltos y al operador de Laplace-Beltrami en la interfaz. Realizamos algunas simulaciones numéricas 3D en un cluster (ver un ejemplo en la Figura 9), discutiendo el uso de los precondicionadores utilizados en la literatura existente para las diferentes físicas, en particular para las ecuaciones de Navier-Stokes en estado estacionario que es la parte más exigente. En cuanto a la resolución numérica de las ecuaciones de convección-difusión aproximadas, utilizamos el MEF discontinuo de Nitsche del Capítulo 2.

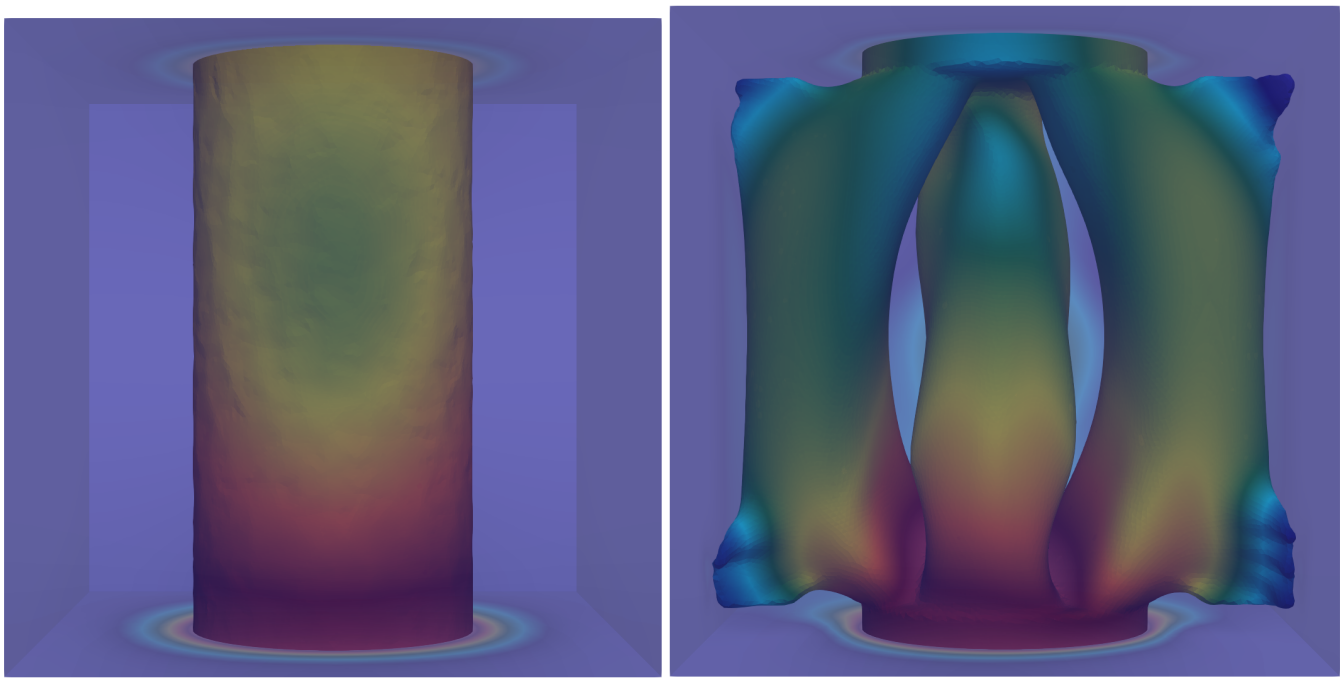

(a) Dominio inicial Ω.

(b) Dominio final Ω.

Figure 3: Un ejemplo de los resultados obtenidos al optimizar la forma de un intercambiador de calor.

La mayor parte del contenido de este capítulo está en proceso de revisión en la revista SIAM Journal on Scientific Computing:

F. Caubet, C. Conca, M. Dambrine and R. Zelada. Shape optimization with Ventcel transmission conditions: application to the design of a heat exchanger. *Under revisions in SIAM Journal on Scientific Computing.*

Apéndice A: Derivada de forma de Hadamard

En este apéndice, comenzamos recordando las principales nociones relacionadas con la optimización de forma, como la definición fundamental de la derivada de la forma en el sentido de Hadamard. A continuación, recordamos algunas fórmulas de integración útiles y explicamos cómo derivar una EDP mediante la derivada material y la derivada de forma. Además, explicamos las principales herramientas numéricas para resolver un problema de optimización de forma, en particular, la función de level-set, el método de redistancia, la advección de la interfaz y el remallado.

Introduction

Cette thèse s'inscrit dans deux domaines majeurs des mathématiques : l'analyse numérique des EDP et l'optimisation de forme et de topologie. Motivés par un problème réel d'échangeur de chaleur issu des travaux de nos collègues *Aldor et al.* du SIAME (Laboratoire des Sciences pour l'Ingénieur Appliquées à la Mécanique et au génie Electrique), qui ont proposé un nouvel échangeur de chaleur sinusoïdal [3], nous nous intéressons à la conception optimale d'un échangeur de chaleur. L'objectif est de considérer le cas d'un échangeur de chaleur à deux fluides en régime de convection forcée, dans le cas où les fluides sont séparés par une couche mince solide, comme sur la Figure 4. Ensuite, en abordant les défis posés par des conditions de transmission non standard, ce travail contribue à faire progresser les outils théoriques et numériques utilisés pour traiter les systèmes physiques couplés et l'optimisation de forme.

Nous commençons par proposer un modèle asymptotique qui prend en compte l'échange de chaleur dans la couche mince impliquant des conditions de transmission de type Ventcel à l'interface. Tout d'abord, la résolution numérique de ce modèle est étudiée, où nous développons et analysons une méthode d'éléments finis de type Nitsche qui est consistent, stable et nous fournissons des estimations d'erreur, validées à la fois théoriquement et numériquement. Ensuite, nous nous intéressons à un problème d'optimisation de forme motivé par l'isolation thermique : nous obtenons des dérivées de forme pour le problème de conception optimale consistant à minimiser le flux de chaleur à l'extérieur d'un tuyau entouré d'un isolant thermique de volume fixe, et nous mettons en place des simulations numériques à l'aide de la méthode des lignes de niveaux. Enfin, nous nous concentrons sur la conception d'échangeurs de chaleur fluide-fluide en 3D : pour maximiser l'échange de chaleur sous des contraintes de dissipation d'énergie et de volume, nous considérons un modèle couplé impliquant les équations de Navier-Stokes stationnaires et une équation de convection-diffusion avec des conditions de transmission de type Ventcel, nous analysons la sensibilité de la forme du système et nous fournissons des simulations numériques 3D.

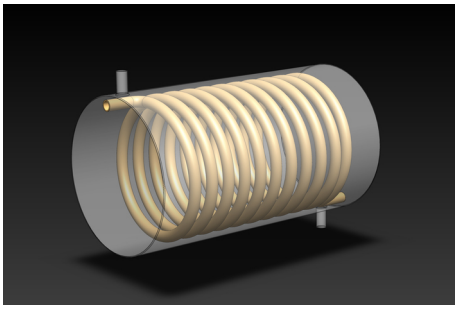

Figure 4: Échangeur de chaleur d'helice. Figure extraite de [88].

Contexte général de l'optimisation de forme et de topologie

Bien que l'optimisation de forme soit une technique mathématique ancienne, ce n'est qu'au cours des dernières décennies que ce domaine a fait l'objet d'une attention considérable, en raison du besoin de solutions plus efficaces et innovantes exigées par des industries comme dans le cadre de l'aérospatial [114, 103], des échangeurs de chaleur [76, 60, 67], du génie civil [19], de la photonique [77, 82], etc.

L'optimisation de forme consiste à modifier la géométrie en variant les frontières tout en conservant la même topologie. La réponse à ce problème est l'optimisation topologique qui, contrairement à l'optimisation de forme, permet de modifier la topologie. L'objectif de l'optimisation de forme et de topologie est d'améliorer les performances d'un système d'ingénierie par rapport à une quantité ou à un critère physique, comme la réduction de la dissipation d'énergie, la réduction du poids, la minimisation de la compliance, etc. Dans certains cas, la complexité de la conception finale a rendu sa fabrication difficile, voire impossible, mais l'avènement de la fabrication additive a encore élargi les possibilités d'optimisation de forme et de topologie.

D'une part, dans l'optimisation de forme, les deux principales méthodes sont la variation des frontières geométriques et l'approche des lignes de niveaux. D'autre part, l'optimisation topologique comprend la dérivée topologique, l'homogénéisation et les méthodes SIMP (Solid Isotropic Material with Penalization). Nous commençons par examiner brièvement ces deux approches ci-dessous.

Optimisation de forme

Pour résoudre un problème d'optimisation général, la stratégie habituelle consiste à utiliser un algorithme de descente de gradient. Il existe de nombreux algorithmes très bien étudiés, pour les cas avec ou sans contraintes, tels que la méthode du gradient, la méthode de Newton, BFGS, le gradient conjugué ou la programmation linéaire, voir [92]. Pour cela, nous devons fournir au moins la dérivée première (dans certains cas, même la dérivée seconde, comme dans la méthode de Newton). Dans l'optimisation de forme, puisque la variable est un domaine, il s'agit d'un problème d'optimisation de dimension infinie et la dérivée se fait par rapport au domaine. La première étape consiste donc à définir, dans un certain sens, le concept de *dérivée de forme*. Dans son ouvrage fondateur, Hadamard [69] a défini ce concept, qui, grosso modo, prend en compte les petites perturbations de la frontière. La dérivée de forme de Hadamard fournit le cadre théorique et, du point de vue numérique, nous disposons de différentes manières de changer la géométrie à chaque étape du processus d'optimisation.

La première approche, connue sous le nom de *optimisation de forme géométrique*, consiste à avoir une représentation explicite d'un domaine par un maillage et à utiliser les directions de descente pour déplacer les nœuds de ce maillage. Nous renvoyons à [13] pour une mise en œuvre pratique dans le contexte de l'optimisation structurelle ou, plus récemment, à l'article pédagogique de Dapogny *et al.* [50] dans le contexte de la mécanique des fluides, tous les deux utilisant le logiciel libre d'éléments finis FreeFem++. Le principal inconvénient de cette méthode est que le processus de déplacement des sommets peut produire des triangles dégénérés (se chevauchant ou non conformes), ce qui affecte la qualité du maillage. Un autre problème est qu'elle maintient

la même connectivité, il est donc logique de l'utiliser lorsque nous avons une idée a priori de la solution.

Une deuxième approche est basée sur la *méthode des lignes de niveaux*. Cette méthode a été développée par Osher et Sethian dans [95], conçue à l'origine pour suivre l'évolution de fronts ou d'interfaces en mouvement, tels que des courbes ou des surfaces. Il s'est avéré très utile dans plusieurs domaines, tels que la segmentation d'images, la vision par ordinateur, les problèmes d'interaction fluides-structures et, ce qui nous intéresse, l'optimisation des formes et des topologies. En introduisant un domaine de calcul fixe qui contient le domaine d'intérêt original, la fonction des lignes de niveaux permet à la frontière d'être implicitement représentée par le niveau zéro de la fonction. Cette fonction est particulièrement utile pour l'optimisation de forme, qui permet d'obtenir des changements topologiques. Initialement, la fonction des lignes de niveaux a été considérée dans un maillage fixe [12, 111]. Cette méthode présente toutefois un inconvénient. Comme le maillage est fixe et que l'évolution est implicitement suivie par la fonction de lignes de niveaux, les équations aux dérivées partielles considérées ne peuvent pas être résolues directement. Une solution généralement envisagée dans les problèmes d'optimisation de forme consiste à introduire un matériau fictif à remplir entre le domaine de calcul et le domaine d'intérêt, ce qui permet de résoudre ces équations approchées.

Aujourd'hui, l'approche moderne est connue sous le nom de *méthode de déformation du maillage par lignes de niveaux*, introduite par Allaire, *et al.* dans [10]. L'idée principale est d'avoir deux représentations différentes de la géométrie, chacune ayant un objectif différent. Plus précisément, nous utilisons la fonction des lignes de niveaux comme précédemment pour gérer les déformations de la géométrie (changements topologiques possibles) et, à chaque étape d'optimisation, nous remaillons selon le niveau zéro, puis le maillage du domaine peut être utilisé pour résoudre les équations aux dérivées partielles considérées.

Optimisation topologique

La liste des méthodes d'optimisation topologique est assez longue. Nous nous limiterons à une brève description des méthodes les plus couramment utilisées, en particulier dans les applications liées aux échangeurs de chaleur.

Premièrement, en plus de la dérivée de forme, il existe la *dérivée topologique* [93, 94, 14], basée sur des développements asymptotiques, qui vise à créer de petits trous dans le domaine ou à y ajouter de petites bulles en fonction du contexte étudié.

Deuxièmement il existe un autre type de méthode : les méthodes dites *méthodes de densité*, dans lesquelles nous avons la *méthode d'homogénéisation* (voir [90, 100, 43, 105] pour une introduction générale à la théorie mathématique de l'homogénéisation et [6, 41] dans le contexte de l'optimisation de forme et de topologie) et la méthode *SIMP* (Solid Isotropic Material with Penalty) (voir [22, 62]). Ces deux méthodes reposent sur une fonction de densité qui se rapproche de la fonction caractéristique, qui est égale à 1 à l'intérieur du domaine variable et à 0 à l'extérieur. Cela signifie que le problème d'optimisation de forme/topologique est relaxé, en acceptant les structures composites comme admissibles. Alors que la méthode d'homogénéisation préconise la caractérisation des propriétés de la microstructure (ce qui n'est pas une tâche facile), la méthode SIMP les approxime en termes de densité par certaines heuristiques (généralement sous la forme d'un

polynôme de la densité). Le principal inconvénient est que nous obtenons une densité continue que nous devons pénaliser pour obtenir une structure binaire.

Optimisation de forme et de topologie des échangeurs de chaleur

Comme mentionné précédemment, l'un des objectifs de cette thèse est de se concentrer sur la conception d'échangeurs de chaleur. Le problème des échangeurs de chaleur est multi-physique (impliquant la température et l'écoulement des fluides, décrits par les équations de convection-diffusion et de Navier-Stokes, respectivement) et inclut également une contrainte d'épaisseur minimale, garantissant que les fluides ne se mélangent pas, ce qui joue un rôle clé dans ce problème.

Dans la communauté de l'optimisation de forme et de topologie, le problème de l'échangeur de chaleur a été abordé en utilisant les différents outils que nous avons décrits ci-dessus, principalement la méthode SIMP et la méthode de déformation de maillage par lignes de niveaux combinée avec la dérivée d'Hadamard. Les premiers travaux dont nous avons trouvé trace ont été réalisés en 2009, en considérant un seul fluide [51, 52, 112]. Le cas de deux fluides a été traité dans la thèse de master de Papazoglou en 2015 [97], puis suivi par [76, 81]. Comme nous l'avons souligné, le principal inconvénient de la méthode SIMP est la manière d'obtenir la structure binaire en introduisant une pénalisation adéquate qui prend encore plus d'importance dans ce problème multi-physique, avec une géométrie complexe et où la contrainte de distance n'est pas triviale à prendre en compte. C'est pourquoi la méthode de déformation du maillage par lignes de niveaux semble plus adaptée à ce problème : c'est l'approche récemment suivie en 2021 dans la thèse de Feppon [67]. Notons que la méthode SIMP est actuellement préférée par une plus grande communauté d'ingénieurs, malgré les problèmes que nous avons expliqués car la méthode de déformation des maillages par lignes de niveaux avec dérivée de Hadamard a été récemment proposée.

Objectif et principales difficultés

Dans cette thèse, l'objectif principal est d'optimiser un échangeur de chaleur en tenant compte de la couche mince séparant les deux fluides, comme cela se produit généralement dans les applications réelles. Plusieurs difficultés techniques apparaissent dans le processus, que nous expliquons ci-dessous.

Conditions de transmission non standard de Ventcel

Pour mieux comprendre ces difficultés, nous avons besoin d'expliciter les conditions de transmission effectives. Nous expliquerons formellement ces conditions de transmission (les détails rigoureux et les résultats de convergence sont donnés dans le chapitre 1. Soit $\eta > 0$ un petit paramètre. Nous commençons par considérer $\Omega^\eta \subset \mathbb{R}^d$, divisé en trois sous-domaines $\Omega_1^\eta, \Omega_s^\eta, \Omega_2^\eta$, où la partie solide Ω_s^η sépare les domaines contenant les fluides Ω_1^η et Ω_2^η. Le paramètre η représente l'épaisseur du solide Ω_s^η (qui modélise la paroi du tuyau contenant le fluide caloporteur). L'interface entre Ω_i^η et Ω_s^η est appelée $\Gamma_i^\eta := \partial\Omega_i^\eta \cap \partial\Omega_s^\eta$, $i = 1, 2$. Par simplicité dans cette introduction, nous

ne considérons que les conditions aux limites de Dirichlet sur le bord $\partial\Omega^\eta =: \Gamma^\eta_{\mathrm{D}}$, et on définit $\Gamma^\eta_{\mathrm{D},i} := \partial\Omega^\eta_i \setminus \Gamma^\eta_i$ la partie de Dirichlet de Ω^η_i, $i = 1, 2$, et $\Gamma^\eta_{\mathrm{D},s} := \partial\Omega^\eta_i \setminus (\Gamma^\eta_1 \cup \Gamma^\eta_2)$ la partie de Dirichlet de Ω^η_s. Nous supposons que $\Gamma^\eta_{\mathrm{D},i}$ touche Γ^η_i, $i = 1, 2$.

Soit $\kappa_1, \kappa_2, \kappa_s$ trois nombres réels positifs (diffusivités thermiques). Nous considérons alors u^η la solution de l'équation de convection-diffusion dans Ω^η, avec des restrictions $u^\eta_i := u^\eta_{\Omega^\eta_i}$, $i = 1, 2, s$, des conditions de transmission continue sur les interfaces Γ^η_i, $i = 1, 2$ et des conditions aux limites homogènes de Dirichlet sur $\Gamma^\eta_{\mathrm{D,i}}$, $i = 1, 2, s$:

$$\left\{\begin{array}{rll} -\operatorname{div}(\kappa_i \nabla u^\eta_i) &= f|_{\Omega^\eta_i} & \text{dans } \Omega^\eta_i, i = 1, 2, \\ -\operatorname{div}(\kappa_s \nabla u^\eta_s) &= f|_{\Omega^\eta_s} & \text{dans } \Omega^\eta_s, \\ u^\eta_i &= 0 & \text{sur } \Gamma^\eta_{\mathrm{D,i}}, i = 1, 2, s, \\ u^\eta_s &= u^\eta_i & \text{sur } \Gamma^\eta_i, i = 1, 2, \\ \kappa_s \dfrac{\partial u^\eta_s}{\partial n} &= \kappa_i \dfrac{\partial u^\eta_i}{\partial n} & \text{sur } \Gamma^\eta_i, i = 1, 2, \end{array}\right. \tag{3}$$

où $\boldsymbol{n}$ est la normale unitaire à Γ^η_i pointant vers Ω^η_2 et $f \in \mathrm{L}^2(\Omega^\eta)$ tel que $f = 0$ dans Ω^η_s.

Comme Ω^η_s est trop mince, nous ne voulons pas le mailler directement, car il ne serait trop coûteux d'utiliser un maillage aussi raffiné pour résoudre numériquement (en particulier en 3D) les problèmes aux limites. Une technique efficace pour traiter ce type de problème est celle des modèles asymptotiques, comme dans les travaux d'Enquist et Nedelec [58] ou plus récemment dans [110, 16]. Un modèle asymptotique similaire (trois matériaux avec une couche mince au milieu) a été obtenu dans [40] en considérant une physique différente.

L'idée est de passer à la limite sur η dans la géométrie, en obtenant $\Omega_1 \cup \Omega_2$, indépendant de η et sans couche mince, où Ω_i est la limite de Ω^η_i lorsque $\eta \to 0$. Soit $\Gamma := \partial\Omega_1 \cap \partial\Omega_2$ l'interface entre Ω_1 et Ω_2. On définit également $\Gamma_{\mathrm{D,i}} := \partial\Omega_i \setminus \Gamma$.

Une première approche consiste à négliger complètement l'effet du solide, c'est-à-dire à ne pas prendre en compte la diffusion dans Ω^η_s, ce qui conduit au modèle d'ordre zéro :

$$\left\{\begin{array}{rll} -\operatorname{div}(\kappa_i \nabla u^0_i) &= f|_{\Omega_i} & \text{dans } \Omega_i, i = 1, 2, \\ u^0_i &= 0 & \text{sur } \Gamma_{\mathrm{D,i}}, i = 1, 2, \\ u^0_1 &= u^0_2 & \text{sur } \Gamma, \\ \kappa_1 \dfrac{\partial u^0_1}{\partial n} &= \kappa_2 \dfrac{\partial u^0_2}{\partial n} & \text{sur } \Gamma, \end{array}\right.$$

où u^0 est la solution associée du modèle d'ordre zéro, avec les restrictions u^0_1 et u^0_2 à Ω_1 et Ω_2, respectivement. En gros, cela signifie que Ω^η_s est si mince que l'on peut supposer que la température u^η_s est constante suivant la direction normale $\boldsymbol{n}$ dans Ω^η_s.

Nous proposeons un modèle plus complexe où la température n'est plus supposée constante dans la couche mince. Il s'agit d'un modèle d'ordre un, qui prend en compte l'effet de diffusion

dans Ω_s^η en utilisant des conditions de transmission de Ventcel :

$$\begin{cases} -\operatorname{div}(\kappa_i \nabla u_i^1) &= f|_{\Omega_i} & \text{dans } \Omega_i, i=1,2, \\ u_i^1 &= 0 & \text{sur } \Gamma_{\mathrm{D,i}}, i=1,2, \\ \left\langle \kappa \dfrac{\partial u^1}{\partial n} \right\rangle &= -\dfrac{\kappa_s}{\eta}[u^1] & \text{sur } \Gamma, \\ \left[\kappa \dfrac{\partial u^1}{\partial n} \right] &= \eta \operatorname{div}_\tau(\kappa_s \nabla_\tau \left\langle u^1 \right\rangle) - \kappa_s H[u^1] & \text{sur } \Gamma, \end{cases} \tag{4}$$

où u^1 est la solution associée du modèle d'ordre un, avec les restrictions u_1^1 et u_2^1 à Ω_1 et Ω_2, respectivement, div_τ est la divergence tangentielle, ∇_τ est le gradient tangentiel, H est la courbure moyenne de Γ et $[\cdot]$, $\langle\cdot\rangle$ désignent le saut et la moyenne à Γ, définis pour toute fonction lisse définie dans Ω avec des restrictions $\phi_i := \phi|_{\Omega_i}$ dans Ω_i comme :

$$[\phi] := \phi_1 - \phi_2 \quad \text{et} \quad \langle \phi \rangle := \frac{1}{2}(\phi_1 + \phi_2) \text{ sur } \Gamma.$$

Ici et dans la suite, nous n'utiliserons plus l'exposant ^{1} pour désigner le modèle d'ordre un, de sorte que nous appelons u la solution du modèle asymptotique. Le modèle d'ordre un avec *conditions de transmission non standard de Ventcel* (4) est le modèle que nous considérerons tout au long de cette thèse. En gros, cela signifie que Ω_s^η est trop mince, que la température u_s^η est linéaire suivant la direction normale $\boldsymbol{n}$ dans Ω_s^η. Notez que l'effet de diffusion de volume $\operatorname{div}(\kappa_s \nabla u_s^\eta)$ dans Ω_s^η apparaît clairement comme $\operatorname{div}_\tau(\kappa_s \nabla_\tau \langle u \rangle)$ sur Γ, dans le modèle asymptotique: c'est devenu une diffusion surfacique.

Résolution numérique du problème de la transmission

Il est important de noter que la résolution numérique du modèle asymptotique précédent (4) présente plusieurs difficultés.

- Les conditions de transmission non classiques modifient la nature du problème. La solution du modèle exact u^η appartient à $\mathrm{H}^1(\Omega^\eta)$, tandis que la solution du modèle asymptotique n'est pas globalement H^1, car il y a un saut sur Γ dans les conditions de transmission (4). Le problème est posé dans ce que l'on appelle un *espace de Sobolev brisé*

$$\mathcal{H}^1(\Omega_1, \Omega_2) := \{\phi = (\phi_1, \phi_2) \in \mathrm{H}^1(\Omega_1) \times \mathrm{H}^1(\Omega_2);\ \langle \phi \rangle \in \mathrm{H}^1(\Gamma)\}.$$

- L'implémentation discrète de l'espace de Sobolev brisé $\mathcal{H}^1(\Omega_1, \Omega_2)$ n'est pas simple et n'est pas disponible dans les logiciels d'éléments finis de libre acces (voir [9] pour plus de détails sur ce problème).

- Bien que nous puissions coder une méthode Galerkin discontinue en doublant seulement les degrés de liberté à l'interface (où il y a des discontinuités), si η est trop petit, la matrice de rigidité associée au modèle asymptotique est mal conditionnée, à cause du terme $-\frac{\kappa_s}{\eta}[u]$ qui explose lorsque $\eta \to 0$. Notons qu'il est raisonnable de prendre de petites valeurs de η pour nos expériences numériques, puisque η est le paramètre du développement asymptotique.

Nous avons besoin d'une méthode d'éléments finis qui soit stable et bien conditionnée par rapport à η pour calculer le champ de température. Pour cela, nous introduisons une nouvelle formulation à la Nitsche que nous étudions. Nous montrons que cette formulation répond à notre cahier des charges (voir le chapitre 2 pour les détails).

Analyse de sensibilité de la forme

Pour revenir au problème de conception optimale, nous devons calculer les dérivées de forme des équations impliquées : dans nos applications, nous considérons un problème multi-physique relaint la thermique à un écoulement de fluides. Nous considérons un couplage faible entre les équations de Navier-Stokes et les équations approchées/asymptotiques de convection-diffusion. Comme nous l'avons déjà souligné, des dérivées similaires ont été obtenues dans [63] lorsque la partie solide Ω_s^η n'est pas une couche mince.

En ce qui concerne les équations considérées dans cette thèse, la difficulté supplémentaire par rapport à [63] est la condition de transmission non-standard avec Ventcel. Plus précisément, la dérivée de forme appartient à un espace de Sobolev brisé et la dérivation des dérivées tangentielles (comme ∇_τ) sur la surface est beaucoup plus compliquée que celle des dérivées usuelles dans le volume ∇ dans Ω, en raison de la dépendance de la normale unitaire $\boldsymbol{n}$ à Γ, qui change en même temps que Γ. La difficulté n'est pas de calculer la dérivée de forme de l'opérateur de Laplace-Beltrami : elle est bien connue dans la littérature, voir par exemple [54, 39, 46] dans un contexte simplifié. La vraie difficulté vient du fait que ces dérivées de surface sont impliquées dans une condition de saut sur une interface et sont couplées avec des discontinuités de coefficient. Nous avons aussi la courbure moyenne H, dont la dérivée de forme nécessite un traitement délicat d'un point de vue numérique. Ces questions sont traitées progressivement dans les chapitres 3 et 4.

Résolution numérique de problèmes à grande échelle et difficultés liées au HPC

Enfin, nous nous intéressons aux applications réelles, c'est-à-dire aux simulations numériques en 3D, qui sont coûteuses en termes de calcul, et pour lesquelles nous rassemblerons tous les outils précédents. Au moins une centaine d'itérations sont nécessaires pour atteindre la convergence de l'algorithme d'optimisation. À chaque itération, nous devons résoudre les équations de Navier-Stokes, les équations approchées de convection-diffusion et les adjoints, déduire une direction de descente et ensuite remailler. En particulier, les équations de Navier-Stokes sont la partie la plus coûteuse, car elles comportent des millions de degrés de liberté dans nos cas de test à grande échelle. Cela ne peut être fait sans parallélisme et avec factorisation LU standard, tout d'abord en raison de la mémoire nécessaire. De plus, elle doit être raisonnablement rapide, ce qui nécessite des préconditionneurs adéquats pour accélérer la résolution du système linéaire.

Contributions principales

Cette recherche explore et étend l'application des techniques d'optimisation de forme et de topologie à la conception d'échangeurs de chaleur à couche mince. L'objectif est de développer des modèles plus réalistes qui aboutissent à des solutions réalisables. Les contributions de ce travail concernent deux domaines principaux : l'analyse numérique et l'optimisation de forme.

Basée sur la méthode de Nitsche [91], la méthode de Nitsche pour les conditions aux limites générales [79], et la méthode des éléments finis étendue de Nitsche [70], cette thèse propose une méthode Nitsche modifiée pour résoudre un problème de convection-diffusion non standard. La méthode est conçue pour améliorer le conditionnement de la matrice de rigidité associée aux problèmes de convection-diffusion avec des conditions de transmission non standard. Les principales caractéristiques de la méthode proposée sont la robustesse par rapport à l'épaisseur de la couche tout en restant consistent, stable, et indépendant par rapport aux coefficients de diffusivité. Ce développement fournit un cadre numérique efficace pour traiter les discontinuités et les conditions de transmission complexes dans les problèmes de convection-diffusion.

Ensuite, un nouveau modèle d'optimisation des isolants thermiques est proposé. Ce modèle est plus réaliste que la littérature existante sur l'optimisation de forme des isolants thermiques, comme [27, 28, 108]. En effet, notre modèle tient compte des effets de diffusion à l'interface du domaine solide mince, en utilisant des conditions de transmission de type Ventcel, ce qui le rend plus réaliste pour les applications pratiques. Ce modèle incorpore également un couplage faible entre les équations de Navier-Stokes (décrivant la dynamique des fluides) et l'équation de convection-diffusion (décrivant le transfert de chaleur). Ici, le domaine des fluides est fixe et seulement le matériau isolant est optimisé. Nous considérons le problème d'optimisation de forme qui vise à minimiser le flux de chaleur à l'extérieur d'un isolant de volume donné : nous caractérisons la dérivée de forme de la fonctionnelle objectif et réalisons des simulations numériques 3D en utilisant la méthode de déformation de maillage par lignes des niveaux.

Nous considérons alors notre objectif initial en introduisant un nouveau modèle pour les échangeurs de chaleur 3D fluide-fluide en convection forcée, où la couche mince solide est représentée par des conditions de transmission non standard. Ici encore, ces conditions tiennent compte des effets de diffusion sur l'interface par l'intermédiaire de l'opérateur de Laplace-Beltrami. L'objectif est d'optimiser la forme du tuyau contenant le fluide caloporteur. Dans ce problème, les conditions de transmission de Ventcel sont imposées sur la frontière que l'on cherche à optimiser. Nous effectuons donc une analyse de sensibilité à la forme et calculons les dérivées de forme associées. À notre connaissance, ces dérivées de forme n'ont jamais été calculées auparavant et ont des expressions compliquées. Les résultats obtenus peuvent être considérés comme un complément à des travaux antérieurs tels que ceux de Feppon [63, 67]. En effet, notre modèle inclut la diffusion de surface à l'interface, alors que les travaux précédents supposaient une diffusion de volume à l'intérieur du solide. En outre, nous soulignons que l'analyse de la sensibilité de la forme pour les problèmes de transmission avec des coefficients de diffusivité discontinus mérite une attention et un soin particuliers. Mentionnons les travaux [74, 96, 1] où l'on considère l'équation de la chaleur dans un problème de transmission avec des coefficients de diffusivité discontinus. Il est important de remarquer que la dérivée de forme doit être calculée avec précaution dans ce cas, en raison de la méthode rapide de Cea qui peut conduire à des erreurs dans la formule de la dérivée de forme soit le problème adjoint comme il a été souligné dans [96]. Dans cette thèse, une dérivation

rigoureuse des dérivées de forme est effectuée en utilisant d'abord les dérivées matérielles, en suivant la méthodologie dans [1]. Notre travail peut être considéré comme une extension de [9], où ils ont considéré l'équation de diffusion avec une solution discontinue à l'interface et le flux normal est continu et proportionnel au saut de la solution, plus précisément (avec notre notation) :

$$\begin{aligned} \left[\kappa \frac{\partial u}{\partial n}\right] &= 0 && \text{sur } \Gamma, \\ \left\langle \kappa \frac{\partial u}{\partial n} \right\rangle &= -\kappa_s [u] && \text{sur } \Gamma, \end{aligned}$$

qui modélisent des interfaces imparfaites pour la fabrication additive. Dans notre cas de transmission par diffusion à l'interface, nous avons des conditions de transmission beaucoup plus compliquées à différencier, car le flux normal n'est pas continu et dépend de l'opérateur de Laplace-Beltrami :

$$\begin{aligned} \left[\kappa \frac{\partial u}{\partial n}\right] &= \eta \operatorname{div}_\tau(\kappa_s \nabla_\tau \langle u \rangle) - \kappa_s H[u] && \text{sur } \Gamma, \\ \left\langle \kappa \frac{\partial u}{\partial n} \right\rangle &= -\frac{\kappa_s}{\eta}[u] && \text{sur } \Gamma. \end{aligned}$$

Une dernière contribution est la réalisation de simulations complexes dans le but de progresser vers des applications industrielles qui permettent d'améliorer la conception des échangeurs de chaleur, avec un code qui permet d'intégrer les différents outils pour un problème couplé d'équations multi-physiques et non-standard, dans l'espoir de repousser les limites de l'optimisation de forme avec des couches minces et de fournir des informations qui conduiront à des solutions de gestion thermique plus efficaces sur le plan énergétique et plus durables pour différentes applications.

Organisation de la thèse

Chapitre 1 : Analyse asymptotique pour un problème de diffusion à trois phases

Dans ce chapitre préliminaire, nous considérons un cadre simplifié d'un modèle de diffusion triphasique, avec une couche mince d'épaisseur η entre les deux autres domaines. La convection peut être ajoutée, mais elle ne joue aucun rôle, puisque la vitesse est nulle à l'interface (condition limite de non-glissement).

Nous décrivons comment obtenir un modèle asymptotique, contenant des conditions de transmission effectives d'ordre un. C'est ce modèle que nous considérerons par la suite tout au long de cette thèse. Pour ce faire, nous utilisons les outils classiques du développement asymptotique et nous terminons en fournissant des estimations d'erreur.

Une partie de ce chapitre a été publiée en tant qu'article dans les actes de Monografías Matemáticas "García de Galeano" [35]:

F. Caubet, C. Conca, M. Dambrine and R. Zelada. Shape optimization for heat exchangers with a thin layer. In *Sixteenth International Conference Zaragoza-Pau on Mathematics and its*

Applications, volume 43 of Monogr. Mat. García Galdeano, pages 51–61. Prensas Univ. Zaragoza, Zaragoza, 2024.

Chapitre 2 : Méthode des éléments finis étendue de Nitsche pour un problème de transmission Ventcel avec discontinuités à l'interface

Ce chapitre se concentre sur l'analyse numérique du modèle asymptotique obtenu au chapitre 1. Par souci de simplicité, nous négligeons la partie convective, puisque la vitesse est nulle à l'interface, et nous nous concentrons ici sur les conditions de transmission non standard. Le but de ce chapitre est de proposer une méthode stable et bien conditionnée par rapport à η.

Nous commençons par définir le cadre variationnel et considérons ensuite la version discontinue de Galerkin. Nous notons qu'un terme explose lorsque η est trop petit et que la matrice de rigidité est mal conditionnée. Nous proposons ensuite une méthode d'éléments finis de Nitsche étendue. La formulation variationnelle discrète peut sembler étrange à première vue, donc nous expliquons comment l'obtenir en appliquant la coercivité pour déduire les inégalités qui doivent vérifier certains coefficients. Nous donnons ensuite les estimations d'erreur, qui nécessitent quelques inégalités inverses. Enfin, nous discutons de l'utilisation de certains solveurs itératifs, que nous n'avons pas explorés trop en profondeur et qui pourraient faire l'objet de travaux futurs afin d'avoir des méthodes rapides, en particulier pour les cas tests d'optimisation de forme 3D comme dans le chapitre 4.

La majeure partie du contenu de ce chapitre est un article scientifique ESAIM: Mathematical Modelling and Numerical Analysis [30]:

D. Capatina, F. Caubet, M. Dambrine, and R. Zelada. Nitsche extended finite element method of a Ventcel transmission problem with discontinuities at the interface. ESAIM: Mathematical Modelling and Numerical Analysis, 59(2):999–1021, 2025.

Chapitre 3 : Optimisation de forme d'un isolant thermique

Comme première étape vers l'optimisation de forme d'un échangeur de chaleur à couche mince, nous étudions dans ce chapitre l'optimisation de forme d'un isolant de chaleur où nous considérons un seul fluide et le matériau (solide) de l'isolant, séparés par une interface qui est fixe. Nous nous intéressons à la forme de l'isolant, plus précisément à la position de sa frontière extérieure.

Nous modélisons un isolant thermique en utilisant un couplage faible entre les équations de Navier-Stokes et le modèle asymptotique du chapitre 1, en ajoutant une condition limite de Robin à la frontière extérieure. Nous nous intéressons à la minimisation de l'isolation thermique tout en fixant un certain volume pour le matériau isolant. Tout d'abord, nous montrons la différentiabilité puisqu'il s'agit d'un problème non standard. Ensuite, nous calculons les dérivées de forme pour un cas de température extérieure déterministe et aléatoire. Enfin, nous réalisons des expériences numériques en 3D (voir Figure 5 pour un exemple) pour valider ces formules en appliquant les méthodes numériques développées au chapitre 2 pour calculer les équations de convection-diffusion et ses équations adjointes.

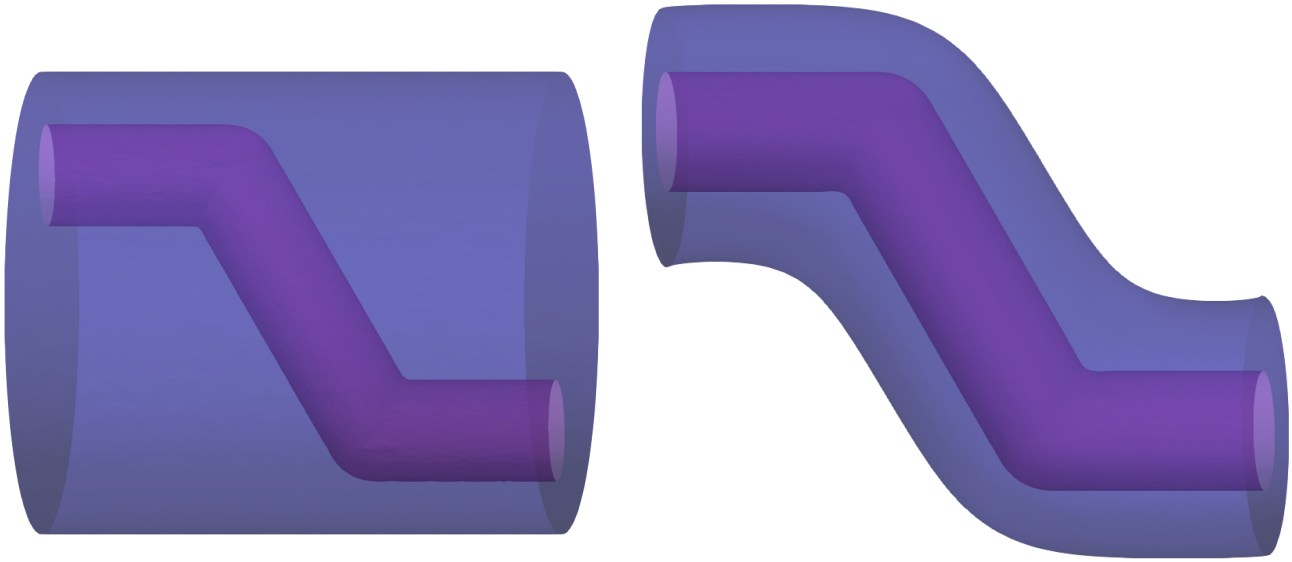

(a) Domaine initial Ω. (b) Domaine final Ω.

Figure 5: Exemple de résultats obtenus pour l'optimisation de la forme d'un isolant thermique.

La majeure partie du contenu de ce chapitre est publié dans un journal scientifique Journal of Optimization Theory and Applications [36]:

F. Caubet, C. Conca, M. Dambrine, and R. Zelada. How to Insulate a Pipe? Journal of Optimization Theory and Applications, 207(3):46, 2025.

Chapitre 4 : Optimisation de forme d'un échangeur de chaleur avec des conditions de transmission Ventcel

Ce chapitre est le cœur de cette thèse, où nous utilisons tous les outils développés dans les chapitres précédents. Nous considérons un échangeur de chaleur à deux fluides en convection forcée, séparé par une interface qui est notre variable soumise à l'optimisation.

Nous le modélisons avec les équations de Navier-Stokes stationnaires et l'équation asymptotique de convection-diffusion. Nous prouvons la différentiabilité et nous calculons ensuite les dérivées de forme, en obtenant une expression compliquée en raison des conditions de transmission non standard impliquant des sauts et l'opérateur Laplace-Beltrami à l'interface. Nous effectuons quelques simulations numériques 3D sur un cluster (voir Figure 6 pour un exemple), en discutant de l'utilisation des préconditionneurs utilisés dans la littérature existante pour les différentes physiques, en particulier pour les équations de Navier-Stokes stationnaires qui sont la partie la plus exigeante. En ce qui concerne la résolution numérique des équations approchées de convection-diffusion, nous utilisons la méthode des élements finis étendue de Nitsche du chapitre 2.

La majeure partie du contenu de ce chapitre est en cours de révision dans la revue SIAM Journal on Scientific Computing:

F. Caubet, C. Conca, M. Dambrine and R. Zelada. Shape optimization with Ventcel transmission

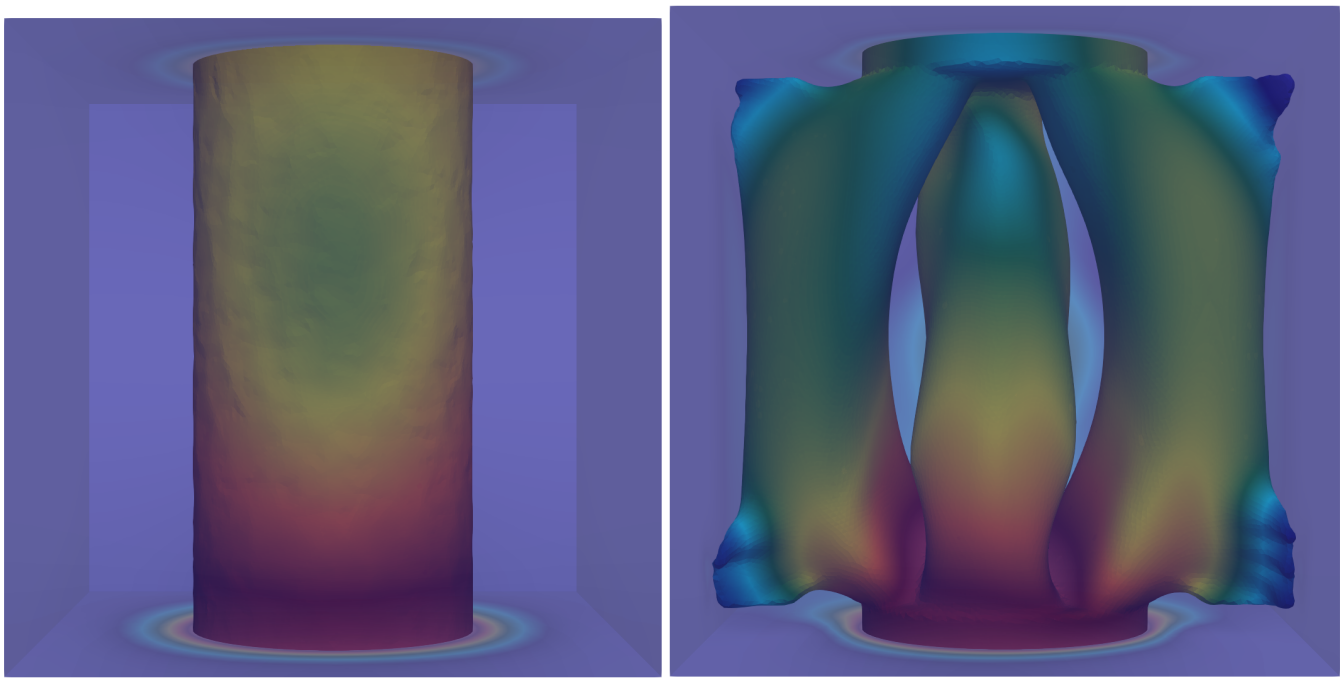

(a) Domaine initial Ω. (b) Domaine final Ω.

Figure 6: Domaine Ω.

conditions: application to the design of a heat exchanger. *Under revisions in SIAM Journal on Scientific Computing*.

Annexe A : Dérivée de forme d'Hadamard

Dans cette annexe, nous commençons par rappeler les principales notions liées à l'optimisation de forme, comme la définition fondamentale de la dérivée de forme au sens de Hadamard. Enseuite, nous donnons quelques formules d'intégration utiles et nous expliquons comment dériver une EDP en utilisant la dérivée matérielle et la dérivée de forme. En outre, nous expliquons les principaux outils numériques permettant de résoudre un problème d'optimisation de forme, en particulier, la fonction de lignes de niveau, la méthode de redistantiation, l'advection de l'interface et le remaillage.

Introduction

This thesis falls within two major areas of mathematics: numerical analysis of PDEs and shape/ topology optimization. Motivated by a real-life heat exchanger problem arising from the work of our colleagues *Aldor et al.* at SIAME (Laboratoire des Sciences pour l'Ingénieur Appliquées à la Mécanique et au génie Electrique), who have proposed a novel sinusoidal heat exchanger [3], we are interested in the optimal design of a heat exchanger. The aim is to consider the case of a two-fluid heat exchanger in a forced convection regime, in the case where the fluids are separated by a thin solid layer, as in Figure 7. Then, by addressing challenges arising from non-standard transmission conditions, this work contributes to advancing the theoretical and numerical tools used to tackle coupled physical systems and shape optimization.

We begin by proposing an asymptotic model that takes into account heat exchange in the thin solid layer involving Ventcel-type transmission conditions at the interface. Firstly, the numerical resolution of this model is studied and we develop and analyze a Nitsche-type finite element method providing consistency, stability, and error estimates, validated both theoretically and numerically. Secondly, we turn to a shape optimization problem motivated by thermal insulation: we compute shape derivatives for the optimal design problem of minimizing the heat flux outside a pipe surrounded by a thermal insulation of fixed volume, and we implement numerical simulations using the level set method. Finally, we focus on the design of 3D fluid-to-fluid heat exchangers: to maximize heat exchange under energy dissipation and volume constraints, we consider a coupled model involving steady-state Navier-Stokes equations and a convection-diffusion equation with Ventcel-type transmission conditions, analyze the shape sensitivity of the system, and provide 3D numerical simulations.

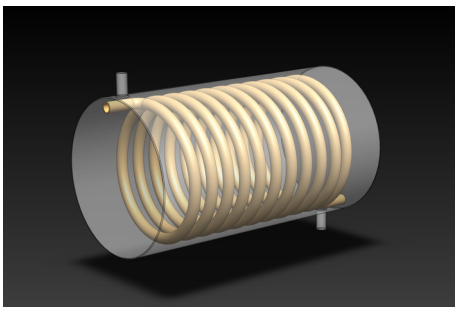

Figure 7: Helicoidal heat exchanger. Figure extracted from [88].

General context of shape and topology optimization

Although shape optimization is an old mathematical technique dating back to 1908 by Jacques Hadamard [69], it is only in the last few decades that this field has received considerable attention, due to the need for more efficient and innovative solutions demanded by industries such as aerospace [114, 103], heat exchangers [76, 60, 67], civil engineering [19], photonics [77, 82], etc.

Shape optimization is about changing the geometry by moving the boundaries while keeping the topology the same. This makes the final design very dependent on the initial domain, and the answer to this problem is called topology optimization, which, unlike shape optimization, allows topology changes. The goal of both shape and topology optimization is to improve the performance of an engineering system with respect to some physical quantity or criterion, such as reducing power dissipation, reducing weight, minimizing compliance, etc., often resulting in designs that are counter-intuitive to traditional engineering methods. In some cases, the complexity of the final design has made it difficult or impossible to manufacture, but the advent of additive manufacturing has further expanded the capabilities of both shape and topology optimization.

On the one hand, in shape optimization, the two main methods are geometric boundary variation and the level set approach. On the other hand, topology optimization includes the topological derivative, homogenization, and SIMP (Solid Isotropic Material with Penalization) methods. We begin by briefly discussing these two approaches below.

Shape optimization

To solve a general optimization problem, the usual strategy is to use a descent algorithm. There are many very well-studied algorithms, for both constrained or unconstrained cases, such as the gradient method, Newton's method, BFGS, conjugate gradient or linear programming, see [92]. For this, we need to provide at least the first derivative (in some cases even the second derivative as in Newton's method). Shape optimization is an infinite dimensional optimization problem where the variable is a domain, and the derivative is with respect to the domain. The first step, then, is to define, in some sense, the concept of *shape derivative*. In his seminal work, Hadamard [69] defined this concept, which roughly speaking takes into account small perturbations of the boundary. Hadamard's shape derivative provides the theoretical framework and, from the numerical point of view, we have different ways of updating the geometry at each step of the optimization process.

The first approach, known as *geometrical shape optimization*, consists of having an explicit representation of a domain by a mesh and using the descent directions to move the nodes of this mesh. We refer to [13] for a practical implementation in the context of structural optimization or, more recently, to the educational paper by Dapogny *et al.* [50] in the context of fluid mechanics, both using the open source finite element software FreeFem++. The main drawback of this method is that the process of moving vertices can produce degenerate triangles (overlapping or non-conforming), which affects the quality of the mesh. Another problem is that it maintains the same connectivity, so it makes sense to use it when we have an *a priori* idea of the solution.

A second approach is based on the *level-set method*. The level-set method was developed by Osher and Sethian in [95], originally conceived to track the evolution of moving fronts or

interfaces, such as curves or surfaces. It turned out to be very useful in several areas, such as image segmentation, computer vision, fluid-structure problems, and what interests us, shape and topology optimization. By introducing a computationally fixed domain that contains the original domain of interest, the level set function allows the boundary to be implicitly represented by the zero level of the function. This is particularly useful in shape optimization, where topological changes can be obtained. Initially, the level set function was considered in a fixed mesh [12, 111]. It does, however, have one drawback. As the mesh is fixed and the evolution is implicitly tracked by the level-set function, the partial differential equations considered cannot be solved directly. A solution usually considered in shape optimization problems is to introduce a fictitious material to fill between the computational domain and the domain of interest, which makes it possible to solve these approximate equations.

Today, the modern approach is known as *the level-set mesh evolution method*, introduced by Allaire *et al.* in [10]. The main idea is to have two different representations of the geometry, each with a different purpose. More precisely, we use the level-set function as before to handle the geometry deformations (possible topology changes) and, at each optimization step, we remesh according to the zero level-set, then the mesh of the domain can be used to solve the partial differential equations under consideration.

Topology optimization

The list of topology optimization methods is quite extensive. We will here limit ourselves to a brief description of the most commonly used ones, especially in heat exchanger applications.

Firstly, in addition to the shape derivative, there exists the *topological derivative* [93, 94, 14], based on asymptotic expansions, which aims to create small holes in the domain or add tiny bubbles to it depending on the context studied.

Secondly, there is another type of method: the so-called *density methods*, in which we have the *homogenization method* (see [90, 100, 43, 105] for a general introduction to the mathematical theory of homogenization and [6, 41] in the context of shape and topology optimization) and the *SIMP method* (Solid Isotropic Material with Penalty) (see [22, 62]). Both of them rely on a density function that approximates the characteristic function, which is 1 inside the variable domain and 0 outside. This means that the shape/topology optimization problem is relaxed, by accepting composite structures as admissible. While the homogenization method advocates to characterize the microstructure properties (which is not an easy task), the SIMP method approximates them in terms of the density via some heuristics (usually as a polynomial function of the density). The main disadvantage is that we get a continuous density which we have to penalize in order to get a binary structure.

Shape and topology optimization for heat exchangers

As mentioned previously, one of the aims of this thesis is to focus on the design of heat exchangers. The heat exchanger problem is multi-physical (involving temperature and fluid flow, described by

the convection-diffusion and Navier-Stokes equations, respectively) and also includes a minimum distance constraint, ensuring that the fluids do not mix, which plays a key role in this problem.

In the shape and topology optimization community, the heat exchanger problem has been addressed by using the different tools that we described above, mainly the SIMP and level-set mesh evolution method combined with Hadamard's derivative. The first works we detected were in 2009, considering a single fluid [51, 52, 112]. The two-fluid case was treated in the master's thesis of Papazoglou in 2015 [97] and then followed by [76, 81]. As we have pointed out, the main drawback of the SIMP method is the difficulty to obtain the binary structure by introducing an adequate penalization which takes even more relevance in this multi-physics problem, with complex geometry and where the distance constraint is not trivial to take into account. This is why the level-set mesh evolution method seems to be more suited for this problem: this is the approach recently followed in 2021 in Feppon's thesis [67]. It should be noted that the SIMP method is currently preferred by a wider community of engineers, despite the problems we have explained, because the level-line mesh deformation method with Hadamard derivative has recently been proposed.

Objective and main difficulties

In this thesis, the main objective is to optimize a heat exchanger by taking into account the thin layer separating the two fluids, as usually happens in real-life applications. Several technical difficulties arise in the process, which we explain below.

Non-standard Ventcel transmission conditions

To better understand these difficulties, we need to explicit the effective transmission conditions. We will formally explain theses transmission conditions (rigorous details and convergence results are given in Chapter 1). Let $\eta > 0$ be a small parameter. We start by considering $\Omega^\eta \subset \mathbb{R}^d$, divided into three subdomains $\Omega_1^\eta, \Omega_s^\eta, \Omega_2^\eta$, where the solid part Ω_s^η separates the fluid domains Ω_1^η and Ω_2^η. The parameter η represents the thickness of the solid Ω_s^η (which models the wall of the pipe containing the heat transfer fluid). The interface between Ω_i^η and Ω_s^η is called $\Gamma_i^\eta := \partial\Omega_i^\eta \cap \partial\Omega_s^\eta$, $i = 1, 2$. For the sake of simplicity in this introduction, we consider only Dirichlet boundary conditions on the boundary $\partial\Omega^\eta =: \Gamma_{\mathrm{D}}^\eta$, and we defined $\Gamma_{\mathrm{D},i}^\eta := \partial\Omega_i^\eta \setminus \Gamma_i^\eta$ the Dirichlet part of Ω_i^η, $i = 1, 2$, and $\Gamma_{\mathrm{D},s}^\eta := \partial\Omega_i^\eta \setminus (\Gamma_1^\eta \cup \Gamma_2^\eta)$ the Dirichlet part of Ω_s^η. We assume that $\Gamma_{\mathrm{D},i}^\eta$ touches Γ_i^η, $i = 1, 2$.

Let $\kappa_1, \kappa_2, \kappa_s$ be three positive real numbers (thermal diffusivities). We then consider u^η the solution of the convection-diffusion equation in Ω^η, with restrictions $u_i^\eta := u|_{\Omega_i^\eta}^\eta$, $i = 1, 2, s$, continuous transmission conditions on the interfaces Γ_i^η, $i = 1, 2$ and homogeneous Dirichlet

boundary condition on $\Gamma^\eta_{\mathrm{D,i}}$, $i = 1, 2, s$:

$$\begin{cases} -\operatorname{div}(\kappa_i \nabla u_i^\eta) &= f|_{\Omega_i^\eta} & \text{in } \Omega_i^\eta, i = 1, 2, \\ -\operatorname{div}(\kappa_s \nabla u_s^\eta) &= f|_{\Omega_s^\eta} & \text{in } \Omega_s^\eta, \\ u_i^\eta &= 0 & \text{on } \Gamma^\eta_{\mathrm{D,i}}, i = 1, 2, s, \\ u_s^\eta &= u_i^\eta & \text{on } \Gamma_i^\eta, i = 1, 2, \\ \kappa_s \dfrac{\partial u_s^\eta}{\partial n} &= \kappa_i \dfrac{\partial u_i^\eta}{\partial n} & \text{on } \Gamma_i^\eta, i = 1, 2, \end{cases} \tag{5}$$

where $\boldsymbol{n}$ is the unit normal at Γ_i^η pointing towards Ω_2^η and $f \in \mathrm{L}^2(\Omega^\eta)$ such that $f = 0$ in Ω_s^η .

Because Ω_s^η is too thin, we cannot mesh it directly, since it would become impractical to solve it numerically (in particular in 3D). An efficient technique to deal with these kind of problems are the asymptotic models as in the work of Enquist and Nedelec [58] or more recently in [110, 16]. A similar asymptotic model (three materials with a thin layer in the middle) was obtained in [40] considering a different physics.

The idea is to pass the limit η, resulting in a geometry featuring two domains, Ω_1, Ω_2, independent of η and without thin layer, where Ω_i is the limit of Ω_i^η when $\eta \to 0$. Let $\Gamma := \partial\Omega_1 \cap \partial\Omega_2$ be the interface between Ω_1 and Ω_2, that coincides with the mid-curve between Γ_1^η and Γ_2^η. Similarly, $\Gamma_{\mathrm{D},i} := \partial\Omega_i \setminus \Gamma$.

A first approach is to completely neglect the solid effect, i.e., not to take into account the diffusion in Ω_s^η, which leads to the order zero model:

$$\begin{cases} -\operatorname{div}(\kappa_i \nabla u_i^0) &= f|_{\Omega_i} & \text{in } \Omega_i, i = 1, 2, \\ u_i^0 &= 0 & \text{on } \Gamma_{\mathrm{D,i}}, i = 1, 2, \\ u_1^0 &= u_2^0 & \text{on } \Gamma, \\ \kappa_1 \dfrac{\partial u_1^0}{\partial n} &= \kappa_2 \dfrac{\partial u_2^0}{\partial n} & \text{on } \Gamma, \end{cases}$$

where u^0 is the associated solution of the order zero model, with restrictions u_1^0 and u_2^0 to Ω_1 and Ω_2, respectively. Rougly speaking, this means that Ω_s^η is too thin, that the temperature u_s^η is constant following the normal direction $\boldsymbol{n}$ in Ω_s^η.

We propose a more complex model where the temperature is no longer assumed to be constant in the thin layer. This is a first-order model, which takes into account the effect of diffusion in Ω_s^η using Ventcel transmission conditions:

$$\begin{cases} -\operatorname{div}(\kappa_i \nabla u_i^1) &= f|_{\Omega_i} & \text{in } \Omega_i, i = 1, 2, \\ u_i^1 &= 0 & \text{on } \Gamma_{\mathrm{D,i}}, i = 1, 2, \\ \left\langle \kappa \dfrac{\partial u^1}{\partial n} \right\rangle &= -\dfrac{\kappa_s}{\eta}[u^1] & \text{on } \Gamma, \\ \left[\kappa \dfrac{\partial u^1}{\partial n} \right] &= \eta \operatorname{div}_\tau(\kappa_s \nabla_\tau \left\langle u^1 \right\rangle) - \kappa_s H[u^1] & \text{on } \Gamma, \end{cases} \tag{6}$$

where u^1 is the associated solution of the order one model, with restrictions u_1^1 and u_2^1 to Ω_1 and Ω_2, respectively, div_τ is the tangential divergence, ∇_τ is the tangential gradient, H is the mean

curvature of Γ and $[\cdot]$, $\langle\cdot\rangle$ denote the jump and mean at Γ, defined for every smooth function defined in Ω with restrictions $\phi_i := \phi|_{\Omega_i}$ in Ω_i as:

$$[\phi] := \phi_1 - \phi_2 \quad \text{and} \quad \langle\phi\rangle := \frac{1}{2}(\phi_1 + \phi_2) \text{ on } \Gamma.$$

Here and in the following we will not use anymore the superscript ^{1} to denote the order one model, so we call u the solution of the asymptotic model. The order one model with *non-standard Ventcel transmission conditions* (6) is the model that we will consider throughout this thesis. Roughly speaking, this means that Ω_s^η is too thin, that the temperature u_s^η is linear following the normal direction $\boldsymbol{n}$ in Ω_s^η. Note that the volume diffusion effect $\mathrm{div}(\kappa_s \nabla u_s^\eta)$ in Ω_s^η appears clearly as $\mathrm{div}_\tau(\kappa_s \nabla_\tau \langle u\rangle)$ on Γ, in the asymptotic model.

Numerical resolution of the transmission problem

It is important to note that the numerical resolution of the previous asymptotic model (6) presents several difficulties.

- The non-classical transmission conditions change the nature of the problem. The solution of the exact model u^η belongs to $\mathrm{H}^1(\Omega^\eta)$, whereas the solution of the asymptotic model is not H^1 globally, since there is a jump on Γ in the transmission conditions (6). The problem is then posed in a so-called *broken Sobolev space*:

$$\mathcal{H}^1(\Omega_1, \Omega_2) := \{\phi = (\phi_1, \phi_2) \in \mathrm{H}^1(\Omega_1) \times \mathrm{H}^1(\Omega_2);\ \langle\phi\rangle \in \mathrm{H}^1(\Gamma)\}.$$

- The discrete implementation of the broken Sobolev space $\mathcal{H}^1(\Omega_1, \Omega_2)$ is not straightforward and it is not available in any Finite Element software (see [9] for more details about this issue).

- Although, we can code an in-house discontinuous Galerkin FEM only doubling the degrees of freedom at the interface (where there are discontinuities), if η is too small, the stiffness matrix associated to the asymptotic model is ill-conditioned, due to the term $-\frac{\kappa_s}{\eta}[u]$ which blows up when $\eta \to 0$. Note that it is reasonable to take small values of η for our numerical experiments, since η is the parameter of the asymptotic development.

We need a finite element method that is stable and well-conditioned with respect to η to calculate the temperature field. To this end, we introduce a new Nitsche formulation, which we study. We show that this formulation meets our requirements (see Chapter 2 for details).

Shape sensitivity analysis

Back to the optimal design problem, we must compute the shape derivatives of the involved equations: in our applications we consider a weak coupling between the Navier-Stokes equations and the approximate/asymptotic convection-diffusion equations, being a multi-physics problem.

As we pointed out before, similar derivatives were obtained in [63] when the solid part Ω_s^η is not a thin layer.

As far as the equations considered in this thesis are concerned, the additional difficulty compared to [63] is the non-standard Ventcel transmission conditions. More specifically, the material and shape derivatives will belong to a broken Sobolev space and moreover the differentiation of tangential terms (such as ∇_τ) on the surface is much more complicated than that of the usual derivatives in the volume due to the dependence of the unit normal $\boldsymbol{n}$ on Γ, which changes when Γ changes. The difficulty is not to compute the shape derivative of the Laplace-Beltrami operator: it is well known in the literature, see for example [54, 39, 46] in a simplified context. The real difficulty comes from the fact that these surface derivatives are involved in a jump condition on an interface and are coupled with coefficient discontinuities. Notice that we have also the mean curvature H, which shape derivative requires delicate treatment from a numerical point of view. These issues are dealt with gradually in the chapters 3 and 4.

Numerical resolution of large scale problems and HPC difficulties

Finally, we are interested in real-life applications, *i.e.* 3D numerical simulations which are computationally expensive, where we will put all the previous tools together. At least a hundred iterations are needed to achieve convergence of the optimization algorithm. In each iteration, we have to solve the Navier-Stokes equations, the approximate convection-diffusion equations and some adjoint equations, deduce a descent direction, and then remesh. In particular, the Navier-Stokes equations are the most expensive part, having millions of degrees of freedom in our large scale test cases. This cannot be done without parallelism and standard LU factorization, first of all because of the required memory. Also, it has to be reasonably fast, which requires suitable preconditioners to speed up the linear system resolution.

Main contributions

This research explores and extends the application of shape and topology optimization techniques to the design of heat exchangers with a thin layer. The aim is to develop more realistic models that result in manufacturable solutions. The contributions of this work concern two main areas: numerical analysis and shape optimization.

Based on the Nitsche method [91], the Nitsche method for general boundary conditions [79], and the Nitsche extended finite element method [70], this thesis first proposes a modified Nitsche method to solve a non-standard convection-diffusion problem. The method is designed to improve the conditioning of the stiffness matrix associated to convection-diffusion problems with non-standard transmission conditions. The main feature of the proposed method is the robustness with respect to the thickness of the layer while remaining consistent, stable, and independent with respect to the diffusivity coefficients. This development provides an efficient numerical framework for dealing with discontinuities and complex transmission conditions in convection-diffusion problems.

Then, a new model for optimizing thermal insulators is proposed. This model is more realistic than existing literature on shape optimization for heat insulators such as [27, 28, 108]. Indeed our model accounts for the diffusion effects at the interface of the thin solid domain, using Ventcel-type transmission conditions, making it more realistic for practical applications. This model also incorporates a weak coupling between the Navier-Stokes equations (describing fluid dynamics) and the convection-diffusion equation (describing heat transfer). Here, the fluid domain is fixed, and only the insulating material is optimized. We consider the shape optimization problem which aims to minimize the heat flux outside an insulator with a given volume: we characterize the shape derivative of the objective functional and perform 3D numerical simulations using the level set evolution method.

Afterwards, we consider our initial objective by introducing a new model for 3D fluid-to-fluid heat exchangers in forced convection, where the thin solid layer is represented via non standard transmission conditions. Here again, these conditions account for diffusion effects on the interface through the Laplace-Beltrami operator. The aim is to optimize the shape of the pipe containing the heat transfer fluid. Then, in this problem, the Ventcel transmission conditions are imposed on the boundary that we will aim to optimize. Hence we perform a shape sensitivity analysis and compute the associated shape derivatives. To the best of our knowledge, these shape derivatives have not been computed before. The results obtained can be seen as a complement to previous work such as that of Feppon [63, 67]. Indeed our model includes surface diffusion at the interface, whereas previous work assumed volume diffusion inside the solid. Moreover, we highlight that the shape sensitivity analysis for transmission problems with discontinuous diffusivity coefficients deserves attention and care. Let us mention the works [74, 96, 1] where the heat equation in a transmission problem with discontinuous diffusivity coefficients is considered. It is important to remark that the shape derivative must be computed with precaution in this case, due to the fast Cea's method can lead to mistakes in the formula of the shape derivative either the adjoint problem as it was pointed out in [96]. In this thesis, a rigorous computation of shape derivatives is performed by first using material derivatives, following the methodology in [1]. Our work can be seen as an extension of [9], where they considered the diffusion equation with a discontinuous solution at the interface and the normal flux is continuous and proportional to the jump of the solution, more precisely (in our notation):

$$\begin{aligned} \left[\kappa \frac{\partial u}{\partial n}\right] &= 0 && \text{on } \Gamma, \\ \left\langle \kappa \frac{\partial u}{\partial n} \right\rangle &= -\kappa_s [u] && \text{on } \Gamma, \end{aligned}$$

which model imperfect interfaces for additive manufacturing. In our case of diffusion transmission at the interface, we have much more complicated transmission conditions to differentiate, since the normal flux is not continuous and depends on the Laplace-Beltrami operator:

$$\begin{aligned} \left[\kappa \frac{\partial u}{\partial n}\right] &= \eta \operatorname{div}_\tau(\kappa_s \nabla_\tau \langle u \rangle) - \kappa_s H[u] && \text{on } \Gamma, \\ \left\langle \kappa \frac{\partial u}{\partial n} \right\rangle &= -\frac{\kappa_s}{\eta}[u] && \text{on } \Gamma. \end{aligned}$$

Finally, the last contribution is the realization of complex simulations with the objective of advancing one step further towards industrial applications that allow to improve the design of

heat exchangers, with a code that allows to integrate the different tools for a coupled problem of multi-physics and non-standard equations. By addressing these problems and technical difficulties, this work aims to push the boundaries of shape optimization involving thin layers and provide insights that will lead to more energy-efficient and sustainable thermal management solutions for different applications.

Organisation of the thesis

Chapter 1: Asymptotic analysis for a three-phase diffusion problem

In this preliminary chapter, we consider a simplified framework of a three-phase diffusion model, with a thin layer of thickness η between the two other domains. The convection can be added but it does not play any role, since the velocity is zero at the interface (no-slip boundary condition).

We describe how to obtain an asymptotic model, containing effective transmission conditions of order one. This is the model that we will consider in the following throughout this thesis. For this purpose, we use the classical tools in asymptotic development and end by providing error estimates.

A small part of this chapter was published as a paper in the proceedings Monografías Matemáticas "García de Galeano" [35]:

F. Caubet, C. Conca, M. Dambrine and R. Zelada. Shape optimization for heat exchangers with a thin layer. In *Sixteenth International Conference Zaragoza-Pau on Mathematics and its Applications*, volume 43 of Monogr. Mat. García Galdeano, pages 51–61. Prensas Univ. Zaragoza, Zaragoza, 2024.

Chapter 2: Nitsche extended finite element method for a Ventcel transmission problem with discontinuities at the interface

This chapter focuses on the numerical analysis of the obtained asymptotic model of Chapter 1. For the sake of simplicity we neglect the convective part, since the velocity is zero at the interface and here we focus on the non-standard transmission conditions. The aim of this chapter is to propose a stable and well-conditioned method with respect to the thickness parameter η.

We start by defining the variational framework and then consider the discrete discontinuous Galerkin version. We note that a term blows up when η is too small and that the stiffness matrix has bad conditioning. Then we propose an extended Nitsche finite element method. The discrete variational formulation may seem strange at first sight, so we explain how to obtain it by enforcing coercivity to deduce the inequalities that must verify some coefficients. Then we give the error estimates, which require some inverse inequalities. Finally, we discuss the use of some iterative solvers, which we have not explored in too much depth and which could be the subject of future work in order to have fast methods, in particular for the 3D shape optimization test cases as in Chapter 4.

Most of the content of this chapter has been published in the journal ESAIM: Mathematical Modelling and Numerical Analysis [30]:

D. Capatina, F. Caubet, M. Dambrine, and R. Zelada. Nitsche extended finite element method of a Ventcel transmission problem with discontinuities at the interface. ESAIM: Mathematical Modelling and Numerical Analysis, 59(2):999–1021, 2025.

Chapter 3: Shape optimization for a heat insulator

As a first step towards the shape optimization for a thin layer heat exchanger, in this chapter we study the shape optimization for a heat insulator where we consider just one fluid and the insulator (solid) material, separated by an interface that is fixed. We are interested in the shape of the insulator, more specifically, its exterior boundary position.

We model a heat insulator by using a weakly coupling between the Navier-Stokes equations and the asymptotic model of Chapter 1, adding a Robin boundary condition to the exterior boundary. We are interested on minimizing the heat insulation while fixing certain volume for the insulator material. First, we show the differentiability since it is a non-standard problem. Second, we compute the shape derivatives for a deterministic and random variable outside temperature case. Finally, we perform some 3D numerical experiments (see an example in Figure 8) to validate these formulas by applying the numerical methods developed in Chapter 2 to compute the convection-diffusion and its adjoint equations.

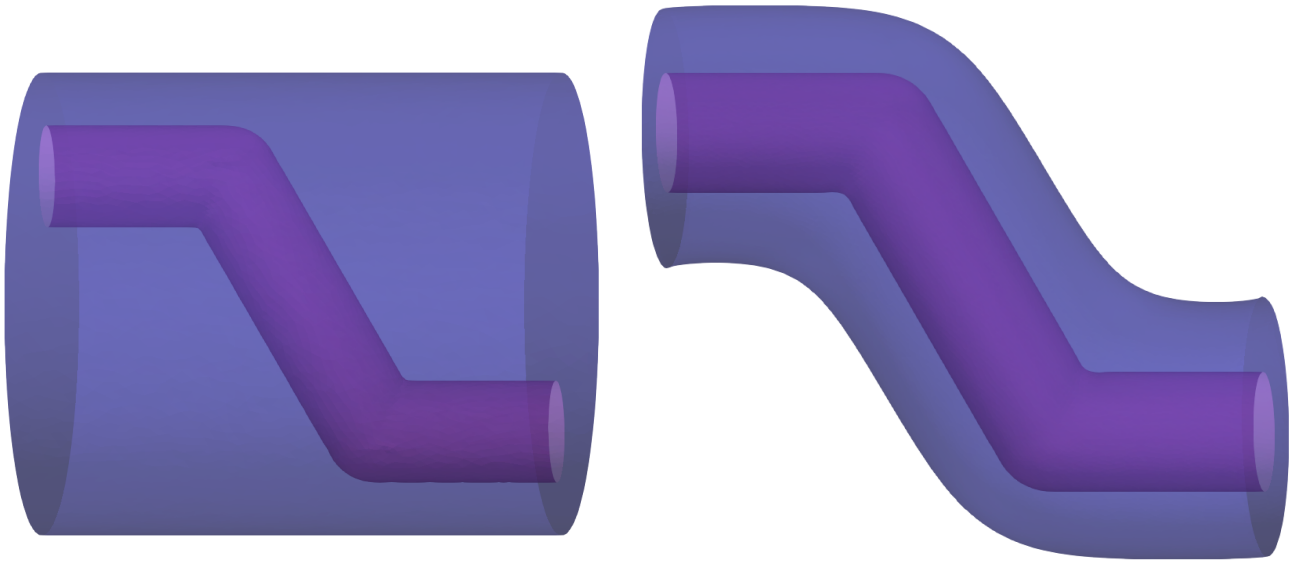

(a) Initial domain Ω. (b) Final domain Ω.

Figure 8: An example of the results obtained for optimising the shape of a thermal insulator.

Most of the content of this chapter has been published in Journal of Optimization Theory and Applications [36]:

F. Caubet, C. Conca, M. Dambrine, and R. Zelada. How to Insulate a Pipe? Journal of Optimization Theory and Applications, 207(3):46, 2025.

Chapter 4: Shape optimization of a heat exchanger with Ventcel transmission conditions

This chapter is the core of this thesis, where we use all the tools developed in the previous chapters. We consider a two fluid heat exchanger in forced convection, separated by an interface that it is our variable subject to optimization.

We model it with the steady-state Navier-Stokes equations and the asymptotic convection-diffusion equation. We prove the differentiability and then we compute the shape derivatives, obtaining a complicated expression due to the non-standard transmission conditions involving jumps and the Laplace-Beltrami operator at the interface. We perform some 3D numerical simulations in a cluster (see an example in Figure 9), discussing the use the preconditioners used in the existing literature for the different physics, in particular for the steady-state Navier-Stokes equations that is the most demanding part. Regarding the numerical resolution of the approximate convection-diffusion equations, we use the Nitsche discontinuous FEM of Chapter 2.

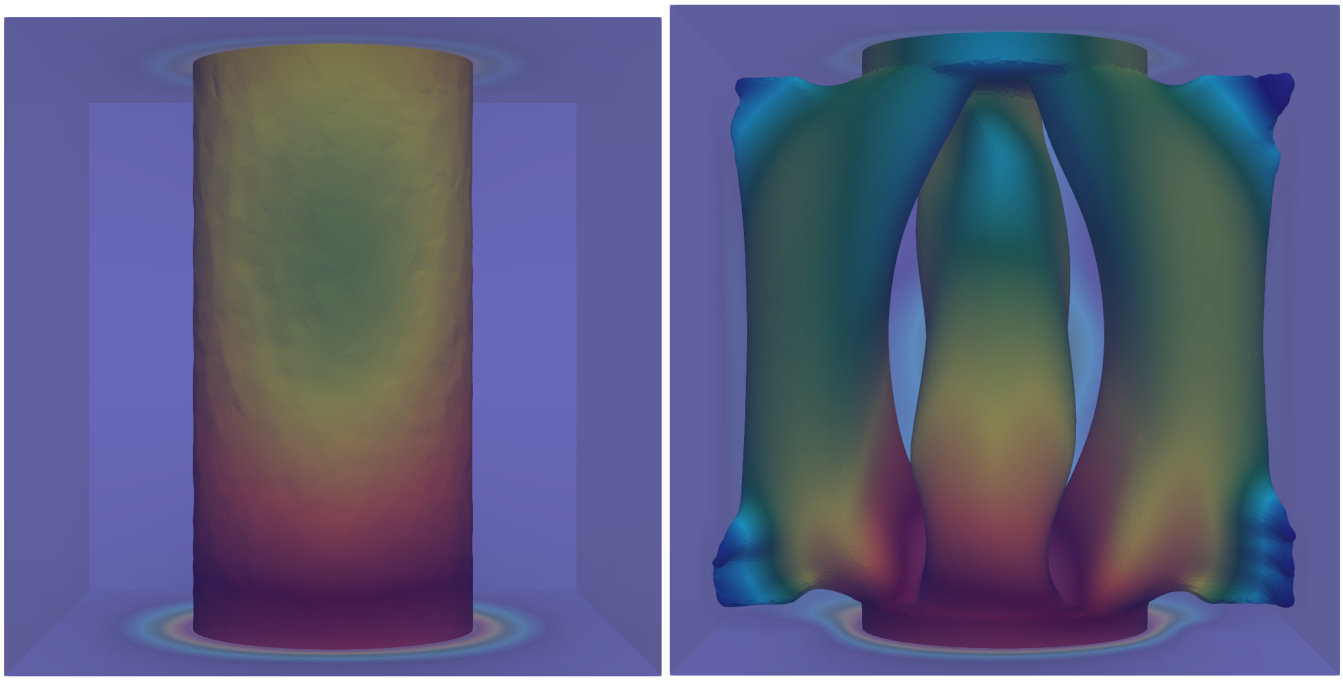

(a) Initial domain Ω. (b) Final domain Ω.

Figure 9: An example of the results obtained for optimising the shape of a heat exchanger.

Most of the content of this chapter is under revision in SIAM Journal on Scientific Computing:

F. Caubet, C. Conca, M. Dambrine and R. Zelada. Shape optimization with Ventcel transmission conditions: application to the design of a heat exchanger. *Under revisions in SIAM Journal on Scientific Computing.*

Annex A: Hadamard's shape derivative

In this appendix, we start by recalling the main notions related to shape optimization as the fundamental definition of shape derivative in the sense of Hadamard. Then, we recall some useful integration formulas and explain how to derive a PDE by means of the material and shape derivative. In addition, we explain the main numerical tools to solve a shape optimization problem, in particular, the level-set function, the redistancing method, the advection of the interface and remeshing.

Notation

Parameters

d	Dimension ($d = 2$ or $d = 3$)
η	The small parameter of the asymptotic model, representing the thickness of the solid
κ_i	Thermal diffusivity of the fluid in Ω_i
κ_s	Thermal diffusivity of the thin solid layer
ν_i	Dynamic viscosity of the fluid in Ω_i

Geometry

Ω	Bounded connected open subset of $\mathbb{R}^d$ which is divided into Ω_1 and Ω_2
Γ	The interface between Ω_1 and Ω_2
Γ_{D}	Dirichlet part of the boundary $\partial\Omega$
Γ_{N}	Neumann part of the boundary $\partial\Omega$

Functional spaces and related definitions

$\mathrm{W}^{p,k}(\Omega_i)^d$	Sobolev space $\mathrm{W}^{p,k}$ of functions defined in Ω_i with values in $\mathbb{R}^d$
$\mathcal{V}_{\boldsymbol{u}_{\mathrm{D,i}}}(\Omega_i)$	Affine space of functions in $\mathrm{H}^1(\Omega_1)^d$, with trace zero on Γ and equal to $\boldsymbol{u}_{\mathrm{D,i}}$ on $\Gamma_{\mathrm{D,i}}$
$\mathcal{V}_{\boldsymbol{u}_{,\mathrm{i}}}(\Omega_i)$	Sobolev space of functions in $\mathrm{H}^1(\Omega_1)^d$, with trace zero on Γ and equal to $\boldsymbol{u}_{\mathrm{D,i}}$ on $\Gamma_{\mathrm{D,i}}$
$\mathcal{H}^1(\Omega_1, \Omega_2)$	Broken Sobolev space of functions in $\mathrm{H}^1(\Omega_1) \times \mathrm{H}^1(\Omega_2)$, with mean $\langle\cdot\rangle$ in $\mathrm{H}^1(\Gamma)$
$\mathcal{H}_{\mathsf{T}_{\mathrm{D}}}(\Omega_1, \Omega_2)$	Affine space of functions in $\mathcal{H}^1(\Omega_1, \Omega_2)$, which trace is equal to T_{D} on Γ_{D}
$\mathcal{H}_0(\Omega_1, \Omega_2)$	Broken Sobolev space of functions in $\mathcal{H}^1(\Omega_1, \Omega_2)$, which trace is zero on Γ_{D}
$u\|_E$	Restriction of the function u to the set E
$[\phi]$	Jump between two smooth functions $\phi_1 := \phi\|_{\Omega_1} \in \mathrm{H}^1(\Omega_1)$ and $\phi_2 := \phi\|_{\Omega_2} \in \mathrm{H}^1(\Omega_2)$
$\langle\phi\rangle$	Mean between two smooth functions $\phi_1 := \phi\|_{\Omega_1} \in \mathrm{H}^1(\Omega_1)$ and $\phi_2 := \phi\|_{\Omega_2} \in \mathrm{H}^1(\Omega_2)$
$\boldsymbol{I}$	Identity mapping from $\mathrm{W}^{1,\infty}(\mathbb{R}^d)^d$ to $\mathrm{W}^{1,\infty}(\mathbb{R}^d)^d$
I	Identity matrix in $\mathbb{R}^d$
$\varepsilon(\boldsymbol{u})$	Symmetric gradient $\varepsilon(\boldsymbol{u}) = \frac{1}{2}(\nabla\boldsymbol{u} + \boldsymbol{u}^t)$
$\sigma(\boldsymbol{u}, p)$	Fluid stress tensor $\sigma(\boldsymbol{u}, p) = 2\nu\varepsilon(\boldsymbol{u}) - p\mathrm{I}$

Differential operators

∇_τ	Tangential gradient at Γ
div_τ	Tangential divergence at Γ

FEM

h	Mesh size
h_K	Diameter of $K \subset \mathbb{R}^d$
$\mathcal{I}_h^k$	the nodal interpolation operator from $\mathrm{H}^{k+1}(\Omega)$ to the polynomial space of degree k, P_h^k
$\mathcal{T}_h$	A regular mesh simplicial mesh of Ω
$\mathcal{F}_h$	Set of faces of $\mathcal{T}_h$
$\mathcal{T}_{h,\Gamma}$	Set of elements of $\mathcal{T}_h$ which have one face on Γ
$\mathcal{F}_{h,\Gamma}$	Set of faces of $\mathcal{T}_{h,\Gamma}$ situated on Γ

Shape and topology optimization

H	Mean curvature of $\partial\Omega_2$
Θ_{ad}	Class of admissible perturbation of $\Omega_1 \cup \Omega_2$
$\boldsymbol{\theta}$	Perturbation of $\Omega_1 \cup \Omega_2$ that belongs to Θ_{ad}
$\Omega_i^{\boldsymbol{\theta}}, \Gamma^{\boldsymbol{\theta}}$	Perturbed domain $\Omega_i^{\boldsymbol{\theta}} = (\boldsymbol{I} + \boldsymbol{\theta})\Omega_i$ and interface $\Gamma^{\boldsymbol{\theta}} = (\boldsymbol{I} + \boldsymbol{\theta})\Gamma$, respectively
$\mathsf{T}_{\boldsymbol{\theta}}$	Solution of the convection-diffusion equation in $\Omega^{\boldsymbol{\theta}}$
$(\boldsymbol{u}_{\boldsymbol{\theta},i}, p_{\boldsymbol{\theta},i})$	Solution of the Navier-Stokes equations in $\Omega_i^{\boldsymbol{\theta}}$
$\overline{\mathsf{T}}$	Transported solution of the convection-diffusion equation $\mathsf{T}_{\boldsymbol{\theta}}$ to Ω, $\overline{\mathsf{T}} = \mathsf{T}_{\boldsymbol{\theta}} \circ (\boldsymbol{I} + \boldsymbol{\theta})$
$(\overline{\boldsymbol{u}}_i, \overline{p}_i)$	Transported solution of the Navier-Stokes equations $(\boldsymbol{u}_{\boldsymbol{\theta},i}, p_{\boldsymbol{\theta},i})$ to Ω_i, $(\overline{\boldsymbol{u}}_i, \overline{p}_i) = (\boldsymbol{u}_{\boldsymbol{\theta},i}, p_{\boldsymbol{\theta},i}) \circ (\boldsymbol{I} + \boldsymbol{\theta})$
$\dot{\phi}$	Material derivative of some function ϕ
ϕ'	Shape derivative of ϕ, $\phi' = \dot{\phi} - \boldsymbol{\theta} \cdot \nabla\phi$

Heat insulation

Γ_{R}	Robin boundary part of $\partial\Omega_2$
$\mathsf{T}_{\mathrm{ext}}$	Exterior temperature to Ω_2, defined on Γ_{R}

Chapter 1

Asymptotic analysis

A small part of this chapter was published as a paper in the proceedings Monografías Matemáticas "García de Galeano" [35]:

F. Caubet, C. Conca, M. Dambrine, and R. Zelada. Shape optimization for heat exchangers with a thin layer. In *Sixteenth International Conference Zaragoza-Pau on Mathematics and its Applications*, volume 43 of Monogr. Mat. García Galdeano, pages 51–61. Prensas Univ. Zaragoza, Zaragoza, 2024.

1.1 Introduction

In this chapter, our goal is to obtain and formally justify the asymptotic model that we will use throughout this thesis. We will consider the case of two materials separated by a thin layer. For the sake of simplicity, we will consider the two-dimensional case. The same arguments are still valid in the three-dimensional case. We follow the approach in [110] of *Ansätz* developed in the case of a thin layer outside a material. In [40] was obtained the effective boundary conditions of order two for a similar geometry to ours for the Bloch-Torrey equation (see [107]) and assuming that the diffusion coefficient is affine to the thickness of the thin layer, using the same *Ansätz* method. In [31] were obtained the effective boundary conditions of order zero for a diffusion problem with a diffusion tensor inversely proportional to the thickness of the thin layer, using a variational approach, and since it was the order zero model the convergence proof is about how to pass the limit when the thickness goes to zero. Concerning the order one or two model is necessary to use the a priori estimates to find the optimal order of convergence with respect to the thickness.

The domains. Let $\eta > 0$ be a small parameter. We consider an open bounded connected domain Ω^η in $\mathbb{R}^2$, which is divided into three open bounded subdomains $\Omega_1^\eta, \Omega_s^\eta, \Omega_2^\eta$. The parameter η represents the thickness of Ω_s^η.

We denote $\Gamma_i^\eta := \partial\Omega_i^\eta \cap \partial\Omega_s^\eta$, the interface between Ω_i^η and Ω_s^η, $i = 1, 2$. We also define $\Gamma^\eta := \Gamma_1^\eta \cup \Gamma_2^\eta$. The boundaries of Ω_i^η are respectively composed by three disjoint regions: $\partial\Omega_i^\eta =: \Gamma_{\mathrm{D,i}}^\eta \cup \Gamma_{\mathrm{N,i}}^\eta \cup \Gamma_i^\eta$, where $\Gamma_{\mathrm{D,i}}^\eta$ is the Dirichlet boundary condition, $\Gamma_{\mathrm{N,i}}^\eta$ represents the Neumann boundary

condition, and the interface with a transmission condition is imposed on Γ_i^η. The boundaries of Ω_s^η are Γ^η and $\Gamma_{\mathrm{N,s}}^\eta := \partial\Omega_s^\eta \setminus \Gamma^\eta$. We define $\Gamma_{\mathrm{D}}^\eta := \Gamma_{\mathrm{D},1}^\eta \cup \Gamma_{\mathrm{D},2}^\eta$ and $\Gamma_{\mathrm{N}}^\eta := \Gamma_{\mathrm{N},1}^\eta \cup \Gamma_{\mathrm{N},2}^\eta$. Finally, let Γ be the mid-curve between Γ_1^η and Γ_2^η.

The model problem. Let $\kappa_1, \kappa_2, \kappa_s$ be positive constants. We consider u^η as the solution of the following system:

$$\begin{cases} -\operatorname{div}(\kappa_i \nabla u_i^\eta) &= G & \text{in } \Omega_i^\eta, i = 1,2, \\ -\operatorname{div}(\kappa_s \nabla u_s^\eta) &= 0 & \text{in } \Omega_s^\eta, \\ u_i^\eta &= u_{\mathrm{D,i}} & \text{on } \Gamma_{\mathrm{D,i}}^\eta, i = 1,2, \\ \kappa_i \dfrac{\partial u_i^\eta}{\partial n} &= 0 & \text{on } \Gamma_{\mathrm{N,i}}^\eta, i = 1,2,s, \\ [u^\eta] &= 0 & \text{on } \Gamma^\eta, \\ \left[\kappa \dfrac{\partial u^\eta}{\partial n}\right] &= 0 & \text{on } \Gamma^\eta, \end{cases} \tag{1.1}$$

where $G, u_{\mathrm{D,i}} \in \mathrm{H}^1(\mathbb{R}^d), i = 1,2$. At the interface Γ^η we suppose continuity of the temperature and the flux, i.e., the jumps are zero.

Remark 1 *This problem is well-posed (by the Lax-Milgram theorem) in*

$$\mathrm{H}^1_{u_{\mathrm{D}}^\eta}(\Omega^\eta) := \{\phi \in \mathrm{H}^1(\Omega^\eta);\ \phi = u_{\mathrm{D,i}} \text{ on } \Gamma_{\mathrm{D,i}}^\eta, i = 1,2\}.$$

1.2 Formal derivation of the effective boundary conditions

In this part we will do a formal derivation of the effective boundary conditions, without precising the details or convergence, which we will leave for the next section.

For the sake of simplicity, here and in the following we will consider an special case: the square. Let $a, b > 0$. Then the domain Ω^η is defined as

$$\Omega^\eta = (-a,a) \times \left(-b - \frac{\eta}{2}, b + \frac{\eta}{2}\right),$$

and Ω_1^η, Ω_2^η, Ω_s^η:

$$\Omega_1^\eta = (-a,a) \times \left(-b - \frac{\eta}{2}, -\frac{\eta}{2}\right), \quad \Omega_s^\eta = (-a,a) \times \left(-\frac{\eta}{2}, \frac{\eta}{2}\right), \quad \Omega_2^\eta = (-a,a) \times \left(\frac{\eta}{2}, b + \frac{\eta}{2}\right).$$

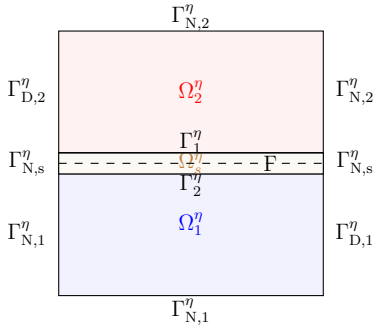

Figure 1.1: Illustration of the domain of the exact problem with a thin layer.

In this case, $\Gamma = (-a, a) \times \{0\}$: see Figure 1.1.

We will make an asymptotic expansion to obtain a new model without thin layer and with new transmission conditions. In this way, we will get rid of the meshing of Ω_s^η associated to the small parameter, but the equations will change. More details about this technique can be found in [110].

Let us introduce $\langle\cdot\rangle_\eta$ the mean and $[\cdot]_\eta$ the jump between Γ_2^η and Γ_1^η, which are given by:

$$\langle v\rangle_\eta(x_\Gamma) := \frac{v_1(x_\Gamma + \frac{\eta}{2}\boldsymbol{n}) + v_2(x_\Gamma - \frac{\eta}{2}\boldsymbol{n})}{2}, \quad [v]_\eta(x_\Gamma) := v_1\left(x_\Gamma - \frac{\eta}{2}\boldsymbol{n}\right) - v_2\left(x_\Gamma + \frac{\eta}{2}\boldsymbol{n}\right),$$

where $x_\Gamma := (x_1, 0) \in \Gamma$, $\boldsymbol{n}$ the unit normal to Γ orientated towards Ω_2^η, that is, $\boldsymbol{n} = (0, 1)$ in the simplified case of the square.

We postulate the following *Ansätz* as the solution of (1.1),

$$\begin{aligned} u_i^\eta(x) &= \sum_{j\geq 0} \eta^j u_i^j(x_1, x_2), x \in \Omega_i^\eta, i = 1, 2, \\ u_s^\eta(x) &= \sum_{j\geq 0} \eta^j u_s^j(x_1, Y), x \in \Omega_s^\eta, \end{aligned}$$

with $Y := \dfrac{x_2}{\eta} \in \left(-\dfrac{1}{2}, \dfrac{1}{2}\right)$. Plugging this into $\operatorname{div}(\kappa_s \nabla u_s) = 0$, we get that for every $Y \in \left(-\dfrac{1}{2}, \dfrac{1}{2}\right)$,

$$\sum_{j\geq 0}\left[\eta^j\left(\operatorname{div}_\tau(\kappa_s\nabla_\tau u_s^j)\right) + \eta^{j-2}\frac{\partial}{\partial Y}\left(\kappa_s\frac{\partial u_s^j}{\partial Y}\right)\right] = 0.$$

Then, by formal identification of powers of η, we obtain in particular the first three terms,

$$\frac{\partial}{\partial Y}\left(\kappa_s\frac{\partial u_s^0}{\partial Y}\right) = 0 \tag{1.2}$$

$$\frac{\partial}{\partial Y}\left(\kappa_s\frac{\partial u_s^1}{\partial Y}\right) = 0 \tag{1.3}$$

$$\frac{\partial}{\partial Y}\left(\kappa_s\frac{\partial u_s^{j+2}}{\partial Y}\right) + \operatorname{div}_\tau\left(\kappa_s\nabla_\tau u_s^j\right) = 0, \qquad \forall j \geq 0. \tag{1.4}$$

Note that the problems solved by u_s^0, u_s^1, u_s^2 are one-dimensional, and x_1 is a parameter to that problem, so we can integrate with respect to Y, getting a first degree polynomial for u_s^0, u_s^1, and a two degree polynomial for u_s^2. In order to determine the coefficients of this polynomial, we use the transmission conditions. The transmission conditions $[u] = 0$ on Γ^η and $\left[\kappa\frac{\partial u}{\partial n}\right] = 0$ on Γ^η become

$$u_s^j\left(x_1, \frac{\pm 1}{2}\right) = u_i^j\left(x_\Gamma \pm \frac{\eta}{2}\boldsymbol{n}\right), \forall j \geq 0 \tag{1.5}$$

$$\kappa_s\frac{\partial u_s^0}{\partial Y}\left(x_1, \pm\frac{1}{2}\right) = 0, \tag{1.6}$$

$$\kappa_s\frac{\partial u_s^{j+1}}{\partial Y}\left(x_1, \pm\frac{1}{2}\right) = \kappa_i\frac{\partial u_i^j}{\partial n}\left(x_\Gamma \pm \frac{\eta}{2}\boldsymbol{n}\right), \quad \forall j \geq 0. \tag{1.7}$$

From (1.2) and the boundary conditions in (1.5) we see that

$$u_s^0(x_1, Y) = \langle u^0 \rangle_\eta(x_\Gamma) - [u^0]_\eta(x_\Gamma)Y.$$

Then, taking into account (1.6) we get

$$[u^0]_\eta = 0, \quad u_s^0\,(x_1, Y) = \langle u^0 \rangle_\eta(x_\Gamma). \tag{1.8}$$

Similarly,

$$u_s^1(x_1, Y) = \langle u^1 \rangle_\eta(x_\Gamma) - [u^1]_\eta(x_\Gamma)Y.$$

Using (1.7), it yields

$$\left[\kappa \frac{\partial u^0}{\partial n}\right]_\eta = 0, \tag{1.9}$$

$$[u^1]_\eta = -\frac{1}{\kappa_s}\left\langle \kappa \frac{\partial u^0}{\partial n}\right\rangle_\eta. \tag{1.10}$$

Then, equation (1.4) becomes

$$\frac{\partial}{\partial Y}\left(\kappa_s \frac{\partial u_s^2}{\partial Y}\right) + \mathrm{div}_\tau\left(\kappa_s \nabla_\tau \langle u^0 \rangle_\eta\right) = 0.$$

Integrating and by (1.5),

$$\kappa_s u_s^2\,(x_1, Y) = \kappa_s \langle u^2 \rangle_\eta(x_\Gamma) + \frac{1}{8}\left(\mathrm{div}_\tau(\kappa_s \nabla_\tau \langle u^0 \rangle_\eta)\right) + \kappa_s [u^2]_\eta(x_\Gamma)Y - \left(\mathrm{div}_\tau(\kappa_s \nabla_\tau \langle u^0 \rangle_\eta\right)\frac{Y^2}{2}.$$

From (1.7) it follows that

$$\left[\kappa \frac{\partial u^1}{\partial n}\right]_\eta = \mathrm{div}_\Gamma(\kappa_s \nabla_\Gamma \langle u^0 \rangle_\eta). \tag{1.11}$$

Finally, since $u_i^\eta = u_i^0 + \eta u_i^1 + \mathcal{O}(\eta^2)$, then summing (1.9) and (1.11),

$$\left[\kappa \frac{\partial u^\eta}{\partial n}\right]_\eta = \eta\, \mathrm{div}_\Gamma(\kappa_s \nabla_\Gamma \langle u^\eta \rangle) + \mathcal{O}(\eta^2). \tag{1.12}$$

Similarly, from (1.8) and (1.10), we get

$$[u^\eta]_\eta = -\frac{\eta}{\kappa_s}\left\langle \kappa \frac{\partial u^\eta}{\partial n}\right\rangle_\eta + \mathcal{O}(\eta^2). \tag{1.13}$$

Thus, we have proved that, $u_i^{\eta,[1]} := u_i^0 + \eta u_i^1$ satisfies

$$\begin{cases} -\operatorname{div}(\kappa_i \nabla u_i^{\eta,[1]}) &= G_i & \text{in } \Omega_i^\eta, i=1,2, \\ u_i^{\eta,[1]} &= u_{\mathrm{D,i}} & \text{on } \Gamma_{\mathrm{D},i}^\eta, i=1,2, \\ \kappa_i \dfrac{\partial u_i^{\eta,[1]}}{\partial n} &= 0 & \text{on } \Gamma_{\mathrm{N,i}}^\eta, i=1,2, \\ [u^0]_\eta &= 0 & \text{on } \Gamma, \\ \left[\kappa \dfrac{\partial u^0}{\partial n}\right]_\eta &= 0 & \text{on } \Gamma, \\ [u^1]_\eta &= -\dfrac{1}{\kappa_s}\left\langle \kappa \dfrac{\partial u^0}{\partial n}\right\rangle_\eta & \text{on } \Gamma, \\ \left[\kappa \dfrac{\partial u^1}{\partial n}\right]_\eta &= \operatorname{div}_\tau(\kappa_s \nabla_\tau \langle u^0\rangle_\eta) & \text{on } \Gamma. \end{cases} \tag{1.14}$$

This motivates to consider the following problem in Ω^η: find v^η such that v^η be linear with respect to $x_2 \in \Omega_s^\eta$ and

$$\begin{cases} -\operatorname{div}(\kappa_i \nabla v_i^\eta) &= G_i & \text{in } \Omega_i^\eta, i=1,2, \\ v_i^\eta &= u_{\mathrm{D,i}} & \text{on } \Gamma_{\mathrm{D,i}}^\eta, i=1,2, \\ \kappa_i \dfrac{\partial v_i^\eta}{\partial n} &= 0 & \text{on } \Gamma_{\mathrm{N,i}}^\eta, i=1,2, \\ \left\langle \kappa \dfrac{\partial v^\eta}{\partial n}\right\rangle_\eta &= -\dfrac{\kappa_s}{\eta}\left[v^\eta\right]_\eta & \text{on } \Gamma, \\ \left[\kappa \dfrac{\partial v^\eta}{\partial n}\right]_\eta &= \eta \operatorname{div}_\tau(\kappa_s \nabla_\tau \langle v^\eta\rangle_\eta) & \text{on } \Gamma. \end{cases} \tag{1.15}$$

Since v^η is linear with respect to x_2 in Ω_s^η, we only need to solve the equation in $\Omega_1^\eta \cup \Omega_2^\eta$ in order to find v^η in the whole domain Ω^η. Furthermore, we can translate Ω_1^η and Ω_2^η in a way that Γ_1^η and Γ_2^η coincide with Γ (as we did in [35] translating with $\pm\frac{\eta}{2}$), then we can call Ω_1 and Ω_2 these translated domains (and similarly for Γ_{D}^η, Γ_{N}^η, G, u_{D}), with interface $\Gamma := \partial\Omega_1 \cap \partial\Omega_2$. Then, considering u the solution of the following problem

$$\begin{cases} -\operatorname{div}(\kappa_i \nabla u_i) &= G & \text{in } \Omega_i, i=1,2, \\ u_i &= u_{\mathrm{D,i}} & \text{on } \Gamma_{\mathrm{D}}, i=1,2, \\ \kappa_i \dfrac{\partial u}{\partial n} &= 0 & \text{on } \Gamma_{\mathrm{N,i}}, i=1,2, \\ \left\langle \kappa \dfrac{\partial u}{\partial n}\right\rangle &= -\dfrac{\kappa_s}{\eta}\left[u\right] & \text{on } \Gamma, \\ \left[\kappa \dfrac{\partial u}{\partial n}\right] &= \eta \operatorname{div}_\tau(\kappa_s \nabla_\tau \langle u\rangle) & \text{on } \Gamma, \end{cases} \tag{1.16}$$

where the jump $[\cdot]$ and mean $\langle\cdot\rangle$ at the interface Γ are defined as:

$$[u] = u_1 - u_2 \quad \text{and} \quad \langle u\rangle = \frac{1}{2}(u_1 + u_2).$$

The equation (1.16) is known as the asymptotic model of order one (and actually in the square case it turns out to be order two).

Note that u is the translation of $v^\eta|_{\Omega_1^\eta \cup \Omega_2^\eta}$ to $\Omega := \Omega_1 \cup \Omega_2$.

Remark 2 *The problem* (1.16) *is well-posed (by the Lax-Milgram theorem) in*

$$\mathcal{H}^1_{u_{\rm D}}(\Omega_1,\Omega_2) := \{\phi = (\phi_1,\phi_2) \in {\rm H}^1(\Omega_1)\times {\rm H}^1(\Omega_2);\ \langle\phi\rangle \in {\rm H}^1(\Gamma);\ \phi_i = u_{\rm D,i} \text{ on } \Gamma_{\rm D,i}, i=1,2\}.$$

A detailed proof will be done in the next chapter.

Remark 3 *All these computations are analogous for the cube case in* $\mathbb{R}^3$*. In the general case in* $\mathbb{R}^2$*, when* Ω_s^η *is not a square (and then* Γ *is not rectilinear). We assume that the thickness of* Ω_s^η *is* η *(constant) and that* Ω_s^η *can be described by the mid-curve* Γ*,*

$$\Omega_s^\eta = \left\{ x \in \Omega^\eta; x = x_\Gamma(t) + r\boldsymbol{n}(t), x_\Gamma(t) \in \Gamma, r \in \left(\frac{-\eta}{2},\frac{\eta}{2}\right)\right\}.$$

We also assume that Γ *is* $\mathcal{C}^2$*. We consider the following parametrization:* $t \in [0,L) \to x_\Gamma(t) \in \Gamma$*, where* L *is the length of* Γ *and* $\left|\frac{dx_\Gamma(t)}{dt}\right| = 1$*, and such that it has a clockwise orientation. Let* $\boldsymbol{n}(t)$ *be the unitary normal vector at* $x_\Gamma(t)$ *directed towards* Ω_i^η *and* $\tau(t) = \frac{dx_\Gamma(t)}{dt}$ *the unitary vector tangential to* Γ *at* $x_\Gamma(t)$*. The curvature* c *is defined by* $c(t) := \boldsymbol{\tau}(t)\cdot\frac{d\boldsymbol{n}(t)}{dt}$*. Then, for each* $x \in \Omega_s^\eta$*, it exists a pair* $(t,r) \in [0,L)\times\left(\frac{-\eta}{2},\frac{\eta}{2}\right)$ *such that*

$$x = \gamma(t,r) := x_\Gamma(t) + r\boldsymbol{n}(t)$$

where $\gamma : [0,L)\times\left(-\frac{\eta}{2},\frac{\eta}{2}\right) \to \Omega_s^\eta$ *is the curvilinear parametrization of* Ω_s^η*. Then,*

$$\begin{aligned}
\nabla u_s &= \frac{1}{(1+rc)}\frac{\partial u_s}{\partial t}\boldsymbol{\tau} + \frac{\partial u_s}{\partial r}\boldsymbol{n}\\
{\rm div}(\kappa_s\nabla u_s) &= \frac{1}{(1+rc)}\frac{\partial}{\partial t}\left(\frac{1}{1+rc}\kappa_s\frac{\partial u_s}{\partial t}\right) + \frac{1}{(1+rc)}\frac{\partial}{\partial r}\left((1+rc)\kappa_s\frac{\partial u_s}{\partial r}\right)\\
&= \frac{1}{(1+rc)}\,{\rm div}_\tau\left(\frac{1}{1+rc}\kappa_s\nabla_\tau u_s\right) + \frac{1}{(1+sc)}\frac{\partial}{\partial r}\left((1+rc)\kappa_s\frac{\partial u_s}{\partial r}\right).
\end{aligned}$$

The only change with respect to (1.14) *is in the jump of the flux, where now appears the curvature*

$$\left[\kappa\frac{\partial u^1}{\partial n}\right]_\eta = {\rm div}_\tau(\kappa_s\nabla_\tau\langle u^0\rangle_\eta) - c\kappa_s[u^1]_\eta \quad \text{ on } \Gamma.$$

This can be obtained after series of technical computations, similar to the rectilinear case.

Theorem 1.2.1 Let $\Omega^\eta = (-a,a)\times\left(-b-\frac{\eta}{2},b+\frac{\eta}{2}\right)$, divided into

$$\Omega_1^\eta = (-a,a)\times\left(-b-\frac{\eta}{2},-\frac{\eta}{2}\right),\quad \Omega_s^\eta = (-a,a)\times\left(-\frac{\eta}{2},\frac{\eta}{2}\right) \text{ and } \Omega_2^\eta = (-a,a)\times\left(\frac{\eta}{2},b+\frac{\eta}{2}\right).$$

Let $\Omega = \Omega_1\cup\Omega_2$, where

$$\Omega_1 = (-a,a)\times(-b,0) \quad \text{ and } \quad \Omega_2 = (-a,a)\times(0,b).$$

Let $u^\eta \in \mathrm{H}^1(\Omega^\eta)$ the solution of the exact diffusion equation (1.1) and $u \in \mathcal{H}^1(\Omega_1, \Omega_2)$ the solution of the asymptotic model (1.16). If $G \in \mathcal{C}^\infty(\Omega_1^\eta \cup \Omega_2^\eta)$, with compact support inside $\Omega_1^\eta \cup \Omega_2^\eta$, then, it exists $C > 0$ independent of η such that,

$$\|\tilde{u}^\eta - u\|_{\mathrm{H}^1(\Omega)} \leq C\eta^2,$$

where $\tilde{u}^\eta(x_1, x_2) := \begin{cases} u_1^\eta(x_1, x_2 + \frac{\eta}{2}) \text{ if } (x_1, x_2) \in \Omega_1^\eta, \\ u_2^\eta(x_1, x_2 - \frac{\eta}{2}) \text{ if } (x_1, x_2) \in \Omega_2^\eta, \end{cases}$.

Proof. The proof is quite standard, it consists of two steps: first, we estimate the truncated error of the original problem and second, we estimate the truncated error of the asymptotic problem and finally combining these two estimates. We conclude by using triangle inequality.

First step: We define the truncated error

$$r_i^{\eta,N} := u_i^\eta - u_i^{\eta,[N]}, i = 1, 2, s,$$

where $u_i^{\eta,[N]} = \sum_{j=0}^{N} \eta^j u_i^j$. We have that,

$$\begin{aligned}
-\operatorname{div}(\kappa_s \nabla r_s^{\eta,N}) &= \operatorname{div}(\kappa_s \nabla u_s^{\eta,[N]}) \\
&= \sum_{j=0}^{N} \eta^j \operatorname{div}(\kappa_s \nabla u_s^j) \\
&= \sum_{j=0}^{N} \eta^j \left(\frac{\partial}{\partial x_1} \left(\kappa_s \frac{\partial u_s^j}{\partial x_1} \right) + \eta^{-2} \frac{\partial}{\partial Y} \left(\kappa_s \frac{\partial u_s^j}{\partial Y} \right) \right) \\
&= \eta^{-2} \sum_{j=0}^{N} \eta^{j+2} \frac{\partial}{\partial x_1} \left(\kappa_s \frac{\partial u_s^j}{\partial x_1} \right) + \eta^{-2} \sum_{j=0}^{N} \eta^j \frac{\partial}{\partial Y} \left(\kappa_s \frac{\partial u_s^j}{\partial Y} \right) \\
&= \eta^{-2} \sum_{j=2}^{N+2} \eta^j \frac{\partial}{\partial x_1} \left(\kappa_s \frac{\partial u_s^{j-2}}{\partial x_1} \right) + \eta^{-2} \sum_{j=2}^{N} \eta^j \frac{\partial}{\partial Y} \left(\kappa_s \frac{\partial u_s^{j-2}}{\partial Y} \right) \\
&\quad + \eta^{-2} \frac{\partial}{\partial Y} \left(\kappa_s \frac{\partial u_s^0}{\partial Y} \right) + \eta^{-1} \frac{\partial}{\partial Y} \left(\kappa_s \frac{\partial u_s^1}{\partial Y} \right) \\
&= \eta^{N-1} \frac{\partial}{\partial x_1} \left(\kappa_s \frac{\partial u_s^{N-1}}{\partial x_1} \right) + \eta^N \frac{\partial}{\partial x_1} \left(\kappa_s \frac{\partial u_s^N}{\partial x_1} \right),
\end{aligned}$$

where in the last identity we have used (1.6) and (1.7). Similarly, for the transmission conditions, we easily verify that $r_i^{\eta,N} = r_s^{\eta,N}$ on Γ. Also,

$$\begin{aligned}
\kappa_i \frac{\partial r_i^{\eta,N}}{\partial n} - \kappa_s \frac{\partial r_s^{\eta,N}}{\partial n} &= \sum_{j=0}^{N} \eta^j \left(\kappa \frac{\partial u_i^j}{\partial n} - \eta^{-1} \kappa_s \frac{\partial u_s^j}{\partial Y} \right) \\
&= \eta^{-1} \sum_{j=1}^{N+1} \eta^j \kappa_s \frac{\partial u_i^{j-1}}{\partial n} - \eta^{-1} \sum_{j=1}^{N} \eta^j \kappa_s \frac{\partial u_s^j}{\partial Y} - \eta^{-1} \kappa_s \frac{\partial u_s^0}{\partial Y} \\
&= \eta^N \kappa_i \frac{\partial u_i^N}{\partial Y}.
\end{aligned}$$

Therefore, $r^{\eta,N}$ verifies

$$\begin{cases} -\operatorname{div}(\kappa_i \nabla r_i^{\eta,N}) &= 0 & \text{in } \Omega_i^\eta, i=1,2, \\ -\operatorname{div}(\kappa_s \nabla r_s^{\eta,N}) &= \mathcal{O}(\eta^{N-1}) & \text{in } \Omega_s^\eta \\ r_i^{\eta,N} &= 0 & \text{on } \Gamma_{\mathrm{D,i}}^\eta, i=1,2, \\ \kappa_i \dfrac{\partial r_i^{\eta,N}}{\partial n} &= 0 & \text{on } \Gamma_{\mathrm{N,i}}^\eta \cup \Gamma_{\mathrm{N,s}}^\eta, i=1,2, \\ r_i^{\eta,N} &= r_s^{\eta,N} & \text{on } \Gamma_i^\eta, i=1,2, \\ \kappa_i \dfrac{\partial r_i^{\eta,N}}{\partial n} &= \kappa_s \dfrac{\partial r_s^{\eta,N}}{\partial n} + \mathcal{O}(\eta^N) & \text{on } \Gamma_i^\eta, i=1,2. \end{cases}$$

Noting that

$$r_i^{\eta,N} = r_i^{\eta,N+2} + \eta^{N+1} u_i^{N+1} + \eta^{N+2} u_i^{N+2}, \quad i=1,2,s.$$

By a priori estimates, there exists a constant $C_N > 0$ independent of η such that:

$$\sum_{i=1}^{2} \|r^{\eta,N}\|_{\mathrm{H}^1(\Omega_i^\eta)} + \sqrt{\eta}\|r_s^{\eta,N}\|_{\mathrm{H}^1(\Omega_s^\eta)} \leq C_N \eta^{N+1}. \tag{1.17}$$

Second step: We define

$$\tilde{u}^{\eta,[1]}(x_1,x_2) := \begin{cases} u_1^{\eta,[1]}(x_1, x_2 + \frac{\eta}{2}) \text{ if } (x_1,x_2) \in \Omega_1^\eta, \\ u_2^{\eta,[1]}(x_1, x_2 - \frac{\eta}{2}) \text{ if } (x_1,x_2) \in \Omega_2^\eta. \end{cases}$$

We define similarly $\tilde{u}^0$ and $\tilde{u}^1$. We consider the *Ansätz* $S_i^\eta = \sum_{j\geq 0} \eta^j S_i^j$, $i=1,2$, that leads to the following recurrence equations, for $j=0$,

$$\begin{cases} -\operatorname{div}(\kappa_i \nabla S_i^0) &= G_i & \text{in } \Omega_i, i=1,2, \\ S_i^0 &= u_{\mathrm{D,i}} & \text{on } \Gamma_{\mathrm{D,i}}, i=1,2, \\ \kappa_i \dfrac{\partial S_i^0}{\partial n} &= 0 & \text{on } \Gamma_{\mathrm{N,i}}, i=1,2, \\ \left[S^0\right] &= 0 & \text{on } \Gamma, \\ \left[\kappa \dfrac{\partial S^1}{\partial n}\right] &= 0 & \text{on } \Gamma, \end{cases}$$

and for each $j \in \mathbb{N}$,

$$\begin{cases} -\operatorname{div}(\kappa_i \nabla S_i^j) &= 0 & \text{in } \Omega_i, i=1,2, \\ S_i^j &= 0 & \text{on } \Gamma_{\mathrm{D,i}}, i=1,2, \\ \kappa_i \dfrac{\partial S_i^j}{\partial n} &= 0 & \text{on } \Gamma_{\mathrm{N,i}}, i=1,2, \\ \left\langle \kappa \dfrac{\partial S^j}{\partial n} \right\rangle &= -\kappa_s [S^{j+1}] & \text{on } \Gamma, \\ \left[\kappa \dfrac{\partial S^{j+1}}{\partial n}\right] &= \operatorname{div}_\tau(\kappa_s \nabla_\tau \left\langle S^j \right\rangle) & \text{on } \Gamma. \end{cases}$$

We note that $\tilde{u}^0, S^0$ and $\tilde{u}^1, S^1$ satisfy the same equations, then

$$\tilde{u}^0 = S^0, \tilde{u}^1 = S^1. \tag{1.18}$$

Conclusion: By triangle inequality,

$$\begin{aligned}\|\tilde{u}^\eta - v\|_{\mathrm{H}^1(\Omega)} &\leq \|\tilde{u}^\eta - \tilde{u}^{\eta,[1]}\|_{\mathrm{H}^1(\Omega)} + \|\tilde{u}^{\eta,[1]} - v\|_{\mathrm{H}^1(\Omega)} \\ &\leq C\eta^2 + \|S^0 + \eta S^1 - v\|_{\mathrm{H}^1(\Omega)},\end{aligned}$$

where it was used inequality (1.17) and identity (1.18). To conclude, we argue in the same way as in the first part in order to estimate $S^0 + \eta S^1 - v$. □

Chapter 2

Nitsche extended finite element method of a Ventcel transmission problem with discontinuities at the interface

Contents

Most of the content of this chapter was published as a paper in the journal ESAIM: Mathematical Modelling and Numerical Analysis [30]:

D. Capatina, F. Caubet, M. Dambrine, and R. Zelada. Nitsche extended finite element method of a Ventcel transmission problem with discontinuities at the interface. ESAIM: Mathematical Modelling and Numerical Analysis, 59(2):999–1021, 2025.

2.1 Introduction

Motivations. In this chapter we consider a heat diffusion problem with an interface. Since our final goal is to optimise the shape of a heat exchanger between two fluids, we are led to study the case where the wall separating the fluids is very thin. Due to the fact that it is very expensive to mesh at the scale of the wall's thickness η, we consider here a model problem obtained by means of an asymptotic analysis as the small parameter η tends to zero. We thus obtain a problem involving discontinuous transmission conditions and surface scattering (also known as *Ventcel conditions*, see [109]). The model problem depends on η, which leads to conditioning problems when using the standard Galerkin discontinuous finite element method. We aim to develop a numerical method that is robust with respect to η, allowing to use iterative solvers.

Setting of the problem. Let us present the studied problem. Let Ω be an open bounded connected domain of $\mathbb{R}^d$ ($d = 2, 3$), divided into two open bounded subdomains Ω_1, Ω_2 which are separated by an interface $\Gamma = \partial\Omega_1 \cap \partial\Omega_2$ that we assume to have non-zero measure in $\mathbb{R}^{d-1}$ and to be smooth enough (see the beginning of section 2.2 for more details). Here and in the following, the subscript $_i$ stands for $_1$ and $_2$. The boundaries of Ω_i are described by $\partial\Omega_i =: \Gamma_{\mathrm{D},i} \cup \Gamma_{\mathrm{N},i} \cup \Gamma$ (see Figure 2.1). We define $\Gamma_{\mathrm{D}} := \Gamma_{\mathrm{D},1} \cup \Gamma_{\mathrm{D},2}$ and similarly, $\Gamma_{\mathrm{N}} := \Gamma_{\mathrm{N},1} \cup \Gamma_{\mathrm{N},2}$. We assume here that $\overline{\Gamma} \cap \overline{\Gamma}_{\mathrm{N}} = \emptyset$ and that $\overline{\Gamma} \cap \overline{\Gamma}_{\mathrm{D}} \neq \emptyset$. Other geometrical configurations could also be treated by changing the functional spaces. Let $\boldsymbol{n}$ be the unit normal to Γ exterior to Ω_1, that is, $\boldsymbol{n} := \boldsymbol{n}_1 = -\boldsymbol{n}_2$. For a piecewise smooth function v defined on Ω, we denote by $v_i := v|_{\Omega_i}$ its restriction to Ω_i and we define the jump and mean of v at Γ, denoted by $[\cdot]$ and $\langle\cdot\rangle$ respectively, as follows:

$$[v] := v_1 - v_2 \text{ on } \Gamma, \quad \text{and} \quad \langle v \rangle := \frac{v_1 + v_2}{2} \text{ on } \Gamma.$$

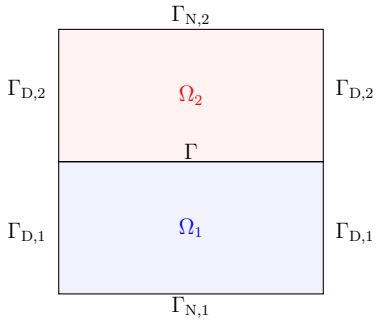

Figure 2.1: Illustration of the domain Ω.

Let $\kappa_1, \kappa_2, \eta, \alpha$ be strictly positive constants and let $\eta > 0$ be fixed. We then consider the

following interface problem:

$$\begin{cases} -\operatorname{div}(\kappa_i \nabla u_i) &= G & \text{in } \Omega_i,\ i=1,2, \\ u_i &= u_{\mathrm{D},i} & \text{on } \Gamma_{\mathrm{D},i},\ i=1,2, \\ \kappa_i \dfrac{\partial u_i}{\partial \boldsymbol{n}} &= 0 & \text{on } \Gamma_{\mathrm{N},i},\ i=1,2, \\ \left\langle \kappa \dfrac{\partial u}{\partial \boldsymbol{n}} \right\rangle + \dfrac{1}{\eta}[u] &= \dfrac{\bar{f}}{\eta} + f & \text{on } \Gamma, \\ \left[\kappa \dfrac{\partial u}{\partial \boldsymbol{n}}\right] - \alpha\eta\Delta_\tau \langle u \rangle &= \alpha\eta\bar{g} + g & \text{on } \Gamma, \end{cases} \tag{2.1}$$

where $G \in \mathrm{L}^2(\Omega)$, $u_{\mathrm{D},i} \in \mathrm{H}_{00}^{1/2}(\Gamma_{\mathrm{D},i}) := \{v|_{\Gamma_{\mathrm{D},i}}, v \in \mathrm{H}^{1/2}(\partial\Omega_i), v|_{\Gamma\cup\Gamma_{\mathrm{N},i}} = 0\}$ for $i = 1, 2$, $f, \bar{f}, g, \bar{g} \in \mathrm{L}^2(\Gamma)$ and $\Delta_{\boldsymbol{\tau}}$ is the *Laplace-Beltrami operator* (see, e.g. [72]). In the sequel, we set $u_{\mathrm{D}} := (u_{\mathrm{D},1}, u_{\mathrm{D},2})$. Note that $f, \overline{f}$ and $g, \overline{g}$ correspond to two different scales appearing in the asymptotic model.

Remark 4 *This problem can be seen as a generalization of the following one studied in [10]:*

$$\begin{cases} -\operatorname{div}(\kappa_i \nabla u_i) &= G & \text{in } \Omega_i,\ i=1,2, \\ u_i &= u_{\mathrm{D},i} & \text{on } \Gamma_{\mathrm{D},i},\ i=1,2, \\ \kappa_i \dfrac{\partial u_i}{\partial \boldsymbol{n}} &= 0 & \text{on } \Gamma_{\mathrm{N},i},\ i=1,2, \\ \left\langle \kappa \dfrac{\partial u}{\partial \boldsymbol{n}} \right\rangle + \dfrac{1}{\eta}[u] &= 0 & \text{on } \Gamma, \\ \left[\kappa \dfrac{\partial u}{\partial \boldsymbol{n}}\right] &= 0 & \text{on } \Gamma. \end{cases}$$

Aim of the present work. At the continuous level, such a boundary problem can be analysed using *broken Sobolev spaces*. Their numerical implementation implies to double the degrees of freedom at the interface, which is not always possible in calculation codes such as FEniCS and FreeFem++. We mention here the work [9] of Allaire *et al.* in a related context of shape optimization of an interface where they overcome this difficulty by using a penalisation/extension method for the numerical approximation, without any error estimates.

In the present work, we aim to carry out the numerical analysis of the previous problem and provide *a priori* error estimates. However, our problem presents an additional difficulty: the presence of the small parameter η which appears at different scales in the transmission conditions.

We first point out that the classical discontinuous Galerkin method is not robust with respect to this small parameter. The conditioning of the associated linear system blows up when η tends to 0. The reason for this is that the solution of the limit problem, which is obtained when η tends to 0, does not belong to the same variational space. Therefore we propose a modification of this first method.

We are inspired by Nitsche's method, which was introduced in [91] to weakly impose Dirichlet boundary conditions. It was adapted by Hansbo and Hansbo in [70] for transmission problems with a non-conforming mesh. In [32], it was used for a scattering problem with Ventcel boundary conditions. It has to be noticed that in [32], there is also a small parameter η but it does not appear

at the order $\frac{1}{\eta}$ in the transmission conditions which makes the problem different. We propose here a method based on [79] to deal with these conditioning problems, adapted to Nitsche's method with Robin-Fourier conditions.

2.2 The continuous problem

2.2.1 Functional setting

Let $k \in \mathbb{N}^*$. It is useful to introduce the broken Sobolev space

$$V^k := \{v = (v_1, v_2) \in \mathrm{H}^k(\Omega_1) \times \mathrm{H}^k(\Omega_2)\}.$$

We assume Γ to be $\mathcal{C}^k$, $k \in \mathbb{N}$. Using [80] for example, we define the following subspace of V^k

$$V_\Gamma^k := \{v \in V^k; \langle v \rangle \in \mathrm{H}_0^1(\Gamma) \cap \mathrm{H}^k(\Gamma)\},$$

endowed with the norm

$$\|v\|_{V_\Gamma^k} := \left(\sum_{i=1}^{2} \|\kappa_i^{1/2} v_i\|^2_{\mathrm{H}^k(\Omega_i)^d} + \|(\alpha\eta)^{1/2} \langle v \rangle\|^2_{\mathrm{H}^k(\Gamma)^d} + \|\eta^{-1/2}[v]\|^2_{\mathrm{H}^{k-1}(\Gamma)} \right)^{1/2}$$

is also a Hilbert space. Let

$$V^k_{\Gamma,u_\mathrm{D}} := \{v \in V_\Gamma^k; v_i = u_{\mathrm{D},i} \text{ on } \Gamma_{\mathrm{D},i}\} \quad \text{and} \quad V^k_{\Gamma,0} := \{v \in V_\Gamma^k; v_i = 0 \text{ on } \Gamma_{\mathrm{D},i}\}.$$

Finally, in the case $k = 1$, it is useful to introduce:

$$\|v\| := \left(\sum_{i=1}^{2} \|\kappa_i^{1/2} \nabla v_i\|^2_{\mathrm{L}^2(\Omega_i)^d} + ||(\alpha\eta)^{1/2} \nabla_\tau \langle v \rangle||^2_{\mathrm{L}^2(\Gamma)^d} \right)^{1/2}$$

and

$$|||v||| := \left(\|v\|^2 + \|\eta^{-1/2}[v]\|^2_{\mathrm{L}^2(\Gamma)} \right)^{1/2}.$$

Due to the trace theorem on Γ, the space $V^1_{\Gamma,0}$ endowed with the norm $|||\cdot|||$ is a Hilbert space.

Remark 5 *Let us discuss on the necessity of the assumption $u_{\mathrm{D},i} \in \mathrm{H}^{1/2}_{00}(\Gamma_{\mathrm{D},i})$.*

Let u be the strong solution of (2.1) that we suppose $V^2_{\Gamma,u_\mathrm{D}}$ and $v \in V^1_{\Gamma,0}$. Using Green's formula on the boundary Γ (see, e.g., [104, Proposition 2.58]), we obtain

$$\int_\Gamma - \mathrm{div}_\tau(\nabla_\tau \langle u \rangle) \langle v \rangle \, \mathrm{d}s = \int_\Gamma \nabla_\tau \langle u \rangle \cdot \langle v \rangle \, \mathrm{d}s - \int_{\partial\Gamma} \langle v \rangle \nabla_\tau \langle u \rangle \cdot \boldsymbol{\tau} \, \mathrm{d}l,$$

where $\boldsymbol{\tau}$ is the unit tangent vector to Γ, normal to $\partial\Gamma$ and $\mathrm{d}l$ is the $(d-2)$ dimensional measure along $\partial\Gamma$. Then the second term of the right hand-side of the previous formula vanishes since $\langle v \rangle = 0$ on $\partial\Gamma$ ($\langle v \rangle \in \mathrm{H}^1_0(\Gamma)$).

Let $U_{\mathrm{D,i}} \in \mathrm{H}^1(\Omega_i)$ be an extension of $u_{\mathrm{D,i}}$. In order to have $u - U_{\mathrm{D}} \in V^1_{\Gamma,0}$, the extension needs to verify:

$$U_{\mathrm{D,i}} = u_{\mathrm{D,i}} \text{ on } \Gamma_{\mathrm{D,i}}, \quad U_{\mathrm{D,i}} = 0 \text{ on } \Gamma \cup \Gamma_{\mathrm{N,i}}.$$

This is guaranteed due to $u_{\mathrm{D,i}} \in \mathrm{H}^{1/2}_{00}(\Gamma_{\mathrm{D,i}})$.

Remark 6 *In the case where $\overline{\Gamma} \cap \overline{\Gamma}_{\mathrm{D}} = \emptyset$ and $\overline{\Gamma} \cap \overline{\Gamma}_{\mathrm{N}} \neq \emptyset$, one assumes that the domain Ω is such that $\tau_\Gamma = \mathrm{n}_{\Gamma_{\mathrm{N}}}$ on $\partial\Gamma$, where τ_Γ is the unit tangent vector to Γ and normal to $\partial\Gamma$, and takes as functional space*

$$V^1_\Gamma = \{v \in V^1; \langle v \rangle \in \mathrm{H}^1(\Gamma), \}. \tag{2.2}$$

In the case with mixed boundary conditions that intersect the interface, that is $\overline{\Gamma} \cap \overline{\Gamma}_{\mathrm{D},j} \cap \overline{\Gamma}_{\mathrm{N},j} \neq \emptyset$, where $j \in \{1,2\}$, one also assumes $\tau_\Gamma = \mathrm{n}_{\Gamma_{\mathrm{N}}}$ on $\partial\Gamma$, and then considers

$$V^1_\Gamma = \{v \in V^1; \langle v \rangle \in \mathrm{H}^1(\Gamma), v_j = 0 \text{ on } \overline{\Gamma} \cap \overline{\Gamma}_{\mathrm{D},j} \cap \overline{\Gamma}_{\mathrm{N},j}\}.$$

Finally, in the case where $\overline{\Gamma} \cap \overline{\Gamma}_{\mathrm{D}} = \overline{\Gamma} \cap \overline{\Gamma}_{\mathrm{N}} = \emptyset$, one uses the functional space (2.2).

2.2.2 Variational formulation

For a fixed value of η, one defines the bilinear forms: for any $u, v \in V^1_\Gamma$,

$$\begin{aligned} b(u,v) &:= \sum_{i=1}^{2} \int_{\Omega_i} \kappa_i \nabla u_i \cdot \nabla v_i \,\mathrm{d}x + \int_\Gamma \alpha\eta \nabla_\tau \langle u \rangle \cdot \nabla_\tau \langle v \rangle \,\mathrm{d}s, \\ c(u,v) &:= \int_\Gamma \frac{1}{\eta}[u][v] \,\mathrm{d}s. \end{aligned}$$

Then, one considers the following variational formulation of Problem (2.1):

$$\text{Find } u \in V^1_{\Gamma,u_{\mathrm{D}}} \text{ such that } \forall v \in V^1_{\Gamma,0}, \quad a(u,v) = l(v), \tag{2.3}$$

where

$$\begin{aligned} a(u,v) &:= b(u,v) + c(u,v), \\ l(v) &:= \int_\Omega Gv \,\mathrm{d}x + \int_\Gamma \left(f[v] + g \langle v \rangle\right) \mathrm{d}s + \int_\Gamma \left(\frac{1}{\eta}\bar{f}[v] + \alpha\eta\bar{g} \langle v \rangle\right) \mathrm{d}s. \end{aligned}$$

We split the bilinear form $a(\cdot,\cdot)$ in order to isolate the term $c(\cdot,\cdot)$ which contains the factor η^{-1}. This blows up when $\eta \to 0$, leading to bad conditioning in the discrete case. How to tackle this difficulty is the core of this work.

In the next theorem we assume, without loss of generality, that $u_{\mathrm{D}} = 0$. Otherwise, consider $\tilde{u}_{\mathrm{D}} = (\tilde{u}_{\mathrm{D},1}, \tilde{u}_{\mathrm{D},2}) \in \mathrm{H}^1(\Omega_1) \times \mathrm{H}^1(\Omega_2)$ such that $\tilde{u}_{\mathrm{D},i} = u_{\mathrm{D},i}$ on $\Gamma_{\mathrm{D},i}$ and then define $\tilde{u} := u - \tilde{u}_{\mathrm{D}}$ which belongs to $V^1_{\Gamma,0}$. In that case, we study the equation that verifies $\tilde{u}$, where the right-hand side becomes $\tilde{G} := G + \mathrm{div}(\kappa_i \nabla \tilde{u}_{\mathrm{D,i}})$ in equation (2.1).

Theorem 2.2.1 (Well-posedness) If $G \in \mathrm{L}^2(\Omega)$, $f, \overline{f}, g, \overline{g} \in \mathrm{L}^2(\Gamma)$ and $u_{\mathrm{D}} = 0$, then Problem (2.3) has a unique solution $u \in V^1_{\Gamma,0}$. Furthermore, the following estimate holds:

$$|||u||| \leq C \max_{i=1,2} \kappa_i^{-1/2} \left(\|G\|_{\mathrm{L}^2(\Omega)} + \|g\|_{\mathrm{L}^2(\Gamma)} + \alpha\eta\|\bar{g}\|_{\mathrm{L}^2(\Gamma)}\right) + \eta^{1/2}\|f\|_{\mathrm{L}^2(\Gamma)} + \eta^{-1/2}\|\bar{f}\|_{\mathrm{L}^2(\Gamma)}, \tag{2.4}$$

with a constant $C > 0$ depending only on the domains Ω_1 and Ω_2.

PROOF. Clearly, $a(\cdot,\cdot)$ is bilinear and symmetric and $l(\cdot)$ is linear. Note that $a(\cdot,\cdot)$ is a scalar product on $V^1_{\Gamma,0}$, of corresponding norm $|||\cdot|||$, so it is continuous and coercive with respect to this norm, with continuity and coercivity constants equal to 1. As regards the continuity of $l(\cdot)$, we first note that the Poincaré inequality yields, for any $v \in V^1_{\Gamma,0}$, that

$$\|v_i\|_{0,\Omega_i} \leq C_P(\Omega_i)\kappa_i^{-1/2}\|\kappa_i^{1/2}\nabla v_i\|_{\mathrm{L}^2(\Omega_i)^d}, \quad i = 1,2,$$

while the trace theorem together with the Poincaré inequality yield:

$$\| \langle v \rangle \|_{\mathrm{L}^2(\Gamma)} \leq \frac{1}{2}\sum_{i=1}^{2} C_T(\Omega_i)\sqrt{1 + C_P(\Omega_i)^2}\kappa_i^{-1/2}\|\kappa_i^{1/2}\nabla v_i\|_{\mathrm{L}^2(\Omega_i)^d}.$$

The $|||\cdot|||$ - continuity of $l(\cdot)$ follows thanks to the Cauchy-Schwarz inequality:

$$|l(v)| \leq |||v||| \left(C \max_{i=1,2} \kappa_i^{-1/2} \left(\|G\|_{\mathrm{L}^2(\Omega)} + \|g\|_{\mathrm{L}^2(\Gamma)} + \alpha\eta\|\bar{g}\|_{\mathrm{L}^2(\Gamma)} \right) + \eta^{1/2}\|f\|_{\mathrm{L}^2(\Gamma)} + \eta^{-1/2}\|\bar{f}\|_{\mathrm{L}^2(\Gamma)} \right).$$

By virtue of the Lax-Milgram theorem, Problem (2.3) has a unique solution in $V^1_{\Gamma,0}$. Estimate (2.4) is classically obtained by testing the weak problem with $v = u$ and by using the previous bound. □

2.2.3 A remark on the limit problem as $\eta \to 0$ at the continuous level

Formally, by making η tend towards 0, Problem (2.1) becomes

$$\begin{cases} -\operatorname{div}(\kappa_i \nabla u_i^0) &= G & \text{in } \Omega_i,\ i = 1,2, \\ u_i^0 &= u_{\mathrm{D},i} & \text{on } \Gamma_{\mathrm{D},i},\ i = 1,2, \\ \kappa_i \dfrac{\partial u_i^0}{\partial \boldsymbol{n}} &= 0 & \text{on } \Gamma_{\mathrm{N},i},\ i = 1,2, \\ [u^0] &= \bar{f} & \text{on } \Gamma, \\ \left[\kappa \dfrac{\partial u^0}{\partial \boldsymbol{n}}\right] &= g & \text{on } \Gamma. \end{cases} \tag{2.5}$$

In this case we need more regularity on $\overline{f}$. We suppose that $\overline{f} \in \mathrm{H}^{1/2}_{00}(\Gamma)$. The natural functional space in order to study Problem (2.5) is the following affine space:

$$U_{\bar{f},u_{\mathrm{D}}} := \{v = (v_1, v_2) \in V^1; [v] = \bar{f} \text{ on } \Gamma; v_i = u_{\mathrm{D,i}} \text{ on } \Gamma_{\mathrm{D,i}}, i = 1,2\}.$$

Endowed with the norm $\|v\|_{U_0} := \displaystyle\sum_{i=1}^{2} \|\kappa_i^{1/2}\nabla v_i\|_{\mathrm{L}^2(\Omega_i)^d}$, the subspace

$$U_0 := \{v = (v_1, v_2) \in V^1; [v] = 0 \text{ on } \Gamma; v_i = 0 \text{ on } \Gamma_{\mathrm{D},i}, i = 1,2\}$$

is a Hilbert space. Hence one can prove that Problem (2.5) has a unique solution $u^0 \in U_{\bar{f}}$: the proof is a mere adaptation of that of the well-posedness of a diffusion problem with mixed boundary conditions, where instead of the Dirichlet boundary condition we have the jump condition in the functional space. Indeed, it is sufficient to use a lifting argument for the non-homogeneous

transmission condition $[u] = \overline{f}$ on Γ and the Dirichlet boundary conditions. More precisely, let $\tilde{u}_{\mathrm{D}} = (\tilde{u}_{\mathrm{D},1}, \tilde{u}_{\mathrm{D},2}) \in V^1$, such that $\tilde{u}_{\mathrm{D},i} = u_{\mathrm{D,i}}$ on $\Gamma_{\mathrm{D},i}$ and $\tilde{u}_{\mathrm{D},i} = 0$ on $\partial\Omega_i \setminus \Gamma_{\mathrm{D},i}$. Let also $\chi = (\chi_1, \chi_2) \in V^1$, such that $[\chi] = \overline{f}$ on Γ and $\chi_i = 0$ on $\Gamma_{\mathrm{D},i}$. Then, we define $\varphi = \tilde{u}_{\mathrm{D}} + \chi \in V^1$ which verifies $\varphi_i = u_{\mathrm{D},i}$ on $\Gamma_{\mathrm{D},i}$ and $[\varphi] = \overline{f}$ on Γ. Then, we conclude by applying the Lax-Milgram theorem to the problem satisfied by $w^0 := u^0 - \varphi$ which belongs to U_0.

Note that the functional spaces associated to Problem (2.1) and Problem (2.5) are different, which suggests numerical difficulties when η tends towards 0. This last point is discussed in the following section.

2.3 Discontinuous Lagrange finite elements approximation

For the sake of simplicity, one assumes that the domain Ω is a polyhedron in $\mathbb{R}^d$ and Γ a finite union of hyperplanes. Let $\mathcal{T}_h$ be a regular simplicial mesh of Ω: there exists a parameter $\sigma > 0$ such that, for all $K \in \mathcal{T}_h$,

$$\frac{h_K}{\rho_K} \leq \sigma,$$

where h_K is the diameter of K and ρ_K is the diameter of the largest ball contained in K. The parameter σ is called the *mesh regularity parameter*. We define $h := \max_{K\in\mathcal{T}_h} h_K$ the mesh size. Assume that the mesh is body-fitted with the interface Γ, i.e., each $K \in \mathcal{T}_h$ is a subset of only one set Ω_i. Finally, we define $\mathcal{T}_h^i := \{K \in \mathcal{T}_h; K \subset \Omega_i\}$, $i = 1, 2$.

Let $\mathcal{F}_h$ be the set of faces of $\mathcal{T}_h$, $\mathcal{F}_{h,\Gamma}$ the set of faces situated on Γ and $\mathcal{T}_{h,\Gamma}$ the set of elements which have one face on Γ. Let h_F be the diameter of the face $F \in \mathcal{F}_{h,\Gamma}$ (in $d = 2$, h_F coincides with the 1-Hausdorff measure of F). Let $k \in \mathbb{N}^*$ and let

$$P_h^k := \{v_h \in V_\Gamma^1; v_h|_{\Omega_i} \in \mathcal{C}(\Omega_i), v_h|_K \in \mathbb{P}^k, \forall K \in \mathcal{T}_h\} \quad \text{and} \quad P_{h,0}^k := P_h^k \cap V_{\Gamma,0}^1.$$

In the sequel, we make the additional assumption that the Dirichlet condition u_{D} belongs to $\mathrm{H}^{k+1/2}(\Gamma_{\mathrm{D},1}) \times \mathrm{H}^{k+1/2}(\Gamma_{\mathrm{D},2})$. Let $u_{\mathrm{D},h} \in P_h^k$ denote a nodal interpolation of u_{D} on Γ_{D}. An intuitive and natural discrete formulation of Problem (2.1) is then:

$$\text{Find } w_h \in P_h^k, \text{ such that } w_h = u_{\mathrm{D},h} \text{ on } \Gamma_{\mathrm{D}} \text{ and } a(w_h, v_h) = l(v_h), \quad \forall v_h \in P_{h,0}^k. \tag{2.6}$$

The aim of this section is first to prove the well-posedness of the discrete formulation and to study the convergence as h tends towards 0 of its solution towards the solution of the continuous problem, and then to study through numerical experiments the behaviour of the discrete scheme, in particular for small values of η.

2.3.1 Analysis of the discrete formulation

Since $P_{h,0}^k \subset V_{\Gamma,0}^1$, taking $v = v_h \in P_{h,0}^k$ in the variational formulation (2.3) immediately yields the consistency of the discrete problem, stated in the next lemma.

Lemma 2.3.1 (Consistency of finite element approximation)**.** *Let u be a smooth solution to* (2.1)*. Then*

$$a(u, v_h) = l(v_h), \quad \forall v_h \in P^k_{h,0}. \tag{2.7}$$

The coercivity and continuity are directly inherited from the continuous problem, which permits to obtain the following lemma.

Lemma 2.3.2 (Discrete coercivity and continuity)**.** *One has that*

$$a(v_h, v_h) = |||v_h|||^2, \quad \forall v_h \in P^k_{h,0} \tag{2.8}$$

and

$$a(w_h, v_h) \leq |||w_h|||\,|||v_h|||, \quad \forall w_h, v_h \in P^k_{h,0}. \tag{2.9}$$

Thus, thanks to the Lax-Milgram theorem, we obtain the following result.

Theorem 2.3.3 Problem (2.6) has a unique solution $w_h \in P^k_h$.

Next, in order to obtain the convergence rate of the approximation error, one needs an interpolation estimate. Similarly to [70] but without cut elements (the mesh being aligned with the interface), for each $k \in \mathbb{N}^*$, we consider

$$(\mathcal{I}^k_h)^* v = (\mathcal{I}^k_h v_1)\mathbb{1}_{\Omega_1} + (\mathcal{I}^k_h v_2)\mathbb{1}_{\Omega_2},$$

where $\mathcal{I}^k_h$ is the standard nodal interpolation operator from $\mathrm{H}^{k+1}(\Omega)$ to P^k_h. Using standard interpolation estimates (see [42, Theorem 3.1.6], [26, Theorem 4.4.20]) and the triangle inequality, one gets the following interpolation result.

Lemma 2.3.4 (Polynomial approximation)**.** *For any $k \in \mathbb{N}^*$ and any $v \in V^{k+1}_{\Gamma,0}$, there exists a constant $C_{\mathrm{ip}} > 0$ independent of $h, \eta, \alpha, \kappa_1$ and κ_2 such that:*

$$|||v - (\mathcal{I}^k_h)^* v||| \leq C_{\mathrm{ip}} h^k \|v\|_{V^{k+1}_\Gamma}. \tag{2.10}$$

Furthermore, if in addition $[v] \in \mathrm{H}^{k+1}(\Gamma)$, then we have

$$|||v - (\mathcal{I}^k_h)^* v||| \leq C_{\mathrm{ip}} h^k \left(\sum_{i=1}^{2} \|\kappa_i^{1/2} v_i\|^2_{\mathrm{H}^{k+1}(\Omega_i)} + \|(\alpha\eta)^{1/2} \langle v \rangle\|^2_{\mathrm{H}^{k+1}(\Gamma)} + h^2 \|\eta^{-1/2}[v]\|^2_{\mathrm{H}^{k+1}(\Gamma)} \right)^{1/2}. \tag{2.11}$$

Remark 7 *Note that if $v \in V^{k+1}_{\Gamma,0}$, then $\langle v \rangle \in \mathrm{H}^{k+1}$ and $[v] \in \mathrm{H}^k(\Gamma)$, that is why we need to take $[v] \in \mathrm{H}^{k+1}(\Gamma)$ to have that $v_1, v_2 \in \mathrm{H}^{k+1}(\Gamma)$.*

Proof of Lemma 2.3.4. Let $v \in V^{k+1}_{\Gamma,0}$. Let $K^i \in \mathcal{T}^i_h$, with $1 \leq i \leq 2$ and $F \in \mathcal{F}_{h,\Gamma}$. By standard interpolation estimates (e.g. [59, Theorem 1.103], [26, Theorem 4.4.20]), there exists a constant $C_{\mathrm{ip}} > 0$ independent of $h, \eta, \alpha, \kappa_1$ and κ_2 such that:

$$\begin{aligned} \|\nabla(v_i - \mathcal{I}^k_h v_i)\|_{\mathrm{L}^2(K^i)^d} &\leq C_{\mathrm{ip}} h^k_{K^i} \|v_i\|_{\mathrm{H}^{k+1}(K^i)}, \\ \|[v] - \mathcal{I}^k_h [v]\|_{\mathrm{L}^2(F)} &\leq C_{\mathrm{ip}} h^k_F \|[v]\|_{\mathrm{H}^k(F)}, \\ \|\nabla_\tau(\langle v \rangle - \mathcal{I}^k_h \langle v \rangle)\|_{\mathrm{L}^2(F)^d} &\leq C_{\mathrm{ip}} h^k_F \| \langle v \rangle \|_{\mathrm{H}^{k+1}(F)}. \end{aligned}$$

Combining these inequalities leads to:

$$\begin{aligned}&|||v-(\mathcal{I}_h^k)^* v|||\\ &\quad\le C_{\rm ip}h^k\left(\sum_{i=1}^{2}\sum_{K^i\in\mathcal{T}_h^i}\|\kappa_i^{1/2}v_i\|^2_{\mathrm{H}^{k+1}(K^i)}+\sum_{F\in\mathcal{F}_{h,\Gamma}}\left(\|\eta^{-1/2}[v]\|^2_{\mathrm{H}^k(F)}+\|(\alpha\eta)^{1/2}\langle v\rangle\|^2_{\mathrm{H}^{k+1}(F)}\right)\right)^{1/2}\end{aligned}$$

which proves (2.10).

Since $[v]\in \mathrm{H}^{k+1}(\Gamma)$, one also has

$$\|[v]-\mathcal{I}_h^k[v]\|_{\mathrm{L}^2(F)}\le C_{\rm ip}h^{k+1}\|[v]\|_{\mathrm{H}^{k+1}(F)}$$

which, together with the previous inequalities, proves (2.11). □

Therefore, Céa's lemma yields the following *a priori* error estimate. For this purpose, we introduce two liftings of $u_{\rm D}$ and $u_{{\rm D},h}$, denoted by $\tilde{u}_{\rm D}$ and $\tilde{u}_{{\rm D},h}$, respectively, such that $\tilde{u}_{\rm D}=u_{\rm D}$, $\tilde{u}_{{\rm D},h}=u_{{\rm D},h}$ on $\Gamma_{\rm D}$ and $\tilde{u}_{\rm D}=\tilde{u}_{{\rm D},h}=0$ on $\partial\Omega\setminus\Gamma_{\rm D}$.

Theorem 2.3.5 (Error estimate) Let $k\in\mathbb{N}^*$ and assume that the solution u of (2.3) belongs to V_Γ^{k+1}. We suppose $\tilde{u}_{\rm D}\in V^{k+1}$ and $\tilde{u}_{{\rm D},h}\in P_h^k$. There exists a constant $C_{\rm e}=C_{\rm ip}>0$ independent of h,η,α,κ_1 and κ_2 such that

$$\begin{aligned}|||\tilde{u}-\tilde{w}_h||| &\le C_{\rm e}h^k\|\tilde{u}\|_{V^k_{\Gamma,0}}\\ &= C_{\rm e}h^k\left(\sum_{i=1}^{2}\|\kappa_i^{1/2}\tilde{u}_i\|^2_{\mathrm{H}^{k+1}(\Omega_i)}+\|(\alpha\eta)^{1/2}\langle\tilde{u}\rangle\|^2_{\mathrm{H}^{k+1}(\Gamma)}+\|\eta^{-1/2}[\tilde{u}]\|^2_{\mathrm{H}^k(\Gamma)}\right)^{1/2}\end{aligned}\qquad(2.12)$$

where $\tilde{u}_i:=u_i-\tilde{u}_{i,\rm D}$, $\tilde{u}:=u-\tilde{u}_{\rm D}$, $\tilde{w}_h:=w_h-\tilde{u}_{{\rm D},h}$ with w_h the solution of (2.6).

Remark 8 *The regularity condition $u\in V_\Gamma^{k+1}$ is a technical assumption necessary to obtain the error estimates. We discuss next in which this assumption is satisfied. On the one hand, the presence of the Ventcel condition has a regularising effect that has been studied for the continuous problem in [25] and in a finite element framework in [80]. The idea of [25] is to rewrite the boundary problem as a non-local problem involving lower order pseudodifferential operators (Dirichlet-to-Neumann maps) at the boundary where the Ventcel condition is applied. Thus this regularity is well obtained if the Ventcel condition is applied to the whole boundary (i.e. $\Omega=\Omega_1$, $\Omega_2=\emptyset$ and $\Gamma=\partial\Omega$). If the interface is disjoint from the edge of the domain, this regularity is also true, as the method of [25] applies directly. On the other hand, if the interface Γ intersects the outer edge, as in the Figure 2.1, the regularity is usually not reasonable. A singularity can develop at the intersection points. Although these singular solutions appear in the general case, they are absent for certain right-hand side terms satisfying a compatibility condition (see [24]).*

Remark 9 *We see that if η is too small with respect to h^2, the third term on the right in* (2.12) *blows up. This is an artefact of the badly scaled term c.*

2.3.2 Numerical tests

Numerical implementation

We consider the two dimensional case for all the numerical simulations. Moreover, for the sake of simplicity, we consider only the case $k = 1$. The broken Sobolev space $P^k_{h,0}$ can be seen as the usual FE space on Ω, enriched with basis functions associated to the nodes situated on the interface. Thus, the degrees of freedom on Γ are doubled. In order to implement this space, let N_Γ be the number of vertices belonging to Γ and N the number of vertices in the whole mesh of Ω. For each vertex belonging to Γ, of global index i^p_Γ, we create a copy of new index $\tilde{i}^p_\Gamma = N + p$, where p is the p^{th} vertex of Γ in ascending order with respect to the index i^p_Γ of the global mesh, i.e. $i^1_\Gamma < \ldots < i^p_\Gamma < \ldots < i^{N_\Gamma}_\Gamma$; for instance, $p = 1$ and $p = N_\Gamma$ for the minimum and the maximum index i^p_Γ, respectively. By convention, we keep the original index i^p_Γ for a vertex situated on the interface Γ when we look at it from $K \in \mathcal{T}^1_h$ and we use $\tilde{i}^p_\Gamma$ when we look at it from $K \in \mathcal{T}^2_h$. Now, in the new mesh structure, we allow for duplicate nodes on the interface (same position but different indices in the global mesh). So, if we ignore the Dirichlet boundary conditions, the linear system can be written as $Ax = b$, where A is a square matrix of size $(N + N_\Gamma)$.

As regards the post-processing, we first reconstruct two vectors of size N: U_1 contains the first N values whereas U_2 contains the first N values, but those corresponding to the index i_Γ are replaced by the values corresponding to $\tilde{i}_\Gamma$. Then, we get u_1 and u_2 by restricting U_1 and U_2 to Ω_1 and Ω_2, respectively. The same idea can be employed for a higher polynomial degree $k > 1$ (of course, the indexing will be different due to the additional degrees of freedom).

Finally we precise that all the numerical simulations presented in this chapter were carried out in `C++`, with PETSc as linear algebra library (see [17, 18]).

Convergence of the method with respect to the mesh size h

In this subsection, the small parameter η is given and fixed. We present some numerical tests in order to validate the error estimate of Theorem 2.3.5 with respect to h. We consider the two following test-cases.

Case 1. We consider the following configuration with mixed boundary conditions (Dirichlet and Neumann): let $\Omega = [0, 1] \times [0, 1]$, where $\Omega_1 = (-0.5, 0.5) \times (-0.5, 0)$ and $\Omega_2 = (-0.5, 0.5) \times (0, 0.5)$ and with boundaries

$$\Gamma = \{y = 0\}, \quad \Gamma_{\mathrm{D},1} = \{(x - 0.5)(x + 0.5) = 0, y \in (-0.5, 0)\}, \quad \Gamma_{\mathrm{N},1} = \{y = -0.5, x \in (-0.5, 0.5)\}$$

and

$$\Gamma_{\mathrm{D},2} = \{(x - 0.5)(x + 0.5) = 0, y \in (0, 0.5)\}, \quad \Gamma_{\mathrm{N},2} = \{y = 0.5, x \in (-0.5, 0.5)\},$$

as illustrated in Figure 2.2.

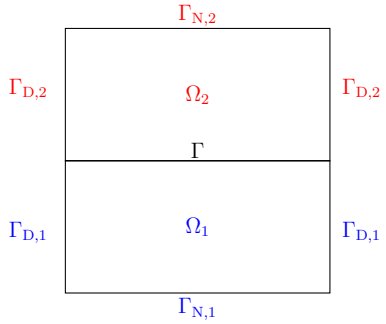

Figure 2.2: Geometry for case 1

We consider the exact solution:

$$u_1(x,y) = \frac{1}{\kappa_1}x^2(e^{y+0.5} - y) \quad \text{and} \quad u_2(x,y) = \frac{1}{\kappa_2}e^x(e^{y-0.5} - y),$$

with the corresponding source term G and

$$f(x,y) = \frac{1}{2}x^2(e^{0.5} - 1) + \frac{1}{2}e^x(e^{-0.5} - 1),$$

$$\bar{f}(x,y) = \frac{1}{\kappa_1}x^2e^{0.5} - \frac{1}{\kappa_2}e^{x-0.5},$$

$$g(x,y) = x^2(e^{0.5} - 1) - e^x(e^{-0.5} - 1.)$$

and

$$\bar{g}(x,y) = -\frac{1}{2}\alpha\eta(\frac{2}{\kappa_1}e^{0.5} + \frac{1}{\kappa_2}e^{x-0.5}).$$

We choose $\kappa_1 = 10^{-3}$, $\kappa_2 = 1$, $\eta = 10^{-2}$ and $\alpha = 10^2$. We observe that the method copes well with the case of highly discontinuous coefficients κ_1 and κ_2 when using the arithmetic mean on the interface and not a weighted mean (as employed in [57, 70, 31] for similar problems).

Case 2. As a second example, we consider a curved interface; even if Γ is now different from Γ_h, with a fine meshing at the interface we should retrieve a good convergence (at least for $k = 1$). Let $\Omega = (-1,1) \times (-0.5,0.5)$, $\Omega_2 = \{(x,y) \in \Omega, x \geq 0, x^2 + y^2 \geq 0.5^2\}$, $\Omega_1 = \Omega \setminus \Omega_2$ with an interface given in polar coordinates by

$$\Gamma = \left\{(0.5\cos\theta, 0.5\sin\theta); \theta \in \left[-\frac{\pi}{2}, \frac{\pi}{2}\right]\right\}$$

and with $\partial\Omega_N = \emptyset$, see Figure 2.3.

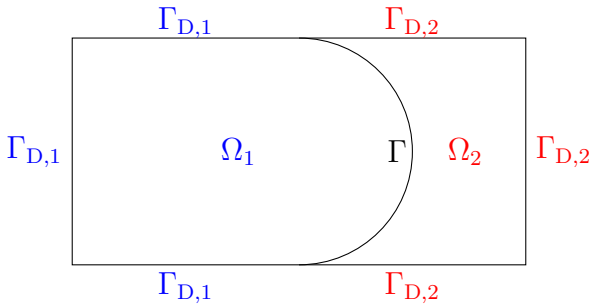

Figure 2.3: Geometry for case 2

We consider the following exact solution:

$$u_1(x,y) = y\mathrm{e}^x \quad \text{and} \quad u_2(x,y) = x\mathrm{e}^y,$$

with the corresponding source term G and with

$$f(x, y = x\mathrm{e}^y(\kappa_1 + \kappa_1 y) + y\mathrm{e}^x(\kappa_2 + \kappa_2 x),$$

$$\bar{f}(x,y) = x\mathrm{e}^y - y\mathrm{e}^x,$$

$$g(x,y) = 2\kappa_2 y\mathrm{e}^x(x+1) - 2\kappa_1 x\mathrm{e}^y(y+1)$$

and

$$\bar{g}(x,y) = -2y\mathrm{e}^x(y^2 - 3x - 1) - 2x\mathrm{e}^y(x^2 - 3y - 1).$$

We choose here $\eta = \kappa_1 = \kappa_2 = \alpha = 1$.

Numerical results. The energy error $e := |||\tilde{u} - \tilde{w}_h|||$ is split into three parts, $e^2 = e_g^2 + e_\tau^2 + e_j^2$ where

- $e_g := \sum_{i=1}^2 \|\kappa_i^{1/2}(\nabla\tilde{u}_i - \nabla\tilde{w}_{h,i})\|_{\mathrm{L}^2(\Omega_i)^d}$ is the gradient error,
- $e_\tau := \|(\alpha\eta)^{1/2}\langle\nabla_\tau\tilde{u} - \nabla_\tau\tilde{w}_h\rangle\|_{\mathrm{L}^2(\Gamma)^d}$ is the tangential error on the interface Γ,
- $e_j := \|\eta^{-1/2}[\tilde{u} - \tilde{w}_h]\|_{\mathrm{L}^2(\Gamma)}$ is the weighted jump error on Γ.

We validate below the convergence with respect to h. For the first case, h varies between 1.4×10^{-3} and 1.17×10^{-1} (which corresponds to 1,000,000 and 144 nodes, respectively) and the energy error e varies between 0.5 and 43.9. For the second case, h varies between 2.1×10^{-3} and 1.1×10^{-1} (2,617,675 and 484 nodes, respectively) and the energy error e varies between 5.4×10^{-3} and 6.1×10^{-2}. Note that in the first example, the mesh is structured and therefore $h = \sqrt{2}N^{-1/2}$, whereas in the second example, the mesh is unstructured since the interface is curved and our mesh is aligned with the discrete interface. So in this case, we only have $\mathcal{O}(h) = \mathcal{O}(N^{-1/2})$ and we plot the errors with respect to $N^{-1/2}$ in this case. In order to use a cartesian mesh in the second example, one could employ a NXFEM type method, see [70, 31] for example.

We observe in Figure 2.4 that in both cases the convergence rate for the energy error e is $\mathcal{O}(h)$, as stated in Theorem 2.3.5. We obtained similar results for the errors e_g and e_τ.

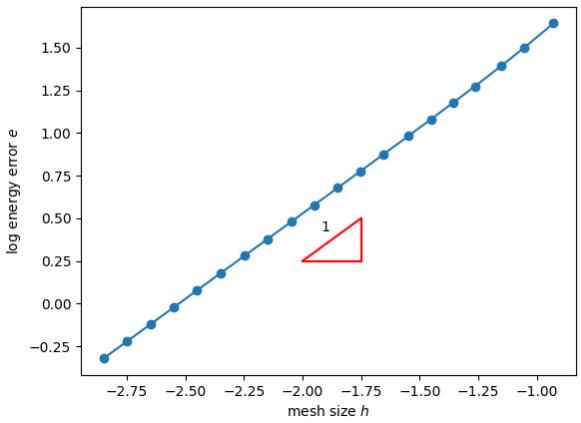

(a) Case 1 with $\eta = 10^{-2}$

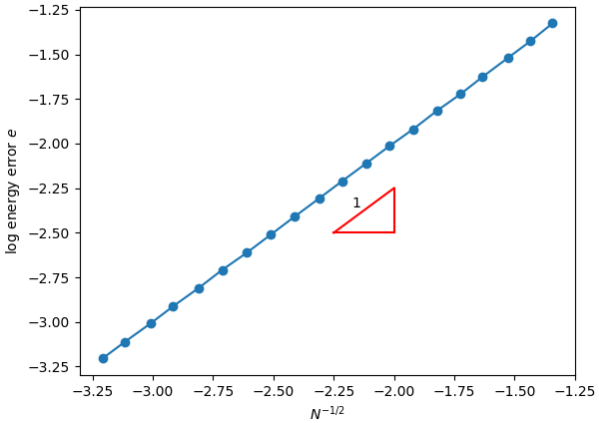

(b) Case 2 with $\eta = 1$

Figure 2.4: Logarithm plot of the energy error e with respect to the mesh size h

Meanwhile, notice that the convergence rate for the jump error e_j is $\mathcal{O}(h^2)$, as shown in Figure 2.5. Note that in this case, the gradient error e_g is larger than the jump error e_j, that is why e is of order one.

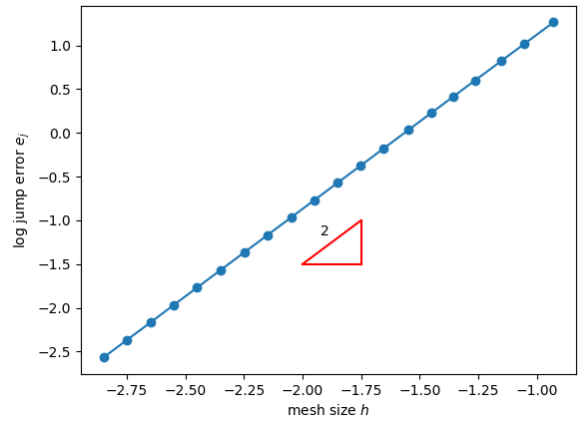

(a) Case 1 with $\eta = 10^{-2}$

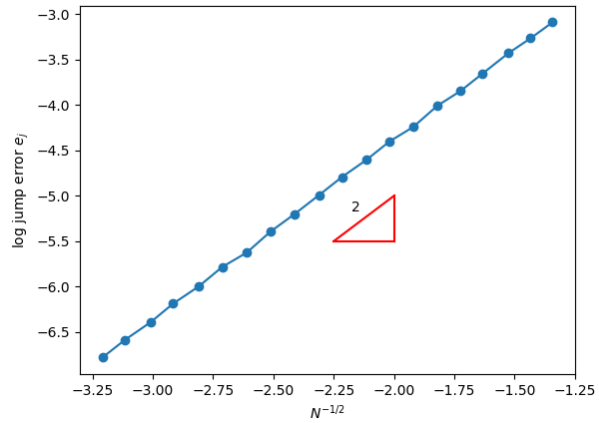

(b) Case 2 with $\eta = 1$

Figure 2.5: Logarithm plot of the jump error e_j with respect to the mesh size h

The numerical convergence rates are summarized in Table 2.1.

	Case 1	Case 2
e_g	1.06	1.00
e_τ	1.00	1.01
e_j	1.99	1.98
e	1.01	1.00

Table 2.1: Convergence rate of each error for the Lagrange discontinuous finite element method

Convergence with respect to η

As previously explained, when η tends towards 0 the transmission boundary condition changes to

$$[u^0] = \bar{f} \text{ on } \Gamma. \tag{2.13}$$

It is then expected to encounter some numerical issues in the limit, since condition (2.13) is included in the functional space whereas our Robin's type interface condition cannot be included in the functional space. In order to illustrate this point, we fix h (which takes different values for each test case) and we let η vary. We can observe in Figure 2.6 that the energy error e blows up as η decreases towards 0. This is due in particular to the jump error e_j, as shown in Figure 2.7. One can see in Figure 2.8 that the tangential gradient error e_τ does not blow up as $\eta \to 0$ (and the same behaviour occurs for the gradient error e_g).

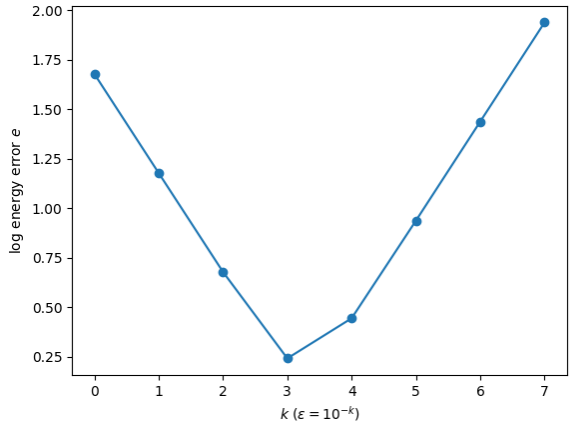

(a) Case 1 with $h = 1.4 \times 10^{-2}$

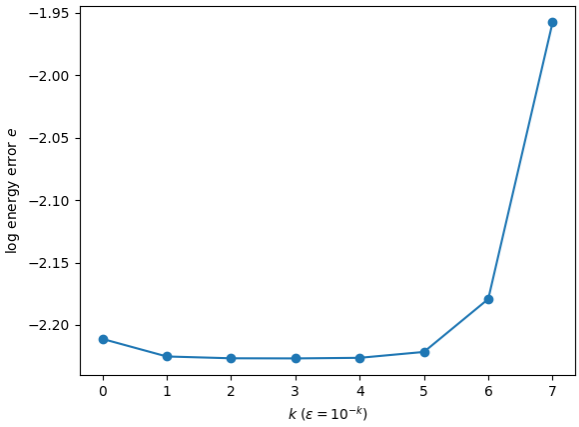

(b) Case 2 with $h = 1.7 \times 10^{-2}$

Figure 2.6: Logarithm plot of the energy error e with respect to η

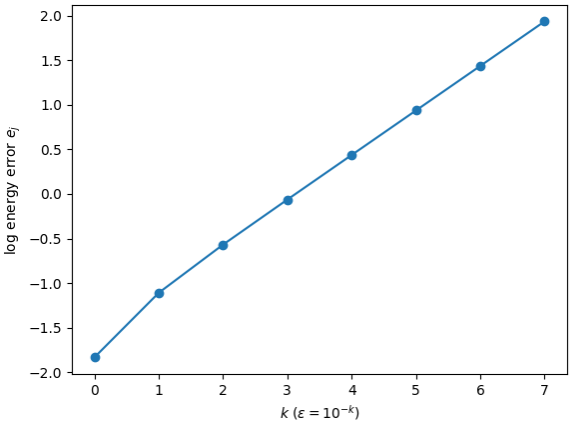

(a) Case 1 with $h = 1.4 \times 10^{-2}$

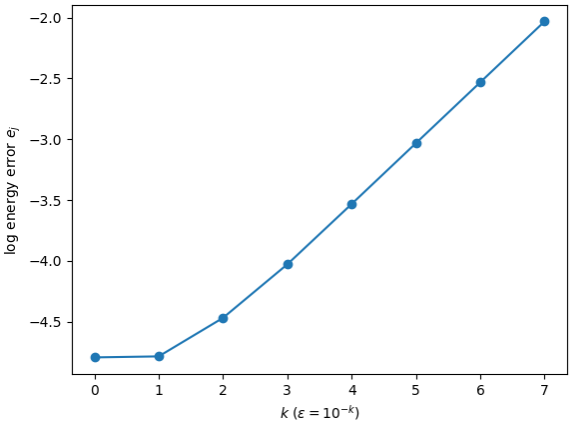

(b) Case 2 with $h = 1.7 \times 10^{-2}$

Figure 2.7: Logarithm plot of the jump error e_j with respect to η

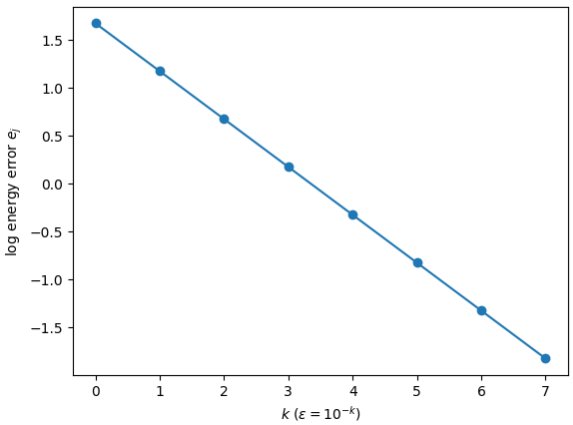

(a) Case 1 with $h = 1.4 \times 10^{-2}$

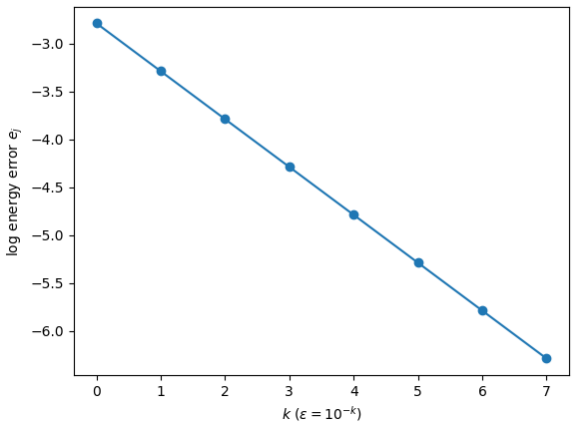

(b) Case 2 with $h = 1.7 \times 10^{-2}$

Figure 2.8: Logarithm plot of the tangential gradient error e_τ with respect to η

Conditioning

We are now interested in the conditioning of the discrete problem in order to explain the bad behaviour of the method when η is too small. We first underline that this has been observed in [79] by Juntunen and Stenberg for the model problem

$$\begin{cases} -\operatorname{div}(\kappa \nabla u) &= G & \text{in } \Omega, \\ \kappa \dfrac{\partial u}{\partial \boldsymbol{n}} &= -\dfrac{1}{\eta} u + \dfrac{\bar{f}}{\eta} + f & \text{on } \Gamma. \end{cases}$$

In this case, they observed that the condition number depends on the value of η as follows:

$$\text{cond} = \mathcal{O}(h^{-2} + (\eta h)^{-1}),$$

which leads to

$$\text{cond} = \begin{cases} \mathcal{O}(h^{-2}) & \text{if } \eta \geq Ch \\ \mathcal{O}((\eta h)^{-1}) & \text{if } \eta \leq Ch \end{cases}$$

for some $C > 0$.

For our problem, we also observe that the condition number (computed as the ratio of the largest singular value to the smallest) for the two previous test-cases depends on η, as shown in Figure 2.9. We considered a fixed value of h, the same parameters as in the previous subsection and plotted the condition number in decimal log scale with respect to $k = -\log_{10} \eta$.

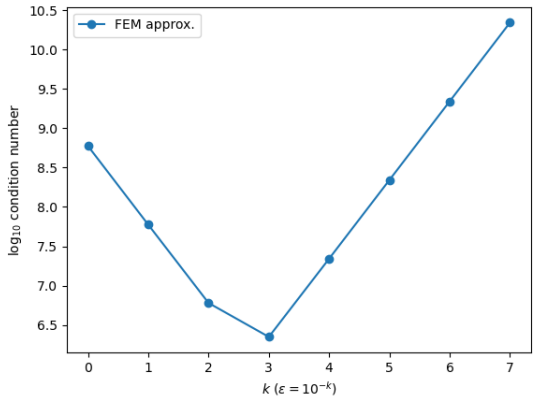

(a) Condition number of case 1 with $h = 1.4 \times 10^{-2}$

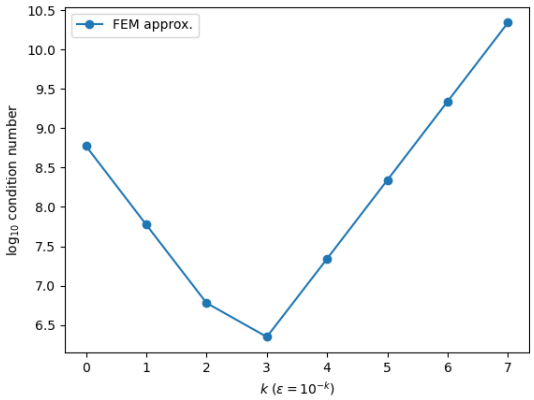

(b) Condition number of case 2 with $h = 5 \times 10^{-2}$

Figure 2.9: Logarithm plot of the condition number for the two test-cases with respect to η

Despite the consistency property and the optimal convergence with respect to h (at fixed η), the discrete problem gets ill-conditioned when η tends towards 0. Therefore, we propose below another numerical method, which is consistent and coercive, but equally well-conditioned and convergent with respect to η.

2.4 Modified Nitsche's type formulation

The Nitsche method was originally designed for the weak imposition of Dirichlet boundary conditions in [91]. It was later adapted in [70] to transmission conditions where the mesh is not necessarily aligned with the interface, leading to NXFEM, Nitsche's extended finite element method. The latter was used in [32] to deal with non-standard transmission conditions involving the Laplace-Beltrami operator.

The main difference between the model problem of [32] and ours is that in [32], the authors considered a simpler jump condition $[u] = \bar{f}$ on Γ, which can be treated by adding to the classical bilinear form the Laplace-Beltrami term. Meanwhile, we consider here a transmission condition of Robin type, involving both the jump and the mean of the normal flux:

$$\left\langle \kappa \frac{\partial u}{\partial \boldsymbol{n}} \right\rangle = -\frac{1}{\eta}[u] + \frac{1}{\eta}\bar{f} + f \quad \text{on } \Gamma. \tag{2.14}$$

Therefore, we have to adapt the standard bilinear form used in Nitsche's method.

The general idea of stabilized methods is to add positive (and often, consistent) terms in order to enhance the discrete coercivity with respect to the new energy norm. Here, the issue is not the loss of coercivity but the dependence on η, due to the presence in the energy norm of the jump term, which is multiplied by $\frac{1}{\eta}$. So contrary to stabilized methods, we propose here to subtract

a positive term multiplied by a stabilisation parameter depending on both η and h, in view of improving the constant in front of the jump term.

Thus, in order to obtain a consistent and symmetric formulation, we introduce the bilinear and linear forms, defined for any $u_h \in P_h^k$, $v_h \in P_{h,0}^k$ by

$$\begin{aligned} a_h(u_h, v_h) &:= a(u_h, v_h) - \sum_{F \in \mathcal{F}_{h,\Gamma}} \beta_F \left(\left\langle \kappa \frac{\partial u_h}{\partial \boldsymbol{n}} \right\rangle + \frac{1}{\eta}[u_h], \left\langle \kappa \frac{\partial v_h}{\partial \boldsymbol{n}} \right\rangle + \frac{1}{\eta}[v_h] \right)_{\mathrm{L}^2(F)}, \\ l_h(v_h) &:= l(v_h) - \sum_{F \in \mathcal{F}_{h,\Gamma}} \beta_F \left(f + \frac{1}{\eta} \bar{f}, \left\langle \kappa \frac{\partial v_h}{\partial \boldsymbol{n}} \right\rangle + \frac{1}{\eta}[v_h] \right)_{\mathrm{L}^2(F)}, \end{aligned}$$

where the parameter $\beta_F > 0$ will be chosen later. We then consider the following Nitsche's type formulation of Problem (2.1):

$$\text{Find } u_h \in P_h^k \text{ such that } u_h = u_{\mathrm{D},h} \text{ on } \Gamma_{\mathrm{D}} \text{ and } a_h(u_h, v_h) = l_h(v_h), \quad \forall v_h \in P_{h,0}^k. \tag{2.15}$$

2.4.1 Analysis of the discrete formulation

The consistency is straightforward, thanks to (2.7) and to the fact that the transmission condition (2.14), which is weakly imposed in the new formulation, is also strongly satisfied by the continuous solution.

Lemma 2.4.1 (Consistency of Nitsche's formulation)**.** *Let u be a smooth solution to* (2.1) *and $\beta_F \in \mathbb{R}$, for any $F \in \mathcal{F}_{h,\Gamma}$. Then*

$$a_h(u, v_h) = l_h(v_h), \quad \forall v_h \in P_h^k.$$

In order to show the discrete coercivity, we need a well-known inverse inequality (see for instance [55, Section 1.4.3]). For the sake of clarity, we recall it below and we sketch its proof.

Lemma 2.4.2 (Inverse inequality)**.** *Let $F \in \mathcal{F}_{h,\Gamma}$ such that $F = \partial K^1 \cap \partial K^2$, with $K^i \in \mathcal{T}_h^i$ for $i = 1, 2$. There exists a constant $C_I > 0$ only dependent of the dimension d, the polynomial degree k, the mesh regularity parameter σ, such that:*

$$h_F \left\| \left\langle \kappa \frac{\partial v_h}{\partial \boldsymbol{n}} \right\rangle \right\|_{\mathrm{L}^2(F)}^2 \leq C_I \sum_{i=1}^{2} \|\kappa_i \nabla v_{h,i}\|_{\mathrm{L}^2(K^i)^d}^2, \quad \forall v_h \in P_h^k.$$

Proof. From the discrete trace inequality combined with a standard inverse inequality (see for example [55, Lemma 1.46]), there exists a positive constant C_{tr}, that depends only on d, k, σ, such that for any $w_{h,i} \in (\mathbb{P}^{k-1}(K^i))^d$, $i = 1, 2$, that

$$\frac{1}{h_F} \|\kappa_i w_{h,i}\|_{\mathrm{L}^2(F)^d}^2 \leq \frac{C_{\mathrm{tr}}}{h_{K^i}^2} \|\kappa_i w_{h,i}\|_{\mathrm{L}^2(K^i)^d}^2.$$

Taking $w_{h,i} = \nabla v_{h,i}$ and noting that $h_F \leq h_{K^i}$ and that $\left| \frac{\partial v_{h,i}}{\partial \boldsymbol{n}} \right| \leq |\nabla v_{h,i}|$, we immediately obtain:

$$h_F \left\| \left\langle \kappa \frac{\partial v_h}{\partial \boldsymbol{n}} \right\rangle \right\|_{\mathrm{L}^2(F)}^2 \leq \frac{1}{2} \sum_{i=1}^{2} h_F \left\| \kappa_i \frac{\partial v_{h,i}}{\partial \boldsymbol{n}} \right\|_{\mathrm{L}^2(F)}^2 \leq C_I \sum_{i=1}^{2} \|\kappa_i \nabla v_{h,i}\|_{\mathrm{L}^2(K^i)^d}^2, \quad \forall v_h \in P_h^k$$

with $C_I = \dfrac{C_{\mathrm{tr}}}{2}$. □

We are next interested in how to choose the stabilization parameter β_F. For this purpose, we write:

$$a_h(v_h, v_h) = b(v_h, v_h) + \frac{1}{\eta} \sum_{F \in \mathcal{F}_{h,\Gamma}} \left(1 - \frac{\beta_F}{\eta}\right) \int_F [v_h]^2 \mathrm{d}s - \sum_{F \in \mathcal{F}_{h,\Gamma}} \beta_F \int_F \left\langle \kappa \frac{\partial v_h}{\partial \boldsymbol{n}} \right\rangle^2 \mathrm{d}s$$
$$- \sum_{F \in \mathcal{F}_{h,\Gamma}} \frac{2\beta_F}{\eta} \int_F \left\langle \kappa \frac{\partial v_h}{\partial \boldsymbol{n}} \right\rangle [v_h] \, \mathrm{d}s.$$

The Cauchy-Schwarz and the Young inequalities yield that:

$$-2 \sum_{F \in \mathcal{F}_{h,\Gamma}} \frac{\beta_F}{\eta} \int_F \left\langle \kappa \frac{\partial v_h}{\partial \boldsymbol{n}} \right\rangle [v_h] \mathrm{d}s \geq -\frac{1}{2\eta} \sum_{F \in \mathcal{F}_{h,\Gamma}} \frac{|\eta - \beta_F|}{\eta} \|[v_h]\|^2_{\mathrm{L}^2(F)} - \sum_{F \in \mathcal{F}_{h,\Gamma}} \frac{2\beta_F^2}{|\eta - \beta_F|} \left\| \left\langle \kappa \frac{\partial v_h}{\partial \boldsymbol{n}} \right\rangle \right\|^2_{\mathrm{L}^2(F)}.$$

Plugging this inequality in the definition of $a_h(v_h, v_h)$ leads to:

$$\begin{aligned} a_h(v_h, v_h) \;\geq\; & b(v_h, v_h) - \sum_{F \in \mathcal{F}_{h,\Gamma}} \frac{\beta_F}{h_F} \left(1 + \frac{2\beta_F}{|\eta - \beta_F|}\right) h_F \left\| \left\langle \kappa \frac{\partial v_h}{\partial \boldsymbol{n}} \right\rangle \right\|^2_{\mathrm{L}^2(F)} \\ & + \frac{1}{\eta^2} \sum_{F \in \mathcal{F}_{h,\Gamma}} \left(\eta - \beta_F - \frac{|\eta - \beta_F|}{2}\right) \|[v_h]\|^2_{\mathrm{L}^2(F)}. \end{aligned}$$

Using next Lemma 2.4.2, we have that:

$$\begin{aligned} a_h(v_h, v_h) \;\geq\; & \sum_{i=1}^{2} \sum_{K^i \in \mathcal{T}_h^i \setminus (\mathcal{T}_h^i \cap \mathcal{T}_{h,\Gamma})} \|\kappa_i^{1/2} \nabla v_{h,i}\|^2_{\mathrm{L}^2(K^i)^d} \\ & + \sum_{i=1}^{2} \sum_{K^i \in \mathcal{T}_h^i \cap \mathcal{T}_{h,\Gamma}} \left(1 - C_I \kappa_{\max} \frac{\beta_F(|\varepsilon - \beta_F| + 2\beta_F)}{h_F |\eta - \beta_F|}\right) \|\kappa_i^{1/2} \nabla v_{h,i}\|^2_{\mathrm{L}^2(K^i)^d} \qquad (2.16) \\ & + \|\alpha^{1/2} \eta^{1/2} \nabla_\tau \langle v_h \rangle\|^2_{\mathrm{L}^2(\Gamma)^d} + \frac{1}{\eta^2} \sum_{F \in \mathcal{F}_{h,\Gamma}} \left(\eta - \beta_F - \frac{|\eta - \beta_F|}{2}\right) \|[v_h]\|^2_{\mathrm{L}^2(F)}, \end{aligned}$$

where $\kappa_{\max} = \max_{i=1,2} \kappa_i$. Thus, in order to obtain the discrete coercivity of $a_h(\cdot, \cdot)$, it is sufficient to choose β_F such that

$$\beta_F < \eta \quad \text{and} \quad \beta_F \frac{\eta + \beta_F}{\eta - \beta_F} < \frac{h_F}{C_I \kappa_{\max}}. \qquad (2.17)$$

Following the idea of [79], where a boundary value problem with similar non-standard boundary conditions was considered, we choose $2\beta_F$ as the harmonic mean of η and $\gamma h_F \kappa_{\max}^{-1}$, where $\gamma > 0$ is a constant independent of η, the discretization and the diffusion coefficients $\kappa_i, i = 1, 2$, that is:

$$\beta_F := \frac{\gamma h_F \eta}{\eta \kappa_{\max} + \gamma h_F}. \qquad (2.18)$$

Then clearly $\beta_F < \eta$, while the second inequality of (2.17) translates into $\dfrac{\gamma(\eta\kappa_{\max} + 2\gamma h_F)}{\eta\kappa_{\max} + \gamma h_F} < \dfrac{1}{C_I}$ and holds true for $\gamma < \dfrac{1}{2C_I}$ since $\dfrac{\eta\kappa_{\max} + 2\gamma h_F}{\eta\kappa_{\max} + \gamma h_F} < 2$. With this choice, the bilinear and linear forms can be written as follows:

$$\begin{aligned}
a_h(u_h, v_h) &= b(u_h, v_h) + \sum_{F\in\mathcal{F}_{h,\Gamma}} \frac{\kappa_{\max}}{\eta\kappa_{\max} + \gamma h_F} \int_F [u_h][v_h]\mathrm{d}s \\
&\quad - \sum_{F\in\mathcal{F}_{h,\Gamma}} \frac{\gamma h_F \eta}{\eta\kappa_{\max} + \gamma h_F} \int_F \left\langle \kappa \frac{\partial u_h}{\partial \boldsymbol{n}} \right\rangle \left\langle \kappa \frac{\partial v_h}{\partial \boldsymbol{n}} \right\rangle \mathrm{d}s \\
&\quad - \sum_{F\in\mathcal{F}_{h,\Gamma}} \frac{\gamma h_F}{\eta\kappa_{\max} + \gamma h_F} \int_F \left(\left\langle \kappa \frac{\partial u_h}{\partial \boldsymbol{n}} \right\rangle [v_h] + \left\langle \kappa \frac{\partial v_h}{\partial \boldsymbol{n}} \right\rangle [u_h] \right) \mathrm{d}s, \\
l_h(v_h) &= \int_\Omega G v_h \mathrm{d}x + \int_\Gamma (g \langle v_h \rangle + \alpha\eta\bar{g} \langle v_h \rangle)\mathrm{d}s \\
&\quad + \sum_{F\in\mathcal{F}_{h,\Gamma}} \frac{\kappa_{\max}}{\eta\kappa_{\max} + \gamma h_F} \int_F (\eta f + \bar{f}) \left([v_h] - \frac{\gamma h_F}{\kappa_{\max}} \left\langle \kappa \frac{\partial v_h}{\partial \boldsymbol{n}} \right\rangle \right) \mathrm{d}s.
\end{aligned}$$

Remark 10 *The case $\gamma = 0$, that is $\beta_F = 0$ for any $F \in \mathcal{F}_{h,\Gamma}$, corresponds to the previous discrete formulation* (2.6)*. The other case when β_F vanishes, that is for $\eta = 0$, is more interesting. Contrary to problem* (2.6)*, we can directly take $\eta = 0$ in the new formulation* (2.15) *and obtain the standard Nitsche formulation of the limit problem* (2.5)*.*

Finally, we introduce the following mesh-dependent norm on P_h^k:

$$|||v_h|||_h := \left(\|v_h\|^2 + \sum_{F\in\mathcal{F}_{h,\Gamma}} \frac{\kappa_{\max}}{\eta\kappa_{\max} + \gamma h_F} \|[v_h]\|^2_{\mathrm{L}^2(F)} \right)^{1/2}$$

and we prove below the main result of this subsection, which yields the well-posedness of the discrete problem (2.15) for γ sufficiently small.

Lemma 2.4.3 (Coercivity and continuity of Nitsche's formulation)**.** *For $\gamma \le C_{\mathrm{I}}/4$, for any u_h, v_h in $P^k_{h,0}$, one has:*

$$a_h(u_h, v_h) \le 2|||u_h|||_h |||v_h|||_h \quad \text{and} \quad a_h(v_h, v_h) \ge \frac{1}{2}|||v_h|||_h^2.$$

Proof. The proof of the continuity is standard. The Cauchy-Schwarz inequality yields, for any $u_h, v_h \in P^k_{h,0}$, that

$$\begin{aligned}
a_h(u_h, v_h) \le \|u_h\|\|v_h\| &+ \sum_{F\in\mathcal{F}_{h,\Gamma}} \frac{\gamma h_F \eta}{\eta\kappa_{\max} + \gamma h_F} \left\| \left\langle \kappa \frac{\partial u_h}{\partial \boldsymbol{n}} \right\rangle \right\|_{\mathrm{L}^2(F)} \left\| \left\langle \kappa \frac{\partial v_h}{\partial \boldsymbol{n}} \right\rangle \right\|_{\mathrm{L}^2(F)} \\
&+ \sum_{F\in\mathcal{F}_{h,\Gamma}} \frac{\kappa_{\max}}{\eta\kappa_{\max} + \gamma h_F} \|[u_h]\|_{\mathrm{L}^2(F)} \|[v_h]\|_{\mathrm{L}^2(F)} \\
&+ \sum_{F\in\mathcal{F}_{h,\Gamma}} \frac{\gamma h_F}{\eta\kappa_{\max} + \gamma h_F} \left(\|[u_h]\|_{\mathrm{L}^2(F)} \left\| \left\langle \kappa \frac{\partial v_h}{\partial \boldsymbol{n}} \right\rangle \right\|_{\mathrm{L}^2(F)} + \left\| \left\langle \kappa \frac{\partial u_h}{\partial \boldsymbol{n}} \right\rangle \right\|_{\mathrm{L}^2(F)} \|[v_h]\|_{\mathrm{L}^2(F)} \right).
\end{aligned}$$

Noting that $\dfrac{\gamma h_F \eta}{\eta\kappa_{\max}+\gamma h_F} \le \dfrac{\gamma h_F}{\kappa_{\max}}$ and that $\dfrac{\gamma h_F}{\eta\kappa_{\max}+\gamma h_F} \le \left(\dfrac{\gamma h_F}{\kappa_{\max}}\right)^{1/2}\left(\dfrac{\kappa_{\max}}{\eta\kappa_{\max}+\gamma h_F}\right)^{1/2}$ and using again the Cauchy–Schwarz inequality, we further obtain

$$a_h(u_h,v_h) \le \left(\|u_h\|^2 + 2\sum_{F\in\mathcal{F}_{h,\Gamma}}\left(\frac{\kappa_{\max}}{\eta\kappa_{\max}+\gamma h_F}\|[u_h]\|^2_{\mathrm{L}^2(F)} + \frac{\gamma h_F}{\kappa_{\max}}\left\|\left\langle \kappa\frac{\partial u_h}{\partial \boldsymbol{n}}\right\rangle\right\|^2_{\mathrm{L}^2(F)}\right)\right)^{1/2}$$
$$\times\left(\|v_h\|^2 + 2\sum_{F\in\mathcal{F}_{h,\Gamma}}\left(\frac{\kappa_{\max}}{\eta\kappa_{\max}+\gamma h_F}\|[v_h]\|^2_{\mathrm{L}^2(F)} + \frac{\gamma h_F}{\kappa_{\max}}\left\|\left\langle \kappa\frac{\partial v_h}{\partial \boldsymbol{n}}\right\rangle\right\|^2_{\mathrm{L}^2(F)}\right)\right)^{1/2}.$$

For $\gamma < \frac{1}{2C_{\mathrm{I}}}$, the first bound is obtained thanks to Lemma 2.4.2.

As regards the uniform coercivity, the choice (2.18) of β_F together with (2.16) yields that

$$a_h(v_h,v_h) \ge \sum_{i=1}^{2}\left(\sum_{K^i\in\mathcal{T}_h^i\setminus(\mathcal{T}_h^i\cap\mathcal{T}_{h,\Gamma})}\|\kappa_i^{1/2}\nabla v_{h,i}\|^2_{\mathrm{L}^2(K^i)^d} + \sum_{K^i\in\mathcal{T}_h^i\cap\mathcal{T}_{h,\Gamma}}(1-2\gamma C_I)\|\kappa_i^{1/2}\nabla v_{h,i}\|^2_{\mathrm{L}^2(K^i)^d}\right)$$
$$+ \|\alpha^{1/2}\nabla_\tau\langle v_h\rangle\|^2_{\mathrm{L}^2(\Gamma)^d} + \frac{1}{2}\sum_{F\in\mathcal{F}_{h,\Gamma}}\frac{\kappa_{\max}}{\eta\kappa_{\max}+\gamma h_F}\|[v_h]\|^2_{\mathrm{L}^2(F)}.$$

Choosing, for instance, $\gamma \le \dfrac{1}{4C_I}$, we obtain the $|||\cdot|||_h$- coercivity with a constant equal to $\dfrac{1}{2}$. □

Lemma 2.4.4 (Polynomial approximation in energy norm)**.** *For any $k\in\mathbb{N}^*$ and $v\in V^{k+1}_{\Gamma,0}$, there exists a constant $\tilde{C}_{\mathrm{ip}}>0$ independent of h, η, α, γ, κ_1 and κ_2 such that:*

$$|||v-(\mathcal{I}_h^k)^*v|||_h \le \tilde{C}_{\mathrm{ip}}h^k\left(\sum_{i=1}^{2}\|\kappa_i^{1/2}v_i\|^2_{\mathrm{H}^{k+1}(\Omega_i)} + \|(\alpha\eta)^{1/2}\langle v\rangle\|^2_{\mathrm{H}^{k+1}(\Gamma)} + \sum_{F\in\mathcal{F}_{h,\Gamma}}\frac{\kappa_{\max}}{\gamma h_F}\|[v]\|^2_{\mathrm{H}^k(F)}\right)^{1/2}. \tag{2.19}$$

Furthermore, if $[v]\in\mathrm{H}^{k+1}(\Gamma)$, then

$$|||v-(\mathcal{I}_h^k)^*v|||_h \le \tilde{C}_{\mathrm{ip}}h^k\left(\sum_{i=1}^{2}\|\kappa_i^{1/2}v_i\|^2_{\mathrm{H}^{k+1}(\Omega_i)} + \|(\alpha\eta)^{1/2}\langle v\rangle\|^2_{\mathrm{H}^{k+1}(\Gamma)} + \sum_{F\in\mathcal{F}_{h,\Gamma}}\frac{\kappa_{\max}h_F}{\gamma}\|[v]\|^2_{\mathrm{H}^{k+1}(F)}\right)^{1/2} \tag{2.20}$$

and

$$|||v-(\mathcal{I}_h^k)^*v|||_h \le \tilde{C}_{\mathrm{ip}}h^k\left(\sum_{i=1}^{2}\|\kappa_i^{1/2}v_i\|^2_{\mathrm{H}^{k+1}(\Omega_i)} + \sum_{i=1}^{2}\frac{\kappa_{\max}}{\gamma}\|v\|^2_{\mathrm{H}^{k+1}(\Omega_i)} + \|(\alpha\eta)^{1/2}\langle v\rangle\|^2_{\mathrm{H}^{k+1}(\Gamma)}\right)^{1/2}. \tag{2.21}$$

Proof. With the same standard interpolation estimates as in Lemma 2.3.4, we immediately get that

$$|||v-(\mathcal{I}_h^k)^*v|||_h^2 \le C_{\mathrm{ip}}^2h^{2k}\left(\sum_{i=1}^{2}\sum_{K^i\in\mathcal{T}_h^i}\|\kappa_i^{1/2}v_i\|^2_{\mathrm{H}^{k+1}(K^i)} + \sum_{F\in\mathcal{F}_{h,\Gamma}}\|(\alpha\eta)^{1/2}\langle v\rangle\|^2_{\mathrm{H}^{k+1}(F)}\right)$$
$$+ C_{\mathrm{ip}}^2h^{2k}\sum_{F\in\mathcal{F}_{h,\Gamma}}\frac{\kappa_{\max}}{\eta\kappa_{\max}+\gamma h_F}\|[v]\|^2_{\mathrm{H}^k(F)},$$

and noting that $\kappa_{\max}(\eta\kappa_{\max}+\gamma h_F)^{-1} < \kappa_{\max}(\gamma h_F)^{-1}$ to get rid of η, we obtain (2.19).
If in addition $[v] \in \mathrm{H}^{k+1}(\Gamma)$, we have:

$$|||v-(\mathcal{I}_h^k)^* v|||_h^2 \leq C_{\mathrm{ip}}^2 h^{2k}\Bigg(\sum_{i=1}^{2}\sum_{K^i\in\mathcal{T}_h^i}\|\kappa_i^{1/2}v_i\|^2_{\mathrm{H}^{k+1}(K^i)} + \sum_{F\in\mathcal{F}_{h,\Gamma}}\|(\alpha\eta)^{1/2}\langle v\rangle\|^2_{\mathrm{H}^{k+1}(F)}\Bigg) + C_{\mathrm{ip}}^2 h^{2k}\sum_{F\in\mathcal{F}_{h,\Gamma}}\frac{\kappa_{\max}h_F^2}{\eta\kappa_{\max}+\gamma h_F}\|[v]\|^2_{\mathrm{H}^{k+1}(F)},$$

and noting that $\gamma h_F(\eta\kappa_{\max}+\gamma h_F)^{-1} \leq 1$, we immediately obtain (2.20). As regards estimate (2.21), it follows from the well-known trace inequality (e.g. [55, Lemma 1.49]): there exists $C_1 > 0$ such that for any $F \in \mathcal{F}_{h,\Gamma}$ with $F = \partial K^1 \cap \partial K^2$ and any $w_i \in \mathrm{H}^1(K^i)$ with $1 \leq i \leq 2$,

$$\frac{1}{\sqrt{h_F}}\|[w]\|_{\mathrm{L}^2(F)} \leq C_1\sum_{i=1}^{2}\left(\frac{1}{h_{K^i}}\|w_i\|_{\mathrm{L}^2(K^i)} + \|w_i\|_{\mathrm{H}^1(K^i)}\right).$$

Using next standard interpolation estimates, there exists a constant $C_2 > 0$ independent of h, η, α, γ, κ_1 and κ_2 such that, for any $F \in \mathcal{F}_{h,\Gamma}$, one has that

$$\frac{\kappa_{\max}}{\eta\kappa_{\max}+\gamma h_F}\|[v]-(\mathcal{I}_h^k)^*[v]]\|^2_{\mathrm{L}^2(F)} \leq \frac{\kappa_{\max}}{\gamma}C_2^2\sum_{i=1}^{2}h_{K^i}^{2k}\|v_i\|^2_{\mathrm{H}^{k+1}(K^i)}.$$

The estimate (2.21) is obtained by summing upon $F \in \mathcal{F}_{h,\Gamma}$, with $\tilde{C}_{\mathrm{ip}} = \max\{C_{\mathrm{ip}}, C_2\}$. Since $C_{\mathrm{ip}} < \tilde{C}_{\mathrm{ip}}$, the first estimate (2.20) also holds with constant $\tilde{C}_{\mathrm{ip}}$. □

The *a priori* error estimate for Nitsche's method is given below and follows from Céa's lemma.

Theorem 2.4.5 (Error estimate in energy norm) Let $k \in \mathbb{N}^*$, u the solution of (2.3) and u_h the solution of (2.15). If $u \in V_\Gamma^{k+1}$ and $\tilde{u}_{\mathrm{D}} \in V^{k+1}$, $\tilde{u}_{\mathrm{D},h} \in P_h^k$. For $\gamma \leq \dfrac{1}{4C_{\mathrm{I}}}$, there exists a constant $C_{\mathrm{e}}^N = 5\tilde{C}_{\mathrm{ip}}$ independent of h, η, α, γ, κ_1 and κ_2 such that:

$$|||\tilde{u}-\tilde{u}_h|||_h \leq C_{\mathrm{e}}^N h^k\left(\sum_{i=1}^{2}\|\kappa_i^{1/2}\tilde{u}_i\|^2_{\mathrm{H}^{k+1}(\Omega_i)} + \|(\alpha\eta)^{1/2}\langle\tilde{u}\rangle\|^2_{\mathrm{H}^{k+1}(\Gamma)} + \sum_{F\in\mathcal{F}_{h,\Gamma}}\frac{\kappa_{\max}}{\gamma h_F}\|[\tilde{u}]\|^2_{\mathrm{H}^k(F)}\right)^{1/2}, \tag{2.22}$$

where $\tilde{u} := u - \tilde{u}_{\mathrm{D}}$, $\tilde{u}_h := u_h - \tilde{u}_{\mathrm{D},h}$. Moreover, if $[u], [\tilde{u}_{\mathrm{D}}] \in \mathrm{H}^{k+1}(\Gamma)$, one has

$$|||\tilde{u}-\tilde{u}_h|||_h \leq C_{\mathrm{e}}^N h^k\left(\sum_{i=1}^{2}\|\kappa_i^{1/2}\tilde{u}_i\|^2_{\mathrm{H}^{k+1}(\Omega_i)} + \|(\alpha\eta)^{1/2}\langle\tilde{u}\rangle\|^2_{\mathrm{H}^{k+1}(\Gamma)} + \sum_{F\in\mathcal{F}_{h,\Gamma}}\frac{\kappa_{\max}h_F}{\gamma}\|[\tilde{u}]\|^2_{\mathrm{H}^{k+1}(F)}\right)^{1/2}, \tag{2.23}$$

and

$$|||\tilde{u}-\tilde{u}_h|||_h \leq C_{\mathrm{e}}^N h^k\left(\sum_{i=1}^{2}\|\kappa_i^{1/2}\tilde{u}_i\|^2_{\mathrm{H}^{k+1}(\Omega_i)} + \frac{\kappa_{\max}}{\gamma}\sum_{i=1}^{2}\|\tilde{u}\|^2_{\mathrm{H}^{k+1}(\Omega_i)} + \|(\alpha\eta)^{1/2}\langle\tilde{u}\rangle\|^2_{\mathrm{H}^{k+1}(\Gamma)}\right)^{1/2}. \tag{2.24}$$

Remark 11 *One can note that, contrary to the error estimate* (2.12) *of the first method, estimate* (2.23) *is robust for small values of* η. *Indeed, if* $\eta \leq \dfrac{\gamma h_F}{\kappa_{\max}}$, *then* $\dfrac{\kappa_{\max} h_F}{\gamma} \leq \dfrac{h_F^2}{\eta}$ *and moreover, the weight* $\dfrac{h_F^2}{\eta}$ *blows up as* $\eta \to 0$.

2.4.2 Numerical tests

In this subsection, we carry out some numerical experiments for the same test-cases as in subsection 2.3.2, but using now the new Nitsche's type formulation. The goal is to illustrate that the energy error remains bounded for small values of η, which is the main issue in the numerical examples of the previous section. The energy norm for Nitsche's formulation $e^N := |||\tilde{u} - \tilde{u}_h|||_h$ is also split into three terms, $(e^N)^2 = e_g^2 + e_\tau^2 + (e_j^N)^2$, where e_j^N now denotes the stabilised jump error on the interface,

$$(e_j^N)^2 := \sum_{F \in \mathcal{F}_{h,\Gamma}} \frac{\kappa_{\max}}{\eta \kappa_{\max} + \gamma h_F} \|[\tilde{u} - \tilde{u}_h]\|^2_{\mathrm{L}^2(F)}.$$

Convergence of the method with respect to the mesh size

We use a stabilisation parameter $\gamma = 10^{-1}$ for both cases. We check numerically the error estimate given in Theorem 2.4.5 for the energy norm e^N, more precisely the convergence rate with respect to h at fixed η.

The results are depicted in Figures 2.10 and 2.11 for the energy norm and the jump stabilized norm of the error, respectively. We observe that the results are similar to Figures 2.4 and 2.5. The orders of convergence are summarized in Table 2.2.

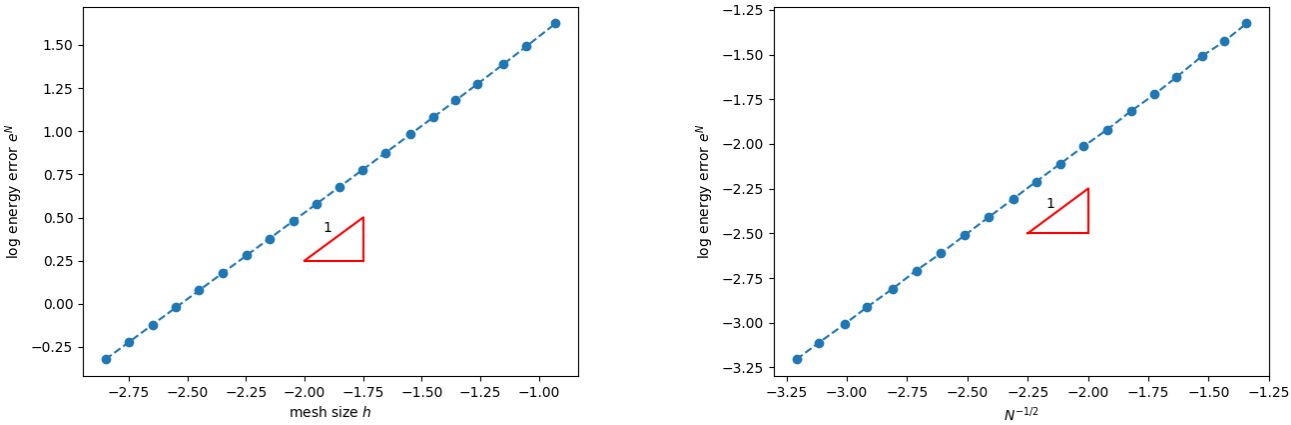

(a) Case 1 with $\eta = 10^{-2}$

(b) Case 2 with $\eta = 1$

Figure 2.10: Logarithm plot of the energy error e^N with respect to the mesh size h

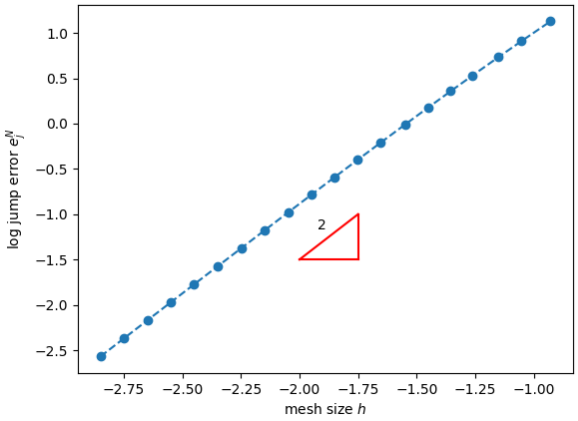

(a) Case 1 with $\eta = 10^{-2}$

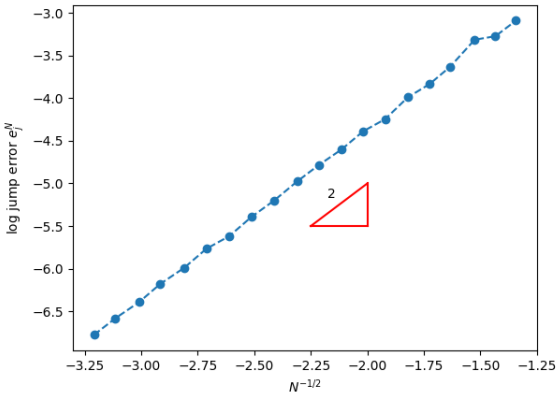

(b) Case 2 with $\eta = 1$

Figure 2.11: Logarithm plot of the jump error e_j^N with respect to the mesh size h

	Case 1	Case 2
e_g^N	1.06	1.00
e_τ^N	1.00	1.02
e_j^N	1.93	1.99
e^N	1.01	1.01

Table 2.2: Convergence rates of each error for Nitsche's method

Convergence with respect to η

Let now h be fixed, for each test-case. We observe from Figure 2.12 that Nitsche's energy error e^N is bounded for small values of η, contrary to the energy error e that blows up. This is due to the fact that Nitsche's jump error is bounded, as shown in Figure 2.13. We note for both methods the good behaviour as η decreases of the gradient and tangential errors, which are not affected by the $\frac{1}{\eta}$-term. The tangential gradient errors are plotted in Figure 2.14.

Conditioning

In Figure 2.15, we observe that the condition number of the Nitsche's method is bounded as η tends towards 0, whereas the condition number of the first method increases, as highlighted in section 2.3.2.

2.4.3 Application: use of iterative solvers

In this subsection, we apply a Krylov subspace method combined with a preconditioner (otherwise none of the methods converge in a reasonable number of iterations, since the classical methods tend to stagnate). To this end we have chosen the conjugate gradient with a Jacobi preconditioner,

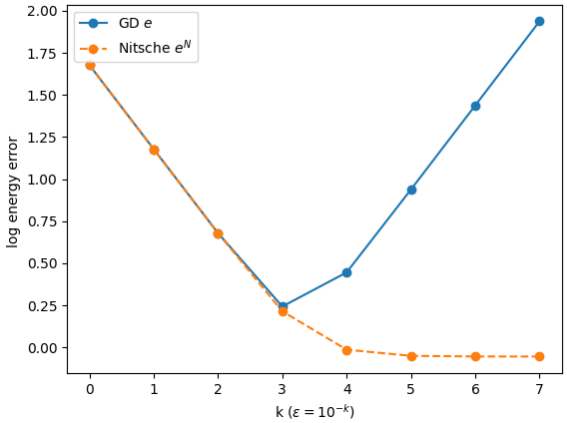

(a) Case 1 with $h = 1.41 \times 10^{-2}$

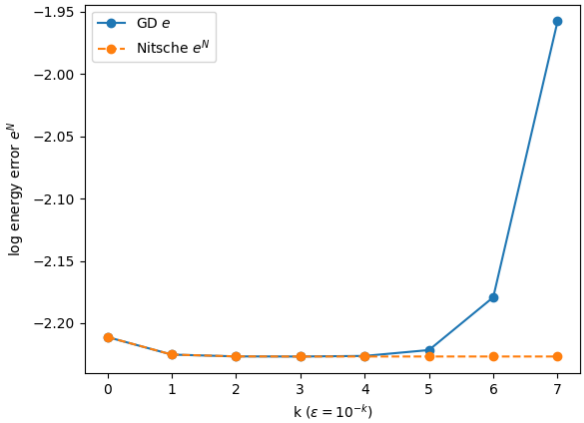

(b) Case 2 with $h = 1.7 \times 10^{-2}$

Figure 2.12: Logarithm plot of the energy errors $e = |||u - w_h|||$ and $e^N = |||u - u_h|||_h$ with respect to η, for FEM and Nitsche's methods respectively.

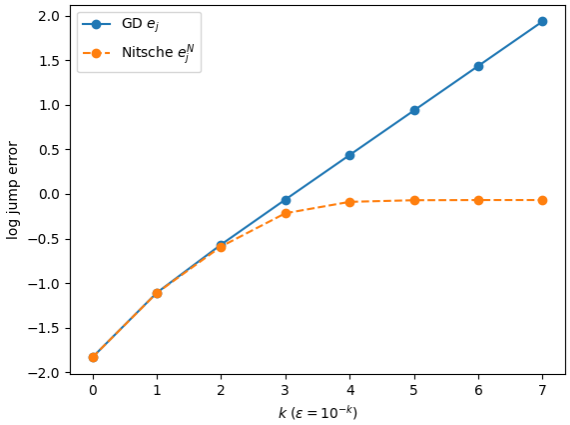

(a) Case 1 with $h = 1.4 \times 10^{-2}$

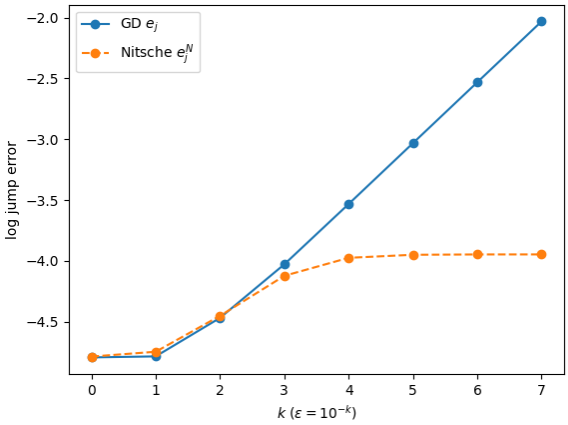

(b) Case 2 with $h = 1.7 \times 10^{-2}$

Figure 2.13: Logarithm plot with respect to η of the jump errors $e_j = \|\eta^{-1/2}(u - w_h)\|_{\mathrm{L}^2(\Gamma)}$ and $e_j^N = \kappa_{\max}(\sum_{F \in \mathcal{F}_{h,\Gamma}} \|(\eta\kappa_{\max} + \gamma h_F)^{-1/2}(u - u_h)\|^2_{\mathrm{L}^2(F)})^{1/2}$, for FEM and Nitsche's methods respectively

due to its flexibility and good performance. For this task, we use the powerful numerical linear algebra library PETSc (see [17, 18]).

Firstly, we consider the test-case 1 as in section 2.3.2, with fixed $h = 1.4 \times 10^{-2}$ ($\mathrm{N} = 10,000$) and $\gamma = 10^{-1}$ for Nitsche's method. We let η vary in order to see how the conditioning affects the performance of each method. We set the absolute tolerance $tol = 10^{-5}$ and the maximum number of iterations I equal to the matrix size, in this case N. Let $r := \|Ax - b\|$ the residual in the last iteration. We can see from Table 2.3 that as η decreases, the number of iterations to reach the fixed tolerance with the first method increases; consequently, the errors increase too,

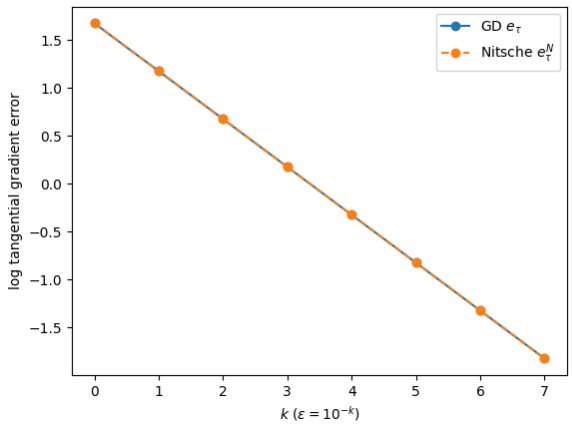

(a) Case 1 with $h = 1.4\ 10^{-2}$

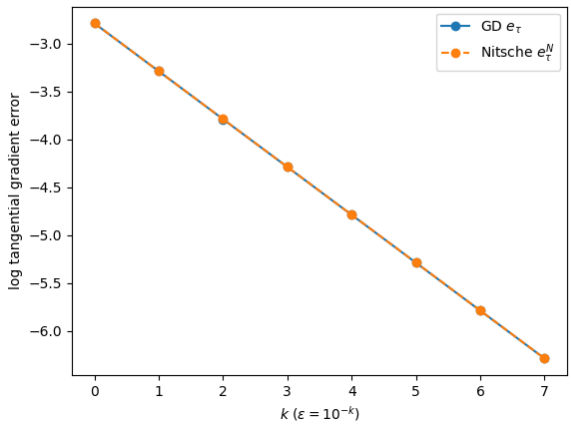

(b) Case 2 with $h = 1.7\ 10^{-2}$

Figure 2.14: Logarithm plot of the tangential gradient errors $e_\tau = \|(\alpha\eta)^{1/2}\nabla_\tau(u - w_h)\|_{\mathrm{L}^2(\Gamma)}$ and $e_\tau^N = \|(\alpha\eta)^{1/2}\nabla_\tau(u - u_h)\|_{\mathrm{L}^2(\Gamma)}$ with respect to η, for FEM and Nitsche's methods respectively

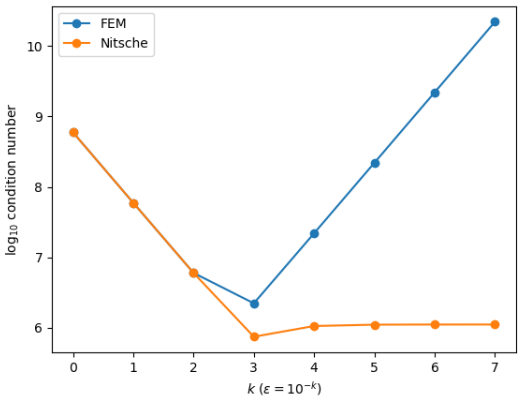

(a) Condition number of case 1 with $h = 3\ 10^{-2}$

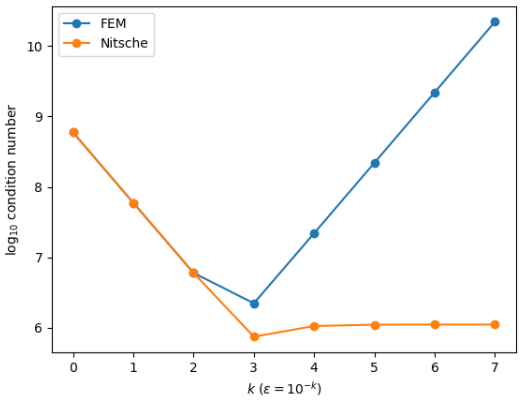

(b) Condition number of case 2 with $h = 5\ 10^{-2}$

Figure 2.15: Logarithm plot with respect to η of the condition number for the two methods

since convergence is not reached in the last iterations. On the other hand, Table 2.4 shows that the number of iterations for Nitsche's method remains limited as η goes to 0, and so do the errors.

η	I	r	e	e_j	e_τ
10^{-3}	967	9.49×10^{-6}	1.75	0.86	1.50
10^{-4}	1,978	8.47×10^{-6}	2.78	2.74	0.47
10^{-5}	10,000	1.44×10^{-5}	8.66	8.66	0.15
10^{-6}	10,000	9.92×10^{-4}	30.66	27.40	0.19
10^{-7}	10,000	2.62×10^{-3}	312.55	86.74	3.47

Table 2.3: Convergence history of conjugate gradient for case 1, using FEM approximation

Secondly, we consider the test-case 2 and we now set an absolute tolerance equal to 10^{-5},

η	I	r	e^N	e_j^N	e_τ^N
10^{-3}	1,144	9.82×10^{-6}	1.63	0.60	1.50
10^{-4}	1,073	9.98×10^{-6}	0.97	0.82	0.48
10^{-5}	1,249	9.73×10^{-6}	0.89	0.85	0.15
10^{-6}	1,368	9.84×10^{-6}	0.88	0.85	0.05
10^{-7}	1,374	9.33×10^{-6}	0.88	0.85	0.02

Table 2.4: Convergence history of conjugate gradient for case 1, using Nitsche's method

$h = 1.7 \times 10^{-2}$ and $\gamma = 10^{-1}$, $N = 26995$ and we fix the maximum number of iterations equal to N. Tables 2.5 and 2.6 show similar results to the test-case 1.

η	I	r	e	e_j	e_τ
10^{-3}	1,075	9.94×10^{-6}	6.07×10^{-3}	1.11×10^{-4}	5.46×10^{-5}
10^{-4}	914	9.99×10^{-6}	6.17×10^{-3}	2.97×10^{-4}	1.92×10^{-5}
10^{-5}	1,953	9.94×10^{-6}	1.03×10^{-2}	9.32×10^{-4}	1.92×10^{-5}
10^{-6}	4,646	9.98×10^{-6}	7.71×10^{-2}	2.95×10^{-3}	5.46×10^{-5}
10^{-7}	26,995	1.27×10^{-5}	8.83×10^{-1}	9.46×10^{-3}	2.19×10^{-4}

Table 2.5: Convergence history of conjugate gradient for case 2, using FEM approximation

η	I	r	e^N	e_j^N	e_τ^N
10^{-3}	1,175	9.95×10^{-6}	6.06×10^{-3}	7.99×10^{-5}	5.46×10^{-5}
10^{-4}	1,020	9.94×10^{-6}	6.02×10^{-3}	1.05×10^{-4}	1.69×10^{-5}
10^{-5}	1,029	9.95×10^{-6}	6.04×10^{-3}	1.12×10^{-4}	5.42×10^{-6}
10^{-6}	1,022	9.87×10^{-6}	6.02×10^{-3}	1.13×10^{-4}	1.70×10^{-6}
10^{-7}	1,022	9.81×10^{-6}	6.02×10^{-3}	1.13×10^{-4}	5.37×10^{-7}

Table 2.6: Convergence history of conjugate gradient for case 2, using Nitsche's method

Chapter 3

Shape optimization for a heat insulator

Contents

Most of the content of this chapter has been published in Journal of Optimization Theory and Applications [36]:

F. Caubet, C. Conca, M. Dambrine, and R. Zelada. How to Insulate a Pipe? Journal of Optimization Theory and Applications, 207(3):46, 2025.

3.1 Introduction and setting of the problem

3.1.1 Motivations

In our daily lives, reducing heat loss is of great importance from an ecological perspective. Indeed this problem appears in various contexts and applications such as hot water pipes, buildings, or electric kettles, for example. A typical question involves optimizing the thermal insulation around a pipe containing hot water, subject to a volume constraint on the insulator. Insulation problems have been studied for a long time. Here are a few recent advances (see, e.g., [27, 28]). In particular, in [27], two thermal insulation problems were addressed by parametrizing the insulator material by means of the tangential and normal coordinates on the boundary of the the hot body (not a fluid) and minimizing with respect to the variable thickness: it was shown that under certain conditions, when the hot body is inside a ball, then the optimal insulator is a ball. Regarding the numerics, in [108], different configurations were compared and a heuristic was proposed to optimize a polygon satisfying certain geometrical constraints, providing insights into how the insulator should be configured.

In this work, we aim to provide pratical numerical solutions of the optimal insulator. We therefore first perform a theoretical sensitivity analysis of the problem of insulating a pipe containing a hot fluid and then implement a descent method -here the null-space algorithm [64]- using the level set framework (see, e.g., [10]).

In many practical applications (see figure 3.1) the wall thickness of the tube (in red in the figure) is very small compared to its length and also small compared to the insulator thickness. For obvious computational reasons, it makes sense not to mesh it. One possibility would be to ignore it. In this work, we propose to take it into account by means of an interface condition written at the edge of the domain occupied by the fluid, obtained by an asymptotic model of order one with respect to the small parameter (i.e. the ratio between this thickness and the length of the pipe). The novelties of this work are: first, the model takes into account the motion of the fluid and thus a convection term appears in the heat equation in the fluid zone; second, the pipe is considered through an interface term rather than with the usual model of insulation.

3.1.2 The physical context

The actual configuration involves three inseparable parts: the fluid, the wall of the pipe, and the insulator. However, the wall thickness is very small compared to the other dimensions, and keeping this wall in a numerical model requires the use of very refined and therefore very expensive meshes, especially in dimension three, to compute the temperature field.

Figure 3.1: The thermal insulation of a pipe (photo by Sönke Kraft aka Arnulf zu Linden on commons.wikimedia.org).

The approximate domains. We therefore propose, in a classical way since the work of Enquist and Nedelec [58], to forget this zone in the geometrical description of the problem, but to take into account its impact on the thermal properties through artificial transmission conditions at the new fluid-insulator interface. We thus obtain, at the cost of a systematic model error, an approximate solution whose calculation is much less costly since it only requires a much coarser mesh (adapted to the internal diameter of the pipe and no longer to the wall thickness). Our idea is to use this inexpensive approximate model to optimize the shape of the insulation around the pipe.

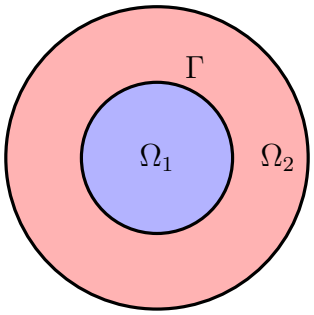

Figure 3.2: The approximate domain.

Let Ω be an open bounded connected domain of $\mathbb{R}^d$ ($d = 2, 3$), divided into two open bounded subdomains Ω_1, Ω_2 which are separated by an interface $\Gamma = \partial\Omega_1 \cap \partial\Omega_2$ that we assume to have non-zero measure in $\mathbb{R}^{d-1}$ and to be $\mathcal{C}^1$ (see Figure 3.2). The boundaries of each subdomain $\partial\Omega_1$ and $\partial\Omega_2$ are respectively decomposed as $\partial\Omega_1 =: \Gamma_{\rm D} \cup \Gamma \cup \Gamma_{\rm N}$ and $\partial\Omega_2 =: \Gamma \cup \Gamma_{\rm R} \cup \Gamma_e$. Moreover, we assume that $\partial\Gamma \subset \partial\Omega$, $\overline{\Gamma} \cap \overline{\Gamma_{\rm D}} \neq \emptyset$ and $\overline{\Gamma} \cap \overline{\Gamma_{\rm N}} \neq \emptyset$. Finally, we assume that Γ intersects $\Gamma_{\rm N}$ and $\Gamma_{\rm D}$ orthogonally. We denote by $\boldsymbol{N}$ the outer unit normal to $\partial\Omega$ and $\boldsymbol{n}$ the outer unit normal to Γ

oriented towards Ω_2, this is $\boldsymbol{n} := \boldsymbol{n}_1 = -\boldsymbol{n}_2$ at Γ, where $\boldsymbol{n}_i$ is the exterior normal of Ω_i. Figure 3.3 illustrates our configuration.

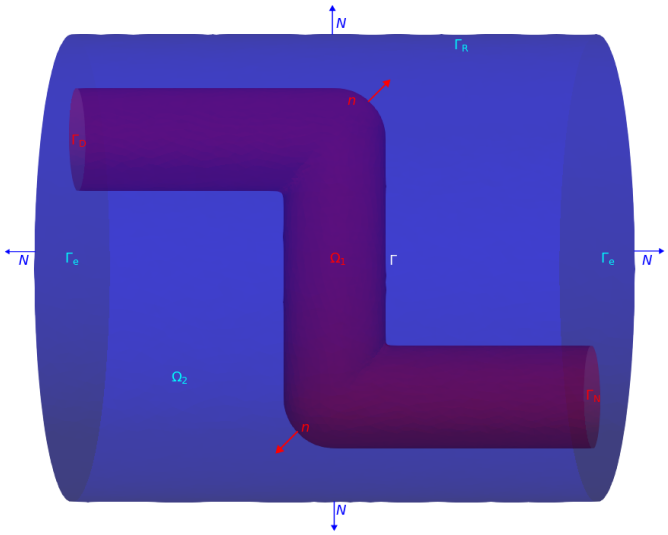

Figure 3.3: Configuration of the 3D thermal insulation problem

We will specify the boundary values problems that we will consider in the following.

The approximate equations. Concerning the fluid, the equations are not affected by this reduction of the domain since there is non-slip boundary condition at the interface. As the pipe may have a complex geometry, the flow of the heat transfer fluid is described by the Navier-Stokes equations (rather than the Stokes equations). We precise that we consider here the steady state case and we denote by $\boldsymbol{u}$ the velocity of the fluid and p the pressure. Let $\nu > 0$ be the kinematic viscosity. The classical non-slip condition $\boldsymbol{u} = 0$ is imposed on Γ. To summarize, the motion of the fluid is described by the following equations:

$$\begin{cases} -\nu\Delta\boldsymbol{u} + (\nabla\boldsymbol{u})\boldsymbol{u} + \nabla p &= 0 & \text{in } \Omega_1, \\ \operatorname{div}(\boldsymbol{u}) &= 0 & \text{in } \Omega_1, \\ \boldsymbol{u} &= \boldsymbol{u}_{\mathrm{D}} & \text{on } \Gamma_{\mathrm{D}}, \\ \sigma(\boldsymbol{u}, p)\boldsymbol{N} &= 0 & \text{on } \Gamma_{\mathrm{N}}, \\ \boldsymbol{u} &= 0 & \text{on } \Gamma, \end{cases} \tag{3.1}$$

where $\boldsymbol{u}_{\mathrm{D}} \in \mathrm{H}_{00}^{1/2}(\Gamma_{\mathrm{D}})^d := \{\boldsymbol{v}|_{\Gamma_{\mathrm{D}}}, \boldsymbol{v} \in \mathrm{H}^1(\Omega_1)^d, \boldsymbol{v}|_{\partial\Omega_1 \setminus \overline{\Gamma_{\mathrm{D}}}} = 0\}$ is the given inlet velocity, $\boldsymbol{n}$ denotes the exterior unit normal, and where $\sigma(\boldsymbol{u}, p)$ is the fluid stress tensor defined by

$$\sigma(\boldsymbol{u}, p) := 2\nu\varepsilon(\boldsymbol{u}) - p\mathrm{I},$$

with $\varepsilon(\boldsymbol{u}) := \frac{1}{2}(\nabla\boldsymbol{u} + \nabla\boldsymbol{u}^t)$ the symmetric gradient and I the identity matrix, and where the superscript ^{t} denotes the transpose matrix. It is well-known that theses stationary Navier-Stokes equations are well-posed if ν is large enough (see, e.g., [68, 106]), which we will assume in the remainder of this work.

As far as the thermal equations are concerned, the omission of the wall of the pipe has a significant impact on the equations. We use the approach introduced in [58] based on now

classic asymptotic techniques. This approach and technical implementation are explained in detail and pedagogically in Vial's thesis [110]. We also mention the work [40] dealing with generalized boundary conditions for an interface problem.

Let $\kappa_1, \kappa_2, \kappa_s$ the thermal diffusivity coefficients that are assumed to be positive numbers. On the Dirichlet part Γ_D, a given temperature is imposed, and a Fourier-Robin condition is imposed on Γ_R the outer boundary Γ_R of Ω_2, stating that the heat flux is proportional to the gap of temperatures with a given rate $\alpha > 0$. Moreover, we impose Neumann boundary conditions on Γ_N. When η is sufficiently small, the following approximate problem of order one is obtained:

$$\left\{\begin{array}{rcll} -\operatorname{div}(\kappa_1 \nabla \mathsf{T}_1) + \boldsymbol{u} \cdot \nabla \mathsf{T}_1 &=& 0 & \text{in } \Omega_1, \\ -\operatorname{div}(\kappa_2 \nabla \mathsf{T}_2) &=& 0 & \text{in } \Omega_2, \\ \mathsf{T}_1 &=& \mathsf{T}_D & \text{on } \Gamma_D, \\ \kappa_1 \dfrac{\partial \mathsf{T}_1}{\partial \boldsymbol{N}} &=& 0 & \text{on } \Gamma_N, \\ \kappa_2 \dfrac{\partial \mathsf{T}_2}{\partial \boldsymbol{N}} &=& 0 & \text{on } \Gamma_e, \\ \kappa_2 \dfrac{\partial \mathsf{T}_2}{\partial \boldsymbol{N}} + \alpha \mathsf{T}_2 &=& \alpha \mathsf{T}_{ext} & \text{on } \Gamma_R, \\ \left\langle \kappa \dfrac{\partial \mathsf{T}}{\partial \boldsymbol{n}} \right\rangle &=& -\dfrac{\kappa_s}{\eta} [\mathsf{T}] & \text{on } \Gamma, \\ \left[\kappa \dfrac{\partial \mathsf{T}}{\partial \boldsymbol{n}} \right] &=& \eta \operatorname{div}_\tau(\kappa_s \nabla_\tau \langle \mathsf{T} \rangle) - \kappa_s H [\mathsf{T}] & \text{on } \Gamma, \\ \dfrac{\partial \langle \mathsf{T} \rangle}{\partial \boldsymbol{N}} &=& 0 & \text{on } \partial\Gamma, \end{array}\right. \tag{3.2}$$

where $\mathsf{T}_D \in \mathrm{H}^{1/2}(\Gamma_D)$ is the given input temperature and $\mathsf{T}_{ext} \in \mathrm{H}^{1/2}(\Gamma_R)$ is the given exterior temperature, and where $\boldsymbol{u}$ solves the Navier-Stokes system (3.1). In the previous equations, div_τ and ∇_τ are respectively the tangential divergence and gradient operator, and H is the mean curvature of Γ. The jump and mean across the interface Γ are defined, for a function ϕ, as

$$[\phi] := \phi_1 - \phi_2 \qquad \text{and} \qquad \langle \phi \rangle := \frac{1}{2}(\phi_1 + \phi_2).$$

The well-posedness of this system is proved below (see Theorem 3.2.1).

The shape optimization problem. We can now set out the main question that we are going to study in this work: *given a pipe with a known fixed geometry and a given quantity of insulation, how should the insulation be positioned to minimize heat loss to the outside world, whose temperature is known?* In other words, the domain Ω_1 being fixed, we are looking for a domain Ω_2 of prescribed volume so that the heat flux across the interface with the outside, i.e. Γ_R, is as small as possible. We therefore define the heat insulation J by

$$J(\Omega_2) := -\int_{\Gamma_R} \kappa_2 \frac{\partial \mathsf{T}_2}{\partial \boldsymbol{N}} \, \mathrm{d}s = \int_{\Gamma_R} \alpha(\mathsf{T}_2 - \mathsf{T}_{ext}) \, \mathrm{d}s \tag{3.3}$$

where the temperature T solves the approximate convection-diffusion problem (3.2).

We thus consider the following shape optimization problem: *given a prescribed volume* $V_0 > 0$, *minimize* J *under the constraint*

$$G(\Omega_2) = 0, \qquad \textit{where } G(\Omega_2) := \int_{\Omega_2} \mathrm{d}x - V_0. \tag{3.4}$$

The fundamental questions of the existence of optimal domains and their regularity have been studied in the work of Bucur *et al.* [28] in a simplified setting (no pipe wall and no fluid circulation just a heated body). This is not the topic of the present work to study these questions. We will here focus on the numerical computation of such a solution, and to this end prove the existence and compute the shape derivatives in this framework.

3.2 Main results

In this section, we claim the main results of our work. All the proofs are detailed in the following section.

3.2.1 Functional spaces and well posedness

We consider the following affine spaces associated to the non-homogeneous Dirichlet boundary data $\boldsymbol{u}_{\mathrm{D}} \in \mathrm{H}^{1/2}_{00}(\Gamma_{\mathrm{D}})^d$ and $\mathsf{T}_{\mathrm{D}} \in \mathrm{H}^{1/2}(\Gamma_{\mathrm{D}})$:

$$\mathcal{V}_{\boldsymbol{u}_{\mathrm{D}}}(\Omega_1) := \{\boldsymbol{w} \in \mathrm{H}^1(\Omega_1)^d;\ \boldsymbol{w} = \boldsymbol{u}_{\mathrm{D}} \text{ on } \Gamma_{\mathrm{D}}, \boldsymbol{w} = 0 \text{ on } \Gamma\},$$

$$\mathcal{H}_{\mathsf{T}_{\mathrm{D}}}(\Omega_1, \Omega_2) := \{\mathsf{S} = (\mathsf{S}_1, \mathsf{S}_2) \in \mathcal{H}^1(\Omega_1, \Omega_2);\ \mathsf{S}_1 = \mathsf{T}_{\mathrm{D}} \text{ on } \Gamma_{\mathrm{D}}\},$$

where,

$$\mathcal{H}^1(\Omega_1, \Omega_2) := \{\mathsf{S} = (\mathsf{S}_1, \mathsf{S}_2) \in \mathrm{H}^1(\Omega_1) \times \mathrm{H}^1(\Omega_2);\ \langle \mathsf{S} \rangle \in \mathrm{H}^1(\Gamma)\}.$$

The spaces $\mathcal{V}_0(\Omega_1)$ and $\mathcal{H}_0(\Omega_1, \Omega_2)$ are Hilbert spaces when they are equipped with the respective norms:

$$\|\boldsymbol{w}\|_{\mathcal{V}_0(\Omega_1)} := \|\boldsymbol{w}\|_{\mathrm{H}^1(\Omega_1)^d} \text{ and } \|\mathsf{S}\|_{\mathcal{H}_0(\Omega_1,\Omega_2)} := \left(\sum_{i=1}^{2} \|\nabla \mathsf{S}_i\|^2_{\mathrm{L}^2(\Omega_i)^d} + \|\nabla_\tau \langle \mathsf{S} \rangle\|^2_{\mathrm{L}^2(\Gamma)^d} + \|[\mathsf{S}]\|^2_{\mathrm{L}^2(\Gamma)} \right)^{1/2}.$$

Then the Navier-Stokes equations (3.1) have the following variational formulation

$$\begin{cases} \text{Find } (\boldsymbol{u}, p) \in \mathcal{V}_{\boldsymbol{u}_{\mathrm{D}}}(\Omega_1) \times \mathrm{L}^2(\Omega_1) \text{ such that, for all } (\boldsymbol{w}, r) \in \mathcal{V}_0(\Omega_1) \times \mathrm{L}^2(\Omega_1), \\ \displaystyle\int_{\Omega_1} (2\nu\varepsilon(\boldsymbol{u}) : \varepsilon(\boldsymbol{w}) + (\nabla \boldsymbol{u})\boldsymbol{u} \cdot \boldsymbol{w} - p \operatorname{div}(\boldsymbol{w}) - r \operatorname{div}(\boldsymbol{u}))\ \mathrm{d}x = 0. \end{cases} \tag{3.5}$$

As previously mentioned, we assume that the viscosity ν is large enough so that the problem (3.1) is well-posed: it has a unique weak solution $(\boldsymbol{u}, p) \in \mathcal{V}_{\boldsymbol{u}_{\mathrm{D}}}(\Omega_1) \times \mathrm{L}^2(\Omega_1)$. For the remainder of this work, we assume that the velocity of the fluid at the outlet, i.e. at the boundary Γ_{N}, actually causes it to exit: there is no recirculation at the outlet. This assumption on the velocity is written as

$$\boldsymbol{u} \cdot \boldsymbol{N} \geq 0 \text{ on } \Gamma_{\mathrm{N}}. \tag{3.6}$$

For the temperature, the corresponding variational formulation of the approximate problem (3.2) is given by

$$\text{Find } \mathsf{T} \in \mathcal{H}_{\mathsf{T}_\mathrm{D}}(\Omega_1,\Omega_2) \text{ such that, for all } \mathsf{S} \in \mathcal{H}_0(\Omega_1,\Omega_2),\ a(\mathsf{T},\mathsf{S}) = l(\mathsf{S}), \tag{3.7}$$

where the bilinear and linear forms are respectively

$$\begin{aligned} a(\mathsf{T},\mathsf{S}) &:= \sum_{i=1}^{2}\int_{\Omega_i}\kappa_i\nabla\mathsf{T}_i\cdot\nabla\mathsf{S}_i\,\mathrm{d}x + \int_{\Omega_1}\mathsf{S}_1\boldsymbol{u}\cdot\nabla\mathsf{T}_1\,\mathrm{d}x + \int_{\Gamma_\mathrm{R}}\alpha\mathsf{T}_2\mathsf{S}_2\,\mathrm{d}s \\ &\quad + \int_{\Gamma}\left(\eta\kappa_\mathrm{s}\nabla_\tau\langle\mathsf{T}\rangle\cdot\nabla_\tau\langle\mathsf{S}\rangle + \kappa_\mathrm{s}H[\mathsf{T}]\langle\mathsf{S}\rangle + \frac{\kappa_\mathrm{s}}{\eta}[\mathsf{T}][\mathsf{S}]\right)\mathrm{d}s, \\ l(\mathsf{S}) &:= \int_{\Gamma_\mathrm{R}}\alpha\mathsf{T}_{\mathrm{ext}}\mathsf{S}_2\,\mathrm{d}x. \end{aligned}$$

Remark 12 *Here we highlight an important point in obtaining the previous variational formulation. Let* T *be the strong solution of* (3.2) *that we suppose* $\mathcal{H}^2(\Omega_1,\Omega_2)$ *and* $\mathsf{S}\in\mathcal{H}_0(\Omega_1,\Omega_2)$*. Using Green's formula on the boundary* Γ *(see, e.g., [104, Proposition 2.58]), we obtain*

$$\int_\Gamma -\operatorname{div}_\tau(\nabla_\tau\langle\mathsf{T}\rangle)\langle\mathsf{S}\rangle\ \mathrm{d}s = \int_\Gamma \nabla_\tau\langle\mathsf{T}\rangle\cdot\langle\mathsf{S}\rangle\ \mathrm{d}s - \int_{\partial\Gamma}\langle\mathsf{S}\rangle\nabla_\tau\langle\mathsf{T}\rangle\cdot\boldsymbol{\tau}\,\mathrm{d}l,$$

where $\boldsymbol{\tau}$ *is the unit tangent vector to* Γ*, normal to* $\partial\Gamma$ *and* $\mathrm{d}l$ *is the* $(d-2)$ *dimensional measure along* $\partial\Gamma$*. In our situation,* $\boldsymbol{\tau}$ *corresponds to the normal to* Γ_D *on* $\overline{\Gamma}\cap\overline{\Gamma}_\mathrm{D}$ *and the normal to* Γ_N *on* $\overline{\Gamma}\cap\overline{\Gamma}_\mathrm{N}$*. Then the second term of the right hand-side of the previous formula vanishes since* $\nabla_\tau\langle\mathsf{T}\rangle\cdot\boldsymbol{\tau} = \dfrac{\partial\langle\mathsf{T}\rangle}{\partial\boldsymbol{N}}$ *and since* $\dfrac{\partial\langle\mathsf{T}\rangle}{\partial\boldsymbol{N}} = 0$ *on* $\partial\Gamma$ *(see Equation 3.2).*

Then the following result claims that this problem is well-posed.

Theorem 3.2.1 (Well-posedness of the state equation for temperature) Assume that the exit condition (3.6) holds. There exists a positive real number η_0 such that, if $0<\eta<\eta_0$, then the convection-diffusion problem (3.7) has a unique solution $\mathsf{T}\in\mathcal{H}_{\mathsf{T}_\mathrm{D}}(\Omega_1,\Omega_2)$.

3.2.2 Shape sensitivity analysis

Now we aim to perform a shape sensitivity analysis and compute the shape derivative of the objective functional J given in (3.3). To do this, we rely on the Hadamard shape derivative (see [104, 72] among many). We suppose Ω_2 to be smooth enough (at least $\mathcal{C}^2$). The main idea is to perturb the domain Ω_2 (in particular, the free boundary Γ_R) using a vector deformation field $\boldsymbol{\theta}\in\mathcal{C}^{1,\infty}(\mathbb{R}^d)^d := \mathcal{C}^1\cap\mathrm{W}^{1,\infty}(\mathbb{R}^d)^d$ with $\|\boldsymbol{\theta}\|_{\mathrm{W}^{1,\infty}(\mathbb{R}^d)^d}<1$, this is,

$$\Omega_2^{\boldsymbol{\theta}} := (\boldsymbol{I}+\boldsymbol{\theta})\Omega_2.$$

We consider the following space of admissible deformations,

$$\Theta_{\mathrm{ad}} := \{\boldsymbol{\theta}\in\mathcal{C}^{1,\infty}(\mathbb{R}^d)^d;\quad \|\boldsymbol{\theta}\|_{\mathrm{W}^{1,\infty}(\mathbb{R}^d)^d}<1,\quad \boldsymbol{\theta}=0 \text{ in } \overline{\Omega_1}\}.$$

Definition 3.2.2. *The shape derivative of a function $J(\Omega_2)$ is defined as the Fréchet derivative at 0 of the map $\boldsymbol{\theta} \in \Theta_{\mathrm{ad}} \mapsto J(\Omega_2^{\boldsymbol{\theta}}) \in \mathbb{R}$. It is denoted by $J'(\Omega_2)$ and it is then given by*

$$J(\Omega_2^{\boldsymbol{\theta}}) = J(\Omega_2) + \langle J'(\Omega_2), \boldsymbol{\theta} \rangle + o(\boldsymbol{\theta}), \text{ with } \lim_{\boldsymbol{\theta} \to 0} \frac{o(\boldsymbol{\theta})}{\|\boldsymbol{\theta}\|_{\mathrm{W}^{1,\infty}(\mathbb{R}^d)^d}} = 0.$$

In the following, we introduce $\mathsf{T}_{\boldsymbol{\theta}} \in \mathcal{H}_{\mathsf{T}_{\mathrm{D}}}(\Omega_1, \Omega_2^{\boldsymbol{\theta}})$ the perturbed solution, i.e. the solution of approximate convection-diffusion Problem (3.2) defined on $\Omega_1 \cup \Omega_2^{\boldsymbol{\theta}}$ instead of $\Omega_1 \cup \Omega_2$.

Proposition 3.2.3 (Existence and characterization of the shape derivative)**.** *If $\mathsf{T}_{\mathrm{ext}} \in \mathrm{H}^2(\mathbb{R}^d)$, then there exists an extension $\tilde{\mathsf{T}}_{\boldsymbol{\theta}} \in \mathrm{H}^1(\mathbb{R}^d) \times \mathrm{H}^1(\mathbb{R}^d)$ of $\mathsf{T}_{\boldsymbol{\theta}}$ such that the mapping $\boldsymbol{\theta} \mapsto \tilde{\mathsf{T}}_{\boldsymbol{\theta}}$ from Θ_{ad} into $\mathrm{L}^2(\mathbb{R}^d) \times \mathrm{L}^2(\mathbb{R}^d)$ is $\mathcal{C}^1$ at 0 and the derivative, denoted T', is called shape derivative of T. In addition, for $\boldsymbol{\theta} \in \Theta_{\mathrm{ad}}$ and assuming that T_2 belongs to $\mathrm{H}^2(\Omega_2)$, the shape derivative $\mathsf{T}' \in \mathcal{H}_0(\Omega_1, \Omega_2)$ is characterized by,*

$$\begin{cases} -\kappa_1 \Delta \mathsf{T}_1' + \nabla \mathsf{T}_1' \cdot \boldsymbol{u} &= 0 \text{ in } \Omega_1, \\ -\kappa_2 \Delta \mathsf{T}_2' &= 0 \text{ in } \Omega_2, \\ \mathsf{T}_1' &= 0 \text{ on } \Gamma_{\mathrm{D}}, \\ \kappa_1 \dfrac{\partial \mathsf{T}_1'}{\partial \boldsymbol{N}} &= 0 \text{ on } \Gamma_{\mathrm{N}}, \\ \kappa_2 \dfrac{\partial \mathsf{T}_2'}{\partial \boldsymbol{N}} &= 0 \text{ on } \Gamma_{\mathrm{e}}, \\ \kappa_2 \dfrac{\partial \mathsf{T}_2'}{\partial \boldsymbol{N}} + \alpha \mathsf{T}_2' &= \mathrm{div}_\tau((\boldsymbol{\theta} \cdot \boldsymbol{N}) \kappa_2 \nabla_\tau \mathsf{T}_2) - \alpha(\boldsymbol{\theta} \cdot \boldsymbol{N}) \left(\dfrac{\partial}{\partial \boldsymbol{N}} (\mathsf{T}_2 - \mathsf{T}_{\mathrm{ext}}) + H(\mathsf{T}_2 - \mathsf{T}_{\mathrm{ext}}) \right) \text{ on } \Gamma_{\mathrm{R}}, \\ \left\langle \kappa \dfrac{\partial \mathsf{T}'}{\partial \boldsymbol{n}} \right\rangle &= -\dfrac{\kappa_{\mathrm{s}}}{\eta} [\mathsf{T}'] \text{ on } \Gamma, \\ \left[\kappa \dfrac{\partial \mathsf{T}'}{\partial \boldsymbol{n}} \right] &= \eta \kappa_{\mathrm{s}} \Delta_\tau \langle \mathsf{T}' \rangle - \kappa_{\mathrm{s}} H [\mathsf{T}'] \text{ on } \Gamma, \\ \dfrac{\partial \langle \mathsf{T}' \rangle}{\partial \boldsymbol{N}} &= 0 \text{ on } \partial\Gamma. \end{cases} \tag{3.8}$$

Finally we can state the result of shape differentiability concerning the objective functional.

Proposition 3.2.4 (Shape derivative of the functional)**.** *If $\mathsf{T}_{\mathrm{ext}} \in \mathrm{H}^2(\mathbb{R}^d)$, then the insulation functional J is shape differentiable in the direction $\boldsymbol{\theta} \in \Theta_{\mathrm{ad}}$ and its shape derivative is given by*

$$J'(\Omega_2)(\boldsymbol{\theta}) = \int_{\Gamma_{\mathrm{R}}} \alpha (1 - \mathsf{R}_2) \left(\mathrm{div}_\tau(\boldsymbol{\theta})(\mathsf{T}_2 - \mathsf{T}_{\mathrm{ext}}) - \nabla \mathsf{T}_{\mathrm{ext}} \cdot \boldsymbol{\theta} \right) \mathrm{d}s + \int_{\Omega_2} \kappa_2 \left((\nabla \boldsymbol{\theta} + \nabla \boldsymbol{\theta}^t - \mathrm{div}(\boldsymbol{\theta}) \mathrm{I}) \nabla \mathsf{T}_2 \cdot \nabla \mathsf{R}_2 \, \mathrm{d}x, \right. \tag{3.9}$$

where $\mathsf{T} = (\mathsf{T}_1, \mathsf{T}_2) \in \mathcal{H}_{\mathsf{T}_{\mathrm{D}}}(\Omega_1, \Omega_2)$ is the solution of the convection-diffusion equation (3.2) and

$\mathsf{R} = (\mathsf{R}_1, \mathsf{R}_2) \in \mathcal{H}_0(\Omega_1, \Omega_2)$ *is the solution of the following adjoint equation*

$$\begin{cases} -\operatorname{div}(\kappa_1 \nabla \mathsf{R}_1 + \mathsf{R}_1 \boldsymbol{u}) &= 0 & \text{in } \Omega_1, \\ -\operatorname{div}(\kappa_2 \nabla \mathsf{R}_2) &= 0 & \text{in } \Omega_2, \\ \mathsf{R}_1 &= 0 & \text{on } \Gamma_{\mathrm{D}}, \\ \kappa_1 \dfrac{\partial \mathsf{R}_1}{\partial \boldsymbol{N}} + \mathsf{R}_1 \boldsymbol{u} \cdot \boldsymbol{N} &= 0 & \text{on } \Gamma_{\mathrm{N}}, \\ \kappa_2 \dfrac{\partial \mathsf{R}_2}{\partial \boldsymbol{N}} &= 0 & \text{on } \Gamma_{\mathrm{e}}, \\ \kappa_2 \dfrac{\partial \mathsf{R}_2}{\partial \boldsymbol{N}} + \alpha \mathsf{R}_2 &= \alpha & \text{on } \Gamma_{\mathrm{R}}, \\ \left\langle \kappa \dfrac{\partial \mathsf{R}}{\partial \boldsymbol{n}} \right\rangle &= -\dfrac{\kappa_{\mathrm{s}}}{\eta} [\mathsf{R}] - \kappa_{\mathrm{s}} H \langle \mathsf{R} \rangle & \text{on } \Gamma, \\ \left[\kappa \dfrac{\partial \mathsf{R}}{\partial \boldsymbol{n}} \right] &= \eta \operatorname{div}_\tau(\kappa_{\mathrm{s}} \nabla_\tau \langle \mathsf{R} \rangle) & \text{on } \Gamma, \\ \dfrac{\partial \langle \mathsf{R} \rangle}{\partial \boldsymbol{N}} &= 0 & \text{on } \partial\Gamma. \end{cases} \tag{3.10}$$

If furthermore $\mathsf{T}_2, \mathsf{R}_2 \in \mathrm{H}^2(\Omega_2)$*, then the shape derivative can be expressed in its surface form as*

$$J'(\Omega_2)(\boldsymbol{\theta}) = \int_{\Gamma_{\mathrm{R}}} f(\mathsf{T}_2, \mathsf{R}_2)(\boldsymbol{\theta} \cdot \boldsymbol{N}) \, \mathrm{d}s, \tag{3.11}$$

with

$$f(\mathsf{T}_2, \mathsf{R}_2) = \alpha(\mathsf{T}_2 - \mathsf{T}_{\mathrm{ext}})(1 - \mathsf{R}_2) \left(H - \frac{2\alpha}{\kappa_2} \right) - \kappa_2 \nabla \mathsf{T}_2 \cdot \nabla \mathsf{R}_2 + \alpha \frac{\partial \mathsf{T}_{\mathrm{ext}}}{\partial \boldsymbol{N}} (\mathsf{R}_2 - 1) \, .$$

3.2.3 Shape sensitivity analysis with random exterior temperature

Notice that previously, we have assumed to know the exterior parameter $\mathsf{T}_{\mathrm{ext}}$ precisely. We want now to consider the more realistic case of an imprecise knowledge of this parameter and we then aim to take into account uncertainties on this data $\mathsf{T}_{\mathrm{ext}}$.

To do that we will assume that we have information about the uncertainties.

Since in this part we consider a random exterior temperature, we will make explicit the dependence on $\mathsf{T}_{\mathrm{ext}}$ by means of the notation:

$$J(\Omega_2, \mathsf{T}_{\mathrm{ext}}) = \int_{\Gamma_{\mathrm{R}}} \alpha(\mathsf{T}_2 - \mathsf{T}_{\mathrm{ext}}) \, \mathrm{d}s,$$

where $\mathsf{T} = (\mathsf{T}_1, \mathsf{T}_2)$ is the solution of the convection-diffusion problem (3.2) with exterior temperature $\mathsf{T}_{\mathrm{ext}}$.

Let $(\Xi, \mathcal{A}, \mathbb{P})$ be a complete probability space. We consider the case where the exterior temperature is given as a random process in the Bochner space $\mathrm{L}^2(\Xi, \mathrm{H}^1(\mathbb{R}^d))$. The temperature $\mathsf{T}(\cdot, \cdot)$

then becomes a random process defined as the unique solution in $\mathcal{H}_{\mathsf{T}_\mathrm{D}}(\Omega_1,\Omega_2)$ to the following system

$$\left\{\begin{array}{rcll} -\operatorname{div}(\kappa_1\nabla\mathsf{T}_1(\cdot,\omega)) + \boldsymbol{u}\cdot\nabla\mathsf{T}_1(\cdot,\omega) &=& 0 & \text{in } \Omega_1,\\ -\operatorname{div}(\kappa_2\nabla\mathsf{T}_2(\cdot,\omega)) &=& 0 & \text{in } \Omega_2,\\ \mathsf{T}_1(\cdot,\omega) &=& \mathsf{T}_\mathrm{D} & \text{on } \Gamma_\mathrm{D},\\ \kappa_1\dfrac{\partial\mathsf{T}_1(\cdot,\omega)}{\partial\boldsymbol{N}} &=& 0 & \text{on } \Gamma_\mathrm{N},\\ \kappa_2\dfrac{\partial\mathsf{T}_2(\cdot,\omega)}{\partial\boldsymbol{N}} &=& 0 & \text{on } \Gamma_\mathrm{e},\\ \kappa_2\dfrac{\partial\mathsf{T}_2(\cdot,\omega)}{\partial\boldsymbol{N}} + \alpha\mathsf{T}_2(\cdot,\omega) &=& \alpha\mathsf{T}_\mathrm{ext}(\cdot,\omega) & \text{on } \Gamma_\mathrm{R},\\ \left\langle\kappa\dfrac{\partial\mathsf{T}(\cdot,\omega)}{\partial\boldsymbol{n}}\right\rangle &=& -\dfrac{\kappa_\mathrm{s}}{\eta}\left[\mathsf{T}(\cdot,\omega)\right] & \text{on } \Gamma,\\ \left[\kappa\dfrac{\partial\mathsf{T}(\cdot,\omega)}{\partial\boldsymbol{n}}\right] &=& \eta\operatorname{div}_\tau(\kappa_\mathrm{s}\nabla_\tau\langle\mathsf{T}(\cdot,\omega)\rangle) - \kappa_\mathrm{s}H[\mathsf{T}(\cdot,\omega)] & \text{on } \Gamma,\\ \dfrac{\partial\langle\mathsf{T}(\cdot,\omega)\rangle}{\partial\boldsymbol{N}} &=& 0 & \text{on } \partial\Gamma. \end{array}\right. \tag{3.12}$$

The objective is now to minimize $\mathbb{E}[J(\Omega_2,\mathsf{T}_\mathrm{ext}(x,\cdot))]$ the expectation of the objective functional J. The functional of interest J is affine in a temperature that depends linearly on the random parameter. This situation fits to the context of the work of Dambrine *et al.* [44]. Note that considering higher order moments can been done by a mere adaptation of the methods (see [45]). The gradient of the objective can be computed thanks to the two-point correlation of the random input T_ext. In order to avoid the needed introduction of tensor calculus for the general case (see [44] for the quadratic case and [38] for the general polynomial case), we restrict ourselves in this work to the particular case where T_ext is a finite sum

$$\mathsf{T}_\mathrm{ext}(x,\omega) = \mathsf{T}^0_\mathrm{ext}(x) + \sum_{k=1}^{m}\xi_k(\omega)\mathsf{T}^k_\mathrm{ext}(x), \quad x\in\Omega,\ \omega\in\Xi, \tag{3.13}$$

where the random variables ξ_k are assumed independent following centered Gaussian distributions with mean σ_k. This case can been dealt with easily but remains representative of the general situation when m the number of terms goes to ∞. The expression (3.13) is a so-called truncated Karhunen-Loeve decomposition [85, Chapter 5.4].

Theorem 3.2.5 (Shape derivative of the expectation of J) Let us consider an uncertain exterior temperature expanded as in (3.13). Let us also assume that the random variables ξ_k mean equal to σ_k and are independent. Then the expectation of J can be computed as

$$\mathbb{E}[J(\Omega_2,\mathsf{T}_\mathrm{ext})] = J(\Omega_2,\mathsf{T}^0_\mathrm{ext}) + \sum_{k=1}^{m}\sigma_k J(\Omega_2,\mathsf{T}^k_\mathrm{ext}) \tag{3.14}$$

and, under regularity assumptions similar to those of Proposition 4.6.3, its shape derivative is then given by

$$\left(\mathbb{E}[J]\right)'(\Omega_2,\mathsf{T}_\mathrm{ext})(\boldsymbol{\theta}) = J'(\Omega_2,\mathsf{T}^0_\mathrm{ext})(\boldsymbol{\theta}) + \sum_{k=1}^{m}\sigma_k J'(\Omega_2,\mathsf{T}^k_\mathrm{ext})(\boldsymbol{\theta}). \tag{3.15}$$

Remark 13 *In the above theorem, we need to define the solution associated to each* $\mathsf{T}^0_{\rm ext}$ *and* $\mathsf{T}^k_{\rm ext}$ *(in order to define the associated functional). Then we specify that (see the corresponding proof), for each* $k = 1, \dots, m$, $\mathsf{T}^k \in \mathcal{H}_0(\Omega_1, \Omega_2)$ *solves Equation 3.2 with respectively* $\mathsf{T}^k_{\rm ext}$ *and* 0 *as conditions on* $\Gamma_{\rm R}$ *and* $\Gamma_{\rm D}$*, and where* $\mathsf{T}^0 \in \mathcal{H}_{\mathsf{T}_{\rm D}}(\Omega_1, \Omega_2)$ *solves Equation* (3.2) *with respectively* $\mathsf{T}^0_{\rm ext}$ *and* $\mathsf{T}_{\rm D}$ *as conditions on* $\Gamma_{\rm R}$ *and* $\Gamma_{\rm D}$*.*

3.3 Proofs

3.3.1 Proof of the well-posedness Theorem 3.2.1

Proof of Theorem 3.2.1. We follow the usual strategy: lift the boundary condition and apply Lax-Milgram theorem in the space $\mathcal{H}_0(\Omega_1, \Omega_2)$. The crucial point is to prove that a is coercive. The presence of an interface condition on Γ is not completely customary. We therefore demonstrate this point.

Let $\mathsf{S} \in \mathcal{H}_0(\Omega_1, \Omega_2)$. We split $a(\mathsf{S}, \mathsf{S})$ into $a_1(\mathsf{S}, \mathsf{S}) + a_2(\mathsf{S}, \mathsf{S}) + a_3(\mathsf{S}, \mathsf{S})$ where

$$\begin{aligned}
a_1(\mathsf{S}, \mathsf{S}) &:= \sum_{i=1}^{2} \int_{\Omega_i} \kappa_i |\nabla \mathsf{S}_i|^2 \,\mathrm{d}x + \kappa_{\rm s} \int_\Gamma \left(\eta |\nabla_\tau \langle \mathsf{S} \rangle|^2 + \frac{1}{\eta} [\mathsf{S}]^2 \right) \mathrm{d}s + \int_{\Gamma_{\rm R}} \alpha \mathsf{S}_2^2 \,\mathrm{d}s, \\
a_2(\mathsf{S}, \mathsf{S}) &:= \int_{\Omega_1} \mathsf{S}_1 (\boldsymbol{u} \cdot \nabla \mathsf{S}_1) \,\mathrm{d}x, \\
a_3(\mathsf{S}, \mathsf{S}) &:= \kappa_{\rm s} \int_\Gamma H [\mathsf{S}] \langle \mathsf{S} \rangle \,\mathrm{d}s.
\end{aligned}$$

The bilinear form a_1 clearly is coercive,

$$a_1(\mathsf{S}, \mathsf{S}) \geq \sum_{i=1}^{2} \kappa_i \|\nabla \mathsf{S}_i\|^2_{\mathrm{L}^2(\Omega_i)^d} + \eta \kappa_{\rm s} \|\nabla_\tau \langle \mathsf{S} \rangle\|^2_{\mathrm{L}^2(\Gamma)^d} + \frac{\kappa_{\rm s}}{\eta} \|[\mathsf{S}]\|^2_{\mathrm{L}^2(\Gamma)}.$$

Concerning a_2, we get after integration by parts

$$a_2(\mathsf{S}, \mathsf{S}) = \int_{\Omega_1} \boldsymbol{u} \cdot \nabla \left(\frac{\mathsf{S}_2^2}{2} \right) \mathrm{d}x = \frac{1}{2} \int_{\Gamma_{\rm N}} \mathsf{S}_2^2 \boldsymbol{u} \cdot \boldsymbol{N} \,\mathrm{d}s.$$

We have used the boundary conditions $\boldsymbol{u} = 0$ on Γ and $\mathsf{S}_1 = 0$ on $\Gamma_{\rm D}$ and the incompressiblility of the fluid $\mathrm{div}(\boldsymbol{u}) = 0$ in Ω_1. Now since the output normal velocity $\boldsymbol{u} \cdot \boldsymbol{N}$ is nonnegative by the exit condition (4.10), we get $a_2(\mathsf{S}, \mathsf{S}) \geq 0$. The difficulty lays in the product $[\mathsf{S}] \langle \mathsf{S} \rangle$ that has no sign. Using successively Cauchy-Schwarz then Young's inequalities, one gets

$$\begin{aligned}
\left| \int_\Gamma H [\mathsf{S}] \langle \mathsf{S} \rangle \,\mathrm{d}s \right| &= \frac{1}{2} \left| \int_\Gamma [\mathsf{S}] \ (H \ \mathsf{S}_1 \ + \ H \ \mathsf{S}_2) \,\mathrm{d}s \right| \\
&\leq \frac{1}{2} \|[\mathsf{S}]\|^2_{\mathrm{L}^2(\Gamma)} \left(\|H \mathsf{S}_1\|^2_{\mathrm{L}^2(\Gamma)} + \|H \mathsf{S}_2\|^2_{\mathrm{L}^2(\Gamma)} \right) \\
&\leq \frac{1}{2} \left(\frac{1}{2\eta} \|[\mathsf{S}]\|^2_{\mathrm{L}^2(\Gamma)} + \frac{\eta}{2} \|H \mathsf{S}_1\|^2_{\mathrm{L}^2(\Gamma)} + \frac{1}{2\eta} \|[\mathsf{S}]\|^2_{\mathrm{L}^2(\Gamma)} + \frac{\eta}{2} \|H \mathsf{S}_2\|^2_{\mathrm{L}^2(\Gamma)} \right) \\
&\leq \frac{1}{2\eta} \|[\mathsf{S}]\|^2_{\mathrm{L}^2(\Gamma)} + \frac{\eta \|H\|^2_\infty}{4} \left(\|\mathsf{S}_1\|^2_{\mathrm{L}^2(\Gamma)} + \|\mathsf{S}_2\|^2_{\mathrm{L}^2(\Gamma)} \right).
\end{aligned}$$

Since $\mathsf{S}_1 = 0$ on $\Gamma_{\rm D}$, one infers from the trace theorem and Poincaré inequality for S_1, the existence of a positive constant $C > 0$, such that, $\|\mathsf{S}_1\|^2_{\mathrm{L}^2(\Gamma)} \leq C\|\nabla \mathsf{S}_1\|^2_{\mathrm{L}^2(\Omega_1)^d}$. This is not the case for S_2. Using the definition of the jump, ones gets

$$\|\mathsf{S}_2\|_{\mathrm{L}^2(\Gamma)} \leq \|\mathsf{S}_1\|_{\mathrm{L}^2(\Gamma)} + \|[\mathsf{S}]\|_{\mathrm{L}^2(\Gamma)} \text{ then } \|\mathsf{S}_2\|^2_{\mathrm{L}^2(\Gamma)} \leq 2\left(\|\mathsf{S}_1\|^2_{\mathrm{L}^2(\Gamma)} + \|[\mathsf{S}]\|^2_{\mathrm{L}^2(\Gamma)}\right)$$

by the triangle inequality. Finally, we have obtained the bound

$$\left|\int_\Gamma H[\mathsf{S}]\,\langle \mathsf{S}\rangle \,\mathrm{d}s\right| \leq \frac{1}{2}\left(\frac{1}{\eta} + \eta\|H\|^2_\infty\right)\|[\mathsf{S}]\|^2_{\mathrm{L}^2(\Gamma)} + \frac{3\eta C\|H\|^2_\infty}{4}\,\|\nabla \mathsf{S}_1\|^2_{\mathrm{L}^2(\Omega_1)^d}.$$

Therefore,

$$a_1(\mathsf{S},\mathsf{S}) + a_3(\mathsf{S},\mathsf{S}) \geq \sum_{i=1}^{2}\kappa_i\|\nabla \mathsf{S}_i\|^2_{\mathrm{L}^2(\Omega_i)^d} - \ \eta\ \frac{3C\kappa_{\rm s}\|H\|^2_\infty}{4}\ \|\nabla \mathsf{S}_1\|^2_{\mathrm{L}^2(\Omega_1)^d} + \eta\kappa_{\rm s}\|\nabla_\tau\,\langle \mathsf{S}\rangle\,\|^2_{\mathrm{L}^2(\Gamma)^d}$$
$$+ \frac{\kappa_{\rm s}}{2}\left(\frac{1}{\eta} - \eta\|H\|^2_\infty\right)\|[\mathsf{S}]\|^2_{\mathrm{L}^2(\Gamma)}.$$

We impose $\eta < \|H\|^{-1}_\infty$ so that the last term is nonnegative. The second term is absorbed by the corresponding term in a_1 if we impose that

$$\kappa_1 - \eta\ \frac{3C\kappa_{\rm s}\|H\|^2_\infty}{4} \geq \frac{1}{2}\kappa_1 \Leftrightarrow \eta \leq \frac{2\kappa_1}{3C\kappa_{\rm s}\|H\|^2_\infty}.$$

In conclusion a is coercive if

$$\eta < \eta_0 := \min\left(\frac{1}{\|H\|_\infty}, \frac{2\kappa_1}{3C\kappa_{\rm s}\|H\|^2_\infty}\right),$$

which concludes the proof.

□

3.3.2 Shape sensitivity analysis

Before proving the main result of this part (Proposition 4.6.3), we need some auxiliary results, as the existence of the derivative. As is classical in shape optimization, the first step is to show the existence of the material derivative and then compute it (see, e.g., [72, 8]). For the sake of simplicity, we assume without loss of generality $\mathsf{T}_{\rm D} = 0$.

We recall that, for $\boldsymbol{\theta} \in \Theta_{\rm ad}$, $\mathsf{T}_{\boldsymbol{\theta}} \in \mathcal{H}_{\mathsf{T}_{\rm D}}(\Omega_1, \Omega_2^{\boldsymbol{\theta}})$ is the solution of the convection-diffusion Problem (3.2) defined in $\Omega_1 \cup \Omega_2^{\boldsymbol{\theta}}$ instead of $\Omega_1 \cup \Omega_2$.

Proposition 3.3.1 (Existence and characterization of the material derivative of T)**.** *For all $\boldsymbol{\theta} \in \Theta_{\rm ad}$, we define the transported solution $\overline{\mathsf{T}}_{\boldsymbol{\theta}} := \mathsf{T}_{\boldsymbol{\theta}} \circ (\boldsymbol{I} + \boldsymbol{\theta})$. If $\mathsf{T}_{\rm ext} \in \mathrm{H}^2(B)$, then*

$$\boldsymbol{\theta} \in \Theta_{\rm ad} \mapsto \overline{\mathsf{T}}_{\boldsymbol{\theta}} \in \mathcal{H}_{\mathsf{T}_{\rm D}}(\Omega_1, \Omega_2)$$

is differentiable in a neighborhood of 0*. Furthermore, its derivative at 0, in the direction* $\boldsymbol{\theta}$*, is called the material derivative of* $\mathsf{T} \in \mathcal{H}_{\mathsf{T}_\mathrm{D}}(\Omega_1, \Omega_2)$*, is denoted by* $\dot{\mathsf{T}} \in \mathcal{H}_0(\Omega_1, \Omega_2)$*, and is the solution of the following variational problem*

$$\begin{cases} \text{Find } \dot{\mathsf{T}} \in \mathcal{H}_0(\Omega_1, \Omega_2) \text{ such that, for all } \phi \in \mathcal{H}_0(\Omega_1, \Omega_2), \\ \displaystyle\sum_{i=1}^{2} \int_{\Omega_i} \kappa_i \nabla \dot{\mathsf{T}}_i \cdot \nabla \phi_i \,\mathrm{d}x + \int_{\Omega_1} \nabla \dot{\mathsf{T}}_1 \cdot \boldsymbol{u} \phi_1 \,\mathrm{d}x + \int_{\Gamma_\mathrm{R}} \alpha \dot{\mathsf{T}}_2 \phi_2 \,\mathrm{d}s \\ \quad + \displaystyle\int_\Gamma \left(\eta \kappa_\mathrm{s} \nabla_\tau \left\langle \dot{\mathsf{T}} \right\rangle \cdot \nabla_\tau \langle \phi \rangle + \kappa_\mathrm{s} H[\dot{\mathsf{T}}] \langle \phi \rangle + \frac{\kappa_\mathrm{s}}{\eta} [\dot{\mathsf{T}}][\phi] \right) \mathrm{d}s \\ = \displaystyle\int_{\Omega_2} \kappa_2 \left(\nabla \boldsymbol{\theta} + \nabla \boldsymbol{\theta}^t - \mathrm{div}(\boldsymbol{\theta}) \mathrm{I} \right) \nabla \mathsf{T}_2 \cdot \nabla \phi_2 \,\mathrm{d}x - \int_{\Gamma_\mathrm{R}} \left(\alpha \,\mathrm{div}_\tau(\boldsymbol{\theta})(\mathsf{T}_2 - \mathsf{T}_{\mathrm{ext}}) \phi_2 - \alpha \nabla \mathsf{T}_{\mathrm{ext}} \cdot \boldsymbol{\theta} \phi_2 \right) \mathrm{d}s. \end{cases} \tag{3.16}$$

The process to prove this result is classical (see [72]) and it is based on the implicit function theorem, although our equation is non standard, so we will do it.

Proof of Proposition 3.3.1. *Step 1: transport on a fixed domain.*
Let $\phi \in \mathcal{H}_0(\Omega_1, \Omega_2)$ and let $\boldsymbol{\theta} \in \Theta_{\mathrm{ad}}$. We define $\phi_{\boldsymbol{\theta}} := \phi \circ (\boldsymbol{I} + \boldsymbol{\theta})^{-1} \in \mathcal{H}_0(\Omega_1, \Omega_2^{\boldsymbol{\theta}})$ and we have

$$\begin{aligned} &\int_{\Omega_2^{\boldsymbol{\theta}}} \kappa_2 \nabla \mathsf{T}_{\boldsymbol{\theta},2} \cdot \nabla \phi_{\boldsymbol{\theta},2} \,\mathrm{d}x + \int_{\Omega_1} \left(\kappa_1 \nabla \mathsf{T}_{\boldsymbol{\theta},1} \cdot \nabla \phi_{\boldsymbol{\theta},1} + \nabla \mathsf{T}_{\boldsymbol{\theta},1} \cdot \boldsymbol{u} \phi_{\boldsymbol{\theta}} \right) \mathrm{d}x + \int_{\Gamma_\mathrm{R}} \alpha \mathsf{T}_{\boldsymbol{\theta},2} \phi_{\boldsymbol{\theta},2} \,\mathrm{d}s \\ &\qquad + \int_{\Gamma^{\boldsymbol{\theta}}} \left(\eta \kappa_\mathrm{s} \nabla_{\tau_{\boldsymbol{\theta}}} \langle \mathsf{T}_{\boldsymbol{\theta}} \rangle \cdot \nabla_{\tau_{\boldsymbol{\theta}}} \langle \phi_{\boldsymbol{\theta}} \rangle + \kappa_\mathrm{s} H_{\boldsymbol{\theta}}[\mathsf{T}_{\boldsymbol{\theta}}] \langle \phi_{\boldsymbol{\theta}} \rangle + \frac{\kappa_\mathrm{s}}{\eta} [\mathsf{T}_{\boldsymbol{\theta}}][\phi_{\boldsymbol{\theta}}] \right) \mathrm{d}s = \int_{\Gamma_\mathrm{R}^{\boldsymbol{\theta}}} \alpha \mathsf{T}_{\mathrm{ext}} \phi_{\boldsymbol{\theta},2} \,\mathrm{d}x. \end{aligned}$$

Changing variables, we get

$$\begin{aligned} &\int_{\Omega_2} \kappa_2 A(\boldsymbol{\theta}) \nabla \overline{\mathsf{T}}_{\boldsymbol{\theta},2} \cdot \nabla \phi_2 \,\mathrm{d}x + \int_{\Omega_1} \left(\kappa_1 \nabla \overline{\mathsf{T}}_{\boldsymbol{\theta},1} \cdot \nabla \phi_1 + \nabla \overline{\mathsf{T}}_{\boldsymbol{\theta},1} \cdot \boldsymbol{u} \phi_1 \right) \mathrm{d}x + \int_{\Gamma_\mathrm{R}} \alpha B(\boldsymbol{\theta}) \overline{\mathsf{T}}_{\boldsymbol{\theta},2} \phi_2 \,\mathrm{d}s \\ &\quad + \int_\Gamma \left(\eta \kappa_\mathrm{s} \nabla_\tau \left\langle \overline{\mathsf{T}}_{\boldsymbol{\theta}} \right\rangle \cdot \nabla_\tau \langle \phi \rangle + \kappa_\mathrm{s} H[\overline{\mathsf{T}}_{\boldsymbol{\theta}}] \langle \phi \rangle + \frac{\kappa_\mathrm{s}}{\eta} [\overline{\mathsf{T}}_{\boldsymbol{\theta}}][\phi] \right) \mathrm{d}s = \int_{\Gamma_\mathrm{R}} \alpha B(\boldsymbol{\theta}) \mathsf{T}_{\mathrm{ext}} \circ (\boldsymbol{I} + \boldsymbol{\theta}) \phi_2 \,\mathrm{d}x, \end{aligned} \tag{3.17}$$

where

$$A(\boldsymbol{\theta}) := |\det(\mathrm{I} + \nabla \boldsymbol{\theta})| (\mathrm{I} + \nabla \boldsymbol{\theta})^{-1} (\mathrm{I} + \nabla \boldsymbol{\theta})^{-t}, B(\boldsymbol{\theta}) := |\det(\mathrm{I} + \nabla \boldsymbol{\theta})| |(\mathrm{I} + \nabla \boldsymbol{\theta})^{-t} \boldsymbol{N}|_{\mathbb{R}^d}, \tag{3.18}$$

and $|\cdot|_{\mathbb{R}^d}$ is the usual Euclidean norm in $\mathbb{R}^d$. *Step 2: implicit function theorem.*
We introduce $\mathcal{F} : \Theta_{\mathrm{ad}} \times \mathcal{H}_0(\Omega_1, \Omega_2) \mapsto (\mathcal{H}_0(\Omega_1, \Omega_2))'$, defined for all $S \in \mathcal{H}_0(\Omega_1, \Omega_2)$ by,

$$\begin{aligned} \langle \mathcal{F}(\boldsymbol{\theta}, \overline{T}), S \rangle := &\int_{\Omega_2} \kappa_2 A(\boldsymbol{\theta}) \nabla \overline{T} \cdot \nabla S \,\mathrm{d}x + \int_{\Omega_1} \left(\kappa_1 \nabla \overline{T} \cdot \nabla S + \nabla \overline{T} \cdot \boldsymbol{u} S \right) \mathrm{d}x + \int_{\Gamma_\mathrm{R}} \alpha B(\boldsymbol{\theta}) \overline{T} S \,\mathrm{d}s \\ &+ \int_\Gamma \kappa_\mathrm{s} \left(\eta \nabla_\tau \left\langle \overline{T} \right\rangle \cdot \nabla_\tau \langle S \rangle + H[\overline{T}] \langle S \rangle + \frac{1}{\eta} [\overline{T}][S] \right) \mathrm{d}s - \int_{\Gamma_\mathrm{R}} \alpha B(\boldsymbol{\theta}) \mathsf{T}_{\mathrm{ext}} \circ (\boldsymbol{I} + \boldsymbol{\theta}) S \,\mathrm{d}s. \end{aligned}$$

By construction $\mathcal{F}(0, \mathsf{T}) = 0$ where T is the solution of the approximate convection-diffusion equation (3.2). Similarly to [72, Theorem 5.5.1], we have that $\boldsymbol{\theta} \in \Theta_{\mathrm{ad}} \mapsto A(\boldsymbol{\theta}) \in \mathrm{L}^\infty(\mathbb{R}^d, \mathcal{M}_d)$,

$\boldsymbol{\theta} \in \Theta_{\rm ad} \mapsto B(\boldsymbol{\theta}) \in \mathcal{C}^0(\Gamma_{\rm R})$ are $\mathcal{C}^\infty$, where $\mathcal{M}_d$ is the space of $d \times d$ matrices and $\boldsymbol{\theta} \in \Theta_{\rm ad} \mapsto G(\boldsymbol{\theta}) := \mathsf{T}_{\rm ext} \circ (\mathsf{I} + \boldsymbol{\theta}) \in \mathrm{H}^1(\mathbb{R}^d)$ is $\mathcal{C}^1$ in a neighborhood of 0. By chain rule we deduce that $\mathcal{F}$ is $\mathcal{C}^1$ in a neighborhood of 0. Finally, the operator $D_{\overline{T}}\mathcal{F}(0, \mathsf{T})$ is an isomorphism from $\mathcal{H}_0(\Omega_1, \Omega_2)$ into $(\mathcal{H}_0(\Omega_1, \Omega_2))'$, since for all $S, \hat{S} \in \mathcal{H}_0(\Omega_1, \Omega_2)$,

$$\langle D_{\overline{T}}\mathcal{F}(0, \mathsf{T})S, \hat{S}\rangle = \sum_{i=1}^{2} \int_{\Omega_i} \kappa_i \nabla S_i \cdot \nabla \hat{S}_i \,\mathrm{d}x + \int_{\Omega_1} \nabla S_1 \cdot \boldsymbol{u}\hat{S}_1 \,\mathrm{d}x + \int_{\Gamma_{\rm R}} \alpha S_2 \hat{S}_2 \,\mathrm{d}s + \int_{\Gamma} \left(\eta\kappa_{\rm s} \nabla_\tau \langle S\rangle \cdot \nabla_\tau \langle \hat{S}\rangle + \kappa_{\rm s} H[S] \left\langle \hat{S} \right\rangle + \frac{\kappa_{\rm s}}{\eta}[S][\hat{S}] \right) \mathrm{d}s.$$

In virtue of the implicit function theorem, there exists a $\mathcal{C}^1$ function $\boldsymbol{\theta} \in \Theta_{\rm ad} \mapsto \overline{T}(\boldsymbol{\theta}) \in \mathcal{H}_0(\Omega_1, \Omega_2)$ in a neighborhood of 0 such that, $\mathcal{F}(0, \overline{T}(\boldsymbol{\theta})) = 0$. By uniqueness of the solution $\overline{\mathsf{T}}_{\boldsymbol{\theta}}$, we deduce $\overline{\mathsf{T}}_{\boldsymbol{\theta}} = \overline{T}(\boldsymbol{\theta})$, then, $\boldsymbol{\theta} \mapsto \overline{\mathsf{T}}_{\boldsymbol{\theta}}$ is $\mathcal{C}^1$.

Step 3: characterization of the material derivative.
To prove that the material derivative $\dot{\mathsf{T}}$ satisfies (3.16), we first recall that (see [72, Section 5.5])

$$DA(0)(\boldsymbol{\theta}) = \mathrm{div}(\boldsymbol{\theta})\mathrm{I} - \nabla\boldsymbol{\theta} - (\nabla\boldsymbol{\theta})^t, \quad DB(0)(\boldsymbol{\theta}) = \mathrm{div}_\tau(\boldsymbol{\theta}) \quad \text{and} \quad DG(0)(\boldsymbol{\theta}) = \nabla\mathsf{T}_{\rm ext} \cdot \boldsymbol{\theta}.$$

Then, differentiating (3.17) at $\boldsymbol{\theta} = 0$, in the direction $\boldsymbol{\theta}$ and using the chain rule of those derivatives, we get (3.16). □

After showing the existence and computing the material derivative, we can do the same for the eulerian derivative, which proof uses the previous results and some integrations by parts.

Proof of Proposition 3.2.3. Let us introduce a linear continuous extension

$$E : \mathcal{H}_0(\Omega_1, \Omega_2) \mapsto \mathrm{H}^1(\mathbb{R}^d) \times \mathrm{H}^1(\mathbb{R}^d).$$

We define $\tilde{\mathsf{T}}_{\boldsymbol{\theta}} := E(\overline{\mathsf{T}}_{\boldsymbol{\theta}}) \circ (\boldsymbol{I} + \boldsymbol{\theta})^{-1} \in \mathcal{H}_0(\Omega_1, \Omega_2)$ and since $\boldsymbol{\theta} \in \Theta_{\rm ad} \mapsto \overline{\mathsf{T}}_{\boldsymbol{\theta}} \in \mathcal{H}_0(\Omega_1, \Omega_2)$ is $\mathcal{C}^1$ in a neighborhood of 0, we obtain the existence of the shape derivative using [72, Lemma 5.3.3].

To characterize the shape derivative $\mathsf{T}' \in \mathcal{H}_0(\Omega_1, \Omega_2)$, we use that $\mathsf{T}'_2 = \dot{\mathsf{T}}_2 - \boldsymbol{\theta} \cdot \nabla\mathsf{T}_2$ belongs to $\mathrm{H}^1(\Omega_2)$ since we have assumed that $\mathsf{T}_2 \in \mathrm{H}^2(\Omega_2)$, and also that $\mathsf{T}'_1 = \dot{\mathsf{T}}_1 \in \mathrm{H}^1(\Omega_1)$ and $\langle \mathsf{T}'\rangle = \left\langle \dot{\mathsf{T}} \right\rangle \in \mathrm{H}^1(\Gamma)$. We use this in the material derivative variational formulation (3.16), this is,

$$
\begin{aligned}
&\int_{\Omega_2} \kappa_2 \nabla \mathsf{T}_2' \cdot \nabla \phi_2 \,\mathrm{d}x + \int_{\Omega_1} (\kappa_1 \nabla \mathsf{T}_1' \cdot \nabla \phi_1 + \phi_1 \nabla \mathsf{T}_1' \cdot \boldsymbol{u}) \,\mathrm{d}x + \int_{\Gamma_\mathrm{R}} \alpha \mathsf{T}_2' \phi_2 \,\mathrm{d}s \\
&\qquad + \int_\Gamma \left(\eta \kappa_\mathrm{s} \nabla_\tau \langle \mathsf{T}' \rangle \cdot \nabla_\tau \langle \phi \rangle + \kappa_\mathrm{s} H [\mathsf{T}'] \langle \phi \rangle + \frac{\kappa_\mathrm{s}}{\eta} [\mathsf{T}'][\phi] \right) \mathrm{d}s \\
&= \int_{\Omega_2} \left(\kappa_2 (\nabla \boldsymbol{\theta} + \nabla \boldsymbol{\theta}^t) \nabla \mathsf{T}_2 \cdot \nabla \phi_2 - \kappa_2 \operatorname{div}(\boldsymbol{\theta}) \nabla \mathsf{T}_2 \cdot \nabla \phi_2 - \kappa_2 \nabla (\boldsymbol{\theta} \cdot \nabla \mathsf{T}_2) \cdot \nabla \phi_2 \right) \mathrm{d}x \\
&\qquad - \int_{\Gamma_\mathrm{R}} (\alpha \operatorname{div}_\tau(\boldsymbol{\theta}) (\mathsf{T}_2 - \mathsf{T}_\mathrm{ext}) \phi_2 + \alpha \phi_2 \boldsymbol{\theta} \cdot \nabla (\mathsf{T}_2 - \mathsf{T}_\mathrm{ext})) \,\mathrm{d}s \\
&= \int_{\Omega_2} \left(\kappa_2 (\nabla \boldsymbol{\theta} - \operatorname{div}(\boldsymbol{\theta}) \mathrm{I}) \nabla \mathsf{T}_2 \cdot \nabla \phi_2 - \kappa_2 (\nabla^2 \mathsf{T}_2) \boldsymbol{\theta} \cdot \nabla \phi_2 \right) \mathrm{d}x \\
&\qquad - \int_{\Gamma_\mathrm{R}} (\alpha \operatorname{div}_\tau(\boldsymbol{\theta}) (\mathsf{T}_2 - \mathsf{T}_\mathrm{ext}) \phi_2 + \alpha \phi_2 \boldsymbol{\theta} \cdot \nabla (\mathsf{T}_2 - \mathsf{T}_\mathrm{ext})) \,\mathrm{d}s \\
&= \int_{\Omega_2} (\kappa_2 \operatorname{div}((\boldsymbol{\theta} \cdot \nabla \phi_2) \nabla \mathsf{T}_2 - (\nabla \mathsf{T}_2 \cdot \nabla \phi_2) \boldsymbol{\theta}) - (\boldsymbol{\theta} \cdot \nabla \phi_2) \kappa_2 \Delta \mathsf{T}_2) \,\mathrm{d}x \\
&\qquad - \int_{\Gamma_\mathrm{R}} (\alpha \operatorname{div}_\tau(\boldsymbol{\theta}) (\mathsf{T}_2 - \mathsf{T}_\mathrm{ext}) \phi_2 + \alpha \phi_2 \boldsymbol{\theta} \cdot \nabla (\mathsf{T}_2 - \mathsf{T}_\mathrm{ext})) \,\mathrm{d}s.
\end{aligned}
$$

Since T is the solution of the convection-diffusion equation (3.2), $\kappa_2 \Delta \mathsf{T}_2 = 0$ in Ω_2 with the boundary condition $\kappa_2 \frac{\partial \mathsf{T}}{\partial \boldsymbol{N}} = \alpha(\mathsf{T}_\mathrm{ext} - \mathsf{T}_2)$ on Γ_R, then

$$
\begin{aligned}
&\int_{\Omega_2} \kappa_2 \nabla \mathsf{T}_2' \cdot \nabla \phi_2 \,\mathrm{d}x + \int_{\Omega_1} (\kappa_1 \nabla \mathsf{T}_1' \cdot \nabla \phi_1 + \phi_1 \nabla \mathsf{T}_1' \cdot \boldsymbol{u}) \,\mathrm{d}x + \int_{\Gamma_\mathrm{R}} \alpha \mathsf{T}_2' \phi_2 \,\mathrm{d}s \\
&\qquad + \int_\Gamma \left(\eta \kappa_\mathrm{s} \nabla_\tau \langle \mathsf{T}' \rangle \cdot \langle \phi \rangle + \kappa_\mathrm{s} H [\mathsf{T}'] \langle \phi \rangle + \frac{\kappa_\mathrm{s}}{\eta} [\mathsf{T}'][\phi] \right) \mathrm{d}s \\
&\qquad = \int_{\Omega_2} (\kappa_2 \operatorname{div}((\boldsymbol{\theta} \cdot \nabla \phi_2) \nabla \mathsf{T}_2 - (\nabla \mathsf{T}_2 \cdot \nabla \phi_2) \boldsymbol{\theta})) \,\mathrm{d}x \\
&\qquad\qquad - \int_{\Gamma_\mathrm{R}} \alpha \left(\operatorname{div}_\tau((\mathsf{T}_2 - \mathsf{T}_\mathrm{ext}) \boldsymbol{\theta}) \phi_2 + (\boldsymbol{\theta} \cdot \boldsymbol{N}) \phi_2 \frac{\partial}{\partial \boldsymbol{N}} (\mathsf{T}_2 - \mathsf{T}_\mathrm{ext}) \right) \mathrm{d}s.
\end{aligned}
$$

By divergence theorem and the fact that $\boldsymbol{\theta} = 0$ on Γ,

$$
\begin{aligned}
&\int_{\Omega_2} \kappa_2 \nabla \mathsf{T}_2' \cdot \nabla \phi_2 \,\mathrm{d}x + \int_{\Omega_1} (\kappa_1 \nabla \mathsf{T}_1' \cdot \nabla \phi_1 + \phi_1 \nabla \mathsf{T}_1' \cdot \boldsymbol{u}) \,\mathrm{d}x + \int_{\Gamma_\mathrm{R}} \alpha \mathsf{T}_2' \phi_2 \,\mathrm{d}s \\
&\qquad + \int_\Gamma \left(\eta \kappa_\mathrm{s} \nabla_\tau \langle \mathsf{T}' \rangle \cdot \langle \phi \rangle + \kappa_\mathrm{s} H [\mathsf{T}'] \langle \phi \rangle + \frac{\kappa_\mathrm{s}}{\eta} [\mathsf{T}'][\phi] \right) \mathrm{d}s \\
&= \int_{\Gamma_\mathrm{R}} \left((\boldsymbol{\theta} \cdot \nabla \phi_2) \kappa \frac{\partial \mathsf{T}_2}{\partial \boldsymbol{N}} - \kappa_2 \nabla \mathsf{T}_2 \cdot \nabla \phi_2 (\boldsymbol{\theta} \cdot \boldsymbol{N}) - \alpha \operatorname{div}_\tau((\mathsf{T}_2 - \mathsf{T}_\mathrm{ext}) \boldsymbol{\theta}) \phi_2 - \alpha (\boldsymbol{\theta} \cdot \boldsymbol{N}) \phi_2 \frac{\partial}{\partial \boldsymbol{N}} (\mathsf{T}_2 - \mathsf{T}_\mathrm{ext}) \right) \mathrm{d}s.
\end{aligned}
$$

Decomposing the gradient as $\nabla \phi = \nabla_\tau \phi + \boldsymbol{N} \frac{\partial \phi}{\partial \boldsymbol{N}}$ and using again that T_2 verifies the Robin

boundary condition at Γ_{R}, we obtain that

$$\begin{aligned}\int_{\Omega_2} \kappa_2 \nabla \mathsf{T}_2' \cdot \nabla \phi_2 \,\mathrm{d}x + \int_{\Omega_1} (\kappa_1 \nabla \mathsf{T}_1' \cdot \nabla \phi_1 + \phi_1 \nabla \mathsf{T}_1' \cdot \boldsymbol{u}) \,\mathrm{d}x + \int_{\Gamma_{\mathrm{R}}} \alpha \mathsf{T}_2' \phi_2 \,\mathrm{d}s \\ + \int_{\Gamma} \left(\eta \kappa_{\mathrm{s}} \nabla_\tau \langle \mathsf{T}' \rangle \cdot \nabla_\tau \langle \phi \rangle + \kappa_{\mathrm{s}} H [\mathsf{T}'] \langle \phi \rangle + \frac{\kappa_{\mathrm{s}}}{\eta} [\mathsf{T}'][\phi] \right) \mathrm{d}s \\ = \int_{\Gamma_{\mathrm{R}}} \left(-\alpha \,\mathrm{div}_\tau(\phi_2(\mathsf{T}_2 - \mathsf{T}_{\mathrm{ext}})\boldsymbol{\theta}) - \kappa_2 \nabla_\tau \mathsf{T}_2 \cdot \nabla_\tau \phi_2 (\boldsymbol{\theta} \cdot \boldsymbol{N}) - \alpha \phi_2 (\boldsymbol{\theta} \cdot \boldsymbol{N}) \frac{\partial}{\partial \boldsymbol{N}} (\mathsf{T}_2 - \mathsf{T}_{\mathrm{ext}}) \right) \mathrm{d}s.\end{aligned}$$

Finally, integrating by parts on the surface Γ_{R} (see [72, Proposition 5.4.9]) yields to the desired formula. □

Finally, afterwards the existence of the shape derivative of T is assured, the shape derivative derivative can be computed by using the chain rule.

Proof of Proposition 4.6.3. *Differentiability.* Let $\boldsymbol{\theta} \in \Theta_{\mathrm{ad}}$. We have

$$J(\Omega_2^{\boldsymbol{\theta}}) = \int_{\Gamma_{\mathrm{R}}^{\boldsymbol{\theta}}} \alpha(\mathsf{T}_{\boldsymbol{\theta},2} - \mathsf{T}_{\mathrm{ext}}) \,\mathrm{d}s.$$

Changing of variables with $\Gamma_{\mathrm{R}}^{\boldsymbol{\theta}} = (\boldsymbol{I} + \boldsymbol{\theta})\Gamma_{\mathrm{R}}$, we get

$$J(\Omega_2^{\boldsymbol{\theta}}) = \int_{\Gamma_{\mathrm{R}}} \alpha(\overline{\mathsf{T}}_{\boldsymbol{\theta},2} - \mathsf{T}_{\mathrm{ext}} \circ (\boldsymbol{I} + \boldsymbol{\theta})) B(\boldsymbol{\theta}) \,\mathrm{d}s,$$

where $B(\boldsymbol{\theta})$ is the one defined in (3.18). We recall that $\boldsymbol{\theta} \in \Theta_{\mathrm{ad}} \mapsto B(\boldsymbol{\theta}) \in \mathcal{C}^0(\Gamma_{\mathrm{R}})$, $\boldsymbol{\theta} \in \Theta_{\mathrm{ad}} \mapsto \mathsf{T}_{\mathrm{ext}} \circ (\mathsf{I} + \boldsymbol{\theta}) \in \mathrm{H}^1(\mathbb{R}^d)$ are $\mathcal{C}^1$ and we have previously proved in Proposition 3.3.1 that $\boldsymbol{\theta} \in \Theta_{\mathrm{ad}} \mapsto \overline{\mathsf{T}}_{\boldsymbol{\theta}} \in \mathcal{H}^1(\Omega_1, \Omega_2)$ is $\mathcal{C}^1$ in a neighborhood of 0, therefore we deduce by chain rule that the heat insulation J (3.3) is shape differentiable and its shape derivative has the following expression:

$$J'(\Omega_2)(\boldsymbol{\theta}) = \int_{\Gamma_{\mathrm{R}}} \alpha(\dot{\mathsf{T}}_2 - \nabla \mathsf{T}_{\mathrm{ext}} \cdot \boldsymbol{\theta}) \,\mathrm{d}s + \int_{\Gamma_{\mathrm{R}}} \alpha(\mathsf{T}_2 - \mathsf{T}_{\mathrm{ext}}) \,\mathrm{div}_\tau(\boldsymbol{\theta}) \,\mathrm{d}s. \tag{3.19}$$

Shape derivative computation. Taking $\phi = \mathsf{R} \in \mathcal{H}_0(\Omega_1, \Omega_2)$ in the material derivative equation (3.16) and testing with $\dot{\mathsf{T}} \in \mathcal{H}_0(\Omega_1, \Omega_2)$ in the adjoint equation (3.10), we get respectively

$$\begin{aligned}\int_{\Omega_2} \kappa_2 \nabla \dot{\mathsf{T}}_2 \cdot \nabla \mathsf{R}_2 \,\mathrm{d}x + \int_{\Omega_1} \left(\kappa_1 \nabla \dot{\mathsf{T}}_1 \cdot \nabla \mathsf{R}_1 + \nabla \dot{\mathsf{T}}_1 \cdot \boldsymbol{u} \mathsf{R}_1 \right) \mathrm{d}x + \int_{\Gamma_{\mathrm{R}}} \alpha \dot{\mathsf{T}}_2 \mathsf{R}_2 \;\mathrm{d}s \\ + \int_{\Gamma} \left(\eta \kappa_{\mathrm{s}} \nabla_\tau \langle \mathsf{R} \rangle \cdot \nabla_\tau \left\langle \dot{\mathsf{T}} \right\rangle + \kappa_{\mathrm{s}} H \langle \mathsf{R} \rangle [\dot{\mathsf{T}}] + \frac{\kappa_{\mathrm{s}}}{\eta} [\mathsf{R}][\dot{\mathsf{T}}] \right) \mathrm{d}s \\ = \int_{\Omega_2} \kappa_2 \left(\nabla \boldsymbol{\theta} + \nabla \boldsymbol{\theta}^t - \mathrm{div}(\boldsymbol{\theta}) \mathrm{I} \right) \nabla \mathsf{T}_2 \cdot \nabla \mathsf{R}_2 \,\mathrm{d}x \\ - \int_{\Gamma_{\mathrm{R}}} (\mathrm{div}_\tau(\boldsymbol{\theta}) \alpha (\mathsf{T}_2 - \mathsf{T}_{\mathrm{ext}}) \mathsf{R}_2 - \alpha \nabla \mathsf{T}_{\mathrm{ext}} \cdot \boldsymbol{\theta} \mathsf{R}_2) \;\mathrm{d}s\end{aligned} \tag{3.20}$$

and

$$\int_{\Omega_2} \kappa_2 \nabla \dot{\mathsf{T}}_2 \cdot \nabla \mathsf{R}_2 \,\mathrm{d}x + \int_{\Omega_1} \left(\kappa_1 \nabla \dot{\mathsf{T}}_1 \cdot \nabla \mathsf{R}_1 + \mathsf{R}_2 \boldsymbol{u} \cdot \nabla \dot{\mathsf{T}}_2 \right) \mathrm{d}x + \int_{\Gamma_{\mathrm{R}}} \alpha \dot{\mathsf{T}}_2 \mathsf{R}_2 \,\mathrm{d}s$$
$$+ \int_{\Gamma} \left(\eta \kappa_{\mathrm{s}} \nabla_\tau \langle \mathsf{R} \rangle \cdot \nabla_\tau \left\langle \dot{\mathsf{T}} \right\rangle + \kappa_{\mathrm{s}} H \langle \mathsf{R} \rangle [\dot{\mathsf{T}}] + \frac{\kappa_{\mathrm{s}}}{\eta} [\mathsf{R}][\dot{\mathsf{T}}] \right) \mathrm{d}s = \int_{\Gamma_{\mathrm{R}}} \alpha \dot{\mathsf{T}}_2 \,\mathrm{d}s. \quad (3.21)$$

Using (3.20) and (3.21), we get

$$\int_{\Gamma_{\mathrm{R}}} \alpha \dot{\mathsf{T}}_2 \,\mathrm{d}s = \int_{\Omega_2} \kappa_2 \left(\nabla \boldsymbol{\theta} + \nabla \boldsymbol{\theta}^t - \mathrm{div}(\boldsymbol{\theta}) \mathrm{I} \right) \nabla \mathsf{T}_2 \cdot \nabla \mathsf{R}_2 \,\mathrm{d}x$$
$$- \int_{\Gamma_{\mathrm{R}}} \left(\mathrm{div}_\tau(\boldsymbol{\theta}) \alpha (\mathsf{T}_2 - \mathsf{T}_{\mathrm{ext}}) \mathsf{R}_2 - \alpha \nabla \mathsf{T}_{\mathrm{ext}} \cdot \boldsymbol{\theta} \mathsf{R}_2 \right) \mathrm{d}s. \quad (3.22)$$

Plugging (3.22) into (3.19), it yields to

$$J'(\Omega_2)(\boldsymbol{\theta}) = \int_{\Gamma_{\mathrm{R}}} \alpha (1 - \mathsf{R}_2) \left(\mathrm{div}_\tau(\boldsymbol{\theta})(\mathsf{T}_2 - \mathsf{T}_{\mathrm{ext}}) - \nabla \mathsf{T}_{\mathrm{ext}} \cdot \boldsymbol{\theta} \right) \mathrm{d}s$$
$$+ \int_{\Omega_2} \kappa_2 (\nabla \boldsymbol{\theta} + \nabla \boldsymbol{\theta}^t - \mathrm{div}(\boldsymbol{\theta}) \mathrm{I}) \nabla \mathsf{T}_2 \cdot \nabla \mathsf{R}_2 \,\mathrm{d}x,$$

obtaining (3.9).
To prove the surface expression (3.11), since now we have more regularity, we can integrate by parts, yielding to the terms $\boldsymbol{\theta} \cdot \boldsymbol{N}$. Differentiating (3.3) and applying chain rule,

$$J'(\Omega_2)(\boldsymbol{\theta}) = \int_{\Gamma_{\mathrm{R}}} \alpha \mathsf{T}_2' \,\mathrm{d}s + \int_{\Gamma_{\mathrm{R}}} \alpha \left(\frac{\partial}{\partial \boldsymbol{N}} (\mathsf{T}_2 - \mathsf{T}_{\mathrm{ext}}) + H (\mathsf{T}_2 - \mathsf{T}_{\mathrm{ext}}) \right) (\boldsymbol{\theta} \cdot \boldsymbol{N}) \,\mathrm{d}s. \quad (3.23)$$

Testing the shape derivative equation of the convection-diffusion (3.8) with $\mathsf{R} \in \mathcal{H}_0(\Omega_1, \Omega_2)$ and the adjoint equation (3.10) with $\mathsf{T}' \in \mathcal{H}_0(\Omega_1, \Omega_2)$, we have respectively

$$\int_{\Omega_2} \kappa_2 \nabla \mathsf{T}_2' \cdot \nabla \mathsf{R}_2 \,\mathrm{d}x + \int_{\Omega_1} \left(\kappa_1 \nabla \mathsf{T}_1' \cdot \nabla \mathsf{R}_1 + \nabla \mathsf{T}_1' \cdot \boldsymbol{u} \mathsf{R}_1 \right) \mathrm{d}x + \int_{\Gamma_{\mathrm{R}}} \alpha \mathsf{T}_2' \mathsf{R}_2 \,\mathrm{d}s$$
$$+ \int_{\Gamma} \left(\eta \kappa_{\mathrm{s}} \nabla_\tau \langle \mathsf{R} \rangle \cdot \nabla_\tau \langle \mathsf{T}' \rangle + \kappa_{\mathrm{s}} H \langle \mathsf{R} \rangle [\mathsf{T}'] + \frac{\kappa_{\mathrm{s}}}{\eta} [\mathsf{R}][\mathsf{T}'] \right) \mathrm{d}s$$
$$= - \int_{\Gamma_{\mathrm{R}}} \left(\kappa_2 \nabla_\tau \mathsf{T}_2 \cdot \nabla_\tau \mathsf{R}_2 + \alpha \mathsf{R}_2 \left(\frac{\partial}{\partial \boldsymbol{N}} (\mathsf{T}_2 - \mathsf{T}_{\mathrm{ext}}) + H (\mathsf{T}_2 - \mathsf{T}_{\mathrm{ext}}) \right) \right) (\boldsymbol{\theta} \cdot \boldsymbol{N}) \,\mathrm{d}s \quad (3.24)$$

and

$$\int_{\Omega_2} \kappa_2 \nabla \mathsf{T}_2' \cdot \nabla \mathsf{R}_2 \,\mathrm{d}x + \int_{\Omega_1} \left(\kappa_1 \nabla \mathsf{T}_1' \cdot \nabla \mathsf{R}_1 + \mathsf{R}_1 \boldsymbol{u} \cdot \nabla \mathsf{T}_1' \,\mathrm{d}x + \int_{\Gamma_{\mathrm{R}}} \alpha \mathsf{T}_2' \mathsf{R}_2 \right) \mathrm{d}s$$
$$+ \int_{\Gamma} \left(\eta \kappa_{\mathrm{s}} \nabla_\tau \langle \mathsf{R} \rangle \cdot \nabla_\tau \langle \mathsf{T}' \rangle + \kappa_{\mathrm{s}} H \langle \mathsf{R} \rangle [\mathsf{T}'] + \frac{\kappa_{\mathrm{s}}}{\eta} [\mathsf{R}][\mathsf{T}'] \right) \mathrm{d}s = \int_{\Gamma_{\mathrm{R}}} \alpha \mathsf{T}_2' \,\mathrm{d}s. \quad (3.25)$$

Using (3.24) and (3.25), we get

$$\int_{\Gamma_{\mathrm{R}}} \alpha \mathsf{T}_2' \,\mathrm{d}s$$
$$= - \int_{\Gamma_{\mathrm{R}}} \left(\kappa_2 \nabla_\tau \mathsf{T}_2 \cdot \nabla_\tau \mathsf{R}_2 + \alpha \mathsf{R}_2 \left(\frac{\partial}{\partial \boldsymbol{N}} (\mathsf{T}_2 - \mathsf{T}_{\mathrm{ext}}) + H (\mathsf{T}_2 - \mathsf{T}_{\mathrm{ext}}) \right) \right) (\boldsymbol{\theta} \cdot \boldsymbol{N}) \,\mathrm{d}s. \quad (3.26)$$

Then, (3.23) becomes

$$\begin{aligned} J'(\Omega_2)(\boldsymbol{\theta}) &= \int_{\Gamma_{\mathrm{R}}} \Bigg(\alpha \frac{\partial}{\partial \boldsymbol{N}} (\mathsf{T}_2 - \mathsf{T}_{\mathrm{ext}}) + \alpha H (\mathsf{T}_2 - \mathsf{T}_{\mathrm{ext}}) - \kappa_2 \nabla_\tau \mathsf{T}_2 \cdot \nabla_\tau \mathsf{R}_2 \\ &\qquad - \alpha \mathsf{R}_2 \Bigg(\frac{\partial}{\partial \boldsymbol{N}} (\mathsf{T}_2 - \mathsf{T}_{\mathrm{ext}}) - H (\mathsf{T}_2 - \mathsf{T}_{\mathrm{ext}}) \Bigg) \Bigg) (\boldsymbol{\theta} \cdot \boldsymbol{N}) \, \mathrm{d}s \\ &= \int_{\Gamma_{\mathrm{R}}} \Bigg(\alpha \frac{\partial \mathsf{T}_2}{\partial \boldsymbol{N}} + \alpha H (\mathsf{T}_2 - \mathsf{T}_{\mathrm{ext}}) - \alpha \mathsf{R}_2 \frac{\partial \mathsf{T}_2}{\partial \boldsymbol{N}} - \alpha H \mathsf{R}_2 (\mathsf{T}_2 - \mathsf{T}_{\mathrm{ext}}) \\ &\qquad - \kappa_2 \nabla_\tau \mathsf{T}_2 \cdot \nabla_\tau \mathsf{R}_2 - \frac{\partial \mathsf{T}_{\mathrm{ext}}}{\partial \boldsymbol{N}} (\alpha - \alpha \mathsf{R}_2) \Bigg) (\boldsymbol{\theta} \cdot \boldsymbol{N}) \, \mathrm{d}s. \end{aligned}$$

Using the boundary conditions $\kappa_2 \frac{\partial \mathsf{T}_2}{\partial \boldsymbol{N}} = \alpha(\mathsf{T}_{\mathrm{ext}} - \mathsf{T}_2)$ and $\kappa_2 \frac{\partial \mathsf{R}_2}{\partial \boldsymbol{N}} = \alpha - \alpha \mathsf{R}_2$ on Γ_{R} and that $\nabla_\tau \mathsf{T}_2 \cdot \nabla_\tau \mathsf{R}_2 = \nabla \mathsf{T}_2 \cdot \nabla \mathsf{R}_2 - \frac{\partial \mathsf{T}_2}{\partial \boldsymbol{N}} \frac{\partial \mathsf{R}_2}{\partial \boldsymbol{N}}$, we obtain (3.11). □

Remark 14 *We also expose an alternative method using the Eulerian derivative in section 3.6.*

3.3.3 Shape sensitivity analysis with random exterior temperature

Proof of Theorem 3.2.5. Let $\omega \in \Xi$ be fixed. Recall that $\mathsf{T}_{\mathrm{ext}}(x, \omega) = \mathsf{T}^0_{\mathrm{ext}}(x) + \sum_{k=1}^{m} \xi_k(\omega) \mathsf{T}^k_{\mathrm{ext}}(x)$, for $x \in \Omega$. Then, by linearity,

$$\mathsf{T}(\cdot, \omega) = \mathsf{T}^0(\cdot) + \sum_{k=1}^{m} \xi_k(\omega) \mathsf{T}^k(\cdot)$$

is the unique solution in $\mathcal{H}_{\mathsf{T}_{\mathrm{D}}}(\Omega_1, \Omega_2)$ of (3.12) where, for each $k = 1, \ldots, m$, $\mathsf{T}^k \in \mathcal{H}_0(\Omega_1, \Omega_2)$ solves Equation (3.2) with respectively $\mathsf{T}^k_{\mathrm{ext}}$ and 0 as conditions on Γ_{R} and Γ_{D}, and where $\mathsf{T}^0 \in \mathcal{H}_{\mathsf{T}_{\mathrm{D}}}(\Omega_1, \Omega_2)$ solves Equation (3.2) with respectively $\mathsf{T}^0_{\mathrm{ext}}$ and T_{D} as conditions on Γ_{R} and Γ_{D}.

Now we will show (3.14). Using that J is quadratic with respect to the temperature gap at the boundary, we have

$$\begin{aligned} \mathbb{E}[J](\Omega_2, \mathsf{T}_{\mathrm{ext}}) &= \mathbb{E}[J(\Omega_2, \mathsf{T}^0_{\mathrm{ext}} + \sum_{k=1}^{m} \xi_k \mathsf{T}^k_{\mathrm{ext}}] = \mathbb{E}\left[\int_{\Gamma_{\mathrm{R}}} \alpha^2 \left((\mathsf{T}^0 - \mathsf{T}^0_{\mathrm{ext}} + \sum_{k=1}^{m} \xi_k (\mathsf{T}^k - \mathsf{T}^k_{\mathrm{ext}}) \right)^2 \right] \\ &= \int_{\Gamma_{\mathrm{R}}} \alpha^2 (\mathsf{T}^0 - \mathsf{T}^0_{\mathrm{ext}})^2 + 2 \sum_{k=1}^{n} \mathbb{E}[\xi_k] \int_{\Gamma_{\mathrm{R}}} (\mathsf{T}^0 - \mathsf{T}^0_{\mathrm{ext}})(\mathsf{T}^k - \mathsf{T}^k_{\mathrm{ext}}) \\ &\quad + \sum_{k,l=1}^{n} \mathbb{E}[\xi_k \xi_l] \int_{\Gamma} (\mathsf{T}^l - \mathsf{T}^l_{\mathrm{ext}})(\mathsf{T}^k - \mathsf{T}^k_{\mathrm{ext}}). \end{aligned}$$

Since the random variables ξ_k are independent and centered, many terms cancel and one gets

$$\mathbb{E}[J](\Omega_2, \mathsf{T}_{\mathrm{ext}}) = J(\Omega_2, \mathsf{T}^0_{\mathrm{ext}}) + \int_{\Xi} \sum_{k=1}^{m} \xi_k^2 J(\Omega_2, \mathsf{T}^k_{\mathrm{ext}}) \mathbb{P}(\mathrm{d}\omega) = J(\Omega_2, \mathsf{T}^0_{\mathrm{ext}}) + \sum_{k=1}^{m} \sigma_k^2 J(\Omega_2, \mathsf{T}^k_{\mathrm{ext}}).$$

The expression of the shape derivative (3.15) follows by linearity of the shape derivative. □

3.4 Numerical methods used to solve the involved problems

In this section we will give the main tools necessary to solve our shape optimization problem: solve the partial differential equations, optimization and remeshing algorithm. More specifically, we will discus the discretization of the convection-diffusion equation (3.2) and its adjoint (3.10). These equations require a special treatment, since they are non standard, discontinuous and when the parameter η is too small, they become ill-conditioned.

We highlight that the approximate convection-diffusion and the adjoint equations can not be implemented directly due to the use of the Broken Sobolev spaces such as $\mathcal{H}_0(\Omega_1, \Omega_2)$. Allaire *et al* proposed a method in [9] to approximate this kind of equations in order to use any finite element software with spaces of continuous functions. However this method involves to duplicate the degrees of freedom, which we do not want for our 3D simulations. Indeed, it becomes too expensive in our context. Domain decomposition method can be used as well, adapting [86] for example. However, it is not clear how many iterations it can take to converge to no mismatch at the interface, in particular in 3D geometries with a large quantity of vertices at the interface (and we require to solve it a lot of times in the shape optimization procedure). Furthermore, the factor $\frac{1}{\eta}$ can lead to poor conditioning of the linear systems and then slow resolution. Finally, in our shape optimization context, we have to compute the shape derivative which is an integral over the interface Γ (which changes at every step of the shape optimization algorithm) and it is then crucial to have precise approximations of this integral. For all these reasons, we solve these equations directly using the dedicated Nitsche method we have introduced in chapter 2. The main advantages is the efficiency and the robustness with respect to the small parameter η.

3.4.1 Nitsche extended finite element method of a Ventcel transmission problem with discontinuities at the interface

For the sake of simplicity, in this part, we suppose $\mathsf{T}_{\mathrm{D}} = 0$. In the case of the convection-diffusion problem (3.7), we decompose $a(\cdot,\cdot)$ into $a(\cdot,\cdot) = b(\cdot,\cdot) + c(\cdot,\cdot)$ where for any $\mathsf{T}, \mathsf{S} \in \mathcal{H}^1(\Omega_1, \Omega_2)$

$$\begin{aligned} b(\mathsf{T},\mathsf{S}) &:= \int_{\Omega_2} \kappa_2 \nabla \mathsf{T}_2 \cdot \nabla \mathsf{S}_2 \,\mathrm{d}x + \int_{\Omega_1} \left(\kappa_1 \nabla \mathsf{T}_1 \cdot \nabla \mathsf{S}_1 + \mathsf{S}_1 \boldsymbol{u} \cdot \nabla \mathsf{T}_1\right) \mathrm{d}x \\ &\quad + \int_{\Gamma_{\mathrm{R}}} \alpha \mathsf{T}_2 \mathsf{S}_2 \,\mathrm{d}s + \int_{\Gamma} \eta \kappa_{\mathrm{s}} \nabla_\tau \langle \mathsf{T} \rangle \cdot \nabla_\tau \langle \mathsf{S} \rangle + \kappa_{\mathrm{s}} H [\mathsf{T}] \langle \mathsf{S} \rangle \,\mathrm{d}s, \\ c(\mathsf{T},\mathsf{S}) &:= \frac{\kappa_{\mathrm{s}}}{\eta} \int_{\Gamma} [\mathsf{T}][\mathsf{S}] \,\mathrm{d}s. \end{aligned}$$

The term $c(\mathsf{T},\mathsf{S})$ produces poor conditioning when η is small. To deal with this, we consider the Nitsche approach previously used in [30] to stabilize our matrix with respect to η, improving the conditioning of the matrix. We first introduce some notations to briefly explain this method.

Let $\mathcal{T}_h$ be a regular simplicial mesh of Ω and let $\mathcal{F}_h$ be the set of faces of $\mathcal{T}_h$, $\mathcal{F}_{h,\Gamma}$ the set of faces situated on Γ and $\mathcal{T}_{h,\Gamma}$ the set of elements which have one face on Γ. Let h_F be the diameter of the face $F \in \mathcal{F}_{h,\Gamma}$ and h the mesh size. We consider the polynomial spaces

$$\mathrm{P}^1_h := \{\mathsf{S}_h \in \mathcal{C}(\Omega_1) \times \mathcal{C}^1(\Omega_2); \mathsf{S}_h|_K \in \mathbb{P}^1, \forall K \in \mathcal{T}_h\} \qquad \text{and} \qquad \mathrm{P}^1_{h,0} := \mathrm{P}^1_h \cap \mathcal{H}_0(\Omega_1, \Omega_2).$$

Then, we define the following mesh-depending bilinear form, for any $\mathsf{T}_h, \mathsf{S}_h \in \mathrm{P}^1_{h,0}$,

$$a_h(\mathsf{T}_h, \mathsf{S}_h) := a(\mathsf{T}_h, \mathsf{S}_h) - \sum_{F \in \mathcal{F}_{h,\Gamma}} \frac{\gamma \eta h_F}{\eta + \gamma \kappa_{\mathrm{s}} h_F} \left(\left\langle \kappa \frac{\partial \mathsf{T}_h}{\partial \boldsymbol{n}} \right\rangle + \frac{\kappa_{\mathrm{s}}}{\eta} [\mathsf{T}_h], \left\langle \kappa \frac{\partial \mathsf{S}_h}{\partial \boldsymbol{n}} \right\rangle + \frac{\kappa_{\mathrm{s}}}{\eta} [\mathsf{S}_h] \right)_{\mathrm{L}^2(F)}.$$

Hence

$$a_h(\mathsf{T}_h, \mathsf{S}_h) \;=\; b(\mathsf{T}_h, \mathsf{S}_h) + c_h(\mathsf{T}_h, \mathsf{S}_h),$$

with

$$\begin{aligned} c_h(\mathsf{T}_h, \mathsf{S}_h) \;:=\; & \sum_{F \in \mathcal{F}_{h,\Gamma}} \int_F \frac{\kappa_{\mathrm{s}}}{\eta + \gamma \kappa_{\mathrm{s}} h_F} [\mathsf{T}_h][\mathsf{S}_h] - \frac{\gamma \eta h_F}{\eta + \gamma \kappa_{\mathrm{s}} h_F} \left\langle \kappa \frac{\partial \mathsf{T}_h}{\partial \boldsymbol{n}} \right\rangle \left\langle \kappa \frac{\partial \mathsf{S}_h}{\partial \boldsymbol{n}} \right\rangle \\ & - \frac{\gamma \kappa_{\mathrm{s}} h_F}{\eta + \gamma \kappa_{\mathrm{s}} h_F} \left(\left\langle \kappa \frac{\partial \mathsf{T}_h}{\partial \boldsymbol{n}} \right\rangle [\mathsf{S}_h] + \left\langle \kappa \frac{\partial \mathsf{S}_h}{\partial \boldsymbol{n}} \right\rangle [\mathsf{T}_h] \right) \mathrm{d}s, \end{aligned}$$

where $\gamma > 0$ is a stabilization parameter, that it is small enough in order to guarantee the coercivity of a_h. Let us remark, that in the decomposition of the new bilinear form a_h, the bilinear form b continues to appear; what it changes is the bilinear form c_h instead of c, which associated matrix has a better conditioning due to the stabilization. Then we consider the following Nitsche problem to approximate the equation (3.7) is

$$\begin{cases} \text{Find } \mathsf{T}_h \in \mathrm{P}^1_{h,0} \text{ such that} \\ a_h(\mathsf{T}_h, \mathsf{S}_h) = l(\mathsf{S}_h), \quad \forall \mathsf{S}_h \in \mathrm{P}^1_{h,0}, \end{cases} \tag{3.27}$$

that estimates the continuous solution T of the convection-diffusion equation (3.2) in the energy sense as it is stated in the next result (the proof is a mere adaptation of [30, Theorem 4.6]).

Theorem 3.4.1 (Error estimate in energy norm) Let $\mathsf{T} \in \mathcal{H}_0(\Omega_1, \Omega_2))$ the solution of the continuous convection-diffusion equation (3.2) and T_h the solution of the (discrete) Nitsche problem (3.27). If in addition $\mathsf{T} \in \mathcal{H}^2(\Omega_1, \Omega_2)$, then for γ sufficiently small, there exists a constant $C > 0$ independent of h and η such that:

$$|||\mathsf{T} - \mathsf{T}_h|||_h \leq Ch \left(\sum_{i=1}^{2} \|\kappa_i^{1/2} \mathsf{T}_i\|^2_{\mathrm{H}^2(\Omega_i)} + \|(\kappa_{\mathrm{s}} \eta)^{1/2} \langle \mathsf{T} \rangle\|^2_{\mathrm{H}^2(\Gamma)} + \sum_{F \in \mathcal{F}_{h,\Gamma}} \frac{\kappa_{\mathrm{s}}}{\gamma h_F} \|[\mathsf{T}]\|^2_{\mathrm{H}^1(F)} \right)^{1/2}, \tag{3.28}$$

where $|||\cdot|||_h := \left(\sum_{i=1}^{2} \|\kappa_i^{1/2} \nabla \cdot\|^2_{\mathrm{L}^2(\Omega_i)^d} + \|(\kappa_s \eta)^{1/2} \nabla_\tau \langle \cdot \rangle\|^2_{\mathrm{L}^2(\Gamma)^d} + \sum_{F \in \mathcal{F}_{h,\Gamma}} \frac{\kappa_s}{\eta + \gamma \kappa_s h_F} \|[\cdot]\|^2_{\mathrm{L}^2(F)} \right)^{1/2}$ is a mesh-dependent norm on P^1_h.

We proceed in a similar way concerning the adjoint equation (3.10). Let $\mathsf{R}, \mathsf{S} \in \mathcal{H}_0(\Omega_1, \Omega_2)$. We define $\tilde{a}(\mathsf{R}, \mathsf{S}) := a(\mathsf{S}, \mathsf{R})$ the bilinear form associated to the adjoint problem (3.10) with right-hand side $\tilde{l}(\mathsf{S}) := \int_{\Gamma_{\mathrm{R}}} \alpha \mathsf{S}_2 \, \mathrm{d}s$. As previously, the matrix associated to the term $c(\cdot, \cdot)$ has poor conditioning. To stabilize it, we define

$$\begin{aligned} \tilde{a}_h(\mathsf{R}, \mathsf{S}) := & \; \tilde{a}(\mathsf{R}, \mathsf{S}) \\ & - \sum_{F \in \mathcal{F}_{h,\Gamma}} \frac{\gamma \eta h_F}{\eta + \gamma \kappa_{\mathrm{m}} h_F} \left(\left\langle \kappa \frac{\partial \mathsf{R}}{\partial \boldsymbol{n}} \right\rangle + \frac{\kappa_{\mathrm{m}}}{\eta} [\mathsf{R}] + \kappa_{\mathrm{m}} H \langle \mathsf{R} \rangle, \left\langle \kappa \frac{\partial \mathsf{S}}{\partial \boldsymbol{n}} \right\rangle + \frac{\kappa_{\mathrm{m}}}{\eta} [\mathsf{S}] + \kappa_{\mathrm{m}} H \langle \mathsf{S} \rangle \right)_{\mathrm{L}^2(F)}. \end{aligned}$$

Therefore, we obtain $\tilde{a}_h(\mathsf{R},\mathsf{S}) = a_h(\mathsf{S},\mathsf{R}) - d_h(\mathsf{R},\mathsf{S})$, where

$$d_h(\mathsf{R},\mathsf{S}) := \sum_{F\in\mathcal{F}_{h,\Gamma}} \frac{\gamma\eta h_F}{\eta+\gamma\kappa_{\mathrm{m}}h_F}\int_F H\langle\mathsf{S}\rangle\left(\left\langle\kappa\frac{\partial\mathsf{R}}{\partial\boldsymbol{n}}\right\rangle+\frac{\kappa_{\mathrm{m}}}{\eta}[\mathsf{R}]\right) + H\langle\mathsf{R}\rangle\left(\left\langle\kappa\frac{\partial\mathsf{S}}{\partial\boldsymbol{n}}\right\rangle+\frac{\kappa_{\mathrm{m}}}{\eta}[\mathsf{S}]\right)+\kappa_{\mathrm{m}}H^2\langle\mathsf{R}\rangle\langle\mathsf{S}\rangle\,\mathrm{d}s.$$

Then the Nitsche problem considered to approximate the adjoint Equation 3.10 is

$$\begin{cases}\text{Find } \mathsf{R}_h\in \mathrm{P}^1_{h,0} \text{ such that}\\ \tilde{a}_h(\mathsf{R}_h,\mathsf{S}_h)=\tilde{l}(\mathsf{S}_h),\quad \forall \mathsf{S}_h\in\mathrm{P}^1_{h,0}.\end{cases} \tag{3.29}$$

The error estimation is similar to the one given in Theorem 4.4.1.

3.4.2 Numerical resolution with FEM

Concerning the Navier-Stokes equations (3.1), they can be solved with any finite element software. We rely on FreeFem++ (see [71]) for this purpose. Since Ω_1 is fixed, the Navier-Stokes equations (3.1) have to be solved just once. However, it is necessary to interpolate the solution in every step of the shape optimization algorithm, since the mesh that describes Ω_1 will change slightly: indeed the remeshing step MMG concerns the level set function that describes the boundary Γ_{R} but then naturally affects the whole mesh.

All the equations involved are solved in parallel by means of FreeFEM++ and PETSc (see [17, 18]), up to the non standard equations (3.2) and (3.10) which involve the discretization of the Sobolev Broken Spaces and are then solved with an optimized sequential version in C++. At this stage it is still not necessary to perfom High Performance Computing (mainly since we just have to solve the Navier-Stokes equations once), with appropiate preconditioners, solvers or to run the simulations in a cluster. We will let it for the next Chapter.

3.4.3 Optimization framework: level set and null space methods

The level-set method. In the context of shape optimization, the level set evolution method was introduced by Allaire *et al.* in [10]. The idea consists in considering a fixed domain D that contains every admissible domain Ω and such that the boundaries Γ_{D}, Γ_{N} and Γ_{e} belong to ∂D. In practice, D is a box. This allows to describe Ω by means of a level set function $\phi : D\to\mathbb{R}$ as follows

$$\begin{cases} x\in\Omega & \Longleftrightarrow \quad \phi(x)<0\\ x\in\Gamma_{\mathrm{R}} & \Longleftrightarrow \quad \phi(x)=0\\ x\in D\setminus\overline{\Omega} & \Longleftrightarrow \quad \phi(x)>0.\end{cases}$$

In particular this allows us to track the boundary Γ_{R} that we aim to optimize. Numerically speaking, there are two representations of shapes $\Omega_1\cup\Omega_2\subset D$:

- Explicit representation: The computational domain $\Omega_1 \cup \Omega_2$ is equipped with a conformal simplicial mesh $\mathcal{T}_{\Omega_1 \cup \Omega_2}$, which is a submesh of a conformal simplicial mesh $\mathcal{T}_D$ that represents D. This representation allows to solve the involved partial differential equations by using the finite element method (see the following subsection).
- Implicit representation: The representation via the level-set function ϕ allows to deal with domain deformations as explained below.

After initialization, at the step n of the shape optimization process, we compute the level set ϕ^n by solving the following equation,

$$\begin{cases} \dfrac{\partial \phi^n}{\partial t} + \boldsymbol{\theta} \cdot \nabla \phi^n = 0, & 0 < t < \tau,\ x \in D \\ \phi^n(0, x) = \phi^{n-1}(x), & x \in D, \end{cases} \tag{3.30}$$

where $\tau > 0$ is the descent step in the shape optimization algorithm and $\boldsymbol{\theta}$ is an appropriate velocity field, such that $\tau \|\boldsymbol{\theta}\|_{\mathrm{L}^\infty(D)^d}$ is of the order of mesh size h. In our applications, we rely on the *null space algorithm* (that we briefly describe below), where $\|\boldsymbol{\theta}\|_{\mathrm{L}^\infty(D)^d}$ is at the mesh size scale h, then we can simply choose $\tau = 1$.

Equation 3.30 can be computed by ADVECT (see [29]) and the remeshing step by MMG (see [47]). Notice that in our case, we have two level set functions, ϕ_1 and ϕ_2 that describe Ω_1 and Ω_2, respectively. Since Ω_1 is fixed, we will just have to update ϕ_2 for the remeshing.

The velocity field $\boldsymbol{\theta}$ that we will use belongs to $\mathrm{H}^1(D)^d$, such that $\boldsymbol{\theta} \cdot \boldsymbol{N} = 0$ on ∂D and $\boldsymbol{\theta} = 0$ in $\overline{\Omega}_1$. It is obtained by solving the following extension-regularization problem,

$$\int_D \left(h^2 \nabla \boldsymbol{\theta} : \nabla \boldsymbol{\psi} + \boldsymbol{\theta} \cdot \boldsymbol{\psi} \right) \mathrm{d}x = \langle J'(\Omega_2), \boldsymbol{\psi} \rangle, \forall \boldsymbol{\psi} \in \left\{ \boldsymbol{\psi} \in \mathrm{H}^1(D)^d;\ \boldsymbol{\psi} \cdot \boldsymbol{N} = 0 \text{ on } \partial D \text{ and } \boldsymbol{\psi} = 0 \text{ in } \overline{\Omega}_1 \right\}. \tag{3.31}$$

It is important to remark, that by construction, $\boldsymbol{\theta}$ is a descent direction.

Remark 15 *The previous procedure is merely formal, since* $\mathrm{H}^1(D)^d$ *is not contained in* $\mathrm{W}^{1,\infty}(D)^d$ *and then* $\langle J'(\Omega_2), \boldsymbol{\psi} \rangle$ *is a priori not well-defined. However, numerically, this works fine in practice (see [11] for more details).*

Null space optimization method. As constrained optimization algorithm, we rely on the *null space algorithm* introduced in [64] under the implementation of Feppon [61]. This method first decreases the violation of the constraint in order to be feasible, then minimizes the objective function. It is particularly well suited when we start from shapes that do not satisfy the constraints and when numerous constraints are considered.

3.5 Numerical examples

We consider the thermal insulation problem in dimension three. We consider the inlet velocity $\boldsymbol{u}_{\mathrm{D}}$ as a parabolic profile with maximum speed at the Γ_{D} centered $(0, y_{\mathrm{c}}, z_{\mathrm{c}})$, equal to 1: in other

words, $\boldsymbol{u}_{\mathrm{D}} := \big((r^2 - (y - y_{\mathrm{c}})^2 - (z - z_{\mathrm{c}})^2)/r^2, 0, 0\big)$, where r is the radius of Ω_1 which is fixed to 0.1 in the simulations below. Moreover, we consider $\mathsf{T}_{\mathrm{D}} \equiv 40$ and $\eta = 1 \cdot 10^{-3}$ in the following examples, and except for the last example, we consider $D = [0,1] \times [0,1] \times [0,1]$. Finally, except for the random outer temperature example of section 3.5.1, we take $\mathsf{T}_{\mathrm{ext}} = 0$. Let us conclude these preliminaries by highlighting two points.

- *On the Robin coefficient α.* From [108], we know that for α small (with respect to κ_2), the functional decreases by removing insulation material, meanwhile for α large enough the functional decreases by adding insulation material, which is more intuitive. blue From a physical point of view, the need to remove material when α is small arises from the fact that, in this case, the convective resistance becomes greater than the conductive resistance (see [23, Chapter 3]). From a (formal) mathematical point of view, we can understand the extreme cases: when $\alpha \to 0$, we get $\kappa_2 \frac{\partial \mathsf{T}_2}{\partial \boldsymbol{N}} = 0$ on Γ_{R}, i.e. there is no influence from the environment (for instance, an external fluid such as air acting on the insulator) and so there is no need to insulate, contrary to the case where $\alpha \to \infty$ for which we get $\mathsf{T}_2 = \mathsf{T}_{\mathrm{ext}}$ on Γ_{R}, i.e. the influence of the environment is very important and then more material is needed to reach equilibrium between the temperature on the insulator and the outside temperature. Hence we will consider this latter case and we summarize the values of the parameters chosen in the following Table 3.1.

κ_1	$1.5 \cdot 10^{-7}$	$m^2 s^{-1}$
κ_2	10^{-7}	$m^2 s^{-1}$
κ_{s}	$1.1 \cdot 10^{-4}$	$m^2 s^{-1}$
α	$2 \cdot 10^{-5}$	$m s^{-1}$
ν	10^{-2}	$m^2 s^{-1}$

Table 3.1: Values of the parameters

- *On the no recirculation at the outlet assumption* (4.10). In the four following examples, we numerically check that the hypothesis $\boldsymbol{u} \cdot \boldsymbol{N} \geq 0$ on Γ_{N} is well satisfied.

All the presented simulations were performed on a personal laptop with an AMD Ryzen 9 4900hs @3.0 GHz, with 40 GB RAM. The meshes considered vary from 300 to 500 thousand vertices and 2 to 3 million tetrahedra. Each numerical simulation took less than four days of computational time. The used codes are available in the github repository: `https://github.com/RodrigoZelada/How-to-insulate-a-pipe/`.

3.5.1 First example: cylinder case

The first example is the cylindric case. We have to mention the work [73] where it was showed, in another context close to our own, that a cylinder is not the optimal solution to minimize the fluid dissipation. We consider here a fixed cylinder Ω_1 of radius $r = 0.1$, of axis (Ox) and with $(y_{\mathrm{c}}, z_{\mathrm{c}}) = (0.5, 0.5)$. The target volume V_0 is the difference between the volume of a cylinder of radius 0.2 and the volume of another cylinder of radius 0.1. It will be chosen similarly in the following examples (changing the cylinder by the respective considered pipes).

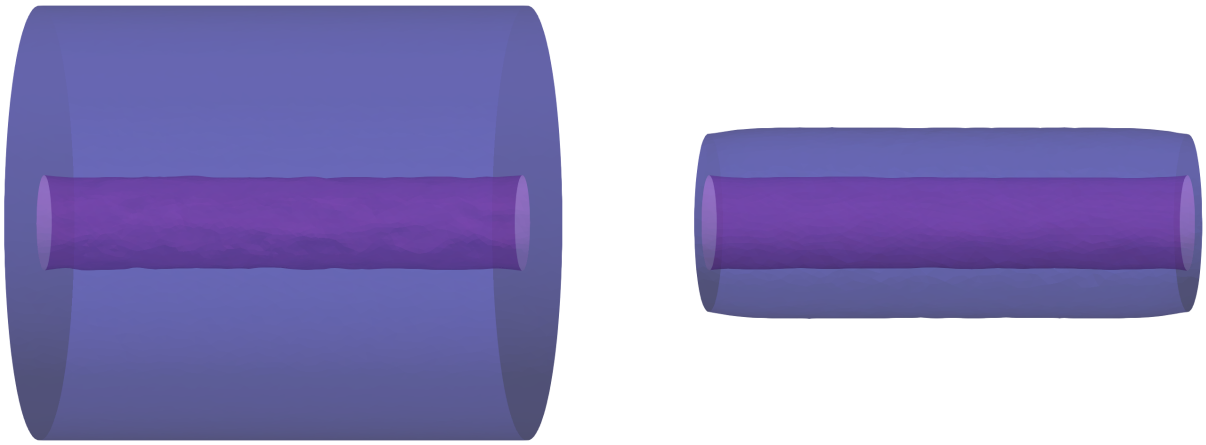

(a) Initial domain Ω. (b) Final domain Ω.

Figure 3.4: First example - initial and final domains in the deterministic case.

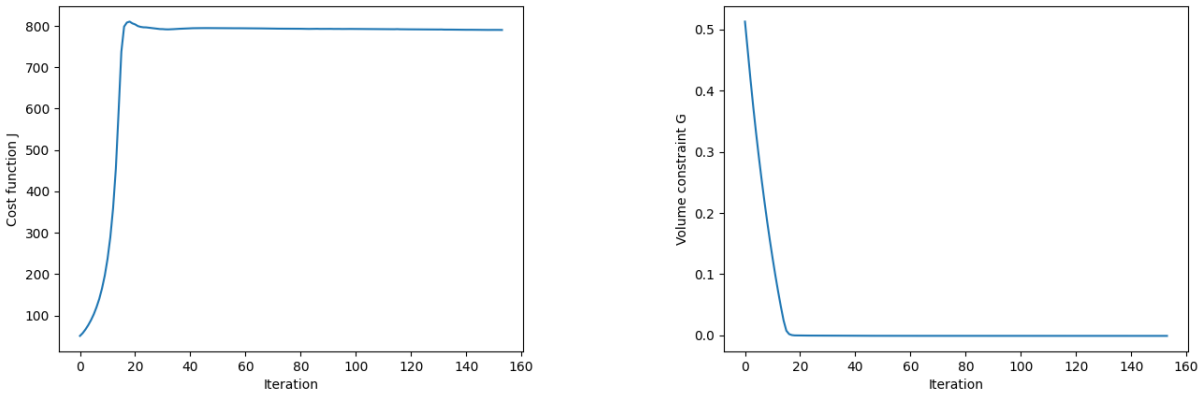

(a) Objective function J. (b) Constraint function G.

Figure 3.5: First example - convergence history in the deterministic case.

Deterministic case

The initial geometry is depicted on Figure 3.4a. The optimized design is shown in Figure 3.4b.

On the one hand, we observe that we do not obtain two concentric cylinders, similarly to what happens in the case of [73]. On the other hand, as expected, the objective functional J increases (see Figure 4.4) until the solution satisfies the volume constraint and then is optimized (it is well-known and natural that if the volume is larger the insulation is better).

With random outside temperature

We now illustrate, on the previous example, the consideration of a random exterior temperature of the form (following the notations introduced in (3.13))

$$\mathsf{T}_{\text{ext}} = \mathsf{T}^0_{\text{ext}} + \xi_1(\omega)\mathsf{T}^1_{\text{ext}}(x,y,z) + \xi_2(\omega)\mathsf{T}^2_{\text{ext}}(x,y,z),$$

where $\mathsf{T}^0_{\text{ext}} = 0, \mathsf{T}^1_{\text{ext}} = 20x$ and $\mathsf{T}^2_{\text{ext}} = 10z$, the random variables ξ_1, ξ_2 are statistically independent, with expected value $\sigma_1 = \mathbb{E}(\xi_1) = 0.5$ and $\sigma_2 = \mathbb{E}(\xi_2) = 0.8$. Figure 3.6 summarizes the obtained result, which is very similar to the deterministic case Figure 3.4. This can be explained as the deterministic component is predominant in the formulas of Theorem 3.2.5 for the chosen values of the outside temperature, for two reasons, first, since the random part, is multiplied by the variance $\sigma_i < 1, i = 1, 2$ and second, since the difference of the values between the outside temperature and inlet Dirichlet temperature is larger for the deterministic case (recall that there are three solutions of the temperature, the deterministic temperature has $\mathsf{T}^0_1 = 40$ on Γ_{D} and $\mathsf{T}^0_{\text{ext}} = 0$ on Γ_{R} as data, meanwhile the random temperatures have $\mathsf{T}^1_1 = 0$ on Γ_{D}, $\mathsf{T}^1_{\text{ext}} = 20z$ on Γ_{R} and $\mathsf{T}^2_1 = 0$ on Γ_{D}, $\mathsf{T}^2_{\text{ext}} = 10x$ on Γ_{R}). The convergence is depicted by Figure 3.7, where we can actually see that the gap between the deterministic and random cases is small with respect to the values of J; the insulation in the random case is slightly larger as expected since it has the random contribution.

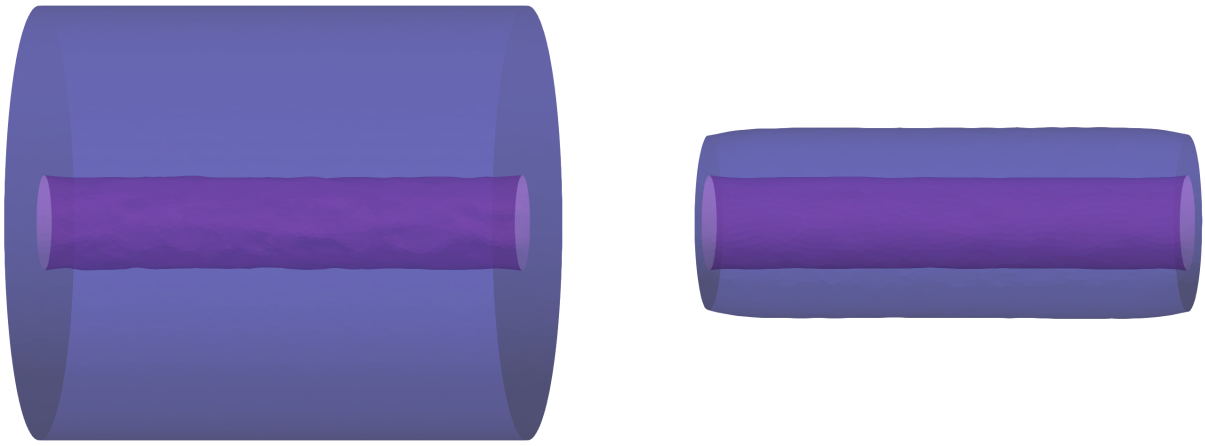

(a) Initial domain Ω.

(b) Final domain Ω.

Figure 3.6: First example - initial and final domains with random temperature.

3.5.2 Second example: perpendicular tubes

In this example, Ω_1 is a pipe of radius $r = 0.1$ with two right-angled bends. The Dirichlet and Neumann boundaries are, respectively,

$$\begin{aligned} \Gamma_{\text{D}} &= \{(0,y,z) \in D;\ (y-0.5)^2 + (z-0.75)^2 = r^2\}, \\ \Gamma_{\text{N}} &= \{(1,y,z) \in D;\ (y-0.5)^2 + (z-0.25)^2 = r^2\}. \end{aligned}$$

The initial geometry is depicted on Figure 3.8a.

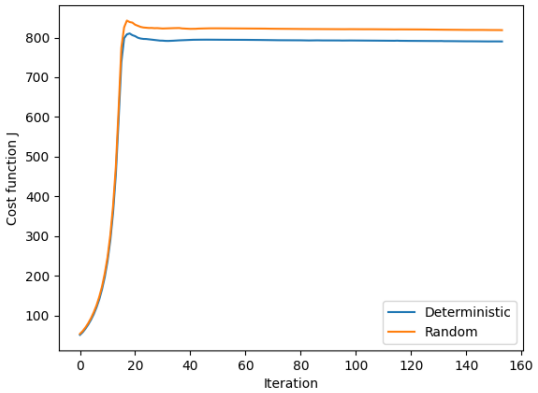

(a) Objective function J.

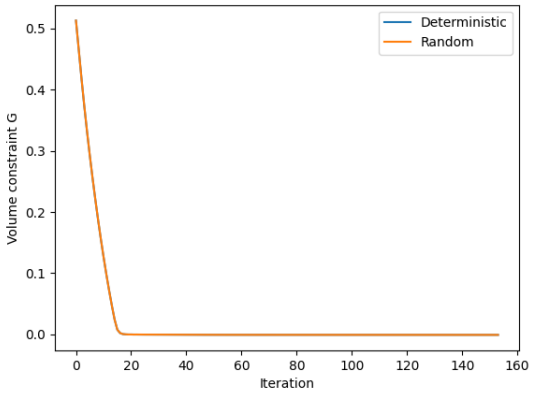

(b) Constraint function G.

Figure 3.7: First example - convergence history with random temperature.

(a) Initial domain Ω.

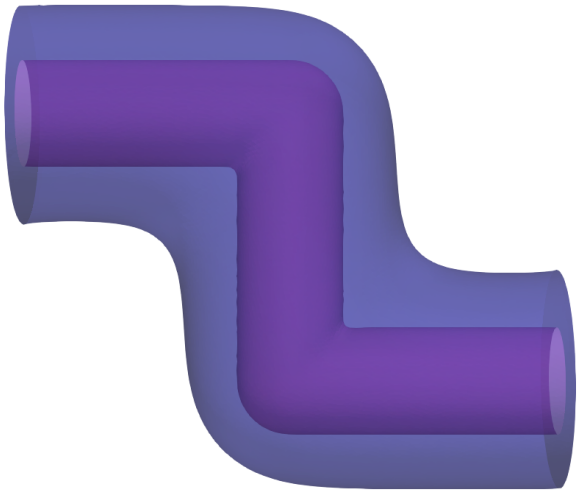

(b) Final domain Ω.

Figure 3.8: Second example - initial and final domains.

The optimized design is shown in Figure 3.8b. Moreover, in Figure 3.9 are displayed the isosurfaces of the temperature at the beginning and the last iteration: we see that the initial temperature is lower on Γ_R than the final temperature, which is reasonable since there is more insulator in the beginning (we do not satisfy the volume constraint). In the optimal domain, the solution satisfies the volume constraint and also keeps better the temperature inside the pipe: this is validated in Figure 3.10 that shows the convergence history which illustrates that in the first 20 iterations the algorithm tries to satisfy the constraint, decreasing the volume but increasing the objective function J until that the constraint is satisfied, and then the objective function decreases.

3.5.3 Third example: tubes with angle of inclination

As a third example, we consider a slight variation to the second one, now with an angle of inclination. In this example, the angle formed by the tube at the bottom and at the middle

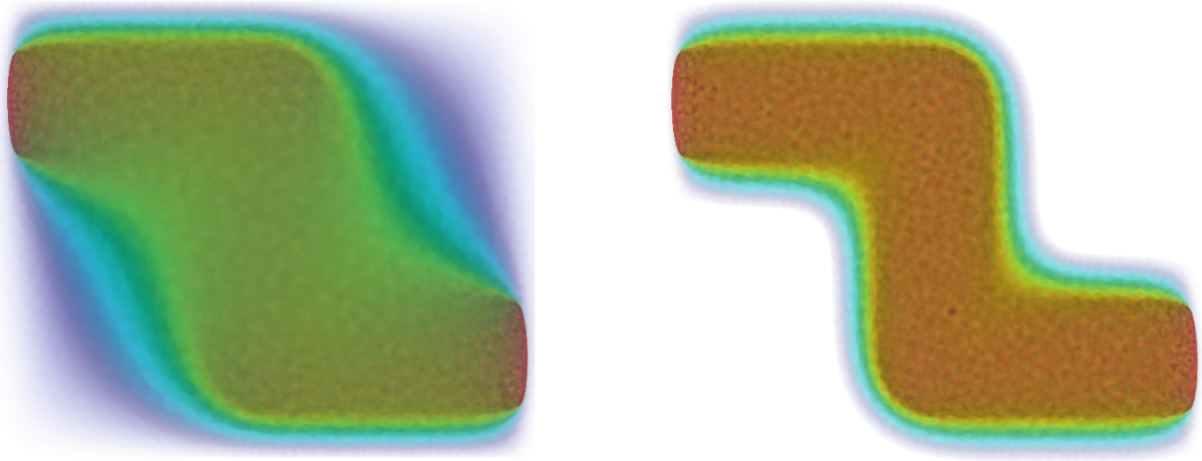

(a) Initial temperature T. (b) Final temperature T.

Figure 3.9: Second example - solution T in the initial and final domains (red means hotter, blue colder, white is almost zero).

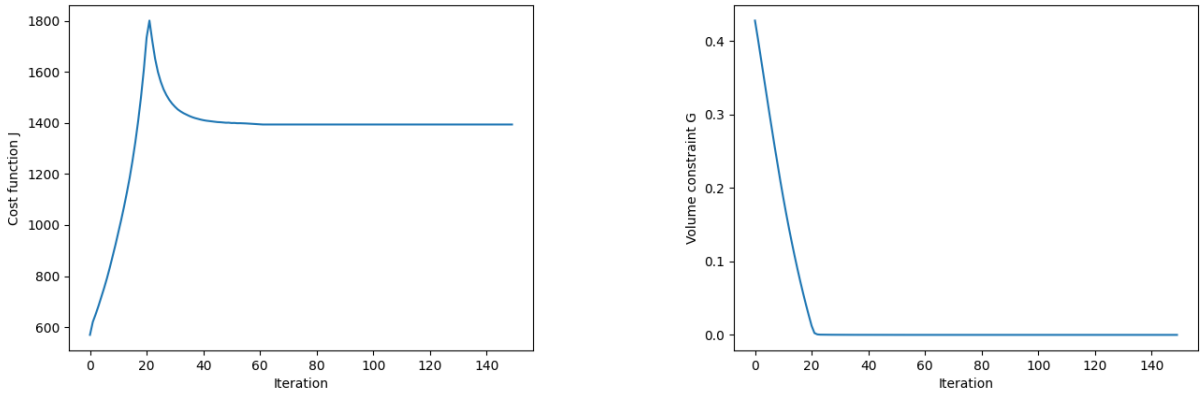

(a) Objective function J. (b) Constraint function G.

Figure 3.10: Second example - convergence history.

is of $\frac{11}{6}\pi$. The results are similar to the previous case as depicted in Figures 3.11 and 3.12.

3.6 Appendix: Shape derivatives of a general functional using a fully Lagrangian approach

In the present chapter, we focus on a specific objective functional J measuring the heart loss given in (3.3). In this appendix, we give some results in order to consider another objective functional which will imply to do some computations (the chain rule part) which can be annoying. In [63] was developed a framework to compute the shape derivatives of general functionals for a multi-physics

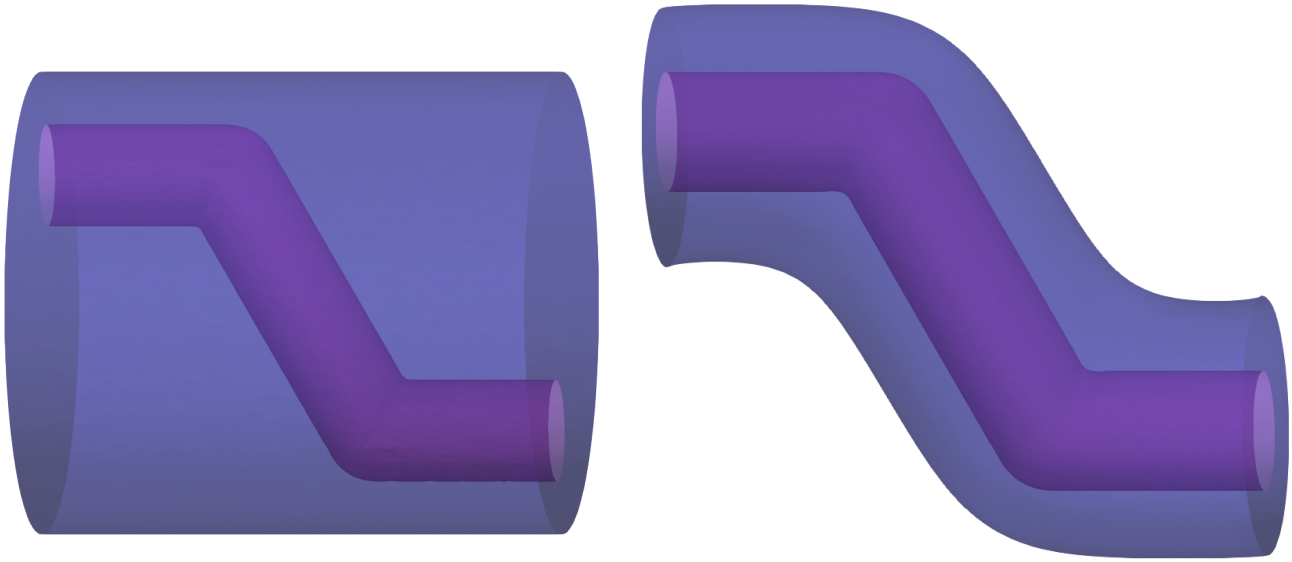

(a) Initial domain Ω. (b) Final domain Ω.

Figure 3.11: Third example - initial and final domains.

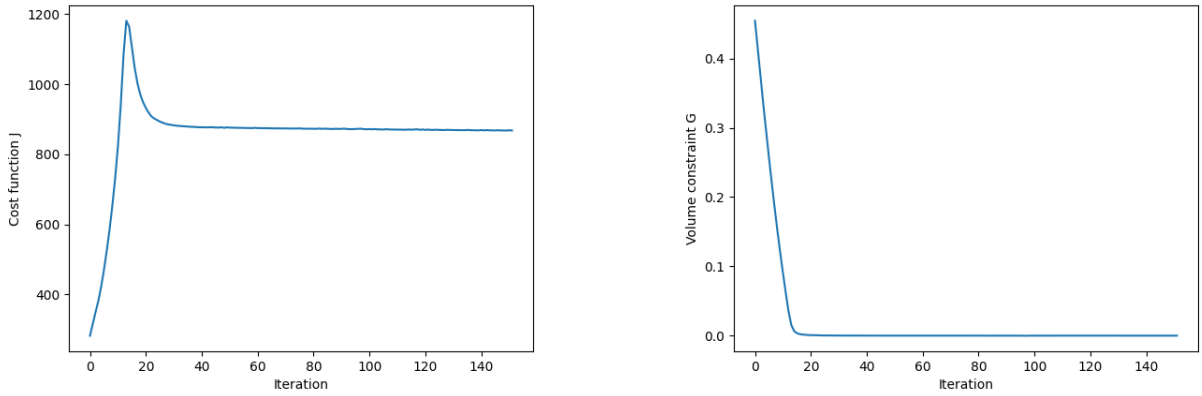

(a) Objective function J. (b) Constraint function G.

Figure 3.12: Third example - convergence history.

problem, that requires only to compute again some partial derivatives.

We keep the same notation than before (see subsection 3.2.2) and consider a general functional J that depends on Ω_2 and on the solution $\mathsf{T} \in \mathcal{H}_{\mathsf{T}_\mathrm{D}}(\Omega_1, \Omega_2)$ of the convection-diffusion problem (3.2). We first recall the concept of *transported functional* given in the following definition.

Definition 3.6.1. *The transported functional of J is the functional $\mathcal{J}$ such that for all $\boldsymbol{\theta} \in \Theta_{\mathrm{ad}}$ and all $\hat{\mathsf{T}} \in \mathcal{H}^1(\Omega_1, \Omega_2)$,*

$$\mathcal{J}(\boldsymbol{\theta}, \hat{\mathsf{T}}) := J(\Omega_2^{\boldsymbol{\theta}}, \hat{\mathsf{T}} \circ (\boldsymbol{I} + \boldsymbol{\theta})^{-1}),$$

where $\Omega_2^{\boldsymbol{\theta}} = (\boldsymbol{I} + \boldsymbol{\theta})\Omega_2$.

We suppose that $\mathcal{J}$ has continuous partial derivatives at $(\boldsymbol{\theta}, \hat{\mathsf{T}}) = (0, \mathsf{T}(\Omega_2))$. To keep notations as simple as possible, we will omit the evaluations of the partial derivatives at $(\boldsymbol{\theta}, \hat{\mathsf{T}}) = (0, \mathsf{T}(\Omega_2))$.

We introduce the solution $\mathsf{R} \in \mathcal{H}_0(\Omega_1, \Omega_2)$ of the following adjoint problem

$$\left\{ \begin{array}{l} \text{Find } \mathsf{R} \in \mathcal{H}_0(\Omega_1, \Omega_2), \text{ such that, for all } \mathsf{S} \in \mathcal{H}_0(\Omega_1, \Omega_2), \\ \displaystyle\int_{\Omega_2} \kappa_2 \nabla \mathsf{R}_2 \cdot \nabla \mathsf{S}_2 \,\mathrm{d}x + \int_{\Omega_1} (\kappa_1 \nabla \mathsf{R}_1 \cdot \nabla \mathsf{S}_1 + \mathsf{R}_1 u \cdot \nabla \mathsf{S}_1) \,\mathrm{d}x + \int_{\Gamma_{\mathrm{R}}} \alpha \mathsf{R}_2 \mathsf{S}_2 \,\mathrm{d}s \\ \displaystyle + \int_{\Gamma} \eta \kappa_{\mathrm{s}} \nabla_\tau \langle \mathsf{R} \rangle \cdot \nabla_\tau \langle \mathsf{S} \rangle + \kappa_{\mathrm{s}} H \langle \mathsf{R} \rangle [\mathsf{S}] + \frac{\kappa_{\mathrm{s}}}{\eta} [\mathsf{R}][\mathsf{S}] \,\mathrm{d}s = \frac{\partial \mathcal{J}}{\partial \hat{\mathsf{T}}}(\mathsf{S}). \end{array} \right. \tag{3.32}$$

Remark 16 *In the particular case of the insulation functional* (3.3)*,*

$$\frac{\partial \mathcal{J}}{\partial \hat{\mathsf{T}}}(\mathsf{S}) \;=\; \int_{\Gamma_{\mathrm{R}}} \alpha \mathsf{S}_2 \,\mathrm{d}s.$$

Then we can give a formula to compute the shape derivative general for any functional, requiring just to compute the partial derivative $\frac{\partial \mathcal{J}}{\partial \boldsymbol{\theta}}(\boldsymbol{\theta})$.

Proposition 3.6.2 (Volume shape derivative)**.** *If $\mathsf{T}_{\mathrm{ext}} \in \mathrm{H}^2(\mathbb{R}^d)$, then J is shape differentiable, then the volume shape derivative is given by*

$$J'(\Omega_2)(\boldsymbol{\theta}) = \frac{\partial \mathcal{J}}{\partial \boldsymbol{\theta}}(\boldsymbol{\theta}) + \int_{\Omega_2} \kappa_2((\nabla \boldsymbol{\theta} + \nabla \boldsymbol{\theta}^t - \mathrm{I}\,\mathrm{div}(\boldsymbol{\theta}))\nabla \mathsf{T}_2) \cdot \nabla \mathsf{R}_2 \,\mathrm{d}x \\ - \int_{\Gamma_{\mathrm{R}}} (\mathrm{div}_\tau(\boldsymbol{\theta}) \alpha (\mathsf{T}_2 - \mathsf{T}_{\mathrm{ext}}) \mathsf{R}_2 - \alpha \nabla \mathsf{T}_{\mathrm{ext}} \cdot \boldsymbol{\theta} \mathsf{R}_2) \,\mathrm{d}s,$$

where T solves the convection-diffusion equation (3.2) *and R solves the adjoint equation* (3.32)*.*

Proof. Let $\dot{\mathsf{T}} \in \mathcal{H}_0(\Omega_1, \Omega_2)$ the material derivative of $\mathsf{T} \in \mathcal{H}_{\mathsf{T}_{\mathrm{D}}}(\Omega_1, \Omega_2)$ given in (3.16). We obtain the result by using the chain rule

$$J'(\Omega_2)(\boldsymbol{\theta}) = \frac{\partial \mathcal{J}}{\partial \boldsymbol{\theta}}(\boldsymbol{\theta}) + \frac{\partial \mathcal{J}}{\partial \hat{\mathsf{T}}}(\dot{\mathsf{T}})$$

and then proceeding as in the proof of Proposition 4.6.3. □

Remark 17 *In the particular case of the insulation functional* (3.3)*,*

$$\frac{\partial \mathcal{J}}{\partial \boldsymbol{\theta}}(\boldsymbol{\theta}) = \int_{\Gamma_{\mathrm{R}}} \alpha \left(\mathrm{div}_\tau(\boldsymbol{\theta})(\mathsf{T}_2 - \mathsf{T}_{\mathrm{ext}}) - \nabla \mathsf{T}_{\mathrm{ext}} \cdot \boldsymbol{\theta} \right) \mathrm{d}s.$$

We can also get a surface expression, which is an integral over the free boundary, that in this case is Γ_{R}, and depending only on the normal component of the perturbation field. The result is obtained by integrating by parts the previous formula and using the structure theorem.

Proposition 3.6.3 (Surface shape derivative)**.** *If $\mathsf{T}_{\mathrm{ext}} \in \mathrm{H}^2(B)$, then J is shape differentiable, and if $\mathsf{T}_2, \mathsf{R}_2 \in \mathrm{H}^2(\Omega_2)$, then the surface shape derivative is given by*

$$J'(\Omega_2)(\boldsymbol{\theta}) = \overline{\frac{\partial \mathcal{J}}{\partial \boldsymbol{\theta}}}(\boldsymbol{\theta}) \\ + \int_{\Gamma_{\mathrm{R}}} \left(\kappa_2 \frac{\partial \mathsf{T}_2}{\partial \boldsymbol{N}} \frac{\partial \mathsf{R}_2}{\partial \boldsymbol{N}} - \kappa_2 \nabla_\tau \mathsf{T}_2 \cdot \nabla_\tau \mathsf{R}_2 - H \alpha (\mathsf{T}_2 - \mathsf{T}_{\mathrm{ext}}) \mathsf{R}_2 + \alpha \frac{\partial \mathsf{T}_{\mathrm{ext}}}{\partial \boldsymbol{N}} \mathsf{R}_2 \right) (\boldsymbol{\theta} \cdot \boldsymbol{N}) \,\mathrm{d}s, \tag{3.33}$$

where $\overline{\dfrac{\partial \mathcal{J}}{\partial \boldsymbol{\theta}}}$ is the part of $\dfrac{\partial \mathcal{J}}{\partial \boldsymbol{\theta}}$ that depends only on $\boldsymbol{\theta} \cdot \boldsymbol{N}$.

Remark 18 *In the particular case of the insulation functional* (3.3),

$$\overline{\frac{\partial \mathcal{J}}{\partial \boldsymbol{\theta}}}(\boldsymbol{\theta}) \;=\; \int_{\Gamma_{\mathrm{R}}} \alpha \left(H(\mathsf{T}_2 - \mathsf{T}_{\mathrm{ext}}) - \frac{\partial \mathsf{T}_{\mathrm{ext}}}{\partial \boldsymbol{N}} \right) (\boldsymbol{\theta} \cdot \boldsymbol{N}) \, \mathrm{d}s.$$

Indeed, changing variables in $\Omega_2^{\boldsymbol{\theta}} = (\boldsymbol{I} + \boldsymbol{\theta})\Omega_2$ *(analogous to the proof of Proposition 3.2.3), we obtain*

$$\frac{\partial \mathcal{J}}{\partial \boldsymbol{\theta}}(\boldsymbol{\theta}) = \int_{\Gamma_{\mathrm{R}}} \alpha \left(\mathrm{div}_\tau(\boldsymbol{\theta})(\mathsf{T}_2 - \mathsf{T}_{\mathrm{ext}}) - \nabla \mathsf{T}_{\mathrm{ext}} \cdot \boldsymbol{\theta} \right) \mathrm{d}s.$$

We conclude by integrating by parts and taking the normal component.

Chapter 4

Shape optimization of a heat exchanger with Ventcel transmission conditions

Contents

Most of the content of this chapter has been submitted for publication as a journal paper under the title *Shape optimization of a heat exchanger with Ventcel transmission conditions*, written in collaboration with Fabien Caubet, Carlos Conca and Marc Dambrine.

4.1 Introduction

In recent years, energy consumption and energy saving have gained more relevance in the society. The scientific community is working to come up with solutions, either by introducing alternative energies, by reducing our waste, or optimizing devices and objects in order to minimize the energy used. A device that is very present in both everyday life and industry is the heat exchanger. Optimising these devices is therefore of great interest (see, e.g., [67, 3, 15, 78]).

To this end, shape and topology optimization techniques provide innovative solutions, usually complex from a geometry and topological point of view but efficient. Due to these complex geometries, it was very difficult to manufacture them (and then test them in practice), until the advent of additive manufacturing (see [33] for a review of additive manufacturing of heat exchangers in aerospace applications). The two most widely used topological optimization methods are the SIMP method [21, 22] and Hadamard's method [89, 13, 72].

In terms of heat exchanger optimization, early works considered a single-phase fluid with forced convection, *i.e.* where the fluid flow is produced by an external source such as a fan or a pump for example (see [52, 112]). The two-fluid case was first discussed in [97] and then followed by [76, 67, 81]. Most of this work is based on the SIMP method, which is easier to implement: it does not require the computation of the Hadamard shape derivatives and then is therefore widely used by the engineering community. However, in the case of heat exchangers it is not straightforward to distinguish fluids from the solid, because this method uses a continuous density function and it is then necessary to use some rules to obtain a binary structure, depending on the problem. This geometry representation issue means that the non-mixing constraint (since the aim is to exchange heat between two fluids, for example, without mixing the fluids) is not easy to implement. Feppon *et al.* proposed an approach based on the Hadamard shape derivatives in [63, 66, 67], combined with the level set evolution method developed in [10], which is able to track the interface implicitly as the zero values of a level set function and then remesh at each iteration of the topology optimization algorithm. This method has the advantage of naturally imposing the non-mixing constraint by means of the signed distance function.

We underline that the natural convection is where the fluid motion is produced by the temperature gradient and that it has been less studied than forced convection, mainly because the temperature and fluid equations are strongly coupled and it is therefore extremely expensive numerically to solve them. Let us mention the early work of Alexandersen *et al.* [4] in the 2D case and then in [5] in the 3D case by using the SIMP method, and the more recent work of Li *et al.* [83] where the level-set with body-fitted mesh is used.

We point out that in the above literature the separation between the fluids is large enough. Motivated by the helical heat exchangers proposed by Aldor *et al.* in [3], the present work aims to take into account that a thin layer separates the two fluids in the heat exchanger. Numerically, this implies meshing the solid region very finely to obtain an accurate solution and be able to reproduce the physics of the problem, which is not numerically viable. Then, we consider an asymptotic model as in our previous works [35, 36], which gets round this difficulty thanks to high-order transmission conditions at the interface that take into account the solid part. It turns out that these transmission conditions are not standard and therefore cannot be solved by classical open-source finite element software. In particular, they involve the Laplace-Beltrami operator and

discontinuities at the interface.

To our knowledge, there is no similar model in the literature. A first work in this spirit was done by Allaire *et al.* in [9], in the context of additive manufacturing, with continuous flux and a kind of discontinuous Robin boundary condition for the jump. They also proposed a variational approximation by introducing a penalization term to solve the equation with the open-source FEM software. Regarding the second-order model we focus on, we studied its numerical resolution in [30] where we noticed that it is ill-conditioned and then proposed a Nitsche-type method as in [91, 70, 79]. Moreover, we consider here the forced convection model, *i.e.* a weak coupling between the steady-state Navier-Stokes equations and the convection-diffusion equation. Finally, in our topology optimization algorithm, we rely on Hadamard's method together with a level set evolution to track the interface, carefully computing the shape derivatives due to the delicate terms involved, such as jumps of solutions, tangential Laplacian and mean curvature of the domain.

4.2 Formulation of the optimal heat exchanger design approximated problem

4.2.1 Problem setting

A heat exchanger between two liquids is a system where two fluids, one a heat transfer fluid and the other to be heated, are separated by a solid wall. This solid wall is often very thin compared to the size of the system. Similar to our first work for a heat exchanger with order zero approximation [35] and recently in the context of a heat insulation problem [36], we propose an approximate model to take into account the effects of the solid thin layer at the interface between the two fluids. Accordingly, we will work with a domain composed of two fluids, where the effect of the solid part appears in the transmission conditions at the interface.

The geometric setting. Let Ω be an open bounded connected domain of $\mathbb{R}^d$ ($d = 2, 3$), divided into two open bounded subdomains Ω_1, Ω_2 which are separated by an interface $\Gamma = \partial\Omega_1 \cap \partial\Omega_2$ that we assume to have non-zero measure in $\mathbb{R}^{d-1}$ and to be $\mathcal{C}^1$. On part of the boundary of each subdomain Ω_i, $i = 1, 2$, Dirichlet and Neumann boundary conditions are imposed, on $\Gamma_{\mathrm{D},i}$ and $\Gamma_{\mathrm{N},i}$ respectively, which in fact correspond to the inlet and outlet of each fluid. We also assume that the inlets are well separated: $\Gamma_{\mathrm{D},1} \cap \Gamma_{\mathrm{D},2} = \emptyset$. The complementary of the boundary of each subdomain is an exterior wall denoted $\Gamma_{\mathrm{e},i}$, and we thus have $\partial\Omega_i = \Gamma_{\mathrm{D},i} \cup \Gamma \cup \Gamma_{\mathrm{N},i} \cup \Gamma_{\mathrm{e},i}$. Moreover, we assume that $\partial\Gamma \subset \partial\Omega$. Finally, we assume that the pipe containing the hot fluid exits the heat exchanger orthogonally to it so that the tangential plane to $\Gamma_{\mathrm{e},2}$ is orthogonal to the tangential plane to Γ on $\partial\Gamma$. Figure 4.1 illustrates our configuration.

The physical models. On the one hand, the motion of the fluids is described by the Navier-Stokes equations. On the other hand, the temperature field is modelled by the convection-diffusion equation. In particular, we consider a weak coupling by neglecting the influence of temperature on the flow. By neglecting fluid expansion, we can work with incompressible fluids, which simplifies

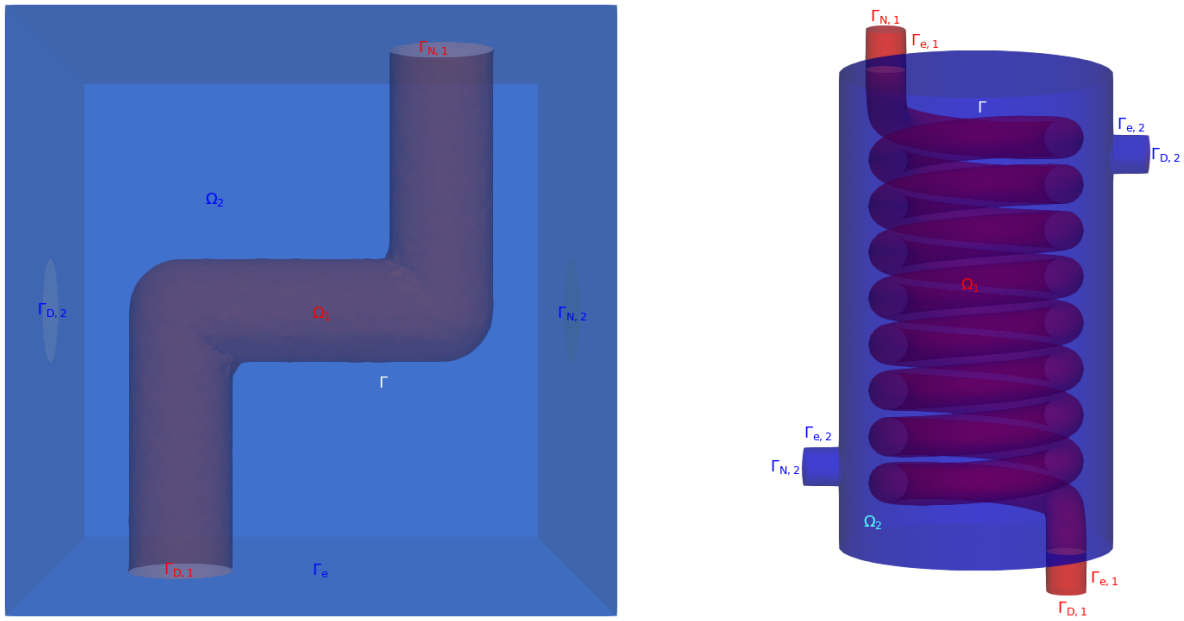

Figure 4.1: Two configurations of the 3D heat exchanger problem. On the left $\Gamma_{\mathrm{e}} = \Gamma_{\mathrm{e},2}$, $\Gamma_{\mathrm{e},1} = \emptyset$, and on the right $\Gamma_{\mathrm{e},1} \neq \emptyset$.

the equations to be treated. This simplified model is already used in the literature, for example in the work of Feppon *et al.* [63].

Concerning the fluids, we denote by $\boldsymbol{u}_i$ the velocity and p_i the pressure in the domain Ω_i, $i = 1, 2$. Let $\nu_i > 0$ be the viscosity, that for the sake of simplicity, we consider constant. The boundary $\Gamma_{\mathrm{D},i}$ represents the inlet of the fluid, so a given inlet velocity $\boldsymbol{u}_{\mathrm{D,i}}$ is given there. On the outlet boundary $\Gamma_{\mathrm{N},i}$, a homogeneous Neumann boundary condition is imposed. Furthermore, Γ and $\Gamma_{\mathrm{e},i}$ are respectively the wall between the fluids and the exterior walls and a non-slip boundary condition is therefore imposed on these boundaries (which ensures in particular that the fluids cannot pass through the wall). This is a modelling choice whose physical relevance is open to debate. To summarize, for each $i = 1, 2$, the fluid flow is described by the following equations:

$$\begin{cases} -\nu_i \Delta \boldsymbol{u}_i + (\nabla \boldsymbol{u}_i)\boldsymbol{u}_i + \nabla p_i &= 0 \quad \text{in } \Omega_i, \\ \mathrm{div}(\boldsymbol{u}_i) &= 0 \quad \text{in } \Omega_i, \\ \boldsymbol{u}_i &= \boldsymbol{u}_{\mathrm{D,i}} \quad \text{on } \Gamma_{\mathrm{D,i}}, \\ \sigma(\boldsymbol{u}_i, p_i)\boldsymbol{N} &= 0 \quad \text{on } \Gamma_{\mathrm{N},i}, \\ \boldsymbol{u}_i &= 0 \quad \text{on } \Gamma \cup \Gamma_{\mathrm{e},i}, \end{cases} \tag{4.1}$$

where $\boldsymbol{u}_{\mathrm{D},i} \in \mathrm{H}^{1/2}_{00}(\Gamma_{\mathrm{D},i})^d = \{\boldsymbol{v}|_{\Gamma_{\mathrm{D,i}}}, \boldsymbol{v} \in \mathrm{H}^1(\Omega_i)^d, \boldsymbol{v}|_{\partial\Omega_i \setminus \overline{\Gamma_{\mathrm{D},i}}} = 0\}$ are the velocities of the fluids at the inlet, where $\boldsymbol{N}$ denotes the exterior unit normal to $\partial\Omega$, and where $\sigma(\boldsymbol{u}, p)$ is the fluid stress tensor defined by

$$\sigma(\boldsymbol{u}, p) = 2\nu\varepsilon(\boldsymbol{u}) - p\mathrm{I},$$

with $\varepsilon(\boldsymbol{u}) = \frac{1}{2}(\nabla \boldsymbol{u} + \nabla \boldsymbol{u}^t)$ the symmetric gradient and I the identity matrix and where the superscript ^{t} denotes the transpose matrix.

In the sequel, for a piece-wise smooth function ϕ defined on Ω, we denote by $\phi_i = \phi|_{\Omega_i}$ its restriction to Ω_i, and we define the jump and mean of ϕ at the interface Γ by $[\cdot]$ and $\langle\cdot\rangle$, respectively, as follows:

$$[\phi] = \phi_1 - \phi_2 \qquad \text{and} \qquad \langle\phi\rangle = \frac{\phi_1 + \phi_2}{2}.$$

We define $\boldsymbol{n}$ the unit normal to Γ exterior to Ω_1 (interior to Ω_2). Then, in terms of temperature, which we denote as T, a given temperature is imposed at the entry of the fluids and a homogeneous Neumann boundary condition at the outlet, meanwhile at the interface there is an effective transmission condition associated to the solid. Then, the associated thermal diffusivity κ_1, κ_2 and κ_s (κ_s is the thermal diffusivity of the solid) are assumed to be constant positive numbers. After asymptotic analysis when the thickness $\eta > 0$ of the solid wall separating the fluids tends to 0, we obtain the following asymptotic model to order 1 in η:

$$\begin{cases} -\operatorname{div}(\kappa_i \nabla \mathsf{T}_i) + \boldsymbol{u}_i \cdot \nabla \mathsf{T}_i = 0 & \text{in } \Omega_i, i = 1, 2, \\ \mathsf{T}_i = \mathsf{T}_{\mathrm{D},i} & \text{on } \Gamma_{\mathrm{D},i}, i = 1, 2, \\ \kappa_i \dfrac{\partial \mathsf{T}_i}{\partial \boldsymbol{N}} = 0 & \text{on } \Gamma_{\mathrm{N},i} \cup \Gamma_{\mathrm{e},i}, i = 1, 2, \\ \left\langle \kappa \dfrac{\partial \mathsf{T}}{\partial \boldsymbol{n}} \right\rangle = -\dfrac{\kappa_s}{\eta} [\mathsf{T}] & \text{on } \Gamma, \\ \left[\kappa \dfrac{\partial \mathsf{T}}{\partial \boldsymbol{n}} \right] = \eta \operatorname{div}_\tau(\kappa_s \nabla_\tau \langle \mathsf{T} \rangle) - \kappa_s H [\mathsf{T}] & \text{on } \Gamma, , \\ \dfrac{\partial \langle \mathsf{T} \rangle}{\partial \boldsymbol{N}} = 0 & \text{on } \partial\Gamma, \end{cases} \tag{4.2}$$

where $\mathsf{T}_{\mathrm{D},i} \in \mathrm{H}^{1/2}(\Gamma_{\mathrm{D},i})$ are the given input temperatures and where $\boldsymbol{u}_i$ is the solution of the Navier-Stokes equations (4.1). Here, H denotes the mean curvature of Γ, div_τ is the tangential divergence and ∇_τ is the tangential gradient.

The shape optimization problem. We want to optimize the shape of the pipe connecting the inlet to the outlet of Ω_1 in order to maximise the heat exchanged between the fluids under two constraints: firstly, the volume of the pipe is prescribed, and secondly, the pressure drop seen from the angle of the energy dissipated by the fluid must remain below a prescribed threshold. To work with a minimization problem, we define the negative heat exchanged W as

$$W(\Gamma) = \int_{\Omega_1} \boldsymbol{u}_1 \cdot \nabla \mathsf{T}_1 \, \mathrm{d}x - \int_{\Omega_2} \boldsymbol{u}_2 \cdot \nabla \mathsf{T}_2 \, \mathrm{d}x, \tag{4.3}$$

where $\boldsymbol{u}_i$ and T_i, $i = 1, 2$, denote the respective solutions of the above problems (4.1) and (4.2).

We consider two constraints: firstly the energy dissipation D_i, with a given threshold $D_{0,i} > 0$ in the fluid labelled by i, defined as

$$D_i(\Gamma) = \int_{\Omega_i} 2\nu_i |\varepsilon(\boldsymbol{u}_i)|^2 \, \mathrm{d}x - D_{0,i}, \tag{4.4}$$

and secondly the gap between the volume occupied by the hot fluid and a target volume $V_0 > 0$ given by

$$V(\Gamma) = \int_{\Omega_1} 1 \, \mathrm{d}x - V_0. \tag{4.5}$$

The problem that we will consider in this chapter is the then following:

$$\min_{\Gamma} W(\Gamma) \quad \text{such that} \quad D_i(\Gamma) \leq 0,\, i = 1, 2, \quad \text{and} \quad V(\Gamma) = 0. \tag{4.6}$$

To numerically address the shape optimization problem (4.6), we need to compute the shape derivative of each shape functional. We highlight that the novelties and difficulties lie in the negative heat exchange W, which involves the solutions of three PDEs (the velocity of the hot and cold fluids and the temperature), in particular the solution of the non-classical convection-diffusion problem (4.2), for which a shape sensitivity analysis will have to be carried out.

Remark 19 *Notice that we could have used a different expression for the objective W. Indeed, note that integrating by parts we get,*

$$W(\Gamma) = \int_{\Gamma_{\mathrm{N},1}\cup\Gamma_{\mathrm{D},1}} \mathsf{T}_1 \boldsymbol{u}_1 \cdot \boldsymbol{n}\, \mathrm{d}s - \int_{\Gamma_{\mathrm{N},2}\cup\Gamma_{\mathrm{D},2}} \mathsf{T}_2 \boldsymbol{u}_2 \cdot \boldsymbol{n}\, \mathrm{d}s,$$

and since $\mathsf{T}_i, \boldsymbol{u}_i$ are known on $\Gamma_{\mathrm{D},i}$ (Dirichlet boundary condition), we could also consider

$$\tilde{W}(\Gamma) = \int_{\Gamma_{\mathrm{N},1}} \mathsf{T}_1 \boldsymbol{u}_1 \cdot \boldsymbol{n}\, \mathrm{d}s - \int_{\Gamma_{\mathrm{N},2}} \mathsf{T}_2 \boldsymbol{u}_2 \cdot \boldsymbol{n}\, \mathrm{d}s. \tag{4.7}$$

4.2.2 Functional setting

To keep the notation as light as possible, we define

$$\Gamma_{\mathrm{D}} = \Gamma_{\mathrm{D},1} \cup \Gamma_{\mathrm{D},2} \qquad \text{and} \qquad \mathsf{T}_{\mathrm{D}} = \mathsf{T}_{\mathrm{D},1} \mathbb{1}_{\Gamma_{\mathrm{D},1}} + \mathsf{T}_{\mathrm{D},2} \mathbb{1}_{\Gamma_{\mathrm{D},2}},$$

where $\mathbb{1}$ denotes the indicator function. We consider the following affine spaces associated to the non-homogeneous Dirichlet boundary data $\boldsymbol{u}_{\mathrm{D},i} \in \mathrm{H}^{1/2}_{00}(\Gamma_{\mathrm{D},i})^d$ and $\mathsf{T}_{\mathrm{D},i} \in \mathrm{H}^{1/2}(\Gamma_{\mathrm{D},i})$:

$$\mathcal{V}_{\boldsymbol{u}_{\mathrm{D}},i}(\Omega_i) = \{\boldsymbol{w} \in \mathrm{H}^1(\Omega_i)^d; \quad \boldsymbol{w} = \boldsymbol{u}_{\mathrm{D},i} \text{ on } \Gamma_{\mathrm{D},i} \text{ and } \boldsymbol{w} = 0 \text{ on } \Gamma \cup \Gamma_{\mathrm{e},i}\},$$

and

$$\mathcal{H}_{\mathsf{T}_{\mathrm{D}}}(\Omega_1, \Omega_2) = \{\phi = (\phi_1, \phi_2) \in \mathcal{H}^1(\Omega_1, \Omega_2);\ \phi = \mathsf{T}_{\mathrm{D}} \text{ on } \Gamma_{\mathrm{D}}\},$$

where

$$\mathcal{H}^k(\Omega_1, \Omega_2) = \{\phi = (\phi_1, \phi_2) \in \mathrm{H}^k(\Omega_1) \times \mathrm{H}^k(\Omega_2);\ \langle\phi\rangle \in \mathrm{H}^k(\Gamma)\}, \quad k \in \mathbb{N}^*.$$

The spaces $\mathcal{V}_0(\Omega_i)$ and $\mathcal{H}_0(\Omega_1, \Omega_2)$ are Hilbert spaces when they are equipped with the respective norms

$$\|\boldsymbol{w}\|_{\mathcal{V}_0(\Omega_i)} = \|\boldsymbol{w}\|_{\mathrm{H}^1(\Omega_i)^d}$$

and

$$\|\phi\|_{\mathcal{H}_0(\Omega_1,\Omega_2)} = \left(\sum_{i=1}^{2} \|\nabla \phi_i\|^2_{\mathrm{L}^2(\Omega_i)^d} + \|\nabla_\tau \langle\phi\rangle\|^2_{\mathrm{L}^2(\Gamma)^d} + \|[\phi]\|^2_{\mathrm{L}^2(\Gamma)} \right)^{1/2}.$$

The space $\mathcal{H}_0(\Omega_1, \Omega_2)$ is called *broken Sobolev space* (see for instance [55] for more details). In the following, we also denote

$$\mathrm{H}^k(\Omega_i, \Gamma) = \{\phi \in \mathrm{H}^k(\Omega_i);\ \phi|_\Gamma \in \mathrm{H}^k(\Gamma)\}, \quad k \in \mathbb{N}^*.$$

Remark 20 *Note that the norm* $\|\cdot\|_{\mathcal{H}_0(\Omega_1,\Omega_2)}$ *is equivalent to the norm*

$$\|\cdot\|_{\mathcal{H}^1(\Omega_1,\Omega_2)} = \left(\sum_{i=1}^{2} \|\nabla\cdot\|^2_{\mathrm{L}^2(\Omega_i)^d} + \|\nabla_\tau \langle\cdot\rangle\|^2_{\mathrm{L}^2(\Gamma)^d}\right)^{1/2},$$

in $\mathcal{H}_0(\Omega_1,\Omega_2)$*, thanks to trace and Poincare's inequalities.*

Firstly, the Navier-Stokes equations (4.1), have the following variational formulation:

$$\left\{\begin{array}{l} \text{Find } (\boldsymbol{u}_i, p_i) \in \mathcal{V}_{\boldsymbol{u}_{\mathrm{D},i}}(\Omega_i)\times \mathrm{L}^2(\Omega_i) \text{ such that for all } (\boldsymbol{w}, r)\in \mathcal{V}_0(\Omega_i)\times \mathrm{L}^2(\Omega_i), \\ \quad \displaystyle\int_{\Omega_i} (2\nu_i \varepsilon(\boldsymbol{u}_i) : \varepsilon(\boldsymbol{w}) + (\nabla \boldsymbol{u}_i)\boldsymbol{u}_i\cdot\boldsymbol{w} - p_i \operatorname{div}(\boldsymbol{w}) - r\operatorname{div}(\boldsymbol{u}_i))\,\mathrm{d}x = 0. \end{array}\right. \tag{4.8}$$

If the viscosity ν_i is large enough, this problem is well-posed, this is, there exists a unique weak solution $(\boldsymbol{u}_i, p_i)\in \mathcal{V}_{\boldsymbol{u}_{\mathrm{D},i}}(\Omega_i)\times \mathrm{L}^2(\Omega_i)$ (see for example [68, 106] for details). As we are interested in questions of optimal design rather than the existence of solutions to this type of problem, we place ourselves in this context and assume that we have a unique solution to these Navier-Stokes equations.

Secondly, for the temperature, the corresponding variational formulation of the approximate convection-diffusion equation (4.2) is given by:

$$\left\{\begin{array}{l} \text{Find } \mathsf{T} = (\mathsf{T}_1, \mathsf{T}_2)\in \mathcal{H}_{\mathsf{T}_\mathrm{D}}(\Omega_1,\Omega_2) \text{ such that for all } \phi = (\phi_1,\phi_2)\in \mathcal{H}_0(\Omega_1,\Omega_2) \\ \quad \displaystyle\sum_{i=1}^{2}\int_{\Omega_i} (\kappa_i \nabla \mathsf{T}_i\cdot\nabla\phi_i + \boldsymbol{u}_i\cdot\nabla \mathsf{T}_i\phi_i)\,\mathrm{d}x \\ \qquad \displaystyle + \int_\Gamma \left(\eta\kappa_\mathrm{s}\nabla_\tau\langle\mathsf{T}\rangle\cdot\nabla_\tau\langle\phi\rangle + \kappa_\mathrm{s} H[\mathsf{T}]\langle\phi\rangle + \frac{\kappa_\mathrm{s}}{\eta}[\mathsf{T}][\phi]\right)\mathrm{d}s = 0. \end{array}\right. \tag{4.9}$$

This problem is non-standard. Its well-posedness was proved in our previous work [36, Theorem 2.1] under the following additional hypothesis. We assume that the fluids leave the domain at the outlet, there is no recirculation there: the normal component of the velocity at the outlet is positive everywhere along the outlet.

$$\boldsymbol{u}_i\cdot\boldsymbol{N}\geq 0 \ \text{ on } \Gamma_{\mathrm{N},i},\ i=1,2. \tag{4.10}$$

Remark 21 *The assumption* $\boldsymbol{u}_{\mathrm{D,i}}\in \mathrm{H}^{1/2}_{00}(\Gamma_{\mathrm{D,i}})^d$ *permits to ensure that the Dirichlet data belongs to* $\mathrm{H}^{1/2}(\Gamma_{\mathrm{D,i}}\cup\Gamma)^d$ *since we have* $\boldsymbol{u}_i = 0$ *on* Γ *and* $\boldsymbol{u}_i = \boldsymbol{u}_{\mathrm{D,i}}$ *on* $\Gamma_{\mathrm{D,i}}$*. Notice that, in particular* $\overline{\Gamma}\cap\overline{\Gamma}_{\mathrm{D},1}\neq\emptyset$*.*

Remark 22 *Let us emphasize a point regarding the way to derive the previous variational formulation. Let* T *the strong solution of* (4.2) *that we suppose* $\mathcal{H}^2(\Omega_1,\Omega_2)$ *and* $\phi\in\mathcal{H}_0(\Omega_1,\Omega_2)$*. Using Green's formula on* Γ*, we get:*

$$\int_\Gamma -(\Delta_\tau\langle\mathsf{T}\rangle)\langle\phi\rangle\,\mathrm{d}s = \int_\Gamma \nabla_\tau\langle\mathsf{T}\rangle\cdot\langle\phi\rangle\,\mathrm{d}s - \int_{\partial\Gamma}\langle\phi\rangle\nabla_\tau\langle\mathsf{T}\rangle\cdot\bar{\boldsymbol{\tau}}\mathrm{d}l,$$

where $\bar{\boldsymbol{\tau}}$ *is the unit tangent vector to* Γ *normal to* $\partial\Gamma$*, and* $\mathrm{d}l$ *is the* $(d-2)$ *dimensional measure along* $\partial\Gamma$*. In our situation,* $\bar{\boldsymbol{\tau}}$ *corresponds to the normal to* Γ_D *on* $\overline{\Gamma}\cap\overline{\Gamma_\mathrm{D}}$ *and the normal to* Γ_N *on* $\overline{\Gamma}\cap\overline{\Gamma_\mathrm{N}}$*. Then*

$$\int_{\partial\Gamma}\langle\phi\rangle\nabla_\tau\langle\mathsf{T}\rangle\cdot\bar{\boldsymbol{\tau}}\mathrm{d}l = 0$$

since $\nabla_\tau \langle \mathsf{T} \rangle \cdot \bar{\boldsymbol{\tau}} = \frac{\partial \langle \mathsf{T} \rangle}{\partial \boldsymbol{N}}$ *and since* $\frac{\partial \langle \mathsf{T} \rangle}{\partial \boldsymbol{N}} = 0$ *on* $\partial\Gamma$.

4.3 Shape sensitivity analysis

Let us now perform a shape sensitivity analysis relying on the Hadamard shape derivative (see [72, 7]). Let us begin by defining the class of admissible deformations. The inlet and outlet boundaries are given and not subject to optimization. Moreover, we introduce a positive real number $\delta > 0$, small enough, and, for $i = 1, 2$, we define

$$\Omega^\delta_{\mathrm{D},i} = \{x \in \Omega_i;\ d(x, \Gamma_\mathrm{D}) < \delta\}.$$

We assume δ small enough in order to have $\overline{\Omega^\delta_{\mathrm{D},1}} \cap \overline{\Omega^\delta_{\mathrm{D},2}} = \emptyset$. We then consider the set of admissible deformations Θ_ad defined as

$$\Theta_\mathrm{ad} = \{\boldsymbol{\theta} \in \mathcal{C}^2(\Omega)^d \cap \mathrm{W}^{2,\infty}(\Omega)^d;\ \|\boldsymbol{\theta}\|_{\mathrm{W}^{2,\infty}(\Omega)^d} < 1,\ \boldsymbol{\theta} = 0 \text{ on } \partial\Omega,\ \boldsymbol{\theta} = 0 \text{ in } \Omega^\delta_{\mathrm{D},i}, i = 1, 2\},$$

and we consider small perturbations of the interface Γ, for $\boldsymbol{\theta} \in \Theta_\mathrm{ad}$:

$$\Gamma^{\boldsymbol{\theta}} = (\boldsymbol{I} + \boldsymbol{\theta})\Gamma \qquad \text{and} \qquad \Omega_i^{\boldsymbol{\theta}} = (\boldsymbol{I} + \boldsymbol{\theta})\Omega_i, \quad i = 1, 2,$$

where $\boldsymbol{I}$ is the identity mapping from $\mathrm{W}^{2,\infty}$ into $\mathrm{W}^{2,\infty}$. Such deformations leave the Ω domain and the vicinity of the inlet and outlet invariant, but allow the shape of the interface between the hot and cold fluids to be modified.

In the following, we introduce $(\boldsymbol{u}_{\boldsymbol{\theta},i}, p_{\boldsymbol{\theta},i}) \in \mathcal{V}_{\boldsymbol{u}_\mathrm{D},i}(\Omega_i^{\boldsymbol{\theta}}) \times \mathrm{L}^2(\Omega_i^{\boldsymbol{\theta}})$ and $\mathsf{T}_{\boldsymbol{\theta}} \in \mathcal{H}_{\mathsf{T}_\mathrm{D}}(\Omega_1^{\boldsymbol{\theta}}, \Omega_2^{\boldsymbol{\theta}})$ the perturbed solutions, *i.e.* the solution of the Navier-Stokes equations defined in $\Omega_i^{\boldsymbol{\theta}}$ (instead of Ω_i) and the approximate convection-diffusion equations (4.2) defined in $\Omega_1^{\boldsymbol{\theta}} \cup \Omega_2^{\boldsymbol{\theta}}$ (instead of $\Omega_1 \cup \Omega_2$).

4.3.1 Shape sensitivity of the velocity and pressure

The shape calculus is well known for the solutions of the Stokes and Navier-Stokes equations: the interested reader can refer to [20, 73] for first order derivatives and [37, 34] for second-order derivatives. Let us recall the expression of the material and shape derivatives of velocity and pressure.

Proposition 4.3.1 (Shape derivative of the Navier-Stokes equations)**.** *For each* $i = 1, 2$*, the material derivative* $(\dot{\boldsymbol{u}}_i, \dot{p}_i) \in \mathcal{V}_0(\Omega_i) \times \mathrm{L}^2(\Omega_i)$ *of the solution* $(\boldsymbol{u}_i, p_i) \in \mathcal{V}_{\boldsymbol{u}_\mathrm{D},i}(\Omega_i) \times \mathrm{L}^2(\Omega_i)$ *of the Navier-Stokes equations* (4.1) *exists and solves the following problem*

$$\left\{\begin{array}{l} \text{Find } (\dot{\boldsymbol{u}}_i, \dot{p}_i) \in \mathcal{V}_0(\Omega_i) \times \mathrm{L}^2(\Omega_i) \text{ such that for all } (\boldsymbol{w}_i, \phi_i) \in \mathcal{V}_0(\Omega_i) \times \mathrm{L}^2(\Omega_i), \\ \displaystyle\int_{\Omega_i} (2\nu_i \varepsilon(\dot{\boldsymbol{u}}_i) : \varepsilon(\boldsymbol{w}_i) + (\nabla \dot{\boldsymbol{u}}_i)\boldsymbol{u}_i \cdot \boldsymbol{w}_i + (\nabla \boldsymbol{u}_i)\dot{\boldsymbol{u}}_i \cdot \boldsymbol{w}_i - \dot{p}_i \operatorname{div}(\boldsymbol{w}_i) - \phi_i \operatorname{div}(\dot{\boldsymbol{u}}_i))\, \mathrm{d}x \\ \quad = \displaystyle\int_{\Omega_i} -\operatorname{div}(\boldsymbol{\theta})(\sigma(\boldsymbol{u}_i, p_i) : \nabla \boldsymbol{w}_i + (\nabla \boldsymbol{u}_i)\boldsymbol{u}_i \cdot \boldsymbol{w}_i)\, \mathrm{d}x \\ \quad + \displaystyle\int_{\Omega_i} (\sigma(\boldsymbol{u}_i, p_i) : (\nabla \boldsymbol{w}_i \nabla \boldsymbol{\theta}) + \sigma(\boldsymbol{w}_i, \phi_i) : (\nabla \boldsymbol{u}_i \nabla \boldsymbol{\theta}) + (\nabla \boldsymbol{u}_i \nabla \boldsymbol{\theta})\boldsymbol{u}_i \cdot \boldsymbol{w}_i)\, \mathrm{d}x. \end{array}\right. \tag{4.11}$$

Furthermore, assuming that $(\boldsymbol{u}_i, p_i)$ *belongs to* $\mathrm{H}^2(\Omega_i)^d \times \mathrm{H}^1(\Omega_i)$*, it is differentiable with respect to the domain and the shape derivatives* $(\boldsymbol{u}_i', p_i') \in \mathrm{H}^1(\Omega_i)^d \times \mathrm{L}^2(\Omega_i)$ *are characterized by*

$$\left\{\begin{array}{rcll} -\nu_i \Delta \boldsymbol{u}_i' + (\nabla \boldsymbol{u}_i)\boldsymbol{u}_i' + (\nabla \boldsymbol{u}_i')\boldsymbol{u}_i + \nabla p_i' &=& 0 & \text{in } \Omega_i, \\ \mathrm{div}(\boldsymbol{u}_i') &=& 0 & \text{in } \Omega_i, \\ \boldsymbol{u}' &=& 0 & \text{on } \Gamma_{\mathrm{D},i} \cup \Gamma_{\mathrm{e},i}, \\ \sigma(\boldsymbol{u}_i', p_i')\boldsymbol{N} &=& 0 & \text{on } \Gamma_{\mathrm{N},i}, \\ \boldsymbol{u}_i' &=& -\dfrac{\partial \boldsymbol{u}_i}{\partial \boldsymbol{n}}(\boldsymbol{\theta}\cdot\boldsymbol{n}) & \text{on } \Gamma. \end{array}\right. \tag{4.12}$$

4.3.2 Shape sensitivity of the temperature

One novelty in our work is the computation of the shape sensitivity analysis and the computation of the shape derivative of the non-standard equation (4.2) dealing with the temperature field. The difficulty is not to compute the shape derivative of the Laplace-Beltrami operator: it is well known in the literature, see for example [54, 39, 46]. The real difficulty comes from the fact that these surface derivatives are involved in a jump condition on an interface and are coupled with coefficient discontinuities.

To compute the shape derivatives for this equation, we need more regularity of the interface Γ, so here and in the following, we assume Γ at least $\mathcal{C}^3$. We use the following overcharged notations. Let d_{Ω_1} be the signed distance function to the domain Ω_1. We set

$$\boldsymbol{n} = \nabla d_{\Omega_1} \quad \text{and} \quad H = \Delta d_{\Omega_1} \text{ in a neighborhood of } \Gamma. \tag{4.13}$$

These functions are defined in the volume and not only on the surface Γ. On the surface Γ, they coincide respectively with the outer unit normal vector and of the mean curvature of Γ (see e.g. [72, Chapter 5, section 4, subsection 3]). Notice that derivation with respect to a shape of terms involving a Laplace-Beltrami operator gives rise to derivatives of curvature, which we can conveniently express using these two functions. In particular, writing $\frac{\partial H}{\partial \boldsymbol{n}}$ makes sense with these definitions, even if it can be confusing at first sight.

Material derivative. Firstly, we prove the following first main result of this section which proves the existence and characterize the material derivative concerning the temperature. It has been well known since [2] that the material derivative is a prerequisite for sensitivity analysis with respect to the form of solutions of problems with coefficients discontinuity. This is done by following the usual procedure given in the book [72]: transport on a fixed domain, differentiability obtained by applying the implicit function theorem and then calculating.

Notice that, in the class Θ_{ad} of deformations, the domain $\Omega_{\mathrm{D},i}^{\delta}$ is untouched by the deformation. Then, we consider a lifting F of the Dirichlet data T_{D}, independent of the deformation field $\boldsymbol{\theta}$, such that

$$F \in \mathrm{H}^1(\Omega), \quad F = \mathsf{T}_{\mathrm{D}} \text{ on } \Gamma_{\mathrm{D}} \quad \text{and} \quad F = 0 \text{ in } \Omega \backslash (\Omega_{\mathrm{D},1}^{\delta} \cup \Omega_{\mathrm{D},2}^{\delta}) \tag{4.14}$$

Such a lifting exists by considering, for instance, the solutions of the two following problems,

for $i = 1, 2$,

$$\begin{cases} -\Delta F_i &= 0 & \text{in } \Omega_i^\delta, \\ F_i &= \mathsf{T}_{\mathrm{D},i} & \text{on } \Gamma_{\mathrm{D},i}, \\ F_i &= 0 & \text{on } \partial\Omega_i^\delta \setminus \partial\Omega, \\ \dfrac{\partial F_i}{\partial \boldsymbol{N}} &= 0 & \text{on } \partial\Omega_i^\delta \cap (\partial\Omega \setminus \Gamma_{\mathrm{D,i}}^\delta), \end{cases}$$

and then extending by 0 to Ω, which extension we continue calling F_i and we define $F := F_1 + F_2$.

Finally, for $\boldsymbol{\theta} \in \Theta_{\mathrm{ad}}$, we recall that $\mathsf{T}_{\boldsymbol{\theta}}$ solution of (4.9) in $\mathcal{H}_{\mathsf{T}_{\mathrm{D}}}(\Omega_1^{\boldsymbol{\theta}}, \Omega_2^{\boldsymbol{\theta}})$ and we introduce its correction by the lifting F of the Dirichlet boundary conditions:

$$\mathsf{R}_{\boldsymbol{\theta}} = \mathsf{T}_{\boldsymbol{\theta}} - F \in \mathcal{H}_0(\Omega_1^{\boldsymbol{\theta}}, \Omega_2^{\boldsymbol{\theta}}).$$

Proposition 4.3.2 (Material derivative of the approximated convection-diffusion equation)**.** *The applications*

$$\boldsymbol{\theta} \in \Theta_{\mathrm{ad}} \mapsto \overline{\mathsf{R}}_{\boldsymbol{\theta}} = \mathsf{R}_{\boldsymbol{\theta}} \circ (\boldsymbol{I} + \boldsymbol{\theta}) \in \mathcal{H}_0(\Omega_1, \Omega_2) \text{ and } \boldsymbol{\theta} \in \Theta_{\mathrm{ad}} \mapsto \overline{\mathsf{T}}_{\boldsymbol{\theta}} = \mathsf{T}_{\boldsymbol{\theta}} \circ (\boldsymbol{I} + \boldsymbol{\theta}) \in \mathcal{H}^1(\Omega_1, \Omega_2)$$

are $\mathcal{C}^1$ in a neighborhood of 0*. Furthermore, the derivative of the last mapping at 0, in the direction $\boldsymbol{\theta}$ is called the material derivative of $\mathsf{T} \in \mathcal{H}_{\mathsf{T}_{\mathrm{D}}}(\Omega_1, \Omega_2)$, is denoted by $\dot{\mathsf{T}}$, and is the solution of the following variational problem*

$$\begin{cases} \text{Find } \dot{\mathsf{T}} \in \mathcal{H}_0(\Omega_1, \Omega_2) \text{ such that for all } \phi \in \mathcal{H}_0(\Omega_1, \Omega_2), \\ \displaystyle\sum_{i=1}^{2} \int_{\Omega_i} \left(\kappa_i \nabla \dot{\mathsf{T}}_i \cdot \nabla \phi_i + \left(\boldsymbol{u}_i \cdot \nabla \dot{\mathsf{T}}_i + \dot{\boldsymbol{u}}_i \cdot \nabla \mathsf{T}_i \right) \phi_i \right) \mathrm{d}x \\ \quad + \displaystyle\int_{\Gamma} \left(\eta \kappa_s \nabla_\tau \left\langle \dot{\mathsf{T}} \right\rangle \cdot \nabla_\tau \langle \phi \rangle + \kappa_s H [\dot{\mathsf{T}}] \langle \phi \rangle + \frac{\kappa_s}{\eta} [\dot{\mathsf{T}}][\phi] \right) \mathrm{d}s \\ = \displaystyle\sum_{i=1}^{2} \int_{\Omega_i} \left(\kappa_i \left(\nabla \boldsymbol{\theta} + \nabla \boldsymbol{\theta}^t - \mathrm{div}(\boldsymbol{\theta}) \mathrm{I} \right) \nabla \mathsf{T}_i \cdot \nabla \phi_i + \left(\left((\nabla \boldsymbol{\theta})\, \boldsymbol{u}_i - \mathrm{div}(\boldsymbol{\theta}) \boldsymbol{u}_i \right) \cdot \nabla \mathsf{T}_i \right) \phi_i \right) \mathrm{d}x \\ \quad + \displaystyle\int_{\Gamma} \eta \kappa_s \left(\left(\nabla_\tau \boldsymbol{\theta} + \nabla_\tau \boldsymbol{\theta}^t - \mathrm{div}_\tau(\boldsymbol{\theta}) \mathrm{I} \right) \nabla_\tau \langle \mathsf{T} \rangle \right) \cdot \nabla_\tau \langle \phi \rangle \, \mathrm{d}s \\ \quad - \displaystyle\int_{\Gamma} \left(\kappa_s H \, \mathrm{div}_\tau(\boldsymbol{\theta}) [\mathsf{T}] \langle \phi \rangle - \kappa_s \Delta_\tau (\boldsymbol{\theta} \cdot \boldsymbol{n}) [\mathsf{T}] \langle \phi \rangle + \kappa_s \nabla H \cdot \theta [\mathsf{T}] \langle \phi \rangle \right) \mathrm{d}s \\ \quad - \displaystyle\int_{\Gamma} \frac{\kappa_s}{\eta} \, \mathrm{div}_\tau(\boldsymbol{\theta}) [\mathsf{T}][\phi] \, \mathrm{d}s. \end{cases} \tag{4.15}$$

Proof. *Step 1: transport on a fixed domain with a fixed interface.* Let $\boldsymbol{\theta} \in \Theta_{\mathrm{ad}}$. We define the transported solution of the Navier-Stokes equations (4.1) $\overline{\boldsymbol{u}}_{\boldsymbol{\theta},i} := \boldsymbol{u}_{\boldsymbol{\theta},i} \circ (\boldsymbol{I} + \boldsymbol{\theta}) \in \mathcal{V}_{\boldsymbol{u}_{\mathrm{D,i}}}(\Omega_i)$. Given $\phi \in \mathcal{H}_0(\Omega_1, \Omega_2)$, we define $\phi_{\boldsymbol{\theta}} = \phi \circ (\boldsymbol{I} + \boldsymbol{\theta})^{-1} \in \mathcal{H}_0(\Omega_1^{\boldsymbol{\theta}}, \Omega_2^{\boldsymbol{\theta}})$. One starts from the weak formulation of the convection-diffusion equation (4.9) on the perturbed domain:

$$\sum_{i=1}^{2} \int_{\Omega_i^{\boldsymbol{\theta}}} (\kappa_i \nabla \mathsf{T}_{\boldsymbol{\theta},i} \cdot \nabla \phi_{\boldsymbol{\theta},i} + \boldsymbol{u}_{\boldsymbol{\theta},i} \cdot \nabla \mathsf{T}_{\boldsymbol{\theta},i} \phi_{\boldsymbol{\theta},i}) \, \mathrm{d}x$$
$$+ \int_{\Gamma^{\boldsymbol{\theta}}} \left(\eta \kappa_s \nabla_{\tau_{\boldsymbol{\theta}}} \langle \mathsf{T}_{\boldsymbol{\theta}} \rangle \cdot \nabla_{\tau_{\boldsymbol{\theta}}} \langle \phi_{\boldsymbol{\theta}} \rangle + \kappa_s H_{\boldsymbol{\theta}} [\mathsf{T}_{\boldsymbol{\theta}}] \langle \phi_{\boldsymbol{\theta}} \rangle + \frac{\kappa_s}{\eta} [\mathsf{T}_{\boldsymbol{\theta}}][\phi_{\boldsymbol{\theta}}] \right) \mathrm{d}s = 0,$$

and $\mathsf{R}_{\boldsymbol{\theta}}$ satisfies,

$$\begin{aligned}
&\sum_{i=1}^{2}\int_{\Omega_i^{\boldsymbol{\theta}}}(\kappa_i\nabla\mathsf{R}_{\boldsymbol{\theta},i}\cdot\nabla\phi_{\boldsymbol{\theta},i}+\boldsymbol{u}_{\boldsymbol{\theta},i}\cdot\nabla\mathsf{R}_{\boldsymbol{\theta},i}\phi_{\boldsymbol{\theta},i})\,\mathrm{d}x\\
&\qquad+\int_{\Gamma^{\boldsymbol{\theta}}}\left(\eta\kappa_s\nabla_{\tau_{\boldsymbol{\theta}}}\langle\mathsf{R}_{\boldsymbol{\theta}}\rangle\cdot\nabla_{\tau_{\boldsymbol{\theta}}}\langle\phi_{\boldsymbol{\theta}}\rangle+\kappa_s H_{\boldsymbol{\theta}}[\mathsf{R}_{\boldsymbol{\theta}}]\langle\phi_{\boldsymbol{\theta}}\rangle+\frac{\kappa_s}{\eta}[\mathsf{R}_{\boldsymbol{\theta}}][\phi_{\boldsymbol{\theta}}]\right)\mathrm{d}s\\
&\qquad\quad=-\sum_{i=1}^{2}\int_{\Omega^{\delta}_{\mathrm{D},i}}(\kappa_i\nabla F\cdot\nabla\phi_i+\boldsymbol{u}_{\boldsymbol{\theta},i}\cdot\nabla F\phi_i)\,\mathrm{d}x-\int_{\Gamma\cap\partial\Omega^{\delta}_{\mathrm{D},1}}\eta\kappa_s\nabla_\tau F\cdot\nabla_\tau\langle\phi\rangle\,\mathrm{d}s,
\end{aligned}$$

where we have used that the lifting F is independent of $\boldsymbol{\theta}$, $[F]=0$ on $\Gamma^{\boldsymbol{\theta}}$, $F=0$ in $\Omega\backslash(\Omega^{\delta}_{\mathrm{D},1}\cup\Omega^{\delta}_{\mathrm{D},2})$ and $\boldsymbol{\theta}\in\Theta$ verifies, $\boldsymbol{\theta}=0$ in $\Omega^{\delta}_{\mathrm{D},1}\cup\Omega^{\delta}_{\mathrm{D},2}$.

After a change of variables to the reference configuration, one gets:

$$\begin{aligned}
&\sum_{i=1}^{2}\int_{\Omega_i}\left(\kappa_i A(\boldsymbol{\theta})\nabla\overline{\mathsf{R}}_{\boldsymbol{\theta},i}\cdot\nabla\phi_i+B(\boldsymbol{\theta})\overline{\boldsymbol{u}}_{\boldsymbol{\theta},i}\cdot\nabla\overline{\mathsf{R}}_{\boldsymbol{\theta},i}\phi_i\right)\mathrm{d}x\\
&\qquad+\int_{\Gamma}\eta\kappa_s C(\boldsymbol{\theta})\Bigg(\left((\mathrm{I}+\nabla\boldsymbol{\theta})^{-1}(\mathrm{I}+\nabla\boldsymbol{\theta})^{-t}\nabla\left\langle\overline{\mathsf{R}}_{\boldsymbol{\theta}}\right\rangle\right)\cdot\nabla\langle\phi\rangle\\
&\qquad\qquad-\left((\mathrm{I}+\nabla\boldsymbol{\theta})^{-t}\nabla\langle\overline{\mathsf{R}}_{\boldsymbol{\theta}}\rangle\cdot\boldsymbol{n}_{\boldsymbol{\theta}}\circ(\boldsymbol{I}+\boldsymbol{\theta})\right)\left((\mathrm{I}+\nabla\boldsymbol{\theta})^{-t}\nabla\langle\phi\rangle\cdot\boldsymbol{n}_{\boldsymbol{\theta}}\circ(\boldsymbol{I}+\boldsymbol{\theta})\right)\Bigg)\mathrm{d}s\\
&\qquad+\int_{\Gamma}\left(\kappa_s C(\boldsymbol{\theta})H_{\boldsymbol{\theta}}\circ(\boldsymbol{I}+\boldsymbol{\theta})[\overline{\mathsf{R}}_{\boldsymbol{\theta}}]\langle\phi\rangle+\frac{\kappa_s}{\eta}C(\boldsymbol{\theta})[\overline{\mathsf{R}}_{\boldsymbol{\theta}}][\phi]\right)\mathrm{d}s\\
&\qquad+\sum_{i=1}^{2}\int_{\Omega^{\delta}_{\mathrm{D},i}}(\kappa_i\nabla F\cdot\nabla\phi_i+\boldsymbol{u}_{\boldsymbol{\theta},i}\cdot\nabla F\phi_i)\,\mathrm{d}x+\int_{\Gamma\cap\partial\Omega^{\delta}_{\mathrm{D},1}}\eta\kappa_s\nabla_\tau F\cdot\nabla_\tau\langle\phi\rangle\,\mathrm{d}s=0,
\end{aligned}\tag{4.16}$$

where

$$\begin{aligned}
A(\boldsymbol{\theta}) &= \det(\mathrm{I}+\nabla\boldsymbol{\theta})(\mathrm{I}+\nabla\boldsymbol{\theta})^{-t}(\mathrm{I}+\nabla\boldsymbol{\theta}),\\
B(\boldsymbol{\theta}) &= \det(\mathrm{I}+\nabla\boldsymbol{\theta})(\mathrm{I}+\nabla\boldsymbol{\theta}),\\
C(\boldsymbol{\theta}) &= \det(\mathrm{I}+\nabla\boldsymbol{\theta})|(\mathrm{I}+\nabla\boldsymbol{\theta})^{-t}\boldsymbol{n}|_{\mathbb{R}^d}.
\end{aligned}$$

Step 2: going for the implicit function theorem. Define $\mathcal{F}:\Theta_{\mathrm{ad}}\times\mathcal{H}_0(\Omega_1,\Omega_2)\mapsto(\mathcal{H}_0(\Omega_1,\Omega_2))'$

by: for all $\phi \in \mathcal{H}_0(\Omega_1, \Omega_2)$,

$$\begin{aligned}\langle \mathcal{F}(\boldsymbol{\theta}, \psi), \phi \rangle = &\sum_{i=1}^{2} \int_{\Omega_i} (\kappa_i A(\boldsymbol{\theta}) \nabla \psi_i \cdot \nabla \phi_i + B(\boldsymbol{\theta}) \overline{\boldsymbol{u}}_{\boldsymbol{\theta},i} \cdot \nabla \psi_i \phi_i) \, \mathrm{d}x \\ &+ \int_{\Gamma} \eta \kappa_s C(\boldsymbol{\theta}) \Big(\big((\mathrm{I} + \nabla \boldsymbol{\theta})^{-1} (\mathrm{I} + \nabla \boldsymbol{\theta})^{-t} \nabla \langle \psi \rangle \big) \cdot \nabla \langle \phi \rangle \\ &\qquad - \big((\mathrm{I} + \nabla \boldsymbol{\theta})^{-t} \nabla \langle \psi \rangle \cdot \boldsymbol{n}_{\boldsymbol{\theta}} \circ (\boldsymbol{I} + \boldsymbol{\theta}) \big) \big((\mathrm{I} + \nabla \boldsymbol{\theta})^{-t} \nabla \langle \phi \rangle \cdot \boldsymbol{n}_{\boldsymbol{\theta}} \circ (\boldsymbol{I} + \boldsymbol{\theta}) \big) \Big) \, \mathrm{d}s \\ &+ \int_{\Gamma} \left(\kappa_s C(\boldsymbol{\theta}) H_{\boldsymbol{\theta}} \circ (\boldsymbol{I} + \boldsymbol{\theta})[\psi] \langle \phi \rangle + \frac{\kappa_s}{\eta} C(\boldsymbol{\theta})[\psi][\phi] \right) \mathrm{d}s \\ &+ \sum_{i=1}^{2} \int_{\Omega_{\mathrm{D},i}^{\delta}} (\kappa_i \nabla F \cdot \nabla \phi_i + \boldsymbol{u}_{\boldsymbol{\theta},i} \cdot \nabla F \phi_i) \, \mathrm{d}x + \int_{\Gamma \cap \partial \Omega_{\mathrm{D},1}^{\delta}} \eta \kappa_s \nabla_\tau F \cdot \nabla_\tau \langle \phi \rangle \, \mathrm{d}s.\end{aligned}$$

Let us check the assumptions of the implicit function theorem.

- By construction
$$\mathcal{F}(0, \mathsf{T} - F) = 0,$$
where T is the solution of the convection-diffusion problem (4.9) (with $\boldsymbol{\theta} = 0$).

- We now study the regularity of $\mathcal{F}$. Let us first recall that $\boldsymbol{\theta} \in \Theta_{\mathrm{ad}} \mapsto \boldsymbol{n}_{\boldsymbol{\theta}} \circ (\boldsymbol{I} + \boldsymbol{\theta}) \in \mathcal{C}^1(\Gamma)^d$ and $\boldsymbol{\theta} \in \Theta_{\mathrm{ad}} \mapsto \boldsymbol{H}_{\boldsymbol{\theta}} \circ (\boldsymbol{I} + \boldsymbol{\theta}) \in \mathcal{C}^0(\Gamma)$ are $\mathcal{C}^1$ (see [104, Lemma 3.4-3.5], [72, Proposition 5.4.14, Lemma 5.4.15]). Also, $\theta \in \Theta_{\mathrm{ad}} \to \overline{\boldsymbol{u}}_{\boldsymbol{\theta},i} \in \mathcal{V}_{0,i}(\Omega_i)$ is $\mathcal{C}^1$ in a neighborhood of 0 as proven in [34] and $\overline{\boldsymbol{u}}_{\boldsymbol{\theta},i} = \boldsymbol{u}_{\boldsymbol{\theta},i}$ in $\Omega_{\mathrm{D,i}}^{\delta}$. Moreover, from [72, Theorem 5.5.1], $\boldsymbol{\theta} \in \Theta_{\mathrm{ad}} \mapsto A(\boldsymbol{\theta}) \in \mathrm{L}^\infty(\Omega, \mathcal{M}_d)$, $\boldsymbol{\theta} \in \Theta_{\mathrm{ad}} \mapsto B(\boldsymbol{\theta}) \in \mathrm{L}^\infty(\Omega, \mathcal{M}_d)$, $\boldsymbol{\theta} \in \Theta_{\mathrm{ad}} \mapsto C(\boldsymbol{\theta}) \in \mathcal{C}^1(\Gamma)$ are $\mathcal{C}^\infty$, where $\mathcal{M}_d$ is the space of $d \times d$ square matrices. Finally, for $\boldsymbol{\theta^*} \in \Theta_{\mathrm{ad}}$, the mapping
$$\mathcal{F}(\boldsymbol{\theta}^*, \cdot) : \mathcal{H}_0(\Omega_1, \Omega_2) \mapsto (\mathcal{H}_0(\Omega_1, \Omega_2))'$$
is linear continuous and then $\mathcal{C}^\infty$. By chain rule, we conclude that $\mathcal{F}$ is $\mathcal{C}^1$ in a neighborhood of 0.

- Finally, we check that the operator $\mathrm{D}_\psi \mathcal{F}(0, \mathsf{T} - F)$ is an isomorphism from $\mathcal{H}_0(\Omega_1, \Omega_2)$ into $(\mathcal{H}_0(\Omega_1, \Omega_2))'$. Indeed for all $S, \hat{S} \in \mathcal{H}_0(\Omega_1, \Omega_2)$, we compute
$$\begin{aligned}\langle \mathrm{D}_\psi \mathcal{F}(0, \mathsf{T} - F) S, \hat{S} \rangle = &\sum_{i=1}^{2} \int_{\Omega_i} \left(\kappa_i \nabla S_i \cdot \nabla \hat{S}_i + \nabla S_i \cdot \boldsymbol{u}_i \hat{S}_i \right) \mathrm{d}x \\ &+ \int_{\Gamma} \left(\eta \kappa_s \nabla_\tau \langle S \rangle \cdot \nabla_\tau \langle \hat{S} \rangle + \kappa_s H[S][\hat{S}] + \frac{\kappa_s}{\eta} [S][\hat{S}] \right) \mathrm{d}s.\end{aligned}$$
This leads to a well-posed problem when the right hand side of the variational problem belongs to $(\mathcal{H}_0(\Omega_1, \Omega_2))'$, thanks to the Lax-Milgram theorem. The proof is analogous to the well-posedness of problem (4.9). Indeed, let us consider $\ell \in (\mathcal{H}_0(\Omega_1, \Omega_2))'$. The coercivity of the bilinear form at the left hand-side was already proved in [36, Theorem 2.1]. The only difference is that we do not have anymore the integral structure at the right hand-side,

but the continuity is straightforward since $\ell \in (\mathcal{H}_0(\Omega_1,\Omega_2))'$. By virtue of the Lax-Milgram theorem, there exists a unique $S_\ell \in \mathcal{H}_0(\Omega_1,\Omega_2)$ such that for all $\hat{S} \in \mathcal{H}_0(\Omega_1,\Omega_2)$,

$$\sum_{i=1}^{2}\int_{\Omega_i}\left(\kappa_i\nabla S_i\cdot\nabla\hat{S}_i+\nabla S_i\cdot\boldsymbol{u}_i\hat{S}_i\right)\mathrm{d}x + \int_\Gamma\left(\eta\kappa_s\nabla_\tau\langle S\rangle\cdot\nabla_\tau\langle\hat{S}\rangle+\kappa_s H[S][\hat{S}]+\frac{\kappa_s}{\eta}[S][\hat{S}]\right)\mathrm{d}s=\left\langle\ell,\hat{S}\right\rangle_{(\mathcal{H}_0(\Omega_1,\Omega_2))',\mathcal{H}_0(\Omega_1,\Omega_2)}.$$

By virtue of the implicit function theorem, there exists a $\mathcal{C}^1$ function

$$\boldsymbol{\theta}\in\Theta_{\mathrm{ad}}\mapsto\psi(\boldsymbol{\theta})\in\mathcal{H}_0(\Omega_1,\Omega_2)$$

in a neighborhood of 0 such that, $\mathcal{F}(0,\psi(\boldsymbol{\theta}))=0$. By uniqueness of the solution $\overline{\mathsf{R}}_{\boldsymbol{\theta}}\in\mathcal{H}_0(\Omega_1,\Omega_2)$, we deduce $\overline{\mathsf{R}}_{\boldsymbol{\theta}}=\psi(\boldsymbol{\theta})$, then, $\boldsymbol{\theta}\in\Theta_{\mathrm{ad}}\mapsto\overline{\mathsf{R}}_{\boldsymbol{\theta}}\in\mathcal{H}_0(\Omega_1,\Omega_2)$ is $\mathcal{C}^1$ in a neighborhood of 0. Since F is independent of θ, we also obtain that $\boldsymbol{\theta}\in\Theta_{\mathrm{ad}}\mapsto\overline{\mathsf{T}}_{\boldsymbol{\theta}}\in\mathcal{H}^1(\Omega_1,\Omega_2)$ is $\mathcal{C}^1$ in a neighborhood of 0.

Step 3: characterization of the material derivative. To prove that the material derivative satisfies (4.15), we proceeded as in [7, Proposition 6.30]. First, we write the variational problem that solves $\mathsf{T}_{\boldsymbol{\theta}}$ after having performed the pull-back on the reference domain:

$$\begin{aligned}&\sum_{i=1}^{2}\int_{\Omega_i}\left(\kappa_i A(\boldsymbol{\theta})\nabla\overline{\mathsf{T}}_{\boldsymbol{\theta},i}\cdot\nabla\phi_i+B(\boldsymbol{\theta})\overline{\boldsymbol{u}}_{\boldsymbol{\theta},i}\cdot\nabla\overline{\mathsf{T}}_{\boldsymbol{\theta},i}\phi_i\right)\mathrm{d}x\\&\quad+\int_\Gamma\eta\kappa_s C(\boldsymbol{\theta})\Big(\left((\mathrm{I}+\nabla\boldsymbol{\theta})^{-1}(\mathrm{I}+\nabla\boldsymbol{\theta})^{-t}\nabla\left\langle\overline{\mathsf{T}}_{\boldsymbol{\theta}}\right\rangle\right)\cdot\nabla\langle\phi\rangle\\&\qquad-\left((\mathrm{I}+\nabla\boldsymbol{\theta})^{-t}\nabla\langle\overline{\mathsf{T}}_{\boldsymbol{\theta}}\rangle\cdot\boldsymbol{n}_{\boldsymbol{\theta}}\circ(\boldsymbol{I}+\boldsymbol{\theta})\right)\left((\mathrm{I}+\nabla\boldsymbol{\theta})^{-t}\nabla\langle\phi\rangle\cdot\boldsymbol{n}_{\boldsymbol{\theta}}\circ(\boldsymbol{I}+\boldsymbol{\theta})\right)\Big)\mathrm{d}s\\&\quad+\int_\Gamma\left(\kappa_s C(\boldsymbol{\theta})H_{\boldsymbol{\theta}}\circ(\boldsymbol{I}+\boldsymbol{\theta})[\overline{\mathsf{T}}_{\boldsymbol{\theta}}]\langle\phi\rangle+\frac{\kappa_s}{\eta}C(\boldsymbol{\theta})[\overline{\mathsf{T}}_{\boldsymbol{\theta}}][\phi]\right)\mathrm{d}s=0.\end{aligned}\tag{4.17}$$

Then, differentiating (4.17) at $\boldsymbol{\theta}=0$ in the direction $\boldsymbol{\theta}$ and using the following derivatives:

$$\begin{aligned}\mathrm{D}A(0)(\boldsymbol{\theta})&=\mathrm{div}(\boldsymbol{\theta})\mathrm{I}-\nabla\boldsymbol{\theta}-(\nabla\boldsymbol{\theta})^t,\\\mathrm{D}B(0)(\boldsymbol{\theta})&=\mathrm{div}(\boldsymbol{\theta})\mathrm{I}-(\nabla\boldsymbol{\theta})^t,\\\mathrm{D}C(0)(\boldsymbol{\theta})&=\mathrm{div}_\tau(\boldsymbol{\theta}),\\\dot{\boldsymbol{n}}&=-\nabla_\tau(\boldsymbol{\theta}\cdot\boldsymbol{n})+(\nabla\boldsymbol{n})\boldsymbol{\theta},\\\dot{H}&=-\Delta_\tau(\boldsymbol{\theta}\cdot\boldsymbol{n})+\nabla H\cdot\boldsymbol{\theta},\end{aligned}$$

where $\dot{\boldsymbol{n}}$ and $\dot{H}$ are the material derivative of the extension of the normal and mean curvature, see [104, Lemma 3.4-3.5]. Finally, we get (4.15) by means of chain rule.

□

Shape derivative. Secondly, we can prove the existence and characterize the shape derivative of the temperature in the following proposition. For this purpose we need the following technical lemma that comes from integrating by parts on the interface.

Lemma 4.3.3. *Let $\boldsymbol{\theta} \in \Theta_{\text{ad}}$. Given $u, \phi \in \mathrm{H}^2(\Gamma)$, we have*

$$-\int_\Gamma \left((\mathrm{div}_\tau(\boldsymbol{\theta})\mathrm{I} - \nabla_\tau\boldsymbol{\theta} - \nabla_\tau\boldsymbol{\theta}^t)\nabla_\tau u \cdot \nabla_\tau\phi + \nabla_\tau(\boldsymbol{\theta}\cdot\nabla_\tau u)\cdot\nabla_\tau\phi - \Delta_\tau u(\boldsymbol{\theta}\cdot\nabla_\tau\phi)\right)\,\mathrm{d}s = \int_\Gamma \mathrm{div}_\tau\left(H(\boldsymbol{\theta}\cdot\boldsymbol{n})\nabla_\tau u - 2(\boldsymbol{\theta}\cdot\boldsymbol{n})(\nabla_\tau\boldsymbol{n})\nabla_\tau u\right)\phi\,\mathrm{d}s.$$

Proof. The idea is to use integration by parts together with the decomposition of the deformation vector $\boldsymbol{\theta} = \boldsymbol{\theta}_\tau + (\boldsymbol{\theta}\cdot\boldsymbol{n})\cdot\boldsymbol{n}$ on Γ. We have,

$$\begin{aligned}
\int_\Gamma \mathrm{div}_\tau(\boldsymbol{\theta})\nabla_\tau u\cdot\nabla_\tau\phi\,\mathrm{d}s &= \int_\Gamma \left(H(\boldsymbol{\theta}\cdot\boldsymbol{n})\nabla_\tau u\cdot\nabla_\tau\phi - \nabla_\tau(\nabla_\tau u\cdot\nabla_\tau\phi)\cdot\boldsymbol{\theta}\right)\,\mathrm{d}s \\
&= \int_\Gamma \left(H(\boldsymbol{\theta}\cdot\boldsymbol{n})\nabla_\tau u\cdot\nabla_\tau\phi - \nabla(\nabla_\tau u\cdot\nabla_\tau\phi)\cdot\boldsymbol{\theta}_\tau\right)\,\mathrm{d}s \\
&= \int_\Gamma \big(H(\boldsymbol{\theta}\cdot\boldsymbol{n})\nabla_\tau u\cdot\nabla_\tau\phi - (\nabla(\nabla_\tau u)^t\nabla_\tau\phi)\cdot\boldsymbol{\theta}_\tau - (\nabla(\nabla_\tau\phi)^t\nabla_\tau u)\cdot\boldsymbol{\theta}_\tau\big)\,\mathrm{d}s, \qquad (4.18)
\end{aligned}$$

$$\begin{aligned}
\int_\Gamma (\nabla_\tau\boldsymbol{\theta}\nabla_\tau u)\cdot\nabla_\tau\phi\,\mathrm{d}s &= \int_\Gamma ((\nabla\boldsymbol{\theta})\nabla_\tau u)\cdot\nabla_\tau\phi\,\mathrm{d}s \\
&= \int_\Gamma \left((\nabla\boldsymbol{\theta}_\tau\nabla_\tau u)\cdot\nabla_\tau\phi + (\boldsymbol{\theta}\cdot\boldsymbol{n})\nabla\boldsymbol{n}\nabla_\tau u\cdot\nabla_\tau\phi\right)\,\mathrm{d}s \qquad (4.19) \\
&= \int_\Gamma ((\boldsymbol{\theta}\cdot\boldsymbol{n})\nabla_\tau\boldsymbol{n}\nabla_\tau u + \nabla\boldsymbol{\theta}_\tau\nabla_\tau u)\cdot\nabla_\tau\phi\,\mathrm{d}s,
\end{aligned}$$

$$\int_\Gamma (\nabla_\tau\boldsymbol{\theta}^t\nabla_\tau u)\cdot\nabla_\tau\phi\,\mathrm{d}s = \int_\Gamma \big((\boldsymbol{\theta}\cdot\boldsymbol{n})\nabla_\tau\boldsymbol{n}\nabla_\tau u + (\nabla\boldsymbol{\theta}_\tau)^t\nabla_\tau u\big)\cdot\nabla_\tau\phi\,\mathrm{d}s, \qquad (4.20)$$

$$\begin{aligned}
\int_\Gamma -\Delta_\tau u(\boldsymbol{\theta}\cdot\nabla_\tau\phi)\,\mathrm{d}s &= \int_\Gamma \nabla_\tau u\cdot\nabla_\tau(\boldsymbol{\theta}\cdot\nabla_\tau\phi)\,\mathrm{d}s \\
&= \int_\Gamma \nabla_\tau u\cdot\nabla(\boldsymbol{\theta}_\tau\cdot\nabla_\tau\phi)\,\mathrm{d}s, \qquad (4.21)
\end{aligned}$$

$$\begin{aligned}
\int_\Gamma \nabla_\tau(\boldsymbol{\theta}\cdot\nabla_\tau u)\cdot\nabla_\tau\phi\,\mathrm{d}s &= \int_\Gamma \nabla(\boldsymbol{\theta}_\tau\cdot\nabla_\tau u)\cdot\nabla_\tau\phi\,\mathrm{d}s \\
&= \int_\Gamma \left(\nabla_\tau\boldsymbol{\theta}^t\nabla_\tau u + \nabla(\nabla_\tau u)^t\boldsymbol{\theta}_\tau\right)\cdot\nabla_\tau\phi\,\mathrm{d}s. \qquad (4.22)
\end{aligned}$$

Summing up the above equations, we get

$$\begin{aligned}
&\int_\Gamma (\mathrm{div}_\tau(\boldsymbol{\theta})\mathrm{I} - \nabla_\tau\boldsymbol{\theta} - \nabla_\tau\boldsymbol{\theta}^t)\nabla_\tau u\cdot\nabla_\tau\phi + \nabla_\tau(\boldsymbol{\theta}\cdot\nabla_\tau u)\cdot\nabla_\tau\phi - \Delta_\tau u(\boldsymbol{\theta}\cdot\nabla_\tau\phi)\,\mathrm{d}s\\
&= \int_\Gamma \left(H(\boldsymbol{\theta}\cdot\boldsymbol{n})\nabla_\tau u\cdot\nabla_\tau\phi - (\nabla(\nabla_\tau u)^t\nabla_\tau\phi)\cdot\boldsymbol{\theta}_\tau + (\nabla(\nabla_\tau\phi)^t\nabla_\tau u)\cdot\boldsymbol{\theta}_\tau\right)\,\mathrm{d}s\\
&\quad - \int_\Gamma 2(\boldsymbol{\theta}\cdot\boldsymbol{n})(\nabla_\tau\boldsymbol{n}\nabla_\tau u)\cdot\nabla_\tau\phi + (\nabla\boldsymbol{\theta}_\tau + \nabla\boldsymbol{\theta}_\tau^t)\nabla_\tau u\cdot\nabla_\tau\phi\,\mathrm{d}s\\
&\quad + \int_\Gamma \nabla_\tau u\cdot\left((\nabla\boldsymbol{\theta})^t\nabla_\tau\phi + \nabla(\nabla_\tau\phi)^t\boldsymbol{\theta}_\tau\right)\,\mathrm{d}s\\
&\quad + \int_\Gamma \left(\nabla\boldsymbol{\theta}_\tau\nabla_\tau u + \nabla(\nabla_\tau u^t)\boldsymbol{\theta}_\tau\right)\cdot\nabla_\tau\phi\,\mathrm{d}s\\
&= \int_\Gamma (H(\boldsymbol{\theta}\cdot\boldsymbol{n})\nabla_\tau u - 2(\boldsymbol{\theta}\cdot\boldsymbol{n})\nabla_\tau\boldsymbol{n}\nabla_\tau u)\cdot\nabla_\tau\phi\,\mathrm{d}s\\
&= \int_\Gamma \mathrm{div}_\tau\left(H(\boldsymbol{\theta}\cdot\boldsymbol{n})\nabla_\tau u - 2(\boldsymbol{\theta}\cdot\boldsymbol{n})(\nabla_\tau\boldsymbol{n})\nabla_\tau u\right)\phi\,\mathrm{d}s.
\end{aligned}$$

□

Remark 23 *We can also simplify the proof of Lemma 4.3.3 supposing $\boldsymbol{\theta} = (\boldsymbol{\theta}\cdot\boldsymbol{n})\boldsymbol{n}$ (since we need this identity to compute the shape derivative and we can justify this assumption by the structure theorem). In this case,*

$$\begin{aligned}
&-\int_\Gamma (\mathrm{div}_\tau(\boldsymbol{\theta})\mathrm{I} - \nabla_\tau\boldsymbol{\theta} - \nabla_\tau\boldsymbol{\theta}^t)\nabla_\tau u\cdot\nabla_\tau\phi + \nabla_\tau(\boldsymbol{\theta}\cdot\nabla_\tau u)\cdot\nabla_\tau\phi - \Delta_\tau u(\boldsymbol{\theta}\cdot\nabla_\tau\phi)\,\mathrm{d}s\\
&= -\int_\Gamma (\mathrm{div}_\tau(\boldsymbol{\theta})\mathrm{I} - \nabla_\tau\boldsymbol{\theta} - \nabla_\tau\boldsymbol{\theta}^t)\nabla_\tau u\cdot\nabla_\tau\phi)\,\mathrm{d}s.
\end{aligned}$$

Integrating by parts on Γ,

$$-\int_\Gamma \mathrm{div}_\tau(\boldsymbol{\theta})\nabla_\tau u\cdot\nabla_\tau\phi\,\mathrm{d}s = -\int_\Gamma H(\nabla_\tau u\cdot\nabla_\tau\phi)(\boldsymbol{\theta}\cdot\boldsymbol{n})\,\mathrm{d}s,$$

and

$$\int_\Gamma (\nabla_\tau\boldsymbol{\theta} + \nabla_\tau\boldsymbol{\theta}^t)\nabla_\tau u\cdot\nabla_\tau\phi\,\mathrm{d}s = 2\int_\Gamma ((\nabla_\tau\boldsymbol{n}\nabla_\tau u)\cdot\nabla_\tau\phi)\,(\boldsymbol{\theta}\cdot\boldsymbol{n})\,\mathrm{d}s,$$

lead to the desired result.

Proposition 4.3.4. *Let d_{Ω_1} be the signed distance function to the domain Ω_1. We define $\boldsymbol{n} = \nabla d_{\Omega_1}$ and $H = \Delta d_{\Omega_1}$ the extension of the unit normal to Ω_1 and mean curvature of $\partial\Omega_1$. If $\partial\Omega_1$ is $\mathcal{C}^3$, then*

$$\frac{\partial H}{\partial\boldsymbol{n}} = -\|\nabla\boldsymbol{n}\|_F^2.$$

Proof. It is known that $\boldsymbol{n} = \nabla d_{\Omega_1}$ is an extension of the unit normal to $\partial\Omega_1$, unitary in a neighborhood of $\partial\Omega_1$ (see, e.g., [53, Theorem 8.5]):

$$\|\boldsymbol{n}\|^2 = \|\nabla d_{\Omega_1}\|^2 = 1 \text{ in a neighborhood of } \partial\Omega_1.$$

Differentiating this identity, in particular we get

$$\Delta(\|\boldsymbol{n}\|^2) = 0 \text{ on } \partial\Omega_1,$$

and using the identity $\Delta(\boldsymbol{u}\cdot\boldsymbol{v}) = \mathrm{I}\Delta\boldsymbol{u}\cdot\boldsymbol{v} + \mathrm{I}\Delta\boldsymbol{v}\cdot\boldsymbol{u} + 2\nabla\boldsymbol{u} : \nabla\boldsymbol{v}$ with $\boldsymbol{u} = \boldsymbol{v} = \boldsymbol{n}$, we obtain:

$$2I\Delta\boldsymbol{n}\cdot\boldsymbol{n} + 2\|\nabla\boldsymbol{n}\|_F^2 = 0.$$

□

Proposition 4.3.5 (Shape derivative of the temperature)**.** *For each $i = 1, 2$, there exists an extension $\tilde{\mathsf{T}}_{\boldsymbol{\theta},i} \in \mathrm{H}^1(\Omega)$ of $\mathsf{T}_{\boldsymbol{\theta},i}$ such that application $\boldsymbol{\theta} \in \Theta_{\mathrm{ad}} \to \tilde{\mathsf{T}}_{\boldsymbol{\theta},i} \in \mathrm{L}^2(\Omega)$ is $\mathcal{C}^1$ at 0 and the derivative, denoted T_i', is called shape derivative of T_i.*

Moreover, if in addition $\mathsf{T} \in \mathrm{H}^2(\Omega_1,\Gamma)\times\mathrm{H}^2(\Omega_2,\Gamma)$ and $\boldsymbol{u}_i \in \mathrm{H}^2(\Omega_i)^d$, then the shape derivative $\mathsf{T}' = (\mathsf{T}_1', \mathsf{T}_2') \in \mathcal{H}_0(\Omega_1,\Omega_2)$ is characterized by,

$$\left\{\begin{array}{rcl} -\operatorname{div}(\kappa_i\nabla\mathsf{T}_i') + \boldsymbol{u}_i\cdot\nabla\mathsf{T}_i' &=& -\boldsymbol{u}_i'\cdot\nabla\mathsf{T}_i \quad \text{in } \Omega_i, i=1,2,\\ \mathsf{T}_i' &=& 0 \quad \text{on } \Gamma_{\mathrm{D},i}, i=1,2,\\ \kappa_i\dfrac{\partial\mathsf{T}_i'}{\partial\boldsymbol{N}} &=& 0 \quad \text{on } \Gamma_{\mathrm{N},i}\cup\Gamma_{\mathrm{e},i}, i=1,2,\\ \left\langle\kappa\dfrac{\partial\mathsf{T}'}{\partial\boldsymbol{n}}\right\rangle &=& -\dfrac{\kappa_s}{\eta}[\mathsf{T}'] + \xi_1(\mathsf{T},\boldsymbol{\theta}\cdot\boldsymbol{n}) \quad \text{on } \Gamma,\\ \left[\kappa\dfrac{\partial\mathsf{T}'}{\partial\boldsymbol{n}}\right] &=& \eta\operatorname{div}_\tau(\kappa_s\nabla_\tau\langle\mathsf{T}'\rangle) - \kappa_s H[\mathsf{T}'] + \xi_2(\mathsf{T},\boldsymbol{\theta}\cdot\boldsymbol{n}) \quad \text{on } \Gamma,\\ \dfrac{\partial\langle\mathsf{T}'\rangle}{\partial\boldsymbol{N}} &=& 0 \quad \text{on } \partial\Gamma, \end{array}\right. \tag{4.23}$$

with

$$\xi_1(\mathsf{T},\boldsymbol{\theta}\cdot\boldsymbol{n}) = \operatorname{div}_\tau((\boldsymbol{\theta}\cdot\boldsymbol{n})\langle\kappa\nabla_\tau\mathsf{T}\rangle) - \frac{\kappa_s}{\eta}\left(H[\mathsf{T}] + \left[\frac{\partial\mathsf{T}}{\partial\boldsymbol{n}}\right]\right)(\boldsymbol{\theta}\cdot\boldsymbol{n}),$$

$$\begin{aligned}\xi_2(\mathsf{T},\boldsymbol{\theta}\cdot\boldsymbol{n}) = \operatorname{div}_\tau((\boldsymbol{\theta}\cdot\boldsymbol{n})[\kappa\nabla_\tau\mathsf{T}]) - \kappa_s\left(H^2[\mathsf{T}] + H\left[\frac{\partial\mathsf{T}}{\partial\boldsymbol{n}}\right] + \frac{\partial H}{\partial\boldsymbol{n}}[\mathsf{T}]\right)(\boldsymbol{\theta}\cdot\boldsymbol{n}) + \kappa_s[\mathsf{T}]\Delta_\tau(\boldsymbol{\theta}\cdot\boldsymbol{n})\\ + \eta\kappa_s\operatorname{div}_\tau(H(\boldsymbol{\theta}\cdot\boldsymbol{n})\nabla_\tau\langle\mathsf{T}\rangle - 2(\boldsymbol{\theta}\cdot\boldsymbol{n})(\nabla_\tau\boldsymbol{n})\nabla_\tau\langle\mathsf{T}\rangle) + \eta\kappa_s\Delta_\tau\left((\boldsymbol{\theta}\cdot\boldsymbol{n})\left\langle\frac{\partial\mathsf{T}}{\partial\boldsymbol{n}}\right\rangle\right).\end{aligned}$$

Proof. Let us introduce two linear continuous extensions $E_i : \mathrm{H}^1(\Omega_i) \mapsto \mathrm{H}^1(\Omega)$, $i = 1, 2$. We define $\tilde{\mathsf{T}}_{\boldsymbol{\theta},i} = E_i(\overline{\mathsf{T}}_{\boldsymbol{\theta},i})\circ(\boldsymbol{I}+\boldsymbol{\theta})^{-1} \in \mathrm{H}^1(\Omega)$ and since $\boldsymbol{\theta} \in \Theta_{\mathrm{ad}} \mapsto \overline{T}_{\boldsymbol{\theta},i} \in \mathrm{H}^1(\Omega_i)$ is $\mathcal{C}^1$ in a neighborhood of 0, by chain rule, we get that $\boldsymbol{\theta} \in \Theta_{\mathrm{ad}} \mapsto E_i(\overline{T}_{\boldsymbol{\theta},i}) \in \mathrm{H}^1(\Omega)$ is $\mathcal{C}^1$ in a neighborhood of 0. By using [72, Lemma 5.3.3], we deduce that $\boldsymbol{\theta} \in \Theta_{\mathrm{ad}} \mapsto E_i(\overline{\mathsf{T}}_{\boldsymbol{\theta},i})\circ(\boldsymbol{I}+\boldsymbol{\theta})^{-1} \in \mathrm{L}^2(\Omega)$ is $\mathcal{C}^1$ in a neighborhood of 0.

If in addition, T_i is $\mathrm{H}^2(\Omega_i,\Gamma)$, then using the relationship between the material and the shape derivative $\mathsf{T}_i' = \dot{\mathsf{T}}_i - \nabla\mathsf{T}_i\cdot\boldsymbol{\theta}, i = 1, 2$ and $\langle\mathsf{T}\rangle' = \langle\dot{\mathsf{T}}\rangle - \nabla\langle\mathsf{T}\rangle\cdot\boldsymbol{\theta}$, yield that T' belongs to $\mathcal{H}_0(\Omega_1,\Omega_2)$. Similarly for the velocity, we have that $\boldsymbol{u}_i' = \dot{\boldsymbol{u}}_i - (\nabla\boldsymbol{u}_i)\boldsymbol{\theta}$, $i = 1, 2$. Then, for any $\phi \in \mathcal{H}_0(\Omega_1,\Omega_2)$,

$$\begin{aligned}\sum_{i=1}^{2}\int_{\Omega_i}(\kappa_i\nabla\mathsf{T}_i'\cdot\nabla\phi_i + (\boldsymbol{u}_i\cdot\nabla\mathsf{T}_i' + \boldsymbol{u}_i'\cdot\nabla\mathsf{T}_i)\,\phi_i)\,\mathrm{d}x\\ + \int_\Gamma\left(\eta\kappa_s\nabla_\tau\langle\mathsf{T}'\rangle\cdot\nabla_\tau\langle\phi\rangle + \kappa_s H[\mathsf{T}']\langle\phi\rangle + \frac{\kappa_s}{\eta}[\mathsf{T}'][\phi]\right)\mathrm{d}s = I_1+I_2+I_3+I_4,\end{aligned}$$

where

$$
\begin{aligned}
I_1 &= \sum_{i=1}^{2} \int_{\Omega_i} \kappa_i \left(\nabla\boldsymbol{\theta} - \operatorname{div}(\boldsymbol{\theta})\nabla\mathsf{T}_i - (\nabla^2\mathsf{T}_i)\boldsymbol{\theta}\right)\cdot\nabla\phi_i \\
&\qquad - \left(\operatorname{div}(\boldsymbol{\theta})\boldsymbol{u}_i\cdot\nabla\mathsf{T}_i + (\nabla^2\mathsf{T}_i)\boldsymbol{u}_i\cdot\boldsymbol{\theta} + (\nabla\boldsymbol{u}_i)\boldsymbol{\theta}\cdot\nabla\mathsf{T}_i\right)\phi_i \,\mathrm{d}x, \\
I_2 &= -\frac{\kappa_s}{\eta}\int_\Gamma \operatorname{div}_\tau(\boldsymbol{\theta})[\mathsf{T}][\phi] + \boldsymbol{\theta}\cdot[\nabla\mathsf{T}][\phi]\,\mathrm{d}s, \\
I_3 &= -\kappa_s\int_\Gamma \left(H\operatorname{div}_\tau(\boldsymbol{\theta})[\mathsf{T}]\langle\phi\rangle - \Delta_\tau(\boldsymbol{\theta}\cdot\boldsymbol{n})[\mathsf{T}]\langle\phi\rangle + (\nabla H\cdot\boldsymbol{\theta})[\mathsf{T}]\langle\phi\rangle + H[\nabla\mathsf{T}]\cdot\boldsymbol{\theta}\langle\phi\rangle\right)\mathrm{d}s, \\
I_4 &= \eta\kappa_s\int_\Gamma \left((\nabla_\tau\boldsymbol{\theta} + \nabla_\tau\boldsymbol{\theta}^t - \operatorname{div}_\tau(\boldsymbol{\theta})\mathrm{I})\nabla_\tau\langle\mathsf{T}\rangle\right)\cdot\nabla_\tau\langle\phi\rangle - \nabla_\tau\left(\nabla\langle\mathsf{T}\rangle\cdot\boldsymbol{\theta}\right)\cdot\nabla_\tau\langle\phi\rangle\Big)\,\mathrm{d}s.
\end{aligned}
$$

Let us first focus on I_1. Using the identity

$$
\operatorname{div}((\boldsymbol{\theta}\cdot\nabla\phi_i)\nabla\mathsf{T}_i - (\nabla\mathsf{T}_i\cdot\nabla\phi_i)\boldsymbol{\theta}) = (\boldsymbol{\theta}\cdot\nabla\phi_i)\Delta\mathsf{T}_i + (\nabla\boldsymbol{\theta})\nabla\mathsf{T}_i\cdot\nabla\phi_i - \operatorname{div}(\boldsymbol{\theta})\nabla\mathsf{T}_i\cdot\nabla\phi_i - \boldsymbol{\theta}\cdot(\nabla^2\mathsf{T}_i)\nabla\phi_i
$$

and that the solution of the convection-diffusion equation (4.2) satisfies $\kappa_i\Delta\mathsf{T}_i = \nabla\mathsf{T}_i\cdot\boldsymbol{u}_i$ in Ω_i, we obtain

$$
\begin{aligned}
I_1 &= \sum_{i=1}^{2}\int_{\Omega_i}\Big(\kappa_i\operatorname{div}\left((\boldsymbol{\theta}\cdot\nabla\phi_i)\nabla\mathsf{T}_i - (\nabla\mathsf{T}_i\cdot\nabla\phi_i)\boldsymbol{\theta}\right) - \boldsymbol{u}_i\cdot\nabla\mathsf{T}_i(\boldsymbol{\theta}\cdot\nabla\phi_i) \\
&\qquad - \left(\operatorname{div}(\boldsymbol{\theta})\boldsymbol{u}_i\cdot\nabla\mathsf{T}_i + (\nabla^2\mathsf{T}_i)\boldsymbol{u}_i\cdot\boldsymbol{\theta} + (\nabla\boldsymbol{u}_i)\boldsymbol{\theta}\cdot\nabla\mathsf{T}_i\right)\phi_i\Big)\,\mathrm{d}x \\
&= \sum_{i=1}^{2}\int_{\Omega_i}\left(\kappa_i\operatorname{div}((\boldsymbol{\theta}\cdot\nabla\phi_i)\nabla\mathsf{T}_i - (\nabla\mathsf{T}_i\cdot\nabla\phi_i)\boldsymbol{\theta}) - \operatorname{div}(\phi_i(\nabla\mathsf{T}_i\cdot\boldsymbol{u}_i)\boldsymbol{\theta})\right)\mathrm{d}x.
\end{aligned}
$$

Then, by the divergence theorem, we get

$$
I_1 = \int_\Gamma\left(\left[\kappa\frac{\partial\mathsf{T}}{\partial\boldsymbol{n}}(\boldsymbol{\theta}\cdot\nabla\phi) - \kappa(\nabla\mathsf{T}\cdot\nabla\phi)(\boldsymbol{\theta}\cdot\boldsymbol{n})\right] - \left[\phi(\nabla\mathsf{T}\cdot\boldsymbol{u})\right](\boldsymbol{\theta}\cdot\boldsymbol{n})\right)\mathrm{d}s,
$$

and using that $\boldsymbol{u}_i = 0$ on Γ and the gradient decomposition $\nabla\phi = \nabla_\tau\phi + \frac{\partial\phi}{\partial\boldsymbol{n}}\boldsymbol{n}$,

$$
I_1 = \int_\Gamma\left[\kappa\frac{\partial\mathsf{T}}{\partial\boldsymbol{n}}(\boldsymbol{\theta}\cdot\nabla_\tau\phi) - (\boldsymbol{\theta}\cdot\boldsymbol{n})\kappa\nabla_\tau\mathsf{T}\cdot\nabla_\tau\phi\right]\mathrm{d}s.
$$

Moreover, integrating by parts on Γ and using the identity $[ab] = [a]\langle b\rangle + \langle a\rangle[b]$, we have

$$
\begin{aligned}
\int_\Gamma[\kappa\nabla_\tau\mathsf{T}\cdot\nabla_\tau\phi](\boldsymbol{\theta}\cdot\boldsymbol{n})\,\mathrm{d}s &= -\int_\Gamma\left[\operatorname{div}_\tau\left((\boldsymbol{\theta}\cdot\boldsymbol{n})\kappa\nabla_\tau\mathsf{T}\right)\phi\right]\mathrm{d}s \\
&= -\int_\Gamma\left(\operatorname{div}_\tau((\boldsymbol{\theta}\cdot\boldsymbol{n})\langle\kappa\nabla_\tau\mathsf{T}\rangle)[\phi] + \operatorname{div}_\tau((\boldsymbol{\theta}\cdot\boldsymbol{n})[\kappa\nabla_\tau\mathsf{T}]\langle\phi\rangle)\right)\mathrm{d}s.
\end{aligned}
$$

Thus, integrating by parts appropriately on Γ and using the boundary conditions

$$
\left\langle\kappa\frac{\partial\mathsf{T}}{\partial\boldsymbol{n}}\right\rangle = -\frac{\kappa_s}{\eta}[\mathsf{T}] \text{ and } \left[\kappa\frac{\partial\mathsf{T}}{\partial\boldsymbol{n}}\right] = \eta\kappa_s\Delta_\tau\langle\mathsf{T}\rangle - \kappa_s H[\mathsf{T}] \text{ on } \Gamma,
$$

we treat the first term

$$\begin{aligned}
I_1 &= \int_\Gamma \left(\left[\kappa \frac{\partial \mathsf{T}}{\partial \boldsymbol{n}} \right] \boldsymbol{\theta} \cdot \nabla_\tau \langle \phi \rangle + \left\langle \kappa \frac{\partial \mathsf{T}}{\partial \boldsymbol{n}} \right\rangle \boldsymbol{\theta} \cdot \nabla_\tau [\phi] \right) \mathrm{d}s \\
&\quad + \int_\Gamma \left(\mathrm{div}_\tau((\boldsymbol{\theta} \cdot \boldsymbol{n}) \langle \kappa \nabla_\tau \mathsf{T} \rangle)[\phi] + \mathrm{div}_\tau((\boldsymbol{\theta} \cdot \boldsymbol{n})[\kappa \nabla_\tau \mathsf{T}]) \langle \phi \rangle \right) \mathrm{d}s \\
&= \int_\Gamma \left((\eta \kappa_s \nabla_\tau \langle \mathsf{T} \rangle - \kappa_s H[\mathsf{T}]) \nabla_\tau \langle \phi \rangle \cdot \theta - \frac{\kappa_s}{\eta} \nabla_\tau [\phi] \cdot \theta \right) \mathrm{d}s \\
&\quad + \int_\Gamma \left(\mathrm{div}_\tau((\boldsymbol{\theta} \cdot \boldsymbol{n}) \langle \kappa \nabla_\tau \mathsf{T} \rangle)[\phi] + \mathrm{div}_\tau((\boldsymbol{\theta} \cdot \boldsymbol{n})[\kappa \nabla_\tau \mathsf{T}]) \langle \phi \rangle \right) \mathrm{d}s \\
&= \int_\Gamma \left(\mathrm{div}_\tau(\kappa_s H[\mathsf{T}]\boldsymbol{\theta}) \langle \phi \rangle - \kappa_s H^2[\mathsf{T}](\boldsymbol{\theta} \cdot \boldsymbol{n}) \langle \phi \rangle + \frac{\kappa_s}{\eta} \mathrm{div}_\tau([\mathsf{T}]\boldsymbol{\theta})[\phi] - \frac{\kappa_s}{\eta} H[\mathsf{T}](\boldsymbol{\theta} \cdot \boldsymbol{n})[\phi] \right) \mathrm{d}s \\
&\quad + \int_\Gamma \left(\mathrm{div}_\tau((\boldsymbol{\theta} \cdot \boldsymbol{n}) \langle \kappa \nabla_\tau \mathsf{T} \rangle)[\phi] + \mathrm{div}_\tau((\boldsymbol{\theta} \cdot \boldsymbol{n})[\kappa \nabla_\tau \mathsf{T}]) \langle \phi \rangle + \eta \kappa_s \Delta_\tau \langle \mathsf{T} \rangle \nabla_\tau \langle \phi \rangle \cdot \boldsymbol{\theta} \right) \mathrm{d}s.
\end{aligned}$$

For I_2 and I_3, we decompose the gradient, which yields to

$$\begin{aligned}
I_2 &= -\frac{\kappa_s}{\eta} \int_\Gamma \left(\mathrm{div}_\tau(\boldsymbol{\theta})[\mathsf{T}][\phi] + (\boldsymbol{\theta} \cdot \boldsymbol{n}) \left[\frac{\partial \mathsf{T}}{\partial \boldsymbol{n}} \right] [\phi] + (\boldsymbol{\theta} \cdot [\nabla_\tau \mathsf{T}])[\phi] \right) \mathrm{d}s \\
&= -\frac{\kappa_s}{\eta} \int_\Gamma \left(\mathrm{div}_\tau([\mathsf{T}]\boldsymbol{\theta})[\phi] + \frac{\partial \mathsf{T}}{\partial \boldsymbol{n}} (\boldsymbol{\theta} \cdot \boldsymbol{n}) \right) \mathrm{d}s
\end{aligned}$$

and

$$\begin{aligned}
I_3 &= -\kappa_s \int_\Gamma \left(H \, \mathrm{div}_\tau(\boldsymbol{\theta})[\mathsf{T}] \langle \phi \rangle + H \boldsymbol{\theta} \cdot [\nabla_\tau \mathsf{T}] \langle \phi \rangle + H (\boldsymbol{\theta} \cdot \boldsymbol{n}) \left[\frac{\partial \mathsf{T}}{\partial \boldsymbol{n}} \right] \langle \phi \rangle \right. \\
&\qquad \left. + \left(-\Delta_\tau (\boldsymbol{\theta} \cdot \boldsymbol{n}) + \frac{\partial H}{\partial \boldsymbol{n}} (\boldsymbol{\theta} \cdot \boldsymbol{n}) + \boldsymbol{\theta} \cdot \nabla_\tau H \right) [\mathsf{T}] \langle \phi \rangle \right) \mathrm{d}s \\
&= -\kappa_s \int_\Gamma \left(H \, \mathrm{div}_\tau([\mathsf{T}]\boldsymbol{\theta}) + H \left[\frac{\partial \mathsf{T}}{\partial \boldsymbol{n}} \right] (\boldsymbol{\theta} \cdot \boldsymbol{n}) - \Delta_\tau (\boldsymbol{\theta} \cdot \boldsymbol{n})[\mathsf{T}] \right. \\
&\qquad \left. + \frac{\partial H}{\partial \boldsymbol{n}} (\boldsymbol{\theta} \cdot \boldsymbol{n})[\mathsf{T}] + \boldsymbol{\theta} \cdot \nabla_\tau H [\mathsf{T}] \right) \langle \phi \rangle \, \mathrm{d}s \\
&= -\kappa_s \int_\Gamma \left(\mathrm{div}_\tau(H[\mathsf{T}]\boldsymbol{\theta}) + H \left[\frac{\partial \mathsf{T}}{\partial \boldsymbol{n}} \right] (\boldsymbol{\theta} \cdot \boldsymbol{n}) - \Delta_\tau (\boldsymbol{\theta} \cdot \boldsymbol{n})[\mathsf{T}] + \frac{\partial H}{\partial \boldsymbol{n}} (\boldsymbol{\theta} \cdot \boldsymbol{n})[\mathsf{T}] \right) \langle \phi \rangle \, \mathrm{d}s.
\end{aligned}$$

Finally, for I_4, thanks to Lemma 4.3.3, we have

$$\begin{aligned}
I_4 &= \eta \kappa_s \int_\Gamma \left(\left(\nabla_\tau \boldsymbol{\theta} + \nabla_\tau \boldsymbol{\theta}^t - \mathrm{div}_\tau(\boldsymbol{\theta}) \mathrm{I} \right) \nabla_\tau \langle \mathsf{T} \rangle - \nabla_\tau \left(\boldsymbol{\theta} \cdot \nabla_\tau \langle \mathsf{T} \rangle \right) \right) \cdot \nabla_\tau \langle \phi \rangle \right) \mathrm{d}s \\
&\quad - \eta \kappa_s \int_\Gamma \nabla_\tau \left((\boldsymbol{\theta} \cdot \boldsymbol{n}) \left\langle \frac{\partial \mathsf{T}}{\partial \boldsymbol{n}} \right\rangle \right) \cdot \nabla_\tau \langle \phi \rangle \, \mathrm{d}s \\
&= \eta \kappa_s \int_\Gamma \left(\mathrm{div}_\tau \left(H(\boldsymbol{\theta} \cdot \boldsymbol{n}) \nabla_\tau \langle \mathsf{T} \rangle - 2(\boldsymbol{\theta} \cdot \boldsymbol{n})(\nabla_\tau \boldsymbol{n}) \nabla_\tau \langle \mathsf{T} \rangle \right) \langle \phi \rangle - \Delta_\tau \langle \mathsf{T} \rangle (\boldsymbol{\theta} \cdot \nabla_\tau \langle \phi \rangle) \right) \mathrm{d}s \\
&\quad - \eta \kappa_s \int_\Gamma \nabla_\tau \left((\boldsymbol{\theta} \cdot \boldsymbol{n}) \left\langle \frac{\partial \mathsf{T}}{\partial \boldsymbol{n}} \right\rangle \right) \cdot \nabla_\tau \langle \phi \rangle \, \mathrm{d}s \\
&= \eta \kappa_s \int_\Gamma \left(\mathrm{div}_\tau \left(H(\boldsymbol{\theta} \cdot \boldsymbol{n}) \nabla_\tau \langle \mathsf{T} \rangle - 2(\boldsymbol{\theta} \cdot \boldsymbol{n})(\nabla_\tau \boldsymbol{n}) \nabla_\tau \langle \mathsf{T} \rangle \right) \langle \phi \rangle - \Delta_\tau \langle \mathsf{T} \rangle (\boldsymbol{\theta} \cdot \nabla_\tau \langle \phi \rangle) \right) \mathrm{d}s \\
&\quad + \eta \kappa_s \int_\Gamma \Delta_\tau \left((\boldsymbol{\theta} \cdot \boldsymbol{n}) \left\langle \frac{\partial \mathsf{T}}{\partial \boldsymbol{n}} \right\rangle \right) \langle \phi \rangle \, \mathrm{d}s.
\end{aligned}$$

We conclude by adding I_1, I_2, I_3 and I_4. □

4.3.3 Shape derivative of the objective functionals

We first recall the definition of the notion of shape derivative of a shape functional in our context.

Definition 4.3.6. *The shape derivative of a function $J(\Gamma)$ is defined as the Fréchet derivative at 0 of the map $\boldsymbol{\theta} \in \Theta_{\mathrm{ad}} \to J(\Gamma^{\boldsymbol{\theta}}) \in \mathbb{R}$. It is denoted by $J'(\Gamma)$ and it is given by*

$$J(\Gamma^{\boldsymbol{\theta}}) = J(\Gamma) + J'(\Gamma)(\boldsymbol{\theta}) + o(\boldsymbol{\theta}), \qquad \textit{with } \lim_{\boldsymbol{\theta}\to 0} \frac{o(\boldsymbol{\theta})}{\|\boldsymbol{\theta}\|_{\mathrm{W}^{2,\infty}(\Omega)^d}} = 0.$$

The objective of this section is to obtain the shape derivatives of the functionals involved in the optimization problem (4.6) on which we focus on, that is the negative heat exchanged (4.3) denoted W, the energy dissipation in the fluids (4.4) denoted D_i, and the volume V.

First of all, it is well-known that the shape derivative of volume V is given, for all $\boldsymbol{\theta} \in \Theta_{\mathrm{ad}}$ by

$$V'(\Gamma)(\boldsymbol{\theta}) = \int_\Gamma \boldsymbol{\theta} \cdot \boldsymbol{n} \, \mathrm{d}s. \tag{4.24}$$

Moreover, we obtain the expression of the shape derivative of the dissipated energy (4.4) using Proposition 4.3.1 and the chain rule (see also [20, 73, 37] for details). In the following, to simplify the writing, we define the region sign s_i as

$$s_i = \begin{cases} 1 & \text{if} \quad i = 1, \\ -1 & \text{if} \quad i = 2. \end{cases}$$

Proposition 4.3.7 (Shape derivative of the dissipation energy)**.** *Let $\boldsymbol{\theta} \in \Theta_{\mathrm{ad}}$ and, for $i = 1, 2$, let $(\boldsymbol{v}_i, q_i) \in \mathcal{V}_0(\Omega_i) \times \mathrm{L}^2(\Omega_i)$ be the solution of the following adjoint equation of the Navier-Stokes equations associated to the dissipation energy:*

$$\left\{ \begin{array}{rll} -\nu_i \Delta \boldsymbol{v}_i + (\nabla \boldsymbol{u}_i)^t \boldsymbol{v}_i - (\nabla \boldsymbol{v}_i)\boldsymbol{u}_i + \nabla q_i &= -2\nu_i \Delta \boldsymbol{u}_i & \textit{in } \Omega_i, \\ \mathrm{div}(\boldsymbol{v}_i) &= 0 & \textit{in } \Omega_i, \\ \boldsymbol{v}_i &= 0 & \textit{on } \Gamma_{\mathrm{D},\mathrm{i}} \cup \Gamma_{\mathrm{e},i} \cup \Gamma, \\ \sigma(\boldsymbol{v}_i, q_i)\boldsymbol{N} + (\boldsymbol{u}_i \cdot \boldsymbol{N})\boldsymbol{v}_i &= 4\nu\varepsilon(\boldsymbol{u}_i)\boldsymbol{N} & \textit{on } \Gamma_{\mathrm{N},i}. \end{array} \right. , \tag{4.25}$$

If $(\boldsymbol{u}_i, p_i), (\boldsymbol{v}_i, q_i) \in \mathrm{H}^2(\Omega_i)^d \times \mathrm{H}^1(\Omega_i)$, then the shape derivative of the dissipation energy is given by

$$D_i'(\Gamma)(\boldsymbol{\theta}) = 2\nu_i \int_\Gamma s_i (\varepsilon(\boldsymbol{u}_i) : \varepsilon(\boldsymbol{v}_i) - |\varepsilon(\boldsymbol{u}_i)|^2)(\boldsymbol{\theta} \cdot \boldsymbol{n}) \, \mathrm{d}s. \tag{4.26}$$

Finally, we state and prove the new result concerning the shape derivative of the negative heat exchanged $W(\Gamma)$ given in (4.3). We define the two following mappings $f_i \in (\mathrm{H}^1(\Omega_i))'$ and $\boldsymbol{g}_i \in (\mathrm{H}^1(\Omega_i)^d)'$, given by:

$$\begin{aligned} \langle f_i, \mathsf{S} \rangle_{(\mathrm{H}^1(\Omega_i))', \mathrm{H}^1(\Omega_i)} &= \int_{\Omega_i} s_i \boldsymbol{u}_i \cdot \nabla \mathsf{S} \, \mathrm{d}x, \quad \forall \mathsf{S} \in \mathrm{H}^1(\Omega_i), \\ \langle \boldsymbol{g}_i, \boldsymbol{w} \rangle_{(\mathrm{H}^1(\Omega_i)^d)', \mathrm{H}^1(\Omega_i)^d} &= \int_{\Omega_i} s_i \boldsymbol{w} \cdot \nabla \mathsf{T}_i \, \mathrm{d}x, \quad \forall \boldsymbol{w} \in \mathrm{H}^1(\Omega_i)^d, \end{aligned}$$

where $\boldsymbol{u}_i$ and T_i are the respective solution of (4.1) and (4.2).

Proposition 4.3.8 (Shape derivative of the exchanged heat)**.** *Let $\boldsymbol{\theta} \in \Theta_{\rm ad}$ and let introduce $\mathsf{R} = (\mathsf{R}_1, \mathsf{R}_2) \in \mathcal{H}_0(\Omega_1, \Omega_2)$ the adjoint of the approximate convection-diffusion equation* (4.1) *associated to the heat exchanged:*

$$\left\{\begin{array}{rcl} -\operatorname{div}(\kappa_i \nabla \mathsf{R}_i + \mathsf{R}_i \boldsymbol{u}_i) &=& f_i \text{ in } \Omega_i, i = 1,2, \\ \mathsf{R}_i &=& 0 \text{ on } \Gamma_{\mathrm{D},i}, i = 1,2, \\ \kappa_i \dfrac{\partial \mathsf{R}_i}{\partial \boldsymbol{N}} &=& 0 \text{ on } \Gamma_{\mathrm{N,i}} \cup \Gamma_{\mathrm{e,i}}, i = 1,2, \\ \left\langle \kappa \dfrac{\partial \mathsf{R}}{\partial \boldsymbol{n}} \right\rangle &=& -\dfrac{\kappa_s}{\eta}[\mathsf{R}] - \kappa_s H \langle \mathsf{R} \rangle \text{ on } \Gamma, \\ \left[\kappa \dfrac{\partial \mathsf{R}}{\partial \boldsymbol{n}} \right] &=& \eta \operatorname{div}_\tau(\kappa_s \nabla_\tau \langle \mathsf{R} \rangle) \text{ on } \Gamma, \\ \dfrac{\partial \langle \mathsf{R} \rangle}{\partial \boldsymbol{N}} &=& 0 \text{ on } \partial\Gamma, \end{array}\right. \tag{4.27}$$

and $(\boldsymbol{v}_i, q_i) \in \mathcal{V}_0(\Omega_i) \times \mathrm{L}^2(\Omega_i)$ the adjoint of the Navier-Stokes equations (4.1) *associated to the heat exchanged:*

$$\left\{\begin{array}{rll} -\nu_i \Delta \boldsymbol{v}_i + (\nabla \boldsymbol{u}_i)^t \boldsymbol{v}_i - (\nabla \boldsymbol{v}_i)\boldsymbol{u}_i + \nabla q_i &= -\mathsf{R}_i \nabla \mathsf{T}_i + \boldsymbol{g}_i & \text{in } \Omega_i, \\ \operatorname{div}(\boldsymbol{v}_i) &= 0 & \text{in } \Omega_i, \\ \boldsymbol{v}_i &= 0 & \text{on } \Gamma_{\mathrm{D,i}} \cup \Gamma \cup \Gamma_{\mathrm{e,i}}, \\ \sigma(\boldsymbol{v}_i, q_i)\boldsymbol{N} &= 0 & \text{on } \Gamma_{\mathrm{N,i}}, \end{array}\right. \tag{4.28}$$

for each $i = 1, 2$.

The heat exchanged W defined in (4.3) *is shape differentiable.*
Furthermore, if $\mathsf{T} = (\mathsf{T}_1, \mathsf{T}_2) \in \mathrm{H}^2(\Omega_1, \Gamma) \times \mathrm{H}^2(\Omega_2, \Gamma)$, $\mathsf{R} = (\mathsf{R}_1, \mathsf{R}_2) \in \mathrm{H}^2(\Omega_1, \Gamma) \times \mathrm{H}^2(\Omega_2, \Gamma)$ and $(\boldsymbol{u}_i, p_i), (\boldsymbol{v}_i, q_i) \in \mathrm{H}^2(\Omega_i)^d \times \mathrm{H}^1(\Omega_i)$, then the shape derivative $W'(\Gamma)(\boldsymbol{\theta})$ can be expressed in the following surface shape derivative form:

$$\begin{aligned} W'(\Gamma)(\boldsymbol{\theta}) = \int_\Gamma \left(2[\nu \varepsilon(\boldsymbol{u}) : \varepsilon(\boldsymbol{v})] - [\kappa \nabla \mathsf{T} \cdot \nabla \mathsf{R}] + 2 \left[\kappa \frac{\partial \mathsf{T}}{\partial \boldsymbol{n}} \frac{\partial \mathsf{R}}{\partial \boldsymbol{n}} \right] \right) (\boldsymbol{\theta} \cdot \boldsymbol{n}) \, \mathrm{d}s \\ - \int_\Gamma \left(\eta \kappa_s (H \mathrm{I} - 2 \nabla_\tau \boldsymbol{n}) \nabla_\tau \langle \mathsf{T} \rangle \cdot \nabla_\tau \langle \mathsf{R} \rangle + \frac{\kappa_s}{\eta} H [\mathsf{T}][\mathsf{R}] \right) (\boldsymbol{\theta} \cdot \boldsymbol{n}) \, \mathrm{d}s \\ - \kappa_s \int_\Gamma \left(H^2 [\mathsf{T}] \langle \mathsf{R} \rangle - \Delta_\tau ([\mathsf{T}] \langle \mathsf{R} \rangle) + \frac{\partial H}{\partial \boldsymbol{n}} [\mathsf{T}] \langle \mathsf{R} \rangle \right) (\boldsymbol{\theta} \cdot \boldsymbol{n}) \, \mathrm{d}s. \end{aligned} \tag{4.29}$$

Remark 24 *Both adjoint equations* (4.27) *and* (4.28) *are well-posed. The adjoint of the approximated convection-diffusion equation is well-posed by Lax-Milgram, analogously to* (4.2) *(see [36]). The equation* (4.25) *is a linearization of the Navier-Stokes (transposed) and the proof is an adaptation of the Navier-Stokes case (see [68, Chapter IV] or [34] for details).*

Proof. *Step 1: differentiability.* The crucial point is the differentiability in a neighborhood of 0, of $\boldsymbol{\theta} \in \Theta_{\rm ad} \mapsto \overline{\mathsf{T}}_{\boldsymbol{\theta}} \in \mathcal{H}^1(\Omega_1, \Omega_2)$ and $\boldsymbol{\theta} \in \Theta_{\rm ad} \mapsto \overline{u}_{\boldsymbol{\theta},i} \in \mathrm{H}^1(\Omega_i)^d, i = 1, 2$. The first one was proved in Proposition 4.3.2 and the second one in [34]. Then, recalling that

$$W(\Gamma^{\boldsymbol{\theta}}) = \sum_{i=1}^{2} \int_{\Omega_i^{\boldsymbol{\theta}}} s_i \boldsymbol{u}_{\boldsymbol{\theta},i} \cdot \nabla \mathsf{T}_{\boldsymbol{\theta},i} \, \mathrm{d}x,$$

and doing a change of variables (similarly to the proof of Proposition 4.3.2), we obtain

$$W(\Gamma^{\boldsymbol{\theta}}) = \sum_{i=1}^{2} \int_{\Omega_i} s_i (\mathrm{I} + \nabla \boldsymbol{\theta})^{-1} \overline{\boldsymbol{u}}_{\boldsymbol{\theta},i} \cdot \nabla \overline{\mathsf{T}}_{\boldsymbol{\theta},i} |\det(\mathrm{I} + \nabla \boldsymbol{\theta})| \, \mathrm{d}x \tag{4.30}$$

Using the chain rule (the differentiability of the other terms is classical, though it was discussed in the proof of Proposition 4.3.2), we conclude that W is shape differentiable.

Step 2: shape derivative computation. Since $\boldsymbol{u}_i \in \mathrm{H}^2(\Omega_i)^d$ and $\mathsf{T}_i \in \mathrm{H}^2(\Omega_i)$, $i = 1, 2$, then thanks to Proposition 4.3.5, $\boldsymbol{u}_i' \in \mathrm{H}^1(\Omega_i)^d$ and $\mathsf{T}_i' \in \mathrm{H}^1(\Omega_i, \Gamma)$. Differentiating (4.3), using the classical formulas of shape derivatives of integral functionals and by chain rule,

$$W'(\Gamma)(\boldsymbol{\theta}) = \sum_{i=1}^{2} \int_{\Omega_i} s_i \left(\boldsymbol{u}_i \cdot \nabla \mathsf{T}_i' + \boldsymbol{u}_i' \cdot \nabla \mathsf{T}_i \right) \mathrm{d}x + \sum_{i=1}^{2} \int_{\Gamma} s_i (\boldsymbol{u}_i \cdot \nabla \mathsf{T}_i)(\boldsymbol{\theta} \cdot \boldsymbol{n}_i) \, \mathrm{d}s,$$

where $\boldsymbol{n}_i$ is the unitary normal at Γ, exterior to Ω_i. Using that $\boldsymbol{u}_i = 0$ on Γ, we obtain:

$$W'(\Gamma)(\boldsymbol{\theta}) = \sum_{i=1}^{2} \int_{\Omega_i} s_i \left(\boldsymbol{u}_i \cdot \nabla \mathsf{T}_i' + \boldsymbol{u}_i' \cdot \nabla \mathsf{T}_i \right) \mathrm{d}x. \tag{4.31}$$

Then, we proceed as it is standard, this is, we multiply each equation of the shape derivative of the states by its respective adjoint, and then we integrate by parts using the boundary conditions that satisfy each solution. Conversely, we multiply the adjoint equation by the corresponding shape derivative and then we integrate. Hence, multiplying (4.23) by R, (4.12) by $\boldsymbol{v}_i$, (4.27) by T', (4.28) by $\boldsymbol{u}_i'$ and integrating in Ω (or Ω_i in the Navier-Stokes case), we get

$$\begin{aligned} \sum_{i=1}^{2} \int_{\Omega_i} (\kappa_i \nabla \mathsf{T}_i' \cdot \nabla \mathsf{R}_i + \mathsf{R}_i \boldsymbol{u}_i \cdot \nabla \mathsf{T}_i' + \mathsf{R}_i \boldsymbol{u}_i' \cdot \nabla \mathsf{T}_i) \, \mathrm{d}x \\ + \int_{\Gamma} \left(\eta \kappa_s \nabla_\tau \langle \mathsf{T}' \rangle \cdot \nabla_\tau \langle \mathsf{R} \rangle + \kappa_s H [\mathsf{T}'] \langle \mathsf{R} \rangle + \frac{\kappa_s}{\eta} [\mathsf{T}'][\mathsf{R}] \right) \mathrm{d}s \\ = \int_{\Gamma} (\xi_1(\mathsf{T}, \boldsymbol{\theta} \cdot \boldsymbol{n})[\mathsf{R}] + \xi_2(\mathsf{T}, \boldsymbol{\theta} \cdot \boldsymbol{n}) \langle \mathsf{R} \rangle) \, \mathrm{d}s, \end{aligned} \tag{4.32}$$

$$\int_{\Omega_i} (2\nu_i \varepsilon(\boldsymbol{u}_i') : \varepsilon(\boldsymbol{v}_i) + (\nabla \boldsymbol{u}_i') \boldsymbol{u}_i \cdot \boldsymbol{v}_i + (\nabla \boldsymbol{u}_i) \boldsymbol{u}_i' \cdot \boldsymbol{v}_i - q_i \operatorname{div}(\boldsymbol{u}_i') - p_i' \operatorname{div}(\boldsymbol{v}_i)) \, \mathrm{d}x = 0, \tag{4.33}$$

$$\begin{aligned} \sum_{i=1}^{2} \int_{\Omega_i} (\kappa_i \nabla \mathsf{R}_i \cdot \nabla \mathsf{T}_i' + \mathsf{R}_i \boldsymbol{u}_i \cdot \nabla \mathsf{T}_i') \, \mathrm{d}x \\ + \int_{\Gamma} \left(\eta \kappa_s \nabla_\tau \langle \mathsf{R} \rangle \cdot \nabla_\tau \langle \mathsf{T}' \rangle + \kappa_s H [\mathsf{R}] \langle \mathsf{T}' \rangle + \frac{\kappa_s}{\eta} [\mathsf{R}][\mathsf{T}'] \right) \mathrm{d}s = \sum_{i=} \int_{\Omega_i} s_i \nabla \mathsf{T}_i' \cdot \boldsymbol{u}_i \, \mathrm{d}x, \end{aligned} \tag{4.34}$$

and

$$\begin{aligned} \int_{\Omega_i} (2\nu_i \varepsilon(\boldsymbol{v}_i) : \varepsilon(\boldsymbol{u}_i') + (\nabla \boldsymbol{u}_i') \boldsymbol{u}_i \cdot \boldsymbol{v}_i + (\nabla \boldsymbol{u}_i) \boldsymbol{u}_i' - q_i \operatorname{div}(\boldsymbol{u}_i') - p_i' \operatorname{div}(\boldsymbol{v}_i)) \, \mathrm{d}x \\ + \int_{\Omega_i} \mathsf{R}_i \nabla \mathsf{T}_i \cdot \boldsymbol{u}_i' \, \mathrm{d}x + \int_{\Gamma} s_i \sigma(\boldsymbol{v}_i, q_i) \boldsymbol{n} \cdot \frac{\partial \boldsymbol{u}_i}{\partial \boldsymbol{n}} (\boldsymbol{\theta} \cdot \boldsymbol{n}) \, \mathrm{d}s = \sum_{i=1}^{2} \int_{\Omega_i} s_i \nabla \mathsf{T}_i \cdot \boldsymbol{u}_i' \, \mathrm{d}x. \end{aligned} \tag{4.35}$$

Using the above identities in (4.31), we obtain

$$W'(\Gamma)(\boldsymbol{\theta}) = \int_\Gamma \left([\sigma(\boldsymbol{v},q)\boldsymbol{n} \cdot \frac{\partial \boldsymbol{u}}{\partial \boldsymbol{n}}(\boldsymbol{\theta}\cdot\boldsymbol{n})] + \xi_1(\mathsf{T},\boldsymbol{\theta}\cdot\boldsymbol{n})[\mathsf{R}] + \xi_2(\mathsf{T},\boldsymbol{\theta}\cdot\boldsymbol{n})\langle \mathsf{R}\rangle \right) \mathrm{d}s.$$

Integrating by parts and using that $\left[\sigma(\boldsymbol{v},q)\boldsymbol{n} \cdot \frac{\partial \boldsymbol{u}}{\partial \boldsymbol{n}}(\boldsymbol{\theta}\cdot\boldsymbol{n})\right] = 2[\varepsilon(\boldsymbol{u}) : \varepsilon(\boldsymbol{v})]$, we get

$$W'(\Gamma)(\boldsymbol{\theta}) \;=\; \int_\Gamma f\,(\boldsymbol{\theta}\cdot\boldsymbol{n})\,\mathrm{d}s,$$

where

$$\begin{aligned} f = 2[\nu\varepsilon(\boldsymbol{u}) : \varepsilon(\boldsymbol{v})] - [\kappa\nabla_\tau \mathsf{T}\cdot\nabla_\tau \mathsf{R}] - \eta\kappa_s(H\mathrm{I} - 2\nabla_\tau \boldsymbol{n})\nabla_\tau\langle \mathsf{T}\rangle\cdot\nabla_\tau\langle \mathsf{R}\rangle + \frac{\kappa_s}{\eta}H[\mathsf{T}][\mathsf{R}] \\ - \kappa_s\left(H^2[\mathsf{T}]\langle \mathsf{R}\rangle - \Delta_\tau([\mathsf{T}]\langle \mathsf{R}\rangle) + \frac{\partial H}{\partial \boldsymbol{n}}[\mathsf{T}]\langle \mathsf{R}\rangle\right) + \eta\kappa_s\Delta_\tau(\langle \mathsf{R}\rangle)\left\langle \frac{\partial \mathsf{T}}{\partial \boldsymbol{n}}\right\rangle \\ - \frac{\kappa_s}{\eta}[\mathsf{R}]\left[\frac{\partial \mathsf{T}}{\partial \boldsymbol{n}}\right] - \kappa_s H\langle \mathsf{R}\rangle\left[\frac{\partial \mathsf{T}}{\partial \boldsymbol{n}}\right]. \end{aligned}$$

Since R is the solution of the adjoint of the convection-diffusion equation (4.28),

$$\eta\kappa_s\Delta_\tau(\langle \mathsf{R}\rangle)\left\langle \frac{\partial \mathsf{T}}{\partial \boldsymbol{n}}\right\rangle - \frac{\kappa_s}{\eta}[\mathsf{R}]\left[\frac{\partial \mathsf{T}}{\partial \boldsymbol{n}}\right] - \kappa_s H\langle \mathsf{R}\rangle\left[\frac{\partial \mathsf{T}}{\partial \boldsymbol{n}}\right] = \left[\kappa\frac{\partial \mathsf{R}}{\partial \boldsymbol{n}}\frac{\partial \mathsf{T}}{\partial \boldsymbol{n}}\right],$$

leading to the same expression as in (4.29). □

4.4 Numerical methods used to solve the involved problems

This section is devoted to the details of the numerical implementation used to perform the simulations to solve the shape optimization problem (4.6). All the equations involved are solved in parallel by means of FreeFem++ [71] and PETSc [17, 18], up to the non-standard equations (4.2) and (4.27) which involve the discretization of the Sobolev Broken Spaces and are then solved with an optimized sequential version in C++. Throughout this section we will detail this. We begin by giving details of the general method used to solve the PDEs involved. Particular attention is paid to the numerical solution of the non-classical convection-diffusion equation (4.2) and the adjoint equation (4.27). We conclude by explaining the framework of the optimization process and the computations of the shape derivatives of the functionals involved.

4.4.1 Nitsche extended finite element method of the Ventcel transmission problem with discontinuities at the interface

In this part we will explain which method we use to discretize the approximate convection-diffusion (4.2) and the adjoint equation (4.27) since they are not the standard FEM. Besides the discontinuous nature, the factor $\frac{1}{\eta}$ in these equations can lead to poor conditioning of the linear systems and then slow resolution. For all these reasons, we solve these equations directly using the Nitsche method we have introduced in our previous work [30]. The main advantages are the efficiency and the robustness with respect to the small parameter η. The main ideas of this method are outlined below.

On the convection-diffusion problem (4.2)**.** For the sake of simplicity, in this part, we assume T_{D} to be a $\mathbb{P}^1$ function. In the case of the variational formulation (4.9) of the convection-diffusion problem (4.2), we decompose the associated bilinear form, denoted by $a(\cdot,\cdot)$, as $a(\cdot,\cdot) = b(\cdot,\cdot) + c(\cdot,\cdot)$, where

$$\begin{aligned} b(\phi,\mathsf{S}) &= \sum_{i=1}^{2}\int_{\Omega_i}(\kappa_i\nabla\phi_i\cdot\nabla\mathsf{S}_i + \mathsf{S}_i\boldsymbol{u}_i\cdot\nabla\phi_i)\,\mathrm{d}x + \int_{\Gamma}(\eta\kappa_{\mathrm{s}}\nabla_\tau\langle\phi\rangle\cdot\nabla_\tau\langle\mathsf{S}\rangle + \kappa_{\mathrm{s}}H[\phi]\langle\mathsf{S}\rangle)\,\mathrm{d}s,\\ c(\phi,\mathsf{S}) &= \frac{\kappa_{\mathrm{s}}}{\eta}\int_{\Gamma}[\phi][\mathsf{S}]\,\mathrm{d}s, \end{aligned}$$

defined for any $\phi,\mathsf{S}\in\mathcal{H}^1(\Omega_1,\Omega_2)$. As mentioned previously, the term $c(\cdot,\cdot)$ produces poor conditioning when η is small. To deal with this, we consider the Nitsche approach previously used in [30] to stabilize our matrix with respect to η, improving the conditioning of the matrix. We now introduce some notations and briefly explain this method: we refer to [30] for details.

Let $\mathcal{T}_h$ be a regular simplicial mesh of Ω. Let $\mathcal{F}_h$ be the set of faces of $\mathcal{T}_h$ and $\mathcal{F}_{h,\Gamma}$ be the set of faces situated on Γ. Let h_F be the diameter of the face $F\in\mathcal{F}_{h,\Gamma}$ and $h>0$ the mesh size. We consider the polynomial spaces

$$\mathrm{P}^1_h = \{\mathsf{S}_h\in\mathcal{C}(\Omega_1)\times\mathcal{C}(\Omega_2);\mathsf{S}_h|_K\in\mathbb{P}^1,\forall K\in\mathcal{T}_h\}\qquad\text{and}\qquad \mathrm{P}^1_{h,0} = \mathrm{P}^1_h\cap\mathcal{H}_0(\Omega_1,\Omega_2). \tag{4.36}$$

Then, we define the following mesh-depending bilinear form, for any $\mathsf{T}_h,\mathsf{S}_h\in\mathrm{P}^1_h$,

$$a_h(\mathsf{T}_h,\mathsf{S}_h) = a(\mathsf{T}_h,\mathsf{S}_h) - \sum_{F\in\mathcal{F}_{h,\Gamma}}\frac{\gamma\eta h_F}{\eta+\gamma\kappa_{\mathrm{s}}h_F}\left(\left\langle\kappa\frac{\partial\mathsf{T}_h}{\partial\boldsymbol{n}}\right\rangle + \frac{\kappa_{\mathrm{s}}}{\eta}[\mathsf{T}_h],\left\langle\kappa\frac{\partial\mathsf{S}_h}{\partial\boldsymbol{n}}\right\rangle + \frac{\kappa_{\mathrm{s}}}{\eta}[\mathsf{S}_h]\right)_{\mathrm{L}^2(F)}.$$

Hence

$$a_h(\mathsf{T}_h,\mathsf{S}_h) = b(\mathsf{T}_h,\mathsf{S}_h) + c_h(\mathsf{T}_h,\mathsf{S}_h),$$

with

$$\begin{aligned} c_h(\mathsf{T}_h,\mathsf{S}_h) = \sum_{F\in\mathcal{F}_{h,\Gamma}}\int_F &\frac{\kappa_{\mathrm{s}}}{\eta+\gamma\kappa_{\mathrm{s}}h_F}[\mathsf{T}_h][\mathsf{S}_h] - \frac{\gamma\eta h_F}{\eta+\gamma\kappa_{\mathrm{s}}h_F}\left\langle\kappa\frac{\partial\mathsf{T}_h}{\partial\boldsymbol{n}}\right\rangle\left\langle\kappa\frac{\partial\mathsf{S}_h}{\partial\boldsymbol{n}}\right\rangle\\ &- \frac{\gamma\kappa_{\mathrm{s}}h_F}{\eta+\gamma\kappa_{\mathrm{s}}h_F}\left(\left\langle\kappa\frac{\partial\mathsf{T}_h}{\partial\boldsymbol{n}}\right\rangle[\mathsf{S}_h] + \left\langle\kappa\frac{\partial\mathsf{S}_h}{\partial\boldsymbol{n}}\right\rangle[\mathsf{T}_h]\right)\mathrm{d}s, \end{aligned}$$

where $\gamma>0$ is a stabilization parameter, that it is small enough in order to guarantee the coercivity of $a_h(\cdot,\cdot)$. Note that in the decomposition of the new bilinear form $a_h(\cdot,\cdot)$, the bilinear form $b(\cdot,\cdot)$ continues to appear; what changes is the bilinear form $c_h(\cdot,\cdot)$ instead of $c(\cdot,\cdot)$, whose associated matrix has better conditioning due to the stabilization term. Then we consider the following Nitsche problem to approximate the equation (4.2):

$$\left\{\begin{array}{c} \textit{Find } \mathsf{T}_h\in\mathrm{P}^1_h \textit{ with } \mathsf{T}_h=\mathsf{T}_{\mathrm{D}} \textit{ on } \Gamma_{\mathrm{D}},\ \textit{such that}\\ a_h(\mathsf{T}_h,\mathsf{S}_h)=0,\quad\forall\mathsf{S}_h\in\mathrm{P}^1_{h,0}. \end{array}\right. \tag{4.37}$$

This problem approximates the continuous solution $\mathsf{T}\in\mathcal{H}_{\mathsf{T}_{\mathrm{D}}}(\Omega_1,\Omega_2)$ of the convection-diffusion equation (4.2) in the energy sense as it is stated in the next result (the proof is a mere adaptation of [30, Theorem 4.6]).

Theorem 4.4.1 (Error estimate in energy norm) Let $\mathsf{T} \in \mathcal{H}_{\mathsf{T}_\mathrm{D}}(\Omega_1,\Omega_2)$ the solution of the continuous convection-diffusion equation (4.2) and T_h the solution of the (discrete) Nitsche problem (4.37). If in addition $\mathsf{T} \in \mathcal{H}^2(\Omega_1,\Omega_2)$, then for γ sufficiently small, there exists a constant $C>0$ independent of h and η such that:

$$|||\mathsf{T}-\mathsf{T}_h|||_h \leq Ch\left(\sum_{i=1}^{2}\|\kappa_i^{1/2}(\mathsf{T}_i-\mathsf{T}_{\mathrm{D,i}})\|^2_{\mathrm{H}^2(\Omega_i)} + \|(\kappa_s\eta)^{1/2}\langle\mathsf{T}\rangle\|^2_{\mathrm{H}^2(\Gamma)} + \sum_{F\in\mathcal{F}_{h,\Gamma}}\frac{\kappa_s}{\gamma h_F}\|[\mathsf{T}]\|^2_{\mathrm{H}^1(F)}\right)^{1/2},$$

where the mesh-dependent norm on P^1_h is defined by

$$|||\cdot|||_h = \left(\sum_{i=1}^{2}\|\kappa_i^{1/2}\nabla\cdot\|^2_{\mathrm{L}^2(\Omega_i)^d} + \|(\kappa_s\eta)^{1/2}\nabla_\tau\langle\cdot\rangle\|^2_{\mathrm{L}^2(\Gamma)^d} + \sum_{F\in\mathcal{F}_{h,\Gamma}}\frac{\kappa_s}{\eta+\gamma\kappa_s h_F}\|[\cdot]\|^2_{\mathrm{L}^2(F)}\right)^{1/2}.$$

On the adjoint problem (4.27)**.** We proceed in a similar way concerning the adjoint equation (4.27). Let $\mathsf{R},\mathsf{S}\in\mathcal{H}_0(\Omega_1,\Omega_2)$. We denote

$$\begin{aligned}\tilde{b}(\mathsf{R},\mathsf{S}) &= \sum_{i=1}^{2}\int_{\Omega_i}(\kappa_i\nabla\mathsf{R}_i\cdot\nabla\mathsf{S}_i + \mathsf{R}_i\boldsymbol{u}_i\cdot\nabla\mathsf{S}_i)\,\mathrm{d}x + \int_\Gamma\eta\kappa_\mathrm{s}\nabla_\tau\langle\mathsf{R}\rangle\cdot\nabla_\tau\langle\mathsf{S}\rangle + \kappa_\mathrm{s}H\langle\mathsf{R}\rangle[\mathsf{S}]\,\mathrm{d}s,\\ \tilde{c}(\mathsf{R},\mathsf{S}) &= \int_\Gamma\frac{\kappa_\mathrm{s}}{\eta}[\mathsf{R}][\mathsf{S}]\,\mathrm{d}s\end{aligned}$$

in such a way that the associated bilinear form writes $\tilde{a}(\mathsf{R},\mathsf{S}) = \tilde{b}(\mathsf{R},\mathsf{S}) + \tilde{c}(\mathsf{R},\mathsf{S})$ is the bilinear form associated to the adjoint problem (4.27) with the right-hand side given by:

$$\tilde{\ell}(\mathsf{S}) = \sum_{i=1}^{2}\int_{\Omega_i} s_i\boldsymbol{u}_i\cdot\nabla\mathsf{S}_i\,\mathrm{d}x$$

As previously, the matrix associated to the term $\tilde{c}$ has poor conditioning and, to stabilize it, we define for any P^1_h

$$\begin{aligned}\tilde{a}_h(\mathsf{R},\mathsf{S}) &= \tilde{a}(\mathsf{R},\mathsf{S})\\ &\quad - \sum_{F\in\mathcal{F}_{h,\Gamma}}\frac{\gamma\eta h_F}{\eta+\gamma\kappa_\mathrm{s}h_F}\left(\left\langle\kappa\frac{\partial\mathsf{R}}{\partial\boldsymbol{n}}\right\rangle + \frac{\kappa_\mathrm{s}}{\eta}[\mathsf{R}] + \kappa_\mathrm{s}H\langle\mathsf{R}\rangle, \left\langle\kappa\frac{\partial\mathsf{S}}{\partial\boldsymbol{n}}\right\rangle + \frac{\kappa_\mathrm{s}}{\eta}[\mathsf{S}] + \kappa_\mathrm{s}H\langle\mathsf{S}\rangle\right)_{\mathrm{L}^2(F)}.\end{aligned}$$

Therefore, we obtain $\tilde{a}_h(\mathsf{R},\mathsf{S}) = \tilde{b}(\mathsf{R},\mathsf{S}) + c_h(\mathsf{R},\mathsf{S}) - d_h(\mathsf{R},\mathsf{S})$, where

$$\begin{aligned}d_h(\mathsf{R},\mathsf{S}) = \sum_{F\in\mathcal{F}_{h,\Gamma}}\frac{\gamma\kappa_\mathrm{s}\eta h_F}{\eta+\gamma\kappa_\mathrm{s}h_F}\int_F H\langle\mathsf{S}\rangle\left(\left\langle\kappa\frac{\partial\mathsf{R}}{\partial\boldsymbol{n}}\right\rangle + \frac{\kappa_\mathrm{s}}{\eta}[\mathsf{R}]\right)\\ + H\langle\mathsf{R}\rangle\left(\left\langle\kappa\frac{\partial\mathsf{S}}{\partial\boldsymbol{n}}\right\rangle + \frac{\kappa_\mathrm{s}}{\eta}[\mathsf{S}]\right) + \kappa_\mathrm{s}H^2\langle\mathsf{R}\rangle\langle\mathsf{S}\rangle\,\mathrm{d}s.\end{aligned}$$

The Nitsche problem considered to approximate the adjoint equation (4.27) is then:

$$\left\{\begin{array}{c}\textit{Find } \mathsf{R}_h\in\mathrm{P}^1_{h,0} \textit{ such that}\\ \tilde{a}_h(\mathsf{R}_h,\mathsf{S}_h) = \tilde{l}(\mathsf{S}_h),\quad \forall\mathsf{S}_h\in\mathrm{P}^1_{h,0}.\end{array}\right. \tag{4.38}$$

The error estimates is similar to the one given in Theorem 4.4.1.

4.4.2 Numerical resolution of PDEs

The numerical resolution of the PDEs (4.1), (4.28), (4.37), (4.38) (and also of the problem (4.40) below) are very expensive when solved by direct solvers as LU in 3D, in particular with respect to memory storage. In our case, since the size of the matrix of the linear systems considered is too large, we will use iterative methods. The more classical ones are the conjugate gradient in the symmetric definite positive case and the Generalized Minimal Residual Method (GMRES) in a general case. Notice that these methods are not enough to solve the linear system since they tend to stagnate. This is why they are used together with a preconditioner (as the Jacobi preconditioner) to speed up the convergence. We underline that the Portable, Extensible Toolkit for Scientific Computation (PETSc) provides a large number of iterative solvers (Krylov methods) and preconditioners in a highly flexible way: we have chosen it for our numerical resolutions and give details below.

Moreover, in parallel computing, the most powerful methods add the mesh information to the preconditioner, with strategies such as domain decomposition (Additive Schwarz Method), multigrid (HYPRE) and component-wise decomposition of vector-valued problems (fieldsplit). Notice that these kind of methods cannot be directly used in the resolution of the non-classical transmission problems (4.37) and (4.38) that we consider (such an adaptation does not fall within the scope of this thesis).

On the one hand, we rely on FreeFem++ for the finite elements discretization of the classical equations (4.1), (4.28) and (4.40) and, once discretized, we use PETSc as linear algebra library to solve the linear (or nonlinear) systems. In the case of the Riesz equation (4.40), we use HYPRE as a preconditionner. Concerning the Navier-Stokes equations (4.1), we rely on the augmented Lagrangian preconditionner proposed by [87]: this is to penalize the divergence and use a Newton iteration method with a fieldsplit structure (which in some way allows to separate the equations of velocity and pressure). We proceed similarly for the adjoint equation (4.28), but of course without a Newton iteration method since the equation is linear.

On the other hand, concerning the non-standard convection-diffusion equations (4.37) and (4.38), we implemented the resolution in C++ with PETSc.
As mentioned, we have not yet implemented a fully parallel version using domain decomposition. For the moment, in sequential, we assemble a distributed memory matrix to be able to solve the linear system in parallel by means of SuperLU_DIST [84].

4.4.3 Numerical shape optimization framework

Level set method. In our shape optimization context, we use the so-called level set evolution method, introduced by Allaire *et al.* in [10]. The domain Ω is fixed, we describe each subdomain Ω_i by means of a level set function $\phi : \Omega \to \mathbb{R}$ to track the interface Γ that we aim to optimize. Then, the mesh on Ω is done based on the level-set ϕ, identifying Γ to the zero level set of ϕ:

$$\begin{cases} x \in \Omega_1 & \Longleftrightarrow & \phi(x) < 0 \\ x \in \Gamma & \Longleftrightarrow & \phi(x) = 0 \\ x \in \Omega_2 & \Longleftrightarrow & \phi(x) > 0. \end{cases}$$

In particular this allows us to track the interface Γ that we aim to optimize. Then, the mesh is done following the level set function, which implies that there is no cut element on Γ. After initialization, at the step n of the shape optimization process, we compute the level set ϕ^n by solving the following equation:

$$\begin{cases} \dfrac{\partial \phi^n}{\partial t} + \boldsymbol{\theta} \cdot \nabla \phi^n = 0, & 0 < t < \tau,\ x \in \Omega, \\ \phi^n(0,x) = \phi^{n-1}(x), & x \in \Omega, \end{cases} \tag{4.39}$$

for some $\tau > 0$, where $\boldsymbol{\theta}$ is an appropriate velocity field described below. Numerically speaking, the equation (4.39) is computed by ADVECT [29] and the remeshing step by MMG [47]). The velocity field $\boldsymbol{\theta}$ that we use is obtained by solving the following extension-regularization problem:
find $\boldsymbol{\theta} \in \Theta_{\text{er}} := \{\boldsymbol{\psi} \in \mathrm{H}^1(\Omega)^d;\ \boldsymbol{\psi} = 0 \text{ on } \partial\Omega;\ \boldsymbol{\psi} = 0 \text{ in } \Omega^\delta_{\mathrm{D},1} \cup \Omega^\delta_{\mathrm{D},2}\}$, such that for all $\boldsymbol{\psi} \in \Theta_{\text{er}}$,

$$\int_\Omega 100h^2 \nabla\boldsymbol{\theta} : \nabla\boldsymbol{\psi} + \boldsymbol{\theta} \cdot \boldsymbol{\psi} \,\mathrm{d}x = J'(\Gamma)(\boldsymbol{\psi}), \tag{4.40}$$

where h is the mesh size and $J(\Gamma)$ is a linear combination between the functionals involved in the problem: $W(\Gamma), D_1(\Gamma), D_2(\Gamma)$ and $V(\Gamma)$, which weights depend on the optimization algorithm used. More specifically, we rely on the null space algorithm [64] that we briefly explain below. It is important to remark, that by construction, $\boldsymbol{\theta}$ is a descent direction.

Null space algorithm. As constrained optimization algorithm, we use the so-called null space algorithm introduced by Feppon *et al.* in [64] under the implementation [61]. The idea is to solve an ordinary differential equation by using the shape gradient, with a kind of gradient flow $\dot{x} = \nabla J(x)$, where $\dot{x}$ will be the deformation field $\boldsymbol{\theta}$. This method first decreases the violation of the constraint in order to be feasible, then minimizes the objective function. It is particularly well suited when we start from shapes that does not satisfy the constraints and when numerous constraints are considered.

Implementation of the shape derivatives. We conclude this part by highlighting some original features and difficulties in computing the shape derivatives involved in the problem under consideration. In particular, we recall how to compute numerically a regularized version of the discretized unit normal and a discretized version of the mean curvature. Finally, there is a term in the shape derivative expressions (4.29) that is delicate to treat: $\frac{\partial H}{\partial \boldsymbol{n}}$ and consequently, we will explain how we deal with it. The issue comes when we use $\mathbb{P}^1$ finite elements as discretization of the signed distance function d_{Ω_1}.

Let us first explain how to compute the extensions of the unit normal and the mean curvature. As we said earlier in (4.13), we have that

$$\boldsymbol{n} = \nabla d_{\Omega_1} \quad \text{and} \quad H = \Delta d_{\Omega_1} \quad \text{on } \Gamma.$$

Numerically, we compute d_{Ω_1} by using MSHDIST [49], discretized as a $\mathbb{P}^1$ function denoted d_h in the following. Then, we follow the work [65] that proposes a variational method to regularize and approximate the mean curvature in the following two steps. Firstly, we solve the following

problem:

$$\begin{cases} \textit{Find } \boldsymbol{g}_h \in (\mathrm{H}^1(\Omega) \cap \mathbb{P}^1)^d \textit{ such that, for all } \boldsymbol{\varphi}_h \in (\mathrm{H}^1(\Omega) \cap \mathbb{P}^1)^d, \\ \displaystyle\int_\Omega \boldsymbol{g}_h \cdot \boldsymbol{\varphi}_h \,\mathrm{d}x = \int_\Omega \nabla d_h \cdot \boldsymbol{\varphi}_h \,\mathrm{d}x. \end{cases}$$

Then, $\boldsymbol{g}_h$ is a regularized version of $\boldsymbol{n}_h = \nabla d_h$, since it is $\mathbb{P}^1$ instead of $\mathbb{P}^0$. Similarly, we compute a discretized version of the mean curvature H to be $\mathbb{P}^1$, denoted by H_h as :

$$\begin{cases} \text{Find } H_h \in \mathrm{H}^1(\Omega) \cap \mathbb{P}^1 \text{ such that, for all } \phi_h \in \mathrm{H}^1(\Omega) \cap \mathbb{P}^1, \\ \displaystyle\int_\Omega \left(10h^2 \nabla H_h \cdot \nabla \phi_h + H_h \phi_h\right) \,\mathrm{d}x = \int_\Omega \mathrm{div}(g_h)\phi_h \,\mathrm{d}x. \end{cases}$$

Finally, instead of computing $\frac{\partial H}{\partial \boldsymbol{n}}$ directly as $\frac{\partial H_h}{\partial \boldsymbol{n}}$, we prefer to use the following identity (for the sake of completeness we detail the proof in the appendix, see Proposition 4.3.4, following for instance [75, 56]):

$$\frac{\partial H}{\partial \boldsymbol{n}} = -\|\nabla \boldsymbol{n}\|_F^2, \tag{4.41}$$

where $\|\cdot\|_F$ denotes the Frobenius norm of a matrix. Hence we use the previous formula with $\boldsymbol{g}_h$ as discretization of $\boldsymbol{n}$.

4.4.4 Summary: brief description of the algorithm used

To summarize the complete shape optimization procedure, we present below each step with the associated computational code or library we use in 1.

Algorithm 1 Level-set mesh evolution method

Require an initial split domain $\Omega_1^0, \Omega_2^0 \subset \Omega$.
for $n = 0, \ldots, n_{\text{maxiter}}$ **do**
  Current subdomains Ω_1^n, Ω_2^n represented by the mesh $\mathcal{T}_{\Omega_i^n} \subset \mathcal{T}_\Omega$, $i = 1, 2$.
  Solve (4.1): the Navier-Stokes equations. ▷ FreeFem++
  Solve (4.25): the adjoint equation of the Navier-Stokes equations associated to the dissipation energy. ▷ FreeFem++
  Solve (4.2): the convection-diffusion equation, using Nitsche method. ▷ C++ in-house code
  Solve (4.27): the adjoint equation of the convection-diffusion equation associated to the heat exchanged, using Nitsche method. ▷ C++ in-house code
  Solve (4.28): the adjoint equation of the Navier-Stokes equations associated to the heat exchanged. ▷ FreeFem++
  Compute the gradients by extension-regularization. ▷ FreeFem++
  Compute the deformation field $\boldsymbol{\theta}$. ▷ Null-space algorithm
  Update the level-set function ϕ^{n+1} by advection. ▷ mshdist and advect
  Remesh thanks to ϕ^{n+1}. ▷ mmg
end for

4.5 Numerical results

In this final section, we present the numerical simulations that we have performed in the three-dimensional case. We will solve the problem (4.6) for two different test cases where we choose $D_{0,i}$, $i = 1, 2$ as k times ($k \in \mathbb{N}^*$) the initial dissipation of the fluid i and V_0 as the initial volume of the hot fluid.

In the following, we consider the box $\Omega = [0,1] \times [0,1] \times [0,1]$. Moreover, we fix some constants $r_1, r_2, y_c, Y_c > 0$ (described below for each case) and we then define

$$\begin{aligned}
\Gamma_{\mathrm{D},1} &= \{(x,y,0) \in \Omega; (x-0.5)^2 + (y-y_c)^2 = r_1^2\},\\
\Gamma_{\mathrm{N},1} &= \{(x,y,1) \in \Omega; (x-0.5)^2 + (y-Y_c)^2 = r_1^2\},\\
\Gamma_{\mathrm{D},2} &= \{(x,0,z) \in \Omega; (x-0.5)^2 + (z-0.5)^2 = r_2^2\},\\
\Gamma_{\mathrm{N},2} &= \{(x,1,z) \in \Omega; (x-0.5)^2 + (z-0.5)^2 = r_2^2\}.
\end{aligned}$$

Additionally, we consider the following inlet velocity

$$\begin{aligned}
\boldsymbol{u}_{\mathrm{D},1}(x,y) &= (0,0,(r_1^2 - (x-0.5)^2 - (y-y_c)^2)/r_1^2),\\
\boldsymbol{u}_{\mathrm{D},2}(x,y) &= (0,(r_2^2 - (x-0.5)^2 - (z-0.5)^2)/r_2^2, 0),
\end{aligned}$$

that follows a parabolic profile, and the inlet temperature $\mathsf{T}_{\mathrm{D},1} = 10$, $\mathsf{T}_{\mathrm{D},2} = 0$. Finally, we use the parameters given in Table 4.1.

κ_1	4×10^{-3}	$m^2 s^{-1}$
κ_2	10^{-3}	$m^2 s^{-1}$
κ_s	10^{-2}	$m^2 s^{-1}$
ν_1	2	$m^2 s^{-1}$
ν_2	10	$m^2 s^{-1}$
η	10^{-2}	

Table 4.1: Values of the physical parameters

We will focus on two typical situations in heat exchangers: crossflow and co-current flow as illustrated in Figure 4.2. The purpose of these simulations is to illustrate our results and prove the feasibility and effectiveness of the proposed method. In this way, we obtain new designs that increase the performance of the initial heat exchanger design while verifying the constraints. We performed medium/large scale numerical simulations, ranging from 100 to 500 thousand vertices and 1 to 2.5 million tetrahedra. The used codes are available in the github repository: `https://github.com/RodrigoZelada/HeatExchanger/`. One node of a cluster with 64 cores was used to perfom the simulations and the execution time of the whole optimization process it took approximately 2 weeks for each test case.

4.5.1 First example: Crossflow cylinder case

The first configuration considered is that of a crossflow, as depicted in Figure 4.2a. In this case, we choose $y_c = Y_c = 0.5$, $r_1 = r_2 = 0.25$ and $D_{0,i}$, $i = 1, 2$ to be 5 times the initial dissipation value

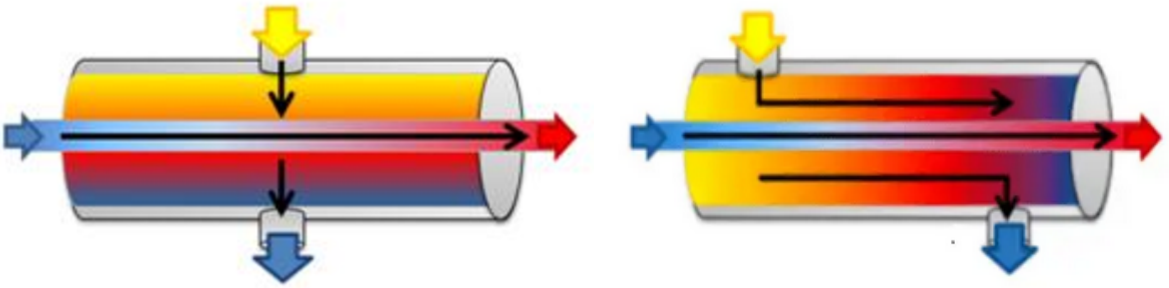

(a) Crossflow configuration. (b) Co-current configuration .

Figure 4.2: Studied configurations (images taken from [99]).

of the respective fluid, which gives in the presented simulation

$$D_{0,1} = 60 \quad D_{0,2} = 25 \text{ and } V_0 = \pi r_1^2 \approx 0.194.$$

It should be noted that the most time-consuming part is the resolution of the Navier-Stokes equations, since the degrees of freedom are about 2 and 4 millions for the cold and hot Navier-Stokes equations, respectively.

The obtained results are shown in Figure 4.3.

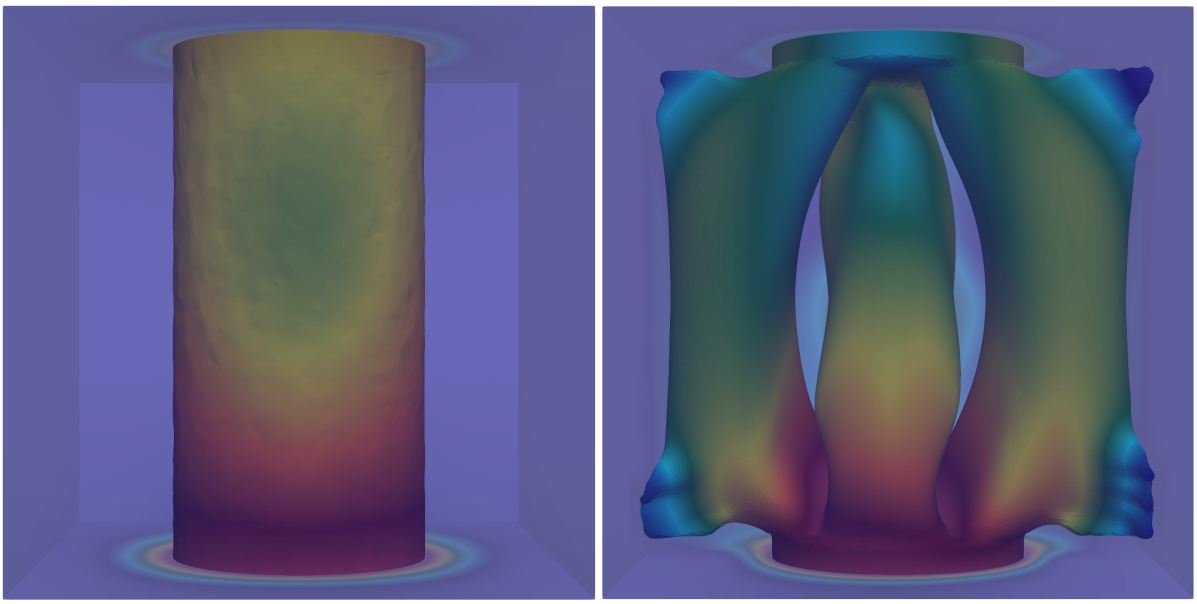

(a) Initial domain Ω. (b) Final domain Ω.

Figure 4.3: Initial and final domain Ω for the first example.

The convergence history for the functionals is depicted on Figure 4.4, where the exchanged heat improved is about 126%.

Remark 25 *We observe that there is a change in the topology. This can be explained by the fact that, since we are considering a co-current flow, the cold fluid has to 'pass through' the thermal*

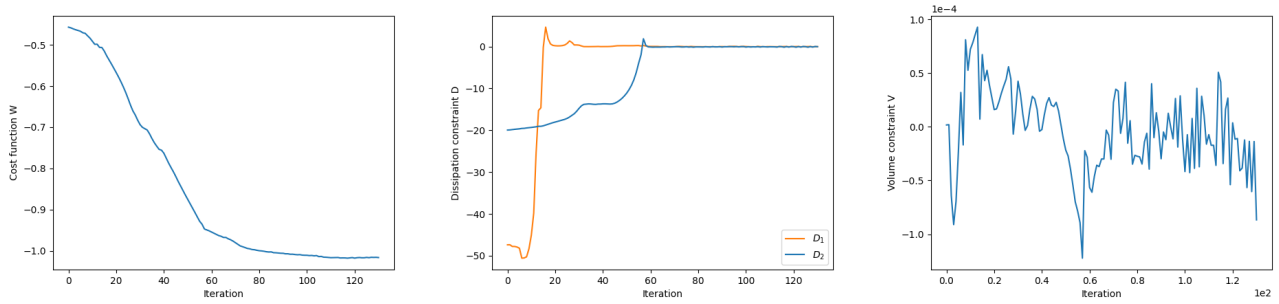

(a) Objective function W. (b) Dissipation constraints D_i. (c) Volume constraint V.

Figure 4.4: Convergence history for the first example.

fluid instead of 'avoiding' it to increase the heat exchanged. In addition, the contact surface has increased, which makes sense because it allows more exchange zones.

4.5.2 Second example: Co-current flow tube case

The second configuration considered is that of a co-current flow, as depicted in Figure 4.2b. In this case, we consider $y_c = 0.25$, $Y_c = 0.75$, $r_1 = 0.1, r_2 = 0.1$ and $D_{0,i}$, $i = 1, 2$ to be 5 times the initial dissipation value of the respective value, which gives in the presented simulations $D_{0,1} = 85$, $D_{0,2} = 5$, and $V_0 \approx 0.0456$. We consider here a more complicated initial configuration and thinner hot domain. Here, the hot and cold Navier-Stokes equations have about $5 \cdot 10^5$ and $1.5 \cdot 10^6$ degrees of freedom, respectively. The obtained results are shown in Figures 4.5 and 4.6. The convergence

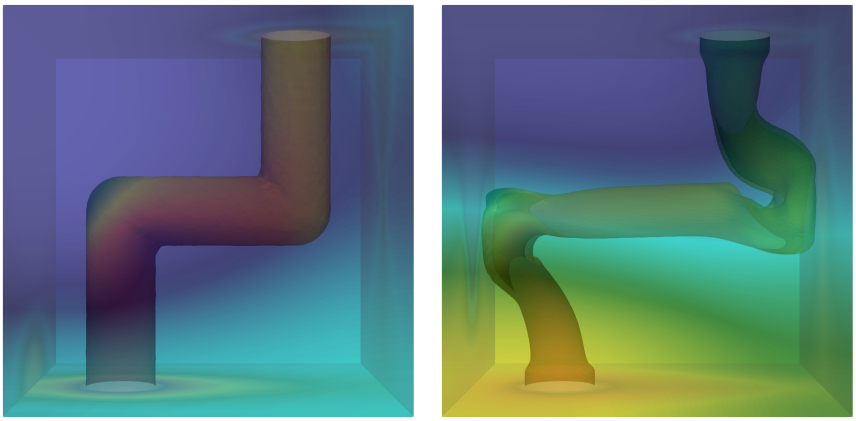

(a) Initial domain Ω. (b) Final domain Ω.

Figure 4.5: Initial and final domain Ω for the second example.

history is depicted on Figure 4.7, where the exchanged heat improved in about 50%.

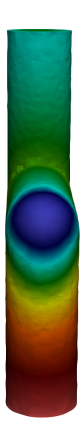

(a) Initial hot temperature T_1.

(b) Initial hot temperature T_1.

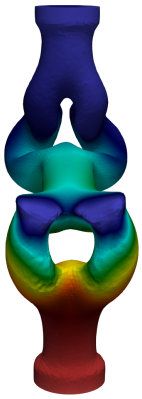

(c) Final hot temperature T_1.

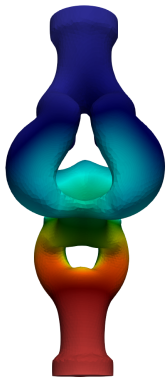

(d) Final hot temperature T_1.

Figure 4.6: Initial and final hot temperature in Ω_1 for the second example.

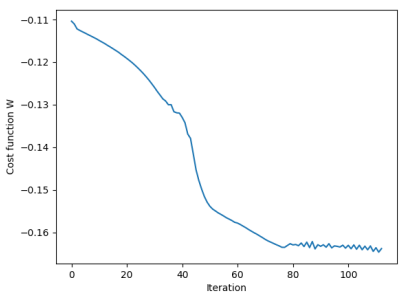

(a) Objective function W.

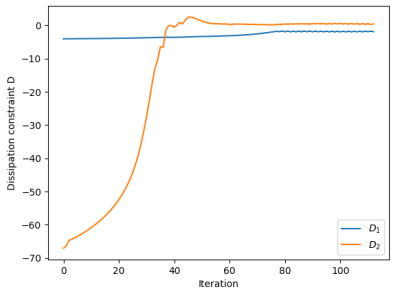

(b) Dissipation constraints D_i.

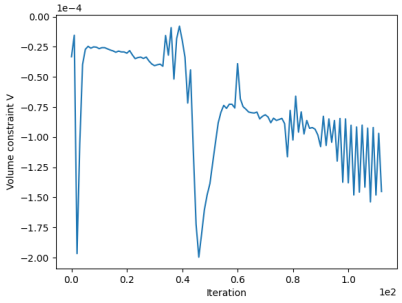

(c) Volume constraint V.

Figure 4.7: Convergence history for the second example.

4.6 Complementary results

In this section we decided to give some additional results for the sake of completness. More specifically, the volume shape derivative of the heat exchanged W and also some formulas for the shape derivatives of a general functional.

4.6.1 Volume shape derivative

Although we have already stated the differentiability and given a formula for the surface shape derivative of the heat exchanged in Proposition 4.3.7, for the sake of completeness, we provide here a formula for the volume shape derivative, which actually requires less assumptions but is less widely used.

Proposition 4.6.1 (Volume shape derivative)**.** *Let $\boldsymbol{\theta} \in \Theta_{\mathrm{ad}}$. The volume shape derivative of the exchanged heat W is given by*

$$
\begin{aligned}
W'(\Gamma)(\boldsymbol{\theta}) \;=\; & \sum_{i=1}^{2} \int_{\Omega_i} s_i \left(\operatorname{div}(\boldsymbol{\theta}) \boldsymbol{u}_i \cdot \nabla \mathsf{T}_i - (\nabla \boldsymbol{\theta}) \boldsymbol{u}_i \cdot \nabla \mathsf{T}_i\right) \mathrm{d}x \\
& - \sum_{i=1}^{2} \int_{\Omega_i} \operatorname{div}(\boldsymbol{\theta}) (\sigma(\boldsymbol{u}_i, p_i) : \nabla \boldsymbol{v}_i + (\nabla \boldsymbol{u}_i) \boldsymbol{u}_i \cdot \boldsymbol{v}_i) \, \mathrm{d}x \\
& + \sum_{i=1}^{2} \int_{\Omega_i} (\sigma(\boldsymbol{u}_i, p_i) : (\nabla \boldsymbol{v}_i \nabla \boldsymbol{\theta}) + \sigma(\boldsymbol{v}_i, q_i) : (\nabla \boldsymbol{u}_i \nabla \boldsymbol{\theta}) + (\nabla \boldsymbol{u}_i \nabla \boldsymbol{\theta}) \boldsymbol{u}_i \cdot \boldsymbol{v}_i) \, \mathrm{d}x \\
& + \sum_{i=1}^{2} \int_{\Omega_i} \left(\kappa_i (\nabla \boldsymbol{\theta} + \nabla \boldsymbol{\theta}^t - \operatorname{div}(\boldsymbol{\theta}) \mathrm{I}) \nabla \mathsf{T}_i \cdot \nabla \mathsf{R}_i + (\nabla \boldsymbol{\theta} - \operatorname{div}(\boldsymbol{\theta}) \mathrm{I}) \mathsf{R}_i \boldsymbol{u}_i \cdot \nabla \mathsf{T}_i\right) \mathrm{d}x \\
& + \eta \kappa_s \int_{\Gamma} (\nabla_\tau \boldsymbol{\theta} + \nabla_\tau \boldsymbol{\theta}^t - \operatorname{div}_\tau(\boldsymbol{\theta}) \mathrm{I}) \nabla_\tau \langle \mathsf{T} \rangle \cdot \nabla_\tau \langle \mathsf{R} \rangle \, \mathrm{d}s \\
& - \kappa_s \int_{\Gamma} (H \operatorname{div}_\tau(\boldsymbol{\theta}) [\mathsf{T}] \langle \mathsf{R} \rangle - \Delta_\tau(\boldsymbol{\theta} \cdot \boldsymbol{n}) [\mathsf{T}] \langle \phi \rangle + \boldsymbol{\theta} \cdot \nabla H [\mathsf{T}] \langle \mathsf{R} \rangle) \, \mathrm{d}s \\
& - \frac{\kappa_s}{\eta} \int_{\Gamma} \operatorname{div}_\tau(\boldsymbol{\theta}) [\mathsf{T}] [\mathsf{R}] \, \mathrm{d}s,
\end{aligned}
\tag{4.42}
$$

where $\mathsf{T} = (\mathsf{T}_1, \mathsf{T}_2) \in \mathcal{H}_{\mathsf{T}_{\mathrm{D}}}(\Omega_1, \Omega_2)$ is the solution of the convection-diffusion equation (4.2)*, $\mathsf{R} = (\mathsf{R}_1, \mathsf{R}_2) \in \mathcal{H}_0(\Omega_1, \Omega_2)$ is the solution of its adjoint equation associated to the heat exchanged* (4.27) *and $(\boldsymbol{u}_i, p_i) \in \mathcal{V}_{\boldsymbol{u}_{\mathrm{D},i}}(\Omega_i) \times \mathrm{L}^2(\Omega_i)$, $(\boldsymbol{v}_i, q_i) \in \mathcal{V}_0(\Omega_i) \times \mathrm{L}^2(\Omega_i)$, $i = 1, 2$, are the respective solutions of the Navier-Stokes equations* (4.1) *and its adjoint associated to the heat exchanged* (4.28)*.*

Proof. From the proof of Proposition 4.3.7, we got the formula (4.30). Differentiating this formula

and by chain rule, yields to:

$$W'(\Gamma)(\boldsymbol{\theta}) = \sum_{i=1}^{2} \int_{\Omega_i} s_i \left(\boldsymbol{u}_i \cdot \nabla \dot{\mathsf{T}}_i + \dot{\boldsymbol{u}}_i \cdot \nabla \mathsf{T}_i \right) \mathrm{d}x.$$
$$+ \sum_{i=1}^{2} \int_{\Omega_i} s_i \left(\operatorname{div}(\boldsymbol{\theta}) \boldsymbol{u}_i \cdot \nabla \mathsf{T}_i - (\nabla \boldsymbol{\theta}) \boldsymbol{u}_i \cdot \nabla \mathsf{T}_i \right) \mathrm{d}x. \quad (4.43)$$

Taking $\phi = \mathsf{R} \in \mathcal{H}_0(\Omega_1, \Omega_2)$ in the material derivative equation associated to the convection-diffusion equation (4.15) and testing with $\phi = \dot{\mathsf{T}} \in \mathcal{H}_0(\Omega_1, \Omega_2)$ in the adjoint of the convection-diffusion equation (4.27), we have respectively

$$\begin{aligned}
&\sum_{i=1}^{2} \int_{\Omega_i} \left(\kappa_i \nabla \dot{\mathsf{T}}_i \cdot \nabla \mathsf{R}_i + \left(\boldsymbol{u}_i \cdot \nabla \dot{\mathsf{T}}_i + \dot{\boldsymbol{u}}_i \cdot \nabla \mathsf{T}_i \right) \mathsf{R}_i \right) \mathrm{d}x \\
&\qquad + \int_{\Gamma} \left(\eta \kappa_s \nabla_\tau \left\langle \dot{\mathsf{T}} \right\rangle \cdot \nabla_\tau \langle \mathsf{R} \rangle + \kappa_s H [\dot{\mathsf{T}}] \langle \mathsf{R} \rangle + \frac{\kappa_s}{\eta} [\dot{\mathsf{T}}][\mathsf{R}] \right) \mathrm{d}s \\
&= \sum_{i=1}^{2} \int_{\Omega_i} \left(\kappa_i \left(\nabla \boldsymbol{\theta} + \nabla \boldsymbol{\theta}^t - \operatorname{div}(\boldsymbol{\theta}) \mathrm{I} \right) \nabla \mathsf{T}_i \cdot \nabla \mathsf{R}_i + \left(\nabla \boldsymbol{\theta} - \operatorname{div}(\boldsymbol{\theta}) \right) \mathsf{R}_i \boldsymbol{u}_i \cdot \nabla \mathsf{T}_i \right) \mathrm{d}x \\
&\qquad + \int_{\Gamma} \eta \kappa_s \left(\left(\nabla_\tau \boldsymbol{\theta} + \nabla_\tau \boldsymbol{\theta}^t - \operatorname{div}_\tau(\boldsymbol{\theta}) \mathrm{I} \right) \nabla_\tau \langle \mathsf{T} \rangle \right) \cdot \nabla_\tau \langle \mathsf{R} \rangle \, \mathrm{d}s \qquad (4.44) \\
&\qquad - \int_{\Gamma} \left(\kappa_s H \operatorname{div}_\tau(\boldsymbol{\theta}) [\mathsf{T}] \langle \mathsf{R} \rangle - \kappa_s \Delta_\tau (\boldsymbol{\theta} \cdot \boldsymbol{n}) [\mathsf{T}] \langle \mathsf{R} \rangle + \kappa_s \nabla H \cdot \theta [\mathsf{T}] \langle \mathsf{R} \rangle \right) \mathrm{d}s \\
&\qquad - \int_{\Gamma} \frac{\kappa_s}{\eta} \operatorname{div}_\tau(\boldsymbol{\theta}) [\mathsf{T}][\mathsf{R}] \, \mathrm{d}s,
\end{aligned}$$

and

$$\begin{aligned}
&\sum_{i=1}^{2} \int_{\Omega_i} \left(\kappa_i \nabla \mathsf{R}_i \cdot \nabla \dot{\mathsf{T}}_i + \mathsf{R}_i \boldsymbol{u}_i \cdot \nabla \dot{\mathsf{T}}_i \right) \mathrm{d}x \\
&\qquad + \int_{\Gamma} \left(\eta \kappa_s \nabla_\tau \langle \mathsf{R} \rangle \cdot \nabla_\tau \left\langle \dot{\mathsf{T}} \right\rangle + \kappa_s H \langle \mathsf{R} \rangle [\dot{\mathsf{T}}] + \frac{\kappa_s}{\eta} [\mathsf{R}][\dot{\mathsf{T}}] \right) \mathrm{d}s = \sum_{i=1}^{2} \int_{\Omega_i} s_i \boldsymbol{u}_i \cdot \nabla \dot{\mathsf{T}}_i \, \mathrm{d}x. \quad (4.45)
\end{aligned}$$

Using (4.44) and (4.45), it yields to

$$\begin{aligned}
&\sum_{i=1}^{2} \int_{\Omega_i} s_i \nabla \dot{\mathsf{T}}_i \cdot \boldsymbol{u}_i \, \mathrm{d}x - \sum_{i=1}^{2} \int_{\Omega_i} \mathsf{R}_i \dot{\boldsymbol{u}}_i \cdot \nabla \mathsf{T}_i \, \mathrm{d}x \\
&\qquad = \sum_{i=1}^{2} \int_{\Omega_i} \left(\kappa_i \left(\nabla \boldsymbol{\theta} + \nabla \boldsymbol{\theta}^t - \operatorname{div}(\boldsymbol{\theta}) \mathrm{I} \right) \nabla \mathsf{T}_i \cdot \nabla \mathsf{R}_i + \left(\nabla \boldsymbol{\theta} - \operatorname{div}(\boldsymbol{\theta}) \right) \mathsf{R}_i \boldsymbol{u}_i \cdot \nabla \mathsf{T}_i \right) \mathrm{d}x \\
&\qquad + \int_{\Gamma} \eta \kappa_s \left(\left(\nabla_\tau \boldsymbol{\theta} + \nabla_\tau \boldsymbol{\theta}^t - \operatorname{div}_\tau(\boldsymbol{\theta}) \mathrm{I} \right) \nabla_\tau \langle \mathsf{T} \rangle \right) \cdot \nabla_\tau \langle \mathsf{R} \rangle \, \mathrm{d}s \qquad (4.46) \\
&\qquad - \int_{\Gamma} \left(\kappa_s H \operatorname{div}_\tau(\boldsymbol{\theta}) [\mathsf{T}] \langle \mathsf{R} \rangle - \kappa_s \Delta_\tau (\boldsymbol{\theta} \cdot \boldsymbol{n}) [\mathsf{T}] \langle \mathsf{R} \rangle + \kappa_s \nabla H \cdot \theta [\mathsf{T}] \langle \mathsf{R} \rangle \right) \mathrm{d}s \\
&\qquad - \int_{\Gamma} \frac{\kappa_s}{\eta} \operatorname{div}_\tau(\boldsymbol{\theta}) [\mathsf{T}][\mathsf{R}] \, \mathrm{d}s.
\end{aligned}$$

Similarly for Navier-Stokes equations, we take $\boldsymbol{w}_i = \boldsymbol{v}_i \in \mathcal{V}_0(\Omega_i)$, $\phi = q_i \in \mathrm{L}^2(\Omega_i)$ in the material derivative equation associated to the Navier-Stokes equations (4.11) and we test against the functions $\boldsymbol{w}_i = \dot{\boldsymbol{u}}_i \in \mathcal{V}_0(\Omega_i)$, $\phi_i = \dot{p}_i \in \mathrm{L}^2(\Omega_i)$ in the adjoint equation of the Navier-Stokes equations (4.28),

$$\begin{aligned}
&\int_{\Omega_i} (2\nu_i \varepsilon(\dot{\boldsymbol{u}}_i) : \varepsilon(\boldsymbol{v}_i) + (\nabla \dot{\boldsymbol{u}}_i)\boldsymbol{u}_i \cdot \boldsymbol{v}_i + (\nabla \boldsymbol{u}_i)\dot{\boldsymbol{u}}_i \cdot \boldsymbol{v}_i - \dot{p}_i \operatorname{div}(\boldsymbol{v}_i) - q_i \operatorname{div}(\dot{\boldsymbol{u}}_i))\, \mathrm{d}x \\
&\quad = \int_{\Omega_i} -\operatorname{div}(\boldsymbol{\theta})(\sigma(\boldsymbol{u}_i, p_i) : \nabla \boldsymbol{v}_i + (\nabla \boldsymbol{u}_i)\boldsymbol{u}_i \cdot \boldsymbol{v}_i)\, \mathrm{d}x \\
&\quad + \int_{\Omega_i} (\sigma(\boldsymbol{u}_i, p_i) : (\nabla \boldsymbol{v}_i \nabla \boldsymbol{\theta}) + \sigma(\boldsymbol{v}_i, q_i) : (\nabla \boldsymbol{u}_i \nabla \boldsymbol{\theta}) + (\nabla \boldsymbol{u}_i \nabla \boldsymbol{\theta})\boldsymbol{u}_i \cdot \boldsymbol{v}_i)\, \mathrm{d}x,
\end{aligned} \tag{4.47}$$

and

$$\begin{aligned}
&\int_{\Omega_i} (2\nu_i \varepsilon(\boldsymbol{v}_i) : \varepsilon(\dot{\boldsymbol{u}}_i) + ((\nabla \boldsymbol{u}_i)\dot{\boldsymbol{u}}_i + (\nabla \dot{\boldsymbol{u}}_i)\boldsymbol{u}_i) \cdot \boldsymbol{v}_i - q_i \operatorname{div}(\dot{\boldsymbol{u}}_i) - \dot{p}_i \operatorname{div}(\boldsymbol{v}_i))\, \mathrm{d}x \\
&\quad = -\int_{\Omega_i} \mathsf{R}_i \nabla \mathsf{T}_i \cdot \dot{\boldsymbol{u}}_i\, \mathrm{d}x + \int_{\Omega_i} s_i \nabla \mathsf{T}_i \cdot \dot{\boldsymbol{u}}_i\, \mathrm{d}x.
\end{aligned} \tag{4.48}$$

Using (4.47) and (4.48), we get

$$\begin{aligned}
\int_{\Omega_i} s_i \nabla \mathsf{T}_i \cdot \dot{\boldsymbol{u}}_i\, \mathrm{d}x \;=\; &\int_{\Omega_i} \mathsf{R}\dot{\boldsymbol{u}}_i \cdot \nabla \mathsf{T}\, \mathrm{d}x \\
&+ \int_{\Omega_i} -\operatorname{div}(\boldsymbol{\theta})(\sigma(\boldsymbol{u}_i, p_i) : \nabla \boldsymbol{v}_i + (\nabla \boldsymbol{u}_i)\boldsymbol{u}_i \cdot \boldsymbol{v}_i)\, \mathrm{d}x \\
&+ \int_{\Omega_i} (\sigma(\boldsymbol{u}_i, p_i) : (\nabla \boldsymbol{v}_i \nabla \boldsymbol{\theta}) + \sigma(\boldsymbol{v}_i, q_i) : (\nabla \boldsymbol{u}_i \nabla \boldsymbol{\theta}) + (\nabla \boldsymbol{u}_i \nabla \boldsymbol{\theta})\boldsymbol{u}_i \cdot \boldsymbol{v}_i)\, \mathrm{d}x.
\end{aligned} \tag{4.49}$$

Summing (4.46) with (4.49), and replacing in (4.43), we obtain the desired formula. □

4.6.2 Proof by using a fully Lagrangian approach

In the following, we will consider a general functional J of the type

$$J(\Gamma) = J(\Gamma, \mathsf{T}_1(\Omega_1), \mathsf{T}_2(\Omega_2), \boldsymbol{u}_1(\Omega_1), \boldsymbol{u}_2(\Omega_2)), \tag{4.50}$$

depending on the solution $\mathsf{T} \in \mathcal{H}_{\mathsf{T}_\mathrm{D}}(\Omega_1, \Omega_2)$ of the convection-diffusion equation (4.2) and on the solutions $\boldsymbol{u}_i \in \mathcal{V}_{\boldsymbol{u}_{\mathrm{D,i}}}(\Omega_i)$, for $i = 1, 2$, of the Navier-Stokes equations (4.1).

The aim of this part is to obtain general formulas for the shape derivatives, where the functional is not necessarily the exchanged heat $W(\Gamma)$ (4.3), the dissipation $D_i(\Gamma)$ (4.4) or the volume $V(\Gamma)$ (4.5). For this purpose, we require the concept of transported functional.

Definition 4.6.2. *The transported functional (in Γ instead of $\Gamma^{\boldsymbol{\theta}} = (\boldsymbol{I} + \boldsymbol{\theta})\Gamma$) of J, is the functional $\mathcal{J}$ such that, for all $\boldsymbol{\theta} \in \Theta_{\mathrm{ad}}$, $\hat{\mathsf{T}} = (\hat{\mathsf{T}}_1, \hat{\mathsf{T}}_2) \in \mathcal{H}^1(\Omega_1, \Omega_2)$, $\hat{\boldsymbol{u}}_i \in \mathrm{H}^1(\Omega_i)^d$, $i = 1, 2$,*

$$\mathcal{J}(\boldsymbol{\theta}, \hat{\mathsf{T}}_1, \hat{\mathsf{T}}_2, \hat{\boldsymbol{u}}_1, \hat{\boldsymbol{u}}_2) = J(\Gamma^{\boldsymbol{\theta}}, \hat{\mathsf{T}}_1 \circ (\boldsymbol{I} + \boldsymbol{\theta})^{-1}, \hat{\mathsf{T}}_2 \circ (\boldsymbol{I} + \boldsymbol{\theta})^{-1}, \hat{\boldsymbol{u}}_1 \circ (\boldsymbol{I} + \boldsymbol{\theta})^{-1}, \hat{\boldsymbol{u}}_2 \circ (\boldsymbol{I} + \boldsymbol{\theta})^{-1}).$$

To keep as simplest as possible the notation, we will omit the evaluations of the partial derivatives at $(\boldsymbol{\theta}, \hat{\mathsf{T}}_1, \hat{\mathsf{T}}_2, \hat{\boldsymbol{u}}_1, \hat{\boldsymbol{u}}_2) = (0, \mathsf{T}_1(\Omega_1), \mathsf{T}_2(\Omega_2), \boldsymbol{u}_1(\Omega_1), \boldsymbol{u}_2(\Omega_2))$.

To compute the shape derivatives, we need to introduce the following adjoint states. Let us consider $\mathsf{R} = (\mathsf{R}_1, \mathsf{R}_2) \in \mathcal{H}_0(\Omega_1, \Omega_2)$ the solution of the following adjoint problem:

$$\begin{aligned}
&\sum_{i=1}^{2} \int_{\Omega_i} (\kappa_i \nabla \mathsf{R}_i \cdot \nabla \phi_i + \mathsf{R}_i \boldsymbol{u}_i \cdot \nabla \phi_i) \, \mathrm{d}x \\
&+ \int_\Gamma \left(\eta \kappa_s \nabla_\tau \langle \mathsf{R} \rangle \cdot \nabla_\tau \langle \phi \rangle + \kappa_s H \langle \mathsf{R} \rangle [\phi] + \frac{\kappa_s}{\eta} [\mathsf{R}][\phi] \right) \mathrm{d}s \\
&= \sum_{i=1}^{2} \frac{\partial \mathcal{J}}{\partial \hat{\mathsf{T}}_i}(\phi_i), \quad \forall \phi = (\phi_1, \phi_2) \in \mathcal{H}_0(\Omega_1, \Omega_2),
\end{aligned} \tag{4.51}$$

and $(\boldsymbol{v}_i, q_i) \in \mathcal{V}_0(\Omega_i) \times \mathrm{L}^2(\Omega_i)$ the solution of the following adjoint problem:

$$\begin{aligned}
&\int_{\Omega_i} (2\nu_i \varepsilon(\boldsymbol{v}_i) : \varepsilon(\boldsymbol{w}_i) + ((\nabla \boldsymbol{u}_i)\boldsymbol{w}_i + (\nabla \boldsymbol{w}_i)\boldsymbol{u}_i) \cdot \boldsymbol{v}_i - q_i \operatorname{div}(\boldsymbol{w}_i) - \phi_i \operatorname{div}(\boldsymbol{v}_i)) \, \mathrm{d}x \\
&= - \int_{\Omega_i} \mathsf{R}_i \nabla \mathsf{T}_i \cdot \boldsymbol{w}_i \, \mathrm{d}x + \frac{\partial \mathcal{J}}{\partial \hat{\boldsymbol{u}}_i}(\boldsymbol{w}_i), \quad \forall \boldsymbol{w}_i \in \mathcal{V}_0(\Omega_i), \phi_i \in \mathrm{L}^2(\Omega_i),
\end{aligned} \tag{4.52}$$

where $\boldsymbol{u}_i$ is the solution of the Navier-Stokes equations (4.1) and T_i is the restriction to Ω_i of the solution T of the approximate convection-diffusion equation (4.2).

Remark 26 *The well-posedness of the above equations was already discussed in 24.*

Proposition 4.6.3 (Volume shape derivative of a general functional)**.** *Let $\boldsymbol{\theta} \in \Theta_{\mathrm{ad}}$. Let be J the objective function that has the structure* (4.50) *and $\mathcal{J}$ the transported objective function with continuous partial derivatives at $(\boldsymbol{\theta}, \hat{\mathsf{T}}, \hat{\boldsymbol{u}}_1, \hat{\boldsymbol{u}}_2) = (0, \mathsf{T}_1(\Omega_1), \mathsf{T}_2(\Omega_2), \boldsymbol{u}_1(\Omega_1), \boldsymbol{u}_2(\Omega_2))$. The functional J is shape differentiable and the volume shape derivative is given by*

$$\begin{aligned}
J'(\Gamma)(\boldsymbol{\theta}) \;=\; & \frac{\partial \mathcal{J}}{\partial \boldsymbol{\theta}}(\boldsymbol{\theta}) - \sum_{i=1}^{2} \int_{\Omega_i} \operatorname{div}(\boldsymbol{\theta})(\sigma(\boldsymbol{u}_i, p_i) : \nabla \boldsymbol{v}_i + (\nabla \boldsymbol{u}_i)\boldsymbol{u}_i \cdot \boldsymbol{v}_i) \, \mathrm{d}x \\
& + \sum_{i=1}^{2} \int_{\Omega_i} (\sigma(\boldsymbol{u}_i, p_i) : (\nabla \boldsymbol{v}_i \nabla \boldsymbol{\theta}) + \sigma(\boldsymbol{v}_i, q_i) : (\nabla \boldsymbol{u}_i \nabla \boldsymbol{\theta}) + (\nabla \boldsymbol{u}_i \nabla \boldsymbol{\theta})\boldsymbol{u}_i \cdot \boldsymbol{v}_i) \, \mathrm{d}x \\
& + \sum_{i=1}^{2} \int_{\Omega_i} \left(\kappa_i (\nabla \boldsymbol{\theta} + \nabla \boldsymbol{\theta}^t - \operatorname{div}(\boldsymbol{\theta}) \mathrm{I}) \nabla \mathsf{T}_i \cdot \nabla \mathsf{R}_i + (\nabla \boldsymbol{\theta} - \operatorname{div}(\boldsymbol{\theta}) \mathrm{I}) \mathsf{R}_i \boldsymbol{u}_i \cdot \nabla \mathsf{T}_i \right) \mathrm{d}x \\
& + \eta \kappa_s \int_\Gamma (\nabla_\tau \boldsymbol{\theta} + \nabla_\tau \boldsymbol{\theta}^t - \operatorname{div}_\tau(\boldsymbol{\theta}) \mathrm{I}) \nabla_\tau \langle \mathsf{T} \rangle \cdot \nabla_\tau \langle \mathsf{R} \rangle \, \mathrm{d}s \\
& - \kappa_s \int_\Gamma (H \operatorname{div}_\tau(\boldsymbol{\theta}) [\mathsf{T}] \langle \mathsf{R} \rangle - \Delta_\tau(\boldsymbol{\theta} \cdot \boldsymbol{n}) [\mathsf{T}] \langle \mathsf{R} \rangle + \boldsymbol{\theta} \cdot \nabla H [\mathsf{T}] \langle \mathsf{R} \rangle) \, \mathrm{d}s \\
& - \frac{\kappa_s}{\eta} \int_\Gamma \operatorname{div}_\tau(\boldsymbol{\theta}) [\mathsf{T}][\mathsf{R}] \, \mathrm{d}s,
\end{aligned} \tag{4.53}$$

where $\mathsf{T} = (\mathsf{T}_1, \mathsf{T}_2) \in \mathcal{H}_{\mathsf{T}_{\mathrm{D}}}(\Omega_1, \Omega_2)$ is the solution of the convection-diffusion equation (4.2)*, $\mathsf{R} = (\mathsf{R}_1, \mathsf{R}_2) \in \mathcal{H}_0(\Omega_1, \Omega_2)$ is the solution of its adjoint equation* (4.51) *and $(\boldsymbol{u}_i, p_i) \in \mathcal{V}_{\boldsymbol{u}_{\mathrm{D},i}}(\Omega_i) \times \mathrm{L}^2(\Omega_i)$, $(\boldsymbol{v}_i, q_i) \in \mathcal{V}_0(\Omega_i) \times \mathrm{L}^2(\Omega_i)$ are the solutions of the Navier-Stokes* (4.1) *and its adjoint* (4.52) *equations, respectively.*

Proof. Applying the chain rule, we get

$$J'(\Omega)(\boldsymbol{\theta}) = \frac{\partial \mathcal{J}}{\partial \boldsymbol{\theta}}(\boldsymbol{\theta}) + \sum_{i=1}^{2} \left(\frac{\partial \mathcal{J}}{\partial \hat{\boldsymbol{u}}_i}(\dot{\boldsymbol{u}}_i) + \frac{\partial \mathcal{J}}{\partial \hat{\mathsf{T}}_i}(\dot{\mathsf{T}}_i) \right). \tag{4.54}$$

Taking $\phi = \mathsf{R} \in \mathcal{H}_0(\Omega_1, \Omega_2)$ in the material derivative equation associated to the convection-diffusion equation (4.15) and $\phi = \dot{\mathsf{T}} \in \mathcal{H}_0(\Omega_1, \Omega_2)$ in the adjoint of the convection-diffusion equation (4.51), we have respectively

$$\begin{aligned}
&\sum_{i=1}^{2} \int_{\Omega_i} \left(\kappa_i \nabla \dot{\mathsf{T}}_i \cdot \nabla \mathsf{R}_i + \left(\boldsymbol{u}_i \cdot \nabla \dot{\mathsf{T}}_i + \dot{\boldsymbol{u}}_i \cdot \nabla \mathsf{T}_i \right) \mathsf{R}_i \right) \mathrm{d}x \\
&+ \int_{\Gamma} \left(\eta \kappa_s \nabla_\tau \left\langle \dot{\mathsf{T}} \right\rangle \cdot \nabla_\tau \langle \mathsf{R} \rangle + \kappa_s H [\dot{\mathsf{T}}] \langle \mathsf{R} \rangle + \frac{\kappa_s}{\eta} [\dot{\mathsf{T}}][\mathsf{R}] \right) \mathrm{d}s \\
&= \sum_{i=1}^{2} \int_{\Omega_i} \left(\kappa_i \left(\nabla \boldsymbol{\theta} + \nabla \boldsymbol{\theta}^t - \mathrm{div}(\boldsymbol{\theta}) \mathrm{I} \right) \nabla \mathsf{T}_i \cdot \nabla \mathsf{R}_i + \left(\nabla \boldsymbol{\theta} - \mathrm{div}(\boldsymbol{\theta}) \right) \mathsf{R}_i \boldsymbol{u}_i \cdot \nabla \mathsf{T}_i \right) \mathrm{d}x \\
&+ \int_{\Gamma} \eta \kappa_s \left(\left(\nabla_\tau \boldsymbol{\theta} + \nabla_\tau \boldsymbol{\theta}^t - \mathrm{div}_\tau(\boldsymbol{\theta}) \mathrm{I} \right) \nabla_\tau \langle \mathsf{T} \rangle \right) \cdot \nabla_\tau \langle \mathsf{R} \rangle \, \mathrm{d}s \\
&- \int_{\Gamma} \left(\kappa_s H \, \mathrm{div}_\tau(\boldsymbol{\theta}) [\mathsf{T}] \langle \mathsf{R} \rangle - \kappa_s \Delta_\tau (\boldsymbol{\theta} \cdot \boldsymbol{n}) [\mathsf{T}] \langle \mathsf{R} \rangle + \kappa_s \nabla H \cdot \theta [\mathsf{T}] \langle \mathsf{R} \rangle \right) \mathrm{d}s \\
&- \int_{\Gamma} \frac{\kappa_s}{\eta} \mathrm{div}_\tau(\boldsymbol{\theta}) [\mathsf{T}][\mathsf{R}] \, \mathrm{d}s,
\end{aligned} \tag{4.55}$$

and

$$\begin{aligned}
&\sum_{i=1}^{2} \int_{\Omega_i} \left(\kappa_i \nabla \mathsf{R}_i \cdot \nabla \dot{\mathsf{T}}_i + \mathsf{R}_i \boldsymbol{u}_i \cdot \nabla \dot{\mathsf{T}}_i \right) \mathrm{d}x \\
&+ \int_{\Gamma} \left(\eta \kappa_s \nabla_\tau \langle \mathsf{R} \rangle \cdot \nabla_\tau \left\langle \dot{\mathsf{T}} \right\rangle + \kappa_s H \langle \mathsf{R} \rangle [\dot{\mathsf{T}}] + \frac{\kappa_s}{\eta} [\mathsf{R}][\dot{\mathsf{T}}] \right) \mathrm{d}s = \sum_{i=1}^{2} \frac{\partial \mathcal{J}}{\partial \hat{\mathsf{T}}_i}(\dot{\mathsf{T}}_i).
\end{aligned} \tag{4.56}$$

Using (4.55) and (4.56), it yields to

$$\begin{aligned}
&\sum_{i=1}^{2} \frac{\partial \mathcal{J}}{\partial \hat{\mathsf{T}}_i}(\dot{\mathsf{T}}_i(\boldsymbol{\theta})) - \sum_{i=1}^{2} \int_{\Omega_i} \mathsf{R}_i \dot{\boldsymbol{u}}_i \cdot \nabla \mathsf{T}_i \, \mathrm{d}x \\
&= \sum_{i=1}^{2} \int_{\Omega_i} \left(\kappa_i \left(\nabla \boldsymbol{\theta} + \nabla \boldsymbol{\theta}^t - \mathrm{div}(\boldsymbol{\theta}) \mathrm{I} \right) \nabla \mathsf{T}_i \cdot \nabla \mathsf{R}_i + \left(\nabla \boldsymbol{\theta} - \mathrm{div}(\boldsymbol{\theta}) \right) \mathsf{R}_i \boldsymbol{u}_i \cdot \nabla \mathsf{T}_i \right) \mathrm{d}x \\
&+ \int_{\Gamma} \eta \kappa_s \left(\left(\nabla_\tau \boldsymbol{\theta} + \nabla_\tau \boldsymbol{\theta}^t - \mathrm{div}_\tau(\boldsymbol{\theta}) \mathrm{I} \right) \nabla_\tau \langle \mathsf{T} \rangle \right) \cdot \nabla_\tau \langle \mathsf{R} \rangle \, \mathrm{d}s \\
&- \int_{\Gamma} \left(\kappa_s H \, \mathrm{div}_\tau(\boldsymbol{\theta}) [\mathsf{T}] \langle \mathsf{R} \rangle - \kappa_s \Delta_\tau (\boldsymbol{\theta} \cdot \boldsymbol{n}) [\mathsf{T}] \langle \phi \rangle + \kappa_s \nabla H \cdot \theta [\mathsf{T}] \langle \mathsf{R} \rangle \right) \mathrm{d}s \\
&- \int_{\Gamma} \frac{\kappa_s}{\eta} \mathrm{div}_\tau(\boldsymbol{\theta}) [\mathsf{T}][\mathsf{R}] \, \mathrm{d}s.
\end{aligned} \tag{4.57}$$

Similarly for Navier-Stokes equations, we take $\boldsymbol{w}_i = \boldsymbol{v}_i \in \mathcal{V}_0(\Omega_i)$, $\phi_i = q_i \in \mathrm{L}^2(\Omega_i)$ in the material derivative equation associated to the Navier-Stokes equations (4.11) and $\boldsymbol{w}_i = \dot{\boldsymbol{u}}_i \in$

$\mathcal{V}_0(\Omega_i)$, $\phi_i = \dot{p}_i \in \mathrm{L}^2(\Omega_i)$ in the adjoint equation of the Navier-Stokes equations (4.52),

$$\begin{aligned}
&\int_{\Omega_i} (2\nu_i \varepsilon(\dot{\boldsymbol{u}}_i) : \varepsilon(\boldsymbol{v}_i) + (\nabla \dot{\boldsymbol{u}}_i)\boldsymbol{u}_i \cdot \boldsymbol{v}_i + (\nabla \boldsymbol{u}_i)\dot{\boldsymbol{u}}_i \cdot \boldsymbol{v}_i - \dot{p}_i \operatorname{div}(\boldsymbol{v}_i) - q_i \operatorname{div}(\dot{\boldsymbol{u}}_i))\, \mathrm{d}x \\
&= \int_{\Omega_i} -\operatorname{div}(\boldsymbol{\theta})(\sigma(\boldsymbol{u}_i, p_i) : \nabla \boldsymbol{v}_i + (\nabla \boldsymbol{u}_i)\boldsymbol{u}_i \cdot \boldsymbol{v}_i)\, \mathrm{d}x \\
&\quad + \int_{\Omega_i} (\sigma(\boldsymbol{u}_i, p_i) : (\nabla \boldsymbol{v}_i \nabla \boldsymbol{\theta}) + \sigma(\boldsymbol{v}_i, q_i) : (\nabla \boldsymbol{u}_i \nabla \boldsymbol{\theta}) + (\nabla \boldsymbol{u}_i \nabla \boldsymbol{\theta})\boldsymbol{u}_i \cdot \boldsymbol{v}_i)\, \mathrm{d}x,
\end{aligned} \tag{4.58}$$

and

$$\begin{aligned}
&\int_{\Omega_i} (2\nu_i \varepsilon(\boldsymbol{v}_i) : \varepsilon(\dot{\boldsymbol{u}}_i) + ((\nabla \boldsymbol{u}_i)\dot{\boldsymbol{u}}_i + (\nabla \dot{\boldsymbol{u}}_i)\boldsymbol{u}_i) \cdot \boldsymbol{v}_i - q_i \operatorname{div}(\dot{\boldsymbol{u}}_i) - \dot{p}_i \operatorname{div}(\boldsymbol{v}_i))\, \mathrm{d}x \\
&= -\int_{\Omega_i} \mathsf{R}_i \nabla \mathsf{T}_i \cdot \dot{\boldsymbol{u}}_i\, \mathrm{d}x + \frac{\partial \mathcal{J}}{\partial \hat{\boldsymbol{u}}_i}(\dot{\boldsymbol{u}}_i).
\end{aligned} \tag{4.59}$$

Using (4.58) and (4.59), we get

$$\begin{aligned}
\frac{\partial \mathcal{J}}{\partial \hat{\boldsymbol{u}}_i}(\dot{\boldsymbol{u}}_i) &= \int_{\Omega_i} \mathsf{R}\dot{\boldsymbol{u}}_i \cdot \nabla \mathsf{T}\, \mathrm{d}x \\
&\quad + \int_{\Omega_i} -\operatorname{div}(\boldsymbol{\theta})(\sigma(\boldsymbol{u}_i, p_i) : \nabla \boldsymbol{v}_i + (\nabla \boldsymbol{u}_i)\boldsymbol{u}_i \cdot \boldsymbol{v}_i)\, \mathrm{d}x \\
&\quad + \int_{\Omega_i} (\sigma(\boldsymbol{u}_i, p_i) : (\nabla \boldsymbol{v}_i \nabla \boldsymbol{\theta}) + \sigma(\boldsymbol{v}_i, q_i) : (\nabla \boldsymbol{u}_i \nabla \boldsymbol{\theta}) + (\nabla \boldsymbol{u}_i \nabla \boldsymbol{\theta})\boldsymbol{u}_i \cdot \boldsymbol{v}_i)\, \mathrm{d}x.
\end{aligned} \tag{4.60}$$

Summing (4.57) with (4.60), and replacing in (4.54) is obtained the desired formula. □

Proposition 4.6.4 (Surface shape derivative of a general functional)**.** *Under the same hypothesis of the previous Proposition. If in addition the solution* $\mathsf{T} = (\mathsf{T}_1, \mathsf{T}_2)$ *of the convection-diffusion equation* (4.2)*, the solution* $\mathsf{R} = (\mathsf{R}_1, \mathsf{R}_2)$ *of its adjoint equation* (4.51) *belong to* $\in \mathrm{H}^2(\Omega_1, \Gamma) \times \mathrm{H}^2(\Omega_2, \Gamma)$ *and the solution* $(\boldsymbol{u}_i, p_i)$ *of the Navier-Stokes equation* (4.1)*, the solution* $(\boldsymbol{v}_i, q_i)$ *of its adjoint* (4.52) *belong to* $\mathrm{H}^2(\Omega_i)^d \times \mathrm{H}^1(\Omega_i)$*, then* $J'(\Gamma)(\boldsymbol{\theta})$ *can be expressed in the surface shape derivative form, that is given by*

$$\begin{aligned}
J'(\Gamma)(\boldsymbol{\theta}) &= \overline{\frac{\partial \mathcal{J}}{\partial \boldsymbol{\theta}}}(\boldsymbol{\theta}) + \int_\Gamma \left(2[\nu \varepsilon(\boldsymbol{u}) : \varepsilon(\boldsymbol{v})] - [\kappa \nabla \mathsf{T} \cdot \nabla \mathsf{R}] + 2\left[\kappa \frac{\partial \mathsf{T}}{\partial \boldsymbol{n}} \frac{\partial \mathsf{R}}{\partial \boldsymbol{n}}\right]\right)(\boldsymbol{\theta} \cdot \boldsymbol{n})\, \mathrm{d}s \\
&\quad - \int_\Gamma \left(\eta \kappa_s (H\mathrm{I} - 2\nabla_\tau \boldsymbol{n}) \nabla_\tau \langle \mathsf{T} \rangle \cdot \nabla_\tau \langle \mathsf{R} \rangle + \frac{\kappa_s}{\eta} H [\mathsf{T}][\mathsf{R}]\right)(\boldsymbol{\theta} \cdot \boldsymbol{n})\, \mathrm{d}s \\
&\quad - \kappa_s \int_\Gamma \left(H^2 [\mathsf{T}]\langle \mathsf{R} \rangle - \Delta_\tau([\mathsf{T}]\langle \mathsf{R} \rangle) + \frac{\partial H}{\partial \boldsymbol{n}} [\mathsf{T}]\langle \mathsf{R} \rangle\right)(\boldsymbol{\theta} \cdot \boldsymbol{n})\, \mathrm{d}s.
\end{aligned} \tag{4.61}$$

We denote $\overline{\frac{\partial \mathcal{J}}{\partial \boldsymbol{\theta}}}$ *the part of* $\frac{\partial \mathcal{J}}{\partial \boldsymbol{\theta}}$ *that depends only on* $\boldsymbol{\theta} \cdot \boldsymbol{n}$*.*

Proof. It is enough to integrate by parts the integral on Γ (the other integrals were already treated in [63]). We will remove the tangential parts of $\boldsymbol{\theta}$ on Γ arguing as in [63] (or by simplicity, we

can just take $\boldsymbol{\theta} = (\boldsymbol{\theta} \cdot \boldsymbol{n})\boldsymbol{n}$). Then, using integration by parts for surface integrals, it leads to the following identities

$$\begin{aligned}
&\int_\Gamma -\operatorname{div}_\tau(\boldsymbol{\theta}) \left(\eta \kappa_s \nabla_\tau \langle \mathsf{T} \rangle \cdot \nabla_\tau \langle \mathsf{R} \rangle + \kappa_s H [\mathsf{T}] \langle \mathsf{R} \rangle + \frac{\kappa_s}{\eta} [\mathsf{T}][\mathsf{R}] \right) \mathrm{d}s \\
&= -\int_\Gamma H \left(\eta \kappa_s \nabla_\tau \langle \mathsf{T} \rangle \cdot \nabla_\tau \langle \mathsf{R} \rangle + H [\mathsf{T}] \langle \mathsf{R} \rangle + \frac{\kappa_s}{\eta} [\mathsf{T}][\mathsf{R}] \right) (\boldsymbol{\theta} \cdot \boldsymbol{n}) \, \mathrm{d}s,
\end{aligned}$$

$$\int_\Gamma \eta \kappa_s \left(\nabla_\tau \boldsymbol{\theta} + \nabla_\tau \boldsymbol{\theta}^t \right) \nabla_\tau \langle \mathsf{T} \rangle \cdot \nabla_\tau \langle \mathsf{R} \rangle \, \mathrm{d}s = \int_\Gamma 2 \eta \kappa_s (\nabla_\tau \boldsymbol{n} \nabla_\tau \langle \mathsf{T} \rangle) \cdot \nabla_\tau \langle \mathsf{R} \rangle (\boldsymbol{\theta} \cdot \boldsymbol{n}) \, \mathrm{d}s,$$

and

$$\int_\Gamma \Delta_\tau (\boldsymbol{\theta} \cdot \boldsymbol{n}) [\mathsf{T}] \langle \mathsf{R} \rangle \, \mathrm{d}s = \int_\Gamma \Delta_\tau ([\mathsf{T}] \langle \mathsf{R} \rangle) (\boldsymbol{\theta} \cdot \boldsymbol{n}) \, \mathrm{d}s.$$

We use the above identities in the volume shape derivative formula (4.53), getting the desired result. □

Remark 27 *In the particular case of the heat exchanged $W(\Gamma)$ (4.3), we have that for any $\phi \in \mathcal{H}_0(\Omega_1, \Omega_2), \boldsymbol{w}_i \in \mathcal{V}_0(\Omega_i)$,*

$$\begin{aligned}
&\frac{\partial \mathcal{W}}{\partial \hat{\mathsf{T}}}(\phi) = \sum_{i=1}^{2} \int_{\Omega_i} s_i \boldsymbol{u}_i \cdot \nabla \phi_i \, \mathrm{d}x, \frac{\partial \mathcal{W}}{\partial \hat{\boldsymbol{u}}_i}(\boldsymbol{w}_i) = \int_{\Omega_i} s_i \boldsymbol{w}_i \cdot \nabla \mathsf{T}_i \, \mathrm{d}x, \\
&\frac{\partial \mathcal{W}}{\partial \boldsymbol{\theta}}(\boldsymbol{\theta}) = \sum_{i=1}^{2} \int_{\Omega_i} s_i \left(\operatorname{div}(\boldsymbol{\theta}) \boldsymbol{u}_i \cdot \nabla \mathsf{T}_i - (\nabla \boldsymbol{\theta}) \boldsymbol{u}_i \cdot \nabla \mathsf{T}_i \right) \mathrm{d}x, \overline{\frac{\partial \mathcal{W}}{\partial \boldsymbol{\theta}}}(\boldsymbol{\theta}) = 0.
\end{aligned}$$

Chapter 5

Conclusion and perspectives

In this thesis we have studied the optimisation of the shape of a heat exchanger, tackling various mathematical areas such as asymptotic analysis, numerical analysis of PDEs, and shape optimization. Specifically, we developed a Nitsche-based discontinuous finite element method to numerically solve the equations presented in Chapter 1. Building on this foundation, we explored the thermal insulator problem as an initial application of shape optimization. This model offers a more realistic approach compared to existing ones, and we conducted a detailed differentiability analysis to derive the corresponding shape derivatives. Finally, we tackled the primary problem of this thesis, applying the tools developed. Unlike the thermal insulator case, this problem involves more intricate differentiability issues because the interface is the variable, resulting in more complex shape derivative formulas. We obtained new results for the differentiability of discontinuous equations at the interface, particularly involving the Laplace-Beltrami operator.

Despite these advancements and the introduction of more realistic models compared to the existing literature, further work is required to transition toward industrial applications. The following is a list of possible prospects.

- Consider a natural convection regime, i.e., investigate scenarios where temperature gradients induce buoyancy, resulting in a strongly coupled system between the Navier-Stokes and convection-diffusion equations. This strong coupling significantly increases computational complexity and will also modify the expressions for the shape derivatives.
- Consider turbulent flow models. When the viscosity is too small (large Reynolds numbers), the Navier-Stokes equations become unstable. Taking turbulence into account will therefore have an impact on the model, the shape derivative computations and, of course, the numerical resolution of the equations involved. We therefore expect significant changes and certainly potentially different solutions to the optimal design problem.
- Efficient solvers for the asymptotic equation. The non-standard equation studied in Chapter 1 does not have established solvers or preconditioners with good performance for solving it efficiently. Future work could explore preconditioners inspired by those used for Laplace or Navier-Stokes equations, such as Additive Schwarz Methods (ASM) or fieldsplit techniques. It should be noted that the exploration of these methods will require the use of the mesh structure in PETSc format and is intrusive.

Bibliography

[1] L. Afraites, M. Dambrine, and D. Kateb. On second order shape optimization methods for electrical impedance tomography. *SIAM J. Control Optim.*, 47(3):1556–1590, 2008.

[2] L. Afraites, M. Dambrine, and D. Kateb. On second order shape optimization methods for electrical impedance tomography. *SIAM Journal on Control and Optimization*, 47(3):1556–1590, 2008.

[3] A. Aldor, Y. Moguen, K. El Omari, C. Habchi, P.-H. Cocquet, and Y. Le Guer. Heat transfer enhancement by chaotic advection in a novel sine-helical channel geometry. *International Journal of Heat and Mass Transfer*, 193:122870, 2022.

[4] J. Alexandersen, N. Aage, C. S. Andreasen, and O. Sigmund. Topology optimisation for natural convection problems. *Internat. J. Numer. Methods Fluids*, 76(10):699–721, 2014.

[5] J. Alexandersen, O. Sigmund, and N. Aage. Large scale three-dimensional topology optimisation of heat sinks cooled by natural convection. *International Journal of Heat and Mass Transfer*, 100:876–891, 2016.

[6] G. Allaire. *Shape optimization by the homogenization method*, volume 146 of *Applied Mathematical Sciences*. Springer-Verlag, New York, 2002.

[7] G. Allaire. *Conception optimale de structures*, volume 58 of *Mathématiques & Applications (Berlin) [Mathematics & Applications]*. Springer-Verlag, Berlin, 2007. With the collaboration of Marc Schoenauer (INRIA) in the writing of Chapter 8.

[8] G. Allaire. *Numerical analysis and optimization*. Numerical Mathematics and Scientific Computation. Oxford University Press, Oxford, 2007. An introduction to mathematical modelling and numerical simulation, Translated from the French by Alan Craig.

[9] G. Allaire, B. Bogosel, and M. Godoy. Shape optimization of an imperfect interface: steady-state heat diffusion. *J. Optim. Theory Appl.*, 191(1):169–201, 2021.

[10] G. Allaire, C. Dapogny, and P. Frey. A mesh evolution algorithm based on the level set method for geometry and topology optimization. *Struct. Multidiscip. Optim.*, 48(4):711–715, 2013.

[11] G. Allaire, C. Dapogny, and F. c. Jouve. Shape and topology optimization. In *Geometric partial differential equations. Part II*, volume 22 of *Handb. Numer. Anal.*, pages 1–132. Elsevier/North-Holland, Amsterdam, [2021] ©2021.

[12] G. Allaire, F. c. Jouve, and A.-M. Toader. A level-set method for shape optimization. *C. R. Math. Acad. Sci. Paris*, 334(12):1125–1130, 2002.

[13] G. Allaire and O. Pantz. Structural optimization with FreeFem++. *Struct. Multidiscip. Optim.*, 32(3):173–181, 2006.

[14] S. Amstutz. An introduction to the topological derivative. *Engineering Computations*, 39(1):3–33, 2022.

[15] O. P. Arsenyeva, L. L. Tovazhnyansky, P. O. Kapustenko, and G. L. Khavin. Optimal design of plate-and-frame heat exchangers for efficient heat recovery in process industries. *Energy*, 36(8):4588–4598, 2011. PRES 2010.

[16] A. Auvray and G. Vial. Asymptotic expansions and effective boundary conditions: a short review for smooth and nonsmooth geometries with thin layers. In *43-ème Congrès National d'Analyse Numérique, CANUM2016*, volume 61 of *ESAIM Proc. Surveys*, pages 38–54. EDP Sci., Les Ulis, 2018.

[17] S. Balay, S. Abhyankar, M. F. Adams, J. Brown, P. Brune, K. Buschelman, L. Dalcin, A. Dener, V. Eijkhout, W. D. Gropp, D. Kaushik, M. G. Knepley, D. A. May, L. C. McInnes, R. T. Mills, T. Munson, K. Rupp, P. Sanan, B. F. Smith, S. Zampini, H. Zhang, and H. Zhang. PETSc Web page, 2018. http://www.mcs.anl.gov/petsc.

[18] S. Balay, S. Abhyankar, M. F. Adams, J. Brown, P. Brune, K. Buschelman, L. Dalcin, A. Dener, V. Eijkhout, W. D. Gropp, D. Kaushik, M. G. Knepley, D. A. May, L. C. McInnes, R. T. Mills, T. Munson, K. Rupp, P. Sanan, B. F. Smith, S. Zampini, H. Zhang, and H. Zhang. PETSc users manual. Technical Report ANL-95/11 - Revision 3.11, Argonne National Laboratory, 2019.

[19] L. L. Beghini, A. Beghini, N. Katz, W. F. Baker, and G. H. Paulino. Connecting architecture and engineering through structural topology optimization. *Engineering Structures*, 59:716–726, 2014.

[20] J. A. Bello, E. Fernández-Cara, J. Lemoine, and J. Simon. The differentiability of the drag with respect to the variations of a lipschitz domain in a navier–stokes flow. *SIAM Journal on Control and Optimization*, 35(2):626–640, 1997.

[21] M. P. Bendsøe and O. Sigmund. Material interpolation schemes in topology optimization. *Archive of applied mechanics*, 69:635–654, 1999.

[22] M. P. Bendsøe and O. Sigmund. *Topology optimization*. Springer-Verlag, Berlin, 2003. Theory, methods and applications.

[23] T. L. Bergman, A. S. Lavine, F. P. Incropera, and D. P. DeWitt. *Introduction to heat transfer*. John Wiley & Sons, 2011.

[24] R. Bey, J.-P. Lohéac, and M. Moussaoui. Singularities of the solution of a mixed problem for a general second order elliptic equation and boundary stabilization of the wave equation. *J. Math. Pures Appl. (9)*, 78(10):1043–1067, 1999.

[25] V. Bonnaillie-Noël, M. Dambrine, F. Hérau, and G. Vial. On generalized Ventcel's type boundary conditions for Laplace operator in a bounded domain. *SIAM J. Math. Anal.*, 42(2):931–945, 2010.

[26] S. C. Brenner and L. R. Scott. *The mathematical theory of finite element methods*, volume 15 of *Texts in Applied Mathematics*. Springer, New York, third edition, 2008.

[27] D. Bucur, G. Buttazzo, and C. Nitsch. Two optimization problems in thermal insulation. *Notices Amer. Math. Soc.*, 64(8):830–835, 2017.

[28] D. Bucur, M. Nahon, C. Nitsch, and C. Trombetti. Shape optimization of a thermal insulation problem. *Calc. Var. Partial Differential Equations*, 61(5):Paper No. 186, 29, 2022.

[29] C. Bui, C. Dapogny, and P. Frey. An accurate anisotropic adaptation method for solving the level set advection equation. *Internat. J. Numer. Methods Fluids*, 70(7):899–922, 2012.

[30] D. Capatina, F. Caubet, M. Dambrine, and R. Zelada. Nitsche extended finite element method of a Ventcel transmission problem with discontinuities at the interface. *ESAIM Math. Model. Numer. Anal.*, 59(2):999–1021, 2025.

[31] D. Capatina, R. Luce, H. El-Otmany, and N. Barrau. Nxfem for solving non-standard transmission problems. In *Int. Conf." Numerical and Mathematical Modeling of Flow and Transport in Porous Media". Octobre 2014, Dubrovnik, Croatie*, 2014.

[32] D. Capatina, R. Luce, H. El-Otmany, and N. Barrau. Nitsche's extended finite element method for a fracture model in porous media. *Appl. Anal.*, 95(10):2224–2242, 2016.

[33] F. Careri, R. H. Khan, C. Todd, and M. M. Attallah. Additive manufacturing of heat exchangers in aerospace applications: a review. *Applied Thermal Engineering*, 235:121387, 2023.

[34] F. Caubet. Instability of an inverse problem for the stationary Navier-Stokes equations. *SIAM J. Control Optim.*, 51(4):2949–2975, 2013.

[35] F. Caubet, C. Conca, M. Dambrine, and R. Zelada. Shape optimization for heat exchangers with a thin layer. In *Sixteenth International Conference Zaragoza-Pau on Mathematics and its Applications*, volume 43 of *Monogr. Mat. García Galdeano*, pages 51–61. Prensas Univ. Zaragoza, Zaragoza, 2024.

[36] F. Caubet, C. Conca, M. Dambrine, and R. Zelada. How to Insulate a Pipe? *J. Optim. Theory Appl.*, 207(3):46, 2025.

[37] F. Caubet and M. Dambrine. Stability of critical shapes for the drag minimization problem in stokes flow. *Journal de Mathématiques Pures et Appliquées*, 100(3):327–346, 2013.

[38] F. Caubet, M. Dambrine, G. Gargantini, and J. Maynadier. Shape Optimization of Polynomial Functionals under Uncertainties on the Right-Hand Side of the State Equation. preprint hal-04082741, Jan. 2023.

[39] F. Caubet, M. Dambrine, and D. Kateb. Shape optimization methods for the inverse obstacle problem with generalized impedance boundary conditions. *Inverse Problems*, 29(11):115011, 26, 2013.

[40] F. Caubet, H. Haddar, J.-R. Li, and D. V. Nguyen. New transmission condition accounting for diffusion anisotropy in thin layers applied to diffusion MRI. *ESAIM Math. Model. Numer. Anal.*, 51(4):1279–1301, 2017.

[41] A. Cherkaev. *Variational methods for structural optimization*, volume 140 of *Applied Mathematical Sciences*. Springer-Verlag, New York, 2000.

[42] P. G. Ciarlet. *The finite element method for elliptic problems*, volume Vol. 4 of *Studies in Mathematics and its Applications*. North-Holland Publishing Co., Amsterdam-New York-Oxford, 1978.

[43] D. Cioranescu and P. Donato. *An introduction to homogenization*, volume 17 of *Oxford Lecture Series in Mathematics and its Applications*. The Clarendon Press, Oxford University Press, New York, 1999.

[44] M. Dambrine, C. Dapogny, and H. Harbrecht. Shape optimization for quadratic functionals and states with random right-hand sides. *SIAM J. Control Optim.*, 53(5):3081–3103, 2015.

[45] M. Dambrine, H. Harbrecht, and B. Puig. Incorporating knowledge on the measurement noise in electrical impedance tomography. *ESAIM Control Optim. Calc. Var.*, 25:Paper No. 84, 16, 2019.

[46] M. Dambrine, D. Kateb, and J. Lamboley. An extremal eigenvalue problem for the Wentzell–Laplace operator. *Annales de l'I.H.P. Analyse non linéaire*, 33(2):409–450, 2016.

[47] C. Dapogny, C. Dobrzynski, and P. Frey. Three-dimensional adaptive domain remeshing, implicit domain meshing, and applications to free and moving boundary problems. *J. Comput. Phys.*, 262:358–378, 2014.

[48] C. Dapogny and F. Feppon. Shape optimization using a level set based mesh evolution method: an overview and tutorial. *C. R. Math. Acad. Sci. Paris*, 361:1267–1332, 2023.

[49] C. Dapogny and P. Frey. Computation of the signed distance function to a discrete contour on adapted triangulation. *Calcolo*, 49(3):193–219, 2012.

[50] C. Dapogny, P. Frey, F. Omnès, and Y. Privat. Geometrical shape optimization in fluid mechanics using FreeFem++. *Struct. Multidiscip. Optim.*, 58(6):2761–2788, 2018.

[51] E. M. Dede. Multiphysics topology optimization of heat transfer and fluid flow systems. In *proceedings of the COMSOL Users Conference*, volume 715, 2009.

[52] E. M. Dede. Optimization and design of a multipass branching microchannel heat sink for electronics cooling. *Journal of Electronic Packaging*, 134(4):041001, 08 2012.

[53] M. C. Delfour and J.-P. Zolésio. *Shapes and geometries*, volume 4 of *Advances in Design and Control*. Society for Industrial and Applied Mathematics (SIAM), Philadelphia, PA, 2001. Analysis, differential calculus, and optimization.

[54] F. R. Desaint and J.-P. Zolésio. Manifold derivative in the Laplace-Beltrami equation. *J. Funct. Anal.*, 151(1):234–269, 1997.

[55] D. A. Di Pietro and A. Ern. *Mathematical aspects of discontinuous Galerkin methods*, volume 69 of *Mathématiques & Applications (Berlin) [Mathematics & Applications]*. Springer, Heidelberg, 2012.

[56] G. Doğan and R. H. Nochetto. First variation of the general curvature-dependent surface energy. *ESAIM Math. Model. Numer. Anal.*, 46(1):59–79, 2012.

[57] M. Dryja. On discontinuous Galerkin methods for elliptic problems with discontinuous coefficients. *Comput. Methods Appl. Math.*, 3(1):76–85, 2003. Dedicated to Raytcho Lazarov.

[58] B. Engquist and J. Nédélec. Effective boundary conditions for electromagnetic scattering in thin layers. Technical Report 278, CMAP, 1993.

[59] A. Ern and J.-L. Guermond. *Theory and practice of finite elements*, volume 159 of *Applied Mathematical Sciences*. Springer-Verlag, New York, 2004.

[60] A. Fawaz, Y. Hua, S. Le Corre, Y. Fan, and L. Luo. Topology optimization of heat exchangers: A review. *Energy*, 252:124053, 2022.

[61] F. Feppon. Null space optimizer, 2019. `https://gitlab.com/florian.feppon/null-space-optimizer` [Accessed: 21/10/2024].

[62] F. Feppon. Density-based topology optimization with the null space optimizer: a tutorial and a comparison. *Struct. Multidiscip. Optim.*, 67(1):Paper No. 4, 34, 2024.

[63] F. Feppon, G. Allaire, F. Bordeu, J. Cortial, and C. Dapogny. Shape optimization of a coupled thermal fluid-structure problem in a level set mesh evolution framework. *SeMA J.*, 76(3):413–458, 2019.

[64] F. Feppon, G. Allaire, and C. Dapogny. Null space gradient flows for constrained optimization with applications to shape optimization. *ESAIM Control Optim. Calc. Var.*, 26:Paper No. 90, 45, 2020.

[65] F. Feppon, G. Allaire, and C. Dapogny. A variational formulation for computing shape derivatives of geometric constraints along rays. *ESAIM Math. Model. Numer. Anal.*, 54(1):181–228, 2020.

[66] F. Feppon, G. Allaire, C. Dapogny, and P. Jolivet. Topology optimization of thermal fluid-structure systems using body-fitted meshes and parallel computing. *J. Comput. Phys.*, 417:109574, 30, 2020.

[67] F. Feppon, G. Allaire, C. Dapogny, and P. Jolivet. Body-fitted topology optimization of 2D and 3D fluid-to-fluid heat exchangers. *Comput. Methods Appl. Mech. Engrg.*, 376:Paper No. 113638, 36, 2021.

[68] V. Girault and P.-A. Raviart. *Finite element methods for Navier-Stokes equations*, volume 5 of *Springer Series in Computational Mathematics*. Springer-Verlag, Berlin, 1986. Theory and algorithms.

[69] J. Hadamard. *Mémoire sur le problème d'analyse relatif à l'équilibre des plaques élastiques encastrées*, volume 33. Imprimerie nationale, 1908.

[70] A. Hansbo and P. Hansbo. An unfitted finite element method, based on Nitsche's method, for elliptic interface problems. *Comput. Methods Appl. Mech. Engrg.*, 191(47-48):5537–5552, 2002.

[71] F. Hecht. New development in freefem++. *J. Numer. Math.*, 20(3-4):251–265, 2012.

[72] A. Henrot and M. Pierre. *Shape variation and optimization*, volume 28 of *EMS Tracts in Mathematics*. European Mathematical Society (EMS), Zürich, 2018. A geometrical analysis, English version of the French publication [MR2512810] with additions and updates.

[73] A. Henrot and Y. Privat. What is the optimal shape of a pipe? *Arch. Ration. Mech. Anal.*, 196(1):281–302, 2010.

[74] F. Hettlich and W. Rundell. The determination of a discontinuity in a conductivity from a single boundary measurement. *Inverse Problems*, 14(1):67–82, 1998.

[75] M. Hintermüller and W. Ring. A second order shape optimization approach for image segmentation. *SIAM J. Appl. Math.*, 64(2):442–467, 2003/04.

[76] L. C. Høghøj, D. R. Nørhave, J. Alexandersen, O. Sigmund, and C. S. Andreasen. Topology optimization of two fluid heat exchangers. *International Journal of Heat and Mass Transfer*, 163:120543, 2020.

[77] J. S. Jensen and O. Sigmund. Topology optimization for nano-photonics. *Laser & Photonics Reviews*, 5(2):308–321, 2011.

[78] H. Jouhara, S. Almahmoud, A. Chauhan, B. Delpech, G. Bianchi, S. A. Tassou, R. Llera, F. Lago, and J. J. Arribas. Experimental and theoretical investigation of a flat heat pipe heat exchanger for waste heat recovery in the steel industry. *Energy*, 141:1928–1939, 2017.

[79] M. Juntunen and R. Stenberg. Nitsche's method for general boundary conditions. *Math. Comp.*, 78(267):1353–1374, 2009.

[80] T. Kashiwabara, C. M. Colciago, L. Dedè, and A. Quarteroni. Well-posedness, regularity, and convergence analysis of the finite element approximation of a generalized Robin boundary value problem. *SIAM J. Numer. Anal.*, 53(1):105–126, 2015.

[81] H. Kobayashi, K. Yaji, S. Yamasaki, and K. Fujita. Topology design of two-fluid heat exchange. *Struct. Multidiscip. Optim.*, 63(2):821–834, 2021.

[82] N. Lebbe, C. Dapogny, E. Oudet, K. Hassan, and A. Gliere. Robust shape and topology optimization of nanophotonic devices using the level set method. *J. Comput. Phys.*, 395:710–746, 2019.

[83] H. Li, T. Kondoh, P. Jolivet, K. Furuta, T. Yamada, B. Zhu, H. Zhang, K. Izui, and S. Nishiwaki. Optimum design and thermal modeling for 2D and 3D natural convection problems incorporating level set-based topology optimization with body-fitted mesh. *Internat. J. Numer. Methods Engrg.*, 123(9):1954–1990, 2022.

[84] X. S. Li and J. W. Demmel. Superlu_dist: A scalable distributed-memory sparse direct solver for unsymmetric linear systems. *ACM Trans. Math. Softw.*, 29(2):110–140, June 2003.

[85] G. J. Lord, C. E. Powell, and T. Shardlow. *An introduction to computational stochastic PDEs*. Cambridge Texts in Applied Mathematics. Cambridge University Press, New York, 2014.

[86] G. McBain. Domain decomposition techniques for interfacial discontinuities. In *Fourth FreeFem workshop on Generic Solver for PDEs*, Paris, December 2012. Laboratoire Jacques-Louis Lions, Université Pierre et Marie Curie.

[87] J. Moulin, P. Jolivet, and O. Marquet. Augmented Lagrangian preconditioner for large-scale hydrodynamic stability analysis. *Comput. Methods Appl. Mech. Engrg.*, 351:718–743, 2019.

[88] M. A. Mukit, T. Anjum, M. Hossain, and M. Islam. Helical coil heat exchanger design and it's performance analysis. 09 2023.

[89] F. Murat and J. Simon. Sur le contrôle par un domaine géométrique. *Rapport du LA*, 189:76015, 1976.

[90] F. Murat and L. Tartar. H-convergence. *Topics in the mathematical modelling of composite materials*, pages 21–43, 1977.

[91] J. Nitsche. über ein Variationsprinzip zur Lösung von Dirichlet-Problemen bei Verwendung von Teilräumen, die keinen Randbedingungen unterworfen sind. *Abh. Math. Sem. Univ. Hamburg*, 36:9–15, 1971.

[92] J. Nocedal and S. J. Wright. *Numerical optimization*. Springer Series in Operations Research and Financial Engineering. Springer, New York, second edition, 2006.

[93] A. A. Novotny and J. Sokoł owski. *Topological derivatives in shape optimization*. Interaction of Mechanics and Mathematics. Springer, Heidelberg, 2013.

[94] A. A. Novotny and J. Sokoł owski. *An introduction to the topological derivative method*. SpringerBriefs in Mathematics. Springer, Cham, [2020] ©2020. SBMAC SpringerBriefs.

[95] S. Osher and J. A. Sethian. Fronts propagating with curvature-dependent speed: algorithms based on Hamilton-Jacobi formulations. *J. Comput. Phys.*, 79(1):12–49, 1988.

[96] O. Pantz. Sensibilité de l'équation de la chaleur aux sauts de conductivité. *C. R. Math. Acad. Sci. Paris*, 341(5):333–337, 2005.

[97] P. Papazoglou. Topology optimization of heat exchangers. *Master's thesis, TU Delft*, 2015.

[98] J. Qian, Y.-T. Zhang, and H.-K. Zhao. Fast sweeping methods for eikonal equations on triangular meshes. *SIAM J. Numer. Anal.*, 45(1):83–107, 2007.

[99] Y. S. Rajput and A. Arya. Cfd analysis of cross flow heat exchanger with different fin thickness. *Materials Science*, 1(1):1–20, 2019.

[100] E. Sánchez-Palencia. *Nonhomogeneous media and vibration theory*, volume 127 of *Lecture Notes in Physics*. Springer-Verlag, Berlin-New York, 1980.

[101] J. A. Sethian. A fast marching level set method for monotonically advancing fronts. *Proc. Nat. Acad. Sci. U.S.A.*, 93(4):1591–1595, 1996.

[102] J. A. Sethian. *Level set methods and fast marching methods*, volume 3 of *Cambridge Monographs on Applied and Computational Mathematics*. Cambridge University Press, Cambridge, second edition, 1999. Evolving interfaces in computational geometry, fluid mechanics, computer vision, and materials science.

[103] S. N. Skinner and H. Zare-Behtash. State-of-the-art in aerodynamic shape optimisation methods. *Applied Soft Computing*, 62:933–962, 2018.

[104] J. Sokoł owski and J.-P. Zolésio. *Introduction to shape optimization*, volume 16 of *Springer Series in Computational Mathematics*. Springer-Verlag, Berlin, 1992. Shape sensitivity analysis.

[105] L. Tartar. *The general theory of homogenization*, volume 7 of *Lecture Notes of the Unione Matematica Italiana*. Springer-Verlag, Berlin; UMI, Bologna, 2009. A personalized introduction.

[106] R. Temam. *Navier-Stokes equations*. AMS Chelsea Publishing, Providence, RI, 2001. Theory and numerical analysis, Reprint of the 1984 edition.

[107] H. C. Torrey. Bloch equations with diffusion terms. *Physical review*, 104(3):563, 1956.

[108] S. Tozza and G. Toraldo. Numerical hints for insulation problems. *Appl. Math. Lett.*, 123:Paper No. 107609, 8, 2022.

[109] A. D. Ventcel'. On boundary conditions for multi-dimensional diffusion processes. *Theor. Probability Appl.*, 4:164–177, 1959.

[110] G. Vial. Analyse multi-échelle et conditions aux limites approchées pour un probleme avec couche mince dans un domaine coin. *Thèse, Université de Rennes 1*, 2003.

[111] M. Y. Wang, X. Wang, and D. Guo. A level set method for structural topology optimization. *Comput. Methods Appl. Mech. Engrg.*, 192(1-2):227–246, 2003.

[112] G. Yoon. Topological design of heat dissipating structure with forced convective heat transfer. *Journal of Mechanical Science and Technology*, 24:1225–1233, 06 2010.

[113] H. Zhao. A fast sweeping method for eikonal equations. *Math. Comp.*, 74(250):603–627, 2005.

[114] J.-H. Zhu, W.-H. Zhang, and L. Xia. Topology optimization in aircraft and aerospace structures design. *Archives of computational methods in engineering*, 23:595–622, 2016.

Appendix A

Reminders in shape optimization

In this appendix, I gather from the existing literature, as a survival guide for the reader who is not an expert in shape optimization, the tools that I will use throughout this thesis: in particular, the theoretical framework to define and compute shape derivatives and then the numerical algorithms used in the level-set mesh evolution method.

A.1 Shape derivative

First, we will introduce properly the concept of shape derivative to then recall some useful results. More details can be found in the classical textbooks [72, 7, 53, 104].

A.1.1 Definition and structure theorem

Let $\Omega \subset \mathbb{R}^d (d = 2, 3)$, a Lipschitz bounded domain. Let us denote $\boldsymbol{n}$ the outward unit normal to $\partial\Omega$. A shape optimisation problem has four components:

- the physics or PDE: for example the Navier-Stokes equations, linear elasticity, etc.
- a criteria or functional J that is real-valued and depends on the solution of the PDE: for example the fluid dissipation in the case of the Navier-Stokes equations or compliance in linear elasticity, etc.
- some constraints $C_p(\Omega), p = 1, \dots, m$, that can be either geometrical or physical criterias.
- a set of admissible domains $\mathcal{U}_{\text{ad}} \subset \mathbb{R}^d$, where the fixed boundaries are taken into account.

Then, a shape optimization problem is usally stated as follows:

$$\begin{cases} \min_{\Omega \in \Theta_{\text{ad}}} J(\Omega) \\ \text{s.t } C_p(\Omega) \leq 0, p = 1, \dots, m. \end{cases}$$

The key is to consider small perturbations of the domain:

$$\Omega_{\boldsymbol{\theta}} := (\boldsymbol{I} + \boldsymbol{\theta})(\Omega),$$

where $\boldsymbol{\theta}$ is smooth enough. A classical choice is to consider

$$\boldsymbol{\theta} \in \mathrm{W}^{1,\infty}(\mathbb{R}^d)^d := \{\boldsymbol{\theta} \in \mathrm{L}^\infty(\mathbb{R}^d)^d; \nabla\boldsymbol{\theta} \in \mathrm{L}^\infty(\mathbb{R}^d)^{d\times d}\}.$$

In some problems we could require more regularity of the perturbation.

Proposition A.1.1. *Let $\boldsymbol{\theta} \in \mathrm{W}^{1,\infty}(\mathbb{R}^d)^d$. If $\|\boldsymbol{\theta}\|_{W^{1,\infty}(\mathbb{R}^d)^d} < 1$, then $\boldsymbol{I}+\boldsymbol{\theta} : \mathbb{R}^d \to \mathbb{R}^d$ is a Lipschitz homeomorphism.*

Definition A.1.2 (Shape derivative)**.** *The functional $J(\Omega)$ is said to be shape differentiable if the mapping*

$$\boldsymbol{\theta} \in \mathrm{W}^{1,\infty}(\mathbb{R}^d)^d \to \mathcal{J}(\boldsymbol{\theta}) := J(\Omega_{\boldsymbol{\theta}}) \in \mathbb{R}$$

is Fréchet differentiable at 0. Then, there exists $\mathcal{J}'(0) = J'(\Omega) \in (\mathrm{W}^{1,\infty}(\mathbb{R}^d)^d)'$ that verifies:

$$\mathcal{J}(\boldsymbol{\theta}) = \mathcal{J}(0) + \mathcal{J}'(0)(\boldsymbol{\theta}) + o(\boldsymbol{\theta}), \text{ where } \frac{o(\boldsymbol{\theta})}{\|\boldsymbol{\theta}\|_{W^{1,\infty}(\mathbb{R}^d)^d}} \to 0 \text{ when } \boldsymbol{\theta} \to 0,$$

or equivalently,

$$J(\Omega_{\boldsymbol{\theta}}) = J(\Omega) + J'(\Omega)(\boldsymbol{\theta}) + o(\boldsymbol{\theta}), \text{ where } \frac{o(\boldsymbol{\theta})}{\|\boldsymbol{\theta}\|_{W^{1,\infty}(\mathbb{R}^d)^d}} \to 0 \text{ when } \boldsymbol{\theta} \to 0.$$

Note that with this definition, the *geometry* paradigm of finding an optimal shape was changed to find the deformation field and then we must also introduce a set of admissible deformations. We consider $\Theta_{\text{ad}} \subset \mathrm{W}^{1,\infty}(\mathbb{R}^d)^d$ the set of admissible deformations.

An interesting and useful property of shape derivatives is that know as structure theorem. This theorem says that the shape derivative depends only on the normal component of the perturbation field $\boldsymbol{\theta}$. More details can be found in [72, Proposition 5.9.1, Theorem 5.9.2]

Theorem A.1.3 (Hadamard's structure theorem 1) Let $\Omega \subset \mathbb{R}^d$ be a bounded open subset of class $\mathcal{C}^1$ and $J(\Omega)$ be a shape differentiable functional. Let $\boldsymbol{\theta}_1, \boldsymbol{\theta}_2 \in \mathrm{W}^{1,\infty}(\mathbb{R}^d)^d$ be such that $\boldsymbol{\theta}_2 - \boldsymbol{\theta}_1 \in \mathcal{C}^1(\mathrm{R}^d)^d$ and $\boldsymbol{\theta}_1 \cdot \boldsymbol{n} = \boldsymbol{\theta}_2 \cdot \boldsymbol{n}$ on $\partial\Omega$. Then,

$$J'(\Omega)(\boldsymbol{\theta}_1) = J'(\Omega)(\boldsymbol{\theta}_2).$$

Theorem A.1.4 (Hadamard's structure theorem 2) Let $\Omega \subset \mathbb{R}^d$ be a bounded open subset of class $\mathcal{C}^2$ and $J(\Omega)$ be a shape differentiable functional. Then, there exists $l \in (\mathcal{C}^k(\Gamma))'$ such that,

$$J'(\Omega)(\boldsymbol{\theta}) = l(\boldsymbol{\theta} \cdot \boldsymbol{n}), \forall \boldsymbol{\theta} \in \mathcal{C}^{1,\infty}.$$

A.1.2 Useful integral formulas for shape derivatives

Lemma A.1.5 (Change of variables for volume integrals)**.** *Let $\Omega \subset \mathbb{R}^d$ be a bounded, Lipschitz domain and, let $\boldsymbol{T}$ be a $\mathcal{C}^1$ diffeomorphism of $\mathbb{R}^d$. Let $1 \leq p \leq \infty$. Then,*

$$f \in \mathrm{L}^p(\boldsymbol{T}(\Omega)) \text{ if and only if } f \circ \boldsymbol{T} \in L^p(\Omega),$$

and the following identities hold:

$$\int_{\boldsymbol{T}(\Omega)} f \,\mathrm{d}x = \int_{\Omega} f \circ \boldsymbol{T} |\det \nabla \boldsymbol{T}| \,\mathrm{d}x \text{ and } \int_{\boldsymbol{T}(\Omega)} f |\det(\nabla \boldsymbol{T})^{-1}| \,\mathrm{d}x = \int_{\Omega} f \circ \boldsymbol{T} \,\mathrm{d}x.$$

Lemma A.1.6 (Change of variables for surface integrals)**.** *Let $\Omega \subset \mathbb{R}^d$ be a bounded domain of class $\mathcal{C}^1$ and, let $\boldsymbol{T}$ be a $\mathcal{C}^1$ diffeomorphism of $\mathbb{R}^d$. Then,*

$$f \in \mathrm{L}^1(\partial \boldsymbol{T}(\Omega)) \text{ if and only if } f \circ \boldsymbol{T} \in L^1(\partial\Omega),$$

and the following identity holds:

$$\int_{\partial \boldsymbol{T}(\Omega)} f \,\mathrm{d}s = \int_{\partial\Omega} f \circ \boldsymbol{T} |\det \nabla \boldsymbol{T}| \|((\nabla \boldsymbol{T})^{-1})^t \boldsymbol{n}\|_{\mathbb{R}^d} \,\mathrm{d}s.$$

Remark 28 *Evidently, we use $\boldsymbol{T} = \boldsymbol{I} + \boldsymbol{\theta}$ as the diffeomorphism for the change of variables.*

A.1.3 Some differential geometry

Before advancing to the shape derivatives formulas, we require some notations and identities of differential geometry. More specifically, in what concerns the shape derivative of surface integrals which are more delicate to treat. We will take advantage and we will define the Laplace-Beltrami operator, that we will be present in our computations later on. For the interested reader the proofs can be found in [72, Chapter 5, Subsection 5.4.3].

Definition A.1.7 (Tangential gradient)**.** *Let Ω to be of class $\mathcal{C}^1$. Let $f : \partial\Omega \to \mathbb{R}$ be a function of class $\mathcal{C}^1$. Its tangential gradient is defined by*

$$\nabla_\tau f = \nabla \tilde{f} - \frac{\partial \tilde{f}}{\partial \boldsymbol{n}} \boldsymbol{n} \text{ on } \partial\Omega,$$

where $\tilde{f} \in \mathcal{C}^1(\mathbb{R}^d)$ is an extension of f.

Definition A.1.8. *We assume Ω to be of class $\mathcal{C}^1$ and $p \geq 1$. We introduce the following norm, for any $u \in \mathcal{C}^1(\partial\Omega)$,*

$$\|u\|_{\mathrm{W}^{p,1}(\partial\Omega)} := \int_{\partial\Omega} |u|^p + |\nabla_\tau u|^p \,\mathrm{d}s.$$

We denote by $\mathrm{W}^{p,1}(\partial\Omega)$ the closure of $\mathcal{C}^1(\partial\Omega)$, with respect to the norm $\|\cdot\|_{\mathrm{W}^{p,1}(\partial\Omega)}$.

Proposition A.1.9. *We assume Ω to be of class $\mathcal{C}^1$. Then,*

$$\mathrm{W}^{p,1}(\partial\Omega) = \{u \in \mathrm{L}^p(\partial\Omega); \nabla_\tau u \in \mathrm{L}^p(\partial\Omega)^{d-1}\}.$$

Definition A.1.10 (Tangential divergence)**.** *Let $\boldsymbol{V} \in \mathcal{C}^1(\Gamma)^d$. Its tangential divergence is defined by,*

$$\operatorname{div}_\tau \boldsymbol{V} = \operatorname{div} \tilde{\boldsymbol{V}} - (\nabla \tilde{V})\boldsymbol{n} \cdot \boldsymbol{n} \text{ on } \partial\Omega,$$

where $\tilde{\boldsymbol{V}} \in \mathcal{C}^1(\mathbb{R}^d)^d$ is an extension of $\boldsymbol{V}$. By density, $\operatorname{div}_\tau \boldsymbol{V}$ is defined for all $\boldsymbol{V} \in \mathrm{W}^{1,1}(\partial\Omega)^d$.

Remark 29 *These definitions are independent of the choice of the extension.*

Definition A.1.11 (Mean curvature)**.** *We suppose Ω to be an open bounded domain of class $\mathcal{C}^2$. The mean curvature is defined by $H = \operatorname{div}_\tau \boldsymbol{n}$.*

The next result allow us to compute the mean curvature as the divergence of a extension of the normal instead of the tangential divergence of the normal vector (that is only defined on the surface).

Proposition A.1.12. *Let Ω be of class $\mathcal{C}^2$ and let $\boldsymbol{N}$ be any unitary extension of the normal $\boldsymbol{n}$. Then,*

$$H = \operatorname{div} \boldsymbol{N} \text{ on } \partial\Omega.$$

Remark 30 *In the future, sometimes we will not distinguish the notation between the extension of the normal $\boldsymbol{N}$ and the normal $\boldsymbol{n}$ in order to do not overcharge the notation. There will appear some terms as $\nabla \boldsymbol{n}$ or ∇H. Of course, we will be using the extension of the normal in these cases.*

Definition A.1.13 (Tangent component of a field)**.** *Let $\boldsymbol{V}$ a field defined on Γ. We define the tangent component as $\boldsymbol{V}_\tau := \boldsymbol{V} - (\boldsymbol{V} \cdot \boldsymbol{n})\boldsymbol{n}$ on $\partial\Omega$.*

The next result is an integration by parts formula on the surface.

Proposition A.1.14. *Let Ω be of class $\mathcal{C}^2$. Let $f \in \mathrm{W}^{1,1}(\partial\Omega), \boldsymbol{V} \in \mathrm{W}^{1,1}(\partial\Omega)^d$. Then,*

$$\int_{\partial\Omega} \operatorname{div}_\tau \boldsymbol{V} \, \mathrm{d}s = \int_{\partial\Omega} H\boldsymbol{V} \cdot \boldsymbol{n} \, \mathrm{d}s,$$

and

$$\int_{\partial\Omega} \nabla_\tau f \cdot \boldsymbol{V} \, \mathrm{d}s = \int_{\partial\Omega} -f \operatorname{div}_\tau \boldsymbol{V} + Hf\boldsymbol{V} \cdot \boldsymbol{n} \, \mathrm{d}s.$$

Definition A.1.15. *We assume Ω to be of class $\mathcal{C}^2$. We introduce the following scalar product, for any $u, v \in \mathcal{C}^2(\partial\Omega)$,*

$$(u, v)_{\mathrm{H}^2(\partial\Omega)} := \int_{\partial\Omega} (\Delta u \Delta v + \nabla_\tau u \cdot \nabla_\tau v + uv) \, \mathrm{d}s.$$

We denote by $\mathrm{H}^2(\partial\Omega)$ the closure of $\mathcal{C}^2(\partial\Omega)$, with respect to the norm induced by $(\cdot,\cdot)_{\mathrm{H}^2(\partial\Omega)}$.

Proposition A.1.16. *We assume Ω to be of class $\mathcal{C}^2$ and $\partial\Omega$ without boundary. Then,*

$$\mathrm{H}^2(\partial\Omega) = \{u \in \mathrm{H}^1(\partial\Omega); \nabla_\tau u \in \mathrm{H}^1(\partial\Omega)^{d-1}\}.$$

Now, we can define the Laplace-Beltrami operator that plays a key role in this thesis.

Definition A.1.17 (Laplace-Beltrami operator)**.** *Assume Ω to be of class $\mathcal{C}^2$. Let $u \in \mathrm{H}^2(\partial\Omega)$. The Laplace-Beltrami operator Δ_τ is defined as follows*

$$\Delta_\tau u = \mathrm{div}_\tau(\nabla_\tau u).$$

Note that if $u \in \mathrm{H}^2(\partial\Omega)$, then $\Delta_\tau u \in \mathrm{L}^2(\partial\Omega)$ and from Proposition A.1.14, for every $v \in \mathrm{H}^1(\partial\Omega)$,

$$\int_{\partial\Omega} \Delta_\tau u v \,\mathrm{d}s = -\int_{\partial\Omega} \nabla_\tau u \cdot \nabla_\tau v \,\mathrm{d}s.$$

Proposition A.1.18. *Let Ω be an open set of class $\mathcal{C}^2$ and $u \in \mathrm{H}^3(\Omega)$. Then,*

$$\Delta u = \Delta_\tau u + H\frac{\partial u}{\partial n} + \frac{\partial^2 u}{\partial n^2} \text{ on } \partial\Omega.$$

A.1.4 Extension of the unit normal vector

In this part we consider $\boldsymbol{\theta} \in \mathcal{C}^{1,\infty} = \mathcal{C}^1 \cap \mathrm{W}^{1,\infty}(\mathbb{R}^d)^d$.

Definition A.1.19 (Signed distance function)**.** *We define the signed distance function $d_{\partial\Omega}$ as :*

$$d_{\partial\Omega}(x) = \begin{cases} -d(x,\partial\Omega) & \iff \quad x \in \Omega \\ 0 & \iff \quad x \in \partial\Omega \\ d(x,\partial\Omega) & \iff \quad x \in \mathbb{R}^d \setminus \overline{\Omega}, \end{cases}$$

where $d(x,\partial\Omega)$ is the distance from x to $\partial\Omega$ (or in other words, the projecton to the boundary).

The signed distance function is very relevant in shape optimization, in particular in the level-set mesh evolution method, since is a level-set function and then it defines en extension of the unit normal vector to $\partial\Omega$:

$$\boldsymbol{n} = \nabla d_{\partial\Omega}. \tag{A.1}$$

Proposition A.1.20. *Let Ω be of class $\mathcal{C}^2$. Let $\boldsymbol{n} \in \mathcal{C}^1(\mathbb{R}^d)^d$ be an extension of the unit normal vector to $\partial\Omega$. Then,*

$$\boldsymbol{n}_{\boldsymbol{\theta}} := \frac{((\mathrm{I} + \nabla\boldsymbol{\theta})^{-t}\boldsymbol{n}) \circ (\boldsymbol{I} + \boldsymbol{\theta})^{-1}}{\|((\boldsymbol{I} + \boldsymbol{\theta})^{-t}\boldsymbol{n}) \circ (\mathrm{I} + \nabla\boldsymbol{\theta})^{-1}\|} \tag{A.2}$$

is normal to $\partial\Omega_{\boldsymbol{\theta}}$ and the mapping $\boldsymbol{\theta} \in \mathcal{C}^{1,\infty} \to \boldsymbol{n}_{\boldsymbol{\theta}} \in \mathcal{C}^0(\mathbb{R}^d)^d$ is differentiable at 0. Its shape derivative is given by:

$$\boldsymbol{n}' = -\nabla_\tau(\boldsymbol{\theta}\cdot\boldsymbol{n}) - ((\nabla n_0)\boldsymbol{n})(\boldsymbol{\theta}\cdot\boldsymbol{n}) \text{ on } \partial\Omega,$$

where $\boldsymbol{n}_0 = \boldsymbol{n}$ on $\partial\Omega$. In particular, if it is the normal extension defined by the signed distance function (A.1)*, then*

$$\boldsymbol{n}' = -\nabla_\tau(\boldsymbol{\theta}\cdot\boldsymbol{n}) \text{ on } \partial\Omega.$$

The following result anticipate the concept of material of derivative, that we will define in general later on. This result can be found in [104, Lemma 3.4].

Proposition A.1.21 (Material derivative of the unit normal vector)**.** *Under the same hypothesis of the previous proposition, we have that*

$$\boldsymbol{n}_{\boldsymbol{\theta}} \circ (\boldsymbol{I} + \boldsymbol{\theta}) = \frac{(\mathrm{I} + \nabla \boldsymbol{\theta})^{-t} \boldsymbol{n}}{\|(\mathrm{I} + \nabla \boldsymbol{\theta})^{-t} \boldsymbol{n}\|}.$$

The mapping $\boldsymbol{\theta} \in \mathcal{C}^{1,\infty} \to \boldsymbol{n}_{\boldsymbol{\theta}} \circ (\mathrm{I} + \boldsymbol{\theta}) \in \mathcal{C}^0(\Gamma)^d$ is differentiable at 0. This derivative is called material derivative $\dot{\boldsymbol{n}}$ and is given by:

$$\dot{\boldsymbol{n}} = -(\nabla_\tau \boldsymbol{\theta})^t \boldsymbol{n}.$$

In particular, if it is the normal extension defined by the signed distance function (A.1)*, then*

$$\dot{\boldsymbol{n}} = -\nabla_\tau (\boldsymbol{\theta} \cdot \boldsymbol{n}) + (\nabla \boldsymbol{n}) \boldsymbol{\theta} \text{ on } \partial\Omega.$$

We have similar results for the mean curvature [104, Lemma 3.5], [75]. Let $\kappa := \operatorname{div} \boldsymbol{n}$ a extension of the mean curvature. In particular,

$$H = \kappa = \Delta d_{\partial\Omega} \text{ on } \partial\Omega. \tag{A.3}$$

Proposition A.1.22 (Shape derivative of the mean curvature)**.** *Let Ω be of class $\mathcal{C}^3$. Let $\boldsymbol{n} \in \mathcal{C}^2(\mathbb{R}^d)^d$ be an extension of the unit normal vector to $\partial\Omega$. Then,*

$$\kappa_{\boldsymbol{\theta}} = \operatorname{div} \boldsymbol{n}_{\boldsymbol{\theta}} \text{ on } \partial\Omega_{\boldsymbol{\theta}},$$

and the application $\boldsymbol{\theta} \in \mathcal{C}^{2,\infty} \to \kappa_{\boldsymbol{\theta}} \in \mathcal{C}^0(\mathbb{R}^d)$ is $\mathcal{C}^1$. Furthermore, if it is the normal extension defined by the signed distance function (A.1)*, then*

$$\kappa' = -\Delta_\tau (\boldsymbol{\theta} \cdot \boldsymbol{n}) \text{ on } \partial\Omega.$$

Proposition A.1.23 (Material derivative of the mean curvature)**.** *Let Ω be of class $\mathcal{C}^3$. Let $\boldsymbol{n} \in \mathcal{C}^2(\mathbb{R}^d)^d$ be an extension of the unit normal vector to $\partial\Omega$. Then,*

$$\kappa_{\boldsymbol{\theta}} \circ (\boldsymbol{I} + \boldsymbol{\theta}) = \operatorname{tr}[\nabla(\boldsymbol{n}_{\boldsymbol{\theta}} \circ (\boldsymbol{I} + \boldsymbol{\theta}))(\mathrm{I} + \nabla \boldsymbol{\theta})^{-t}] \text{ on } \partial\Omega.$$

The mapping $\boldsymbol{\theta} \in \mathcal{C}^{2,\infty} \to \kappa_{\boldsymbol{\theta}} \circ (\boldsymbol{I} + \boldsymbol{\theta}) \in \mathcal{C}^0(\partial\Omega)$ is differentiable at 0 and this derivative is called the material derivative of κ. Moreover, if it is the normal extension defined by the signed distance function (A.3)*, then*

$$\dot{\kappa} = -\Delta_\tau (\boldsymbol{\theta} \cdot \boldsymbol{n}) + \nabla \kappa \cdot \boldsymbol{\theta} \text{ on } \partial\Omega.$$

A.1.5 Integral shape derivatives

We start by considering functionals that depends only on the domain Ω without having associated a solution of a PDE. These results are the cornerstone of shape optimization.

Theorem A.1.24 Let $f \in \mathrm{W}^{1,1}(\mathbb{R}^d)$ and consider the following functional as a volume integral in Ω that we suppose to be $\mathcal{C}^1$:

$$J(\Omega) = \int_\Omega f(x) \, \mathrm{d}x.$$

Then J is differentiable at Ω and we have

$$J'(\Omega)(\boldsymbol{\theta}) = \int_\Omega \operatorname{div}(f\boldsymbol{\theta})\,\mathrm{d}x = \int_{\partial\Omega} f\boldsymbol{\theta}\cdot\boldsymbol{n}\,\mathrm{d}s,$$

for any $\boldsymbol{\theta} \in \mathrm{W}^{1,\infty}(\mathrm{R}^d)^d$.

The next result gives a similar formula for surface integrals.

Proposition A.1.25. *Let $f \in \mathrm{W}^{2,1}(\mathbb{R}^d)$, then the following funtional as a surface integral on $\partial\Omega$ that we assume to be $\mathcal{C}^2$:*

$$J(\Omega) = \int_{\partial\Omega} f(x)\,\mathrm{d}s(x).$$

Then J is shape differentiable at Ω and, for every $\boldsymbol{\theta} \in \mathcal{C}^1(\mathbb{R}^d)^d$, we have

$$J'(\Omega)(\boldsymbol{\theta}) = \int_{\partial\Omega} \left(\frac{\partial f}{\partial \boldsymbol{n}} + Hf\right)(\boldsymbol{\theta}\cdot\boldsymbol{n})\,\mathrm{d}s,$$

where H is the mean curvature of $\partial\Omega$.

A.1.6 Differentiation of a PDE

In this part, we will introduce the concept of material and shape derivatives or also called Lagrangean and Eulerian derivatives, respectively. We follow the lines of [7, Subsection 6.3.3].

Let $\mathrm{H}(\Omega)$ be a Sobolev space. Let $u_\Omega \in \mathrm{H}$ be a scalar function that depends on the domain Ω. We can think of u as the solution of a PDE variational problem. At first sight, we can think of defining its derivative similarly to the shape derivative of a functional of Ω (Definition A.1.2), this is, for any $x \in \Omega$, we can define the mapping

$$\boldsymbol{\theta} \in \Theta_{\mathrm{ad}} \to \mathcal{U}(\boldsymbol{\theta}, x) := u_{\Omega_{\boldsymbol{\theta}}}(x) \in \mathbb{R},$$

and then the shape derivative of u could be obtained as

$$\mathcal{U}(\boldsymbol{\theta}, x) = \mathcal{U}(0, x) + \mathcal{U}'(0)(\boldsymbol{\theta}) + o(\boldsymbol{\theta}), \text{ with } \lim_{\boldsymbol{\theta}\to 0} \frac{\|o(\boldsymbol{\theta})\|}{\|\boldsymbol{\theta}\|} = 0,$$

or,

$$u_{\Omega_{\boldsymbol{\theta}}}(x) = u_\Omega(x) + u'(\boldsymbol{\theta})(x) + o(\boldsymbol{\theta}), \text{ with } \lim_{\boldsymbol{\theta}\to 0} \frac{\|o(\boldsymbol{\theta})\|}{\|\boldsymbol{\theta}\|} = 0.$$

Even tough this definition works for interior points $x \in \operatorname{int}(\Omega)$, it does not work for boundary points $x \in \partial\Omega$. More precisely, for $\boldsymbol{\theta}$ small enough, if $x \in \Omega$, then x still belongs to $\Omega_{\boldsymbol{\theta}}$. However, if $x \in \partial\Omega$, we cannot guarantee that $x \in \partial\Omega_{\boldsymbol{\theta}}$. This means that u_Ω and $u_{\Omega_{\boldsymbol{\theta}}}$ belongs to different Sobolev spaces.

Remark 31 *Of course, it is not true that $u_{\Omega_{\boldsymbol{\theta}}} = u_\Omega \circ (\boldsymbol{I} + \boldsymbol{\theta})^{-1}$ neither $u_\Omega = u_{\Omega_{\boldsymbol{\theta}}} \circ (\boldsymbol{I} + \boldsymbol{\theta})$.*

This issues leads to consider another type of derivative of u_Ω.

Definition A.1.26 (Transported function)**.** *Let* $\mathrm{H}(\Omega)$ *be a Sobolev and* u_Ω *a scalar function belonging to* $\mathrm{H}(\Omega)$*. We define the transported function* $\overline{u}_\Omega$ *as*

$$\boldsymbol{\theta} \in \Theta_{\mathrm{ad}} \to \overline{u}_\Omega(\boldsymbol{\theta}) = u_{\Omega_{\boldsymbol{\theta}}} \circ (\boldsymbol{I} + \boldsymbol{\theta}) \to \mathrm{H}(\Omega).$$

This transported function belongs to the fixed space $\mathrm{H}(\Omega)$ and then we can derive it without problems. Its derivative it is called material derivative of u_Ω.

Definition A.1.27 (Material derivative)**.** *We assume the transported function from Definition A.1.26 is differentiable at* 0*. Then we define the material derivative of* u_Ω *as the Fŕechet derivative of the mapping* $\boldsymbol{\theta} \to \overline{u}_\Omega$ *and we denote it by* $\dot{u}_\Omega \in \mathrm{V}(\Omega)$*, this is, it verifies,*

$$\overline{u}_\Omega(\boldsymbol{\theta})(x) = \overline{u}_\Omega(0)(x) + \dot{u}_\Omega(\boldsymbol{\theta})(x) + o(\boldsymbol{\theta}), \ \textit{with} \ \lim_{\boldsymbol{\theta}\to 0} \frac{\|o(\boldsymbol{\theta})\|}{\|\boldsymbol{\theta}\|} = 0,$$

where $\mathrm{V}(\Omega) \subset \mathrm{H}(\Omega)$ *is a certain Sobolev space.*

Definition A.1.28. *Under the same hypothesis of the previous definition and also assuming that* $\nabla u_\Omega \in \mathrm{H}(\Omega)$*, we define the shape derivative of* u_Ω *as :*

$$u'_\Omega(\boldsymbol{\theta}) = \dot{u}_\Omega - \nabla u_\Omega \cdot \boldsymbol{\theta} \in \mathrm{H}(\Omega), \ \textit{for any} \ \boldsymbol{\theta} \in \Theta_{\mathrm{ad}}.$$

A.2 Level-set mesh evolution method and numerical tools

In this part we will explain the main ingredients of the level-set evolution method that will use throughout this thesis. For more details refer to [10, 48, 9].

As we have highlighted in the introduction, the level-set method represents implicitly the domain. We start by defining a level-set function:

Definition A.2.1. *A level-set function of the domain* Ω *is any real-valued continuous function* ϕ_Ω *such that:*

$$\begin{cases} \phi_\Omega(x) < 0 \ \textit{iff} \ x \in \Omega, \\ \phi_\Omega(x) = 0 \ \textit{iff} \ x \in \partial\Omega, \\ \phi_\Omega(x) > 0 \ \textit{iff} \ x \in \mathbb{R}^d \setminus \overline{\Omega}. \end{cases}$$

Note that the signed-distance function A.1.19 is a particular case of a level-set function.

In a shape optimization context, we fix a computational domain $B \subset \mathbb{R}^d$ that contains Ω and such that ∂B contains the fixed boundary parts of $\partial\Omega$, to work with variations of Ω inside B. We assume that B is discretized by a conforming mesh $\mathcal{T}$.

The great versatility of this method lies in the fact that we have two representations of the domain Ω. One explicit through a conforming mesh $\mathcal{T}_{int}$ (and $B\setminus\Omega$ is discretized a conforming mesh $\mathcal{T}_{ext}$) and one implicit through the level-set function ϕ_Ω. The explicit representation through $\mathcal{T}$ allows to solve the associated PDEs, while the implicit representation allows to capture the evolution of the Ω domain.

In the following we will describe the steps involving the level-set function within the shape optimization algorithm:

Redistancing algorithm. The easiest way to compute the signed distance (but not the most efficient) $d(x, \partial\Omega)$ for a given vertex x is to iterate through every vertex $y \in \partial\Omega$ of the mesh $\mathcal{T}$ and compute the minimum. Most efficient algorithms such as the Fast Marching Methods [102, 101], Fast Sweeping Method [113, 98] or the so-called redistancing equation [49] involve the resolution of the Eikonal equation:

$$\begin{cases} \dfrac{\partial d_\Omega}{\partial t}(t,x) + sgn(\phi_0)(\|\nabla d_\Omega\| - 1) = 0, \quad \forall (t,x) \in (0,\infty) \times \mathbb{R}^d, \\ d_\Omega(0,x) = \phi_0(x), \forall x \in \mathbb{R}^d, \end{cases}$$

where ϕ_0 is any level-set function of Ω. We rely in the redistancing equation, that is available in the open-source library MSHDIST [1].

Advection. Let $n-1$ be the actual iteration in the shape optimization process. We denote ϕ^{n-1} the level function associated to Ω^{n-1}, with conformal mesh $\mathcal{T}$. Let $\boldsymbol{\theta}$ a given velocity (that actually is a direction descent in the shape optimization algorithm, we will explain how to obtain it later on). In order to obtain ϕ^n we solve the following transport equation:

$$\begin{cases} \dfrac{\partial \phi^n}{\partial t} + \boldsymbol{\theta} \cdot \nabla \phi^n = 0, & 0 < t < \tau, \ x \in \Omega, \\ \phi^n(0,x) = \phi^{n-1}(x), & x \in \Omega, \end{cases} \tag{A.4}$$

for some $\tau > 0$. To solve the equation (A.4) we use ADVECT [2] [29] .

Remesh. Once we have the level-set function of the next step ϕ^n, we remesh with respect to its zero value, getting $\partial\Omega^n$ and the conformal mesh $\mathcal{T}^n$. For this purpose we use the open-source library MMG [3] [47]).

It remains explaining how to obtain $\boldsymbol{\theta}$ of equation (A.4).

Extension-regularization We consider J a shape derivable function. In a shape optimization problem, it will be a linear combination between the objective function and constraints. See Chapters 3 and 4 to fix ideas.

We introduce a Hilbert space such as:

$$H := \{\boldsymbol{\varphi} \in \mathrm{H}(B)^d; \boldsymbol{\varphi} = 0 \text{ on } \partial B\},$$

and the following bilinear form

$$a(\boldsymbol{\theta}, \boldsymbol{\varphi}) := \int_B \left(\gamma^2 \nabla\boldsymbol{\theta} : \nabla\boldsymbol{\varphi} + \boldsymbol{\theta} \cdot \boldsymbol{\varphi}\right) \mathrm{d}x,$$

where $\gamma > 0$ is positive parameter that depends on the mesh size h. Then, we consider the following problem:

$$\text{Find } \boldsymbol{\theta} \in H, \text{ such that } \forall \boldsymbol{\varphi} \in H, a(\boldsymbol{\theta}, \boldsymbol{\varphi}) = J'(\Omega)(\boldsymbol{\theta}).$$

[1] https://github.com/ISCDtoolbox/Mshdist
[2] https://github.com/ISCDtoolbox/Advection
[3] https://github.com/MmgTools/mmg

Even though, this is formal, since H is not embedded into $\mathrm{W}^{1,\infty}(\mathbb{R}^d)^d$, it works well in practice. Refer to [9] for more details about this.